

The effect of a *Mycoplasma hyorhinis*
protein (p37) on gene expression
in mouse fibroblasts

Submitted by

Amber Cathie Gomersall

Bachelor of Biological Sciences (Honours)

A thesis submitted in total fulfilment
of the requirements for the degree of
Doctor of Philosophy

School of Life Sciences

Department of Botany

Faculty of Science, Technology and Engineering

La Trobe University

Bundoora, Victoria 3086

Australia

July 2013

TABLE OF CONTENTS

TABLE OF CONTENTS	II
LIST OF FIGURES	VII
LIST OF TABLES	XI
ABBREVIATIONS	XIII
GENERAL ABBREVIATIONS.....	XIII
ABBREVIATIONS OF DIFFERENT CELL LINES	XV
ABSTRACT	XVI
STATEMENT OF AUTHORSHIP	XVIII
ACKNOWLEDGEMENTS.....	XIX
1. INTRODUCTION	1
1.1 MYCOPLASMA AND CANCER	1
1.2 THE DISCOVERY OF THE P37 PROTEIN	3
1.3 THE P37 OPERON HAS STRUCTURAL SIMILARITIES TO PERIPLASMIC BINDING-PROTEIN DEPENDENT TRANSPORT SYSTEMS	7
1.4 P37 PROTEIN STRUCTURE	11
1.5 P37 BINDING AND LOCALISATION ON MAMMALIAN CELLS	14
1.6 P37 AND CANCER.....	18
1.7 HETEROTYPIC CONTACT INHIBITION OF LOCOMOTION	24
1.8 THE ROLE OF RAC1 AND RHOA IN HETEROTYPIC CONTACT INHIBITION OF LOCOMOTION.....	29
1.9 AIMS	33
2. MATERIALS AND METHODS	34
2.1 REAGENTS.....	34
2.2 CONSTRUCTS	35
2.2.1 pRAP37	35
2.2.2 pSTP37	35
2.3 BACTERIAL STRAINS	36
2.4 MAMMALIAN CELL LINE	36
2.5 OLIGONUCLEOTIDES.....	37
2.5.1 GENERAL OLIGONUCLEOTIDES	37
2.5.2 PCR GENE OLIGONUCLEOTIDES	37
2.5.3 qPCR OLIGONUCLEOTIDES	38
2.6 CLONING	39
2.6.1 XL1-BLUE COMPETENT CELLS (STRATAGENE) HEAT SHOCK TRANSFORMATION	39
2.6.2 ONE SHOT® BL21(DE3) (INVITROGEN) HEAT SHOCK TRANSFORMATION	39
2.6.3 SHORT TERM STORAGE OF BACTERIAL TRANSFORMATIONS	40
2.6.4 LONG TERM STORAGE OF BACTERIAL TRANSFORMATIONS.....	40
2.6.5 ISOLATION OF PLASMID DNA	40
2.6.6 RESTRICTION ENZYME DIGEST	40
2.6.7 DNA PURIFICATION FROM AGAROSE GEL.....	40
2.6.8 DEPHOSPHORYLATION USING SHRIMP ALKALINE PHOSPHATASE (PROMEGA).....	41
2.6.9 LIGATION REACTION	41

2.6.10	QUIKCHANGE II XL SITE-DIRECTED MUTAGENESIS (AGILENT TECHNOLOGIES)	41
2.7	AGAROSE GEL ELECTROPHORESIS	42
2.8	DNA SEQUENCING (AGRF)	42
2.8.1	PLASMID SEQUENCING	42
2.8.2	PCR PRODUCT SEQUENCING	42
2.8.3	SEQUENCE ANALYSES	42
2.9	RNA PURIFICATION AND cDNA SYNTHESIS	43
2.9.1	RNA EXTRACTIONS FROM ANIMAL CELLS	43
2.9.2	REMOVAL OF GENOMIC CONTAMINATION VIA DNASE TREATMENT	43
2.9.3	RNA INTEGRITY AND QUANTIFICATION	43
2.9.4	cDNA SYNTHESIS USING REVERSE TRANSCRIPTION	43
2.10	DNA PURIFICATION	44
2.10.1	GENOMIC DNA ISOLATION	44
2.11	POLYMERASE CHAIN REACTION (PCR)	44
2.11.1	PCR MIXTURE	44
2.11.2	PROOF READING TAQ (KAPA HiFi DNA POLYMERASE)	44
2.11.3	COLONY PCR	44
2.11.4	PCR AMPLIFICATION PROCESS	44
2.11.5	SEMI-QUANTITATIVE RT-PCR	45
2.12	QUANTITATIVE PCR (qPCR) ANALYSIS	45
2.12.1	QUANTITATIVE PCR (qPCR)	45
2.12.2	PRIMER EFFICIENCY: STANDARD CURVE	45
2.12.3	PRIMER EFFICIENCY: CONTAMINATION AND SPECIFICITY	46
2.12.4	NORMALISED CYCLE THRESHOLD (ΔC_T)	46
2.12.5	TRANSCRIPT ABUNDANCE	46
2.12.6	FOLD CHANGE	46
2.12.7	ERROR BARS FOR TRANSCRIPT ABUNDANCE	46
2.12.8	ERROR BARS FOR FOLD CHANGE	47
2.12.9	ANALYSIS OF VARIANCE (ANOVA)	47
2.13	MICROARRAY	47
2.13.1	MICROARRAY	47
2.13.2	MICROARRAY ANALYSIS	48
2.14	RT²PROFILER™ PCR ARRAY SYSTEM	48
2.14.1	SAMPLE PREPARATION	48
2.14.2	RT ² FIRST STRAND SYNTHESIS (SABIOSCIENCES CAT#330401)	48
2.14.3	REAL-TIME PCR	48
2.14.4	ANALYSIS OF DATA	49
2.15	SOLUBLE PROTEIN EXPRESSION AND PURIFICATION	49
2.15.1	PROTEIN EXPRESSION IN ONESHOT® BL21 (DE3)	49
2.15.2	CLARIFICATION OF <i>E. COLI</i> LYSATE UNDER NATIVE CONDITIONS	49
2.15.3	PURIFICATION OF 6X HIS TAG PROTEINS IN NATIVE CONDITIONS	49
2.16	INSOLUBLE PROTEIN EXPRESSION AND PURIFICATION	50
2.16.1	ISOLATION OF INCLUSION BODIES	50
2.16.2	SOLUBILISATION AND PREPARATION OF INCLUSION BODIES	50
2.16.3	PURIFICATION OF 6X HIS TAG PROTEIN FROM INCLUSION BODIES	51
2.17	PROTEIN ANALYSIS	51
2.17.1	SDS-PAGE GELS	51
2.17.2	COOMASSIE BLUE STAINING OF SDS-PAGE GELS	51
2.17.3	WESTERN	52
2.17.4	COLORIMETRIC ANALYSIS OF A WESTERN MEMBRANE USING PRIMARY AND SECONDARY ANTIBODIES	52
2.17.5	ALKALINE PHOSPHATASE COLORIMETRIC DEVELOPMENT OF A WESTERN MEMBRANE	52

2.17.6	PROTEIN SIZE ANALYSIS.....	52
2.17.7	PROTEIN QUANTIFICATION.....	53
2.18	MAMMALIAN TISSUE CULTURE AND TRANSFORMATION	53
2.18.1	PASSAGING	53
2.18.2	FREEZING DOWN.....	54
2.18.3	DEFROSTING CELL CULTURES.....	54
2.18.4	KILL CURVE	55
2.18.5	LIPOFECTION OF NIH3T3 CELLS.....	55
2.18.6	ISOLATING A CLONE	55
2.18.7	MYCOPLASMA DETECTION PCR.....	56
2.18.8	USING A HAEMOCYTOMETER.....	56
2.19	TREATING MAMMALIAN CELLS	56
2.19.1	PREPARING NIH3T3 CELLS FOR TREATMENT	56
2.19.2	TREATING NIH3T3 CELLS WITH THE PURIFIED P37 PROTEIN	56
2.19.3	IL6R/ TREATMENT.....	57
2.19.4	STAT3 INHIBITOR VI (S31-201) TREATMENT.....	57
2.19.5	LPS TREATMENT	57
2.19.6	VIPER OR CP7 TREATMENT	58
2.20	CYTOSKELETON: G-LISA™ RHOA ACTIVATION ASSAY BIOCHEM KIT (ABSORBANCE ASSAY)	58
2.21	WOUND HEALING ASSAYS	58
2.21.1	WOUNDING CELL CULTURE.....	58
2.21.2	ANALYSIS WITH IMAGEJ.....	59
2.21.3	CALCULATING THE MIGRATION CELL SURFACE AREA	60
3.	GENE EXPRESSION PROFILING OF P37 TREATED NIH3T3 (MOUSE) FIBROBLASTS..	61
3.1	INTRODUCTION	61
3.2	RESULTS AND DISCUSSION.....	63
3.2.1	PURIFICATION OF THE P37 PROTEIN	63
3.2.2	GENE EXPRESSION PROFILING OF P37-TREATED NIH3T3 FIBROBLASTS.....	67
3.2.3	VALIDATION OF THE 18 SELECTED GENES INDUCED BY P37 TREATMENT OF NIH3T3 CELLS.....	76
3.2.4	THE EFFECT OF P37 CONCENTRATIONS ON GENE EXPRESSION IN NIH3T3 CELLS.....	80
3.2.5	TEMPORAL INDUCTION PATTERNS OF GENE INDUCTION DUE TO 24HR P37 TREATMENT.....	82
3.2.6	COMPARISON OF P37-INDUCED GENE EXPRESSION OVER THE DIFFERENT EXPERIMENTS.....	84
3.2.7	THE EFFECT OF P37 IN THE INFLAMMATORY RESPONSE AND AUTOIMMUNITY PATHWAYS: AN RT ² PROFILER PCR ARRAY STUDY.....	86
3.2.8	GENES DOWN-REGULATED BY P37	91
4.	THE ROLE OF THE INTERLEUKIN 6 PATHWAY IN ACTIVATION BY P37 OF GENES ENCODING ACUTE PHASE PROTEINS	93
4.1	INTRODUCTION	93
4.2	RESULTS AND DISCUSSION.....	97
4.2.1	EFFECT OF THE IL6R/ ANTIBODY ON THE EXPRESSION OF THE NINETEEN SELECTED GENES	97
4.2.2	THE ROLE OF THE IL6R IN THE ACTIVATION OF P37-INDUCED GENE EXPRESSION	99
4.3	CONCLUSION	102
5.	THE EFFECT OF INHIBITING STAT3 ON P37-INDUCED GENE EXPRESSION	103
5.1	INTRODUCTION	103
5.2	RESULTS AND DISCUSSION.....	105
5.2.1	EFFECTS OF P37 ON <i>STAT3</i> TRANSCRIPTION IN NIH3T3 CELLS	105
5.2.2	EFFECT OF THE STAT3 INHIBITOR S31-201 ON P37-INDUCED GENE EXPRESSION	107
5.2.3	THE EFFECT OF STAT3 INHIBITION ON P37-INDUCED EXPRESSION OF THE INFLAMMATORY RESPONSE AND AUTOIMMUNITY PATHWAY: AN RT ² PROFILER PCR ARRAY STUDY	111

5.3	CONCLUSION	117
6.	P37 ACTIVATES THE EXPRESSION OF ACUTE PHASE PROTEINS VIA TOLL LIKE RECEPTOR 4 PATHWAY	119
6.1	INTRODUCTION	119
6.2	RESULTS AND DISCUSSION.....	122
6.2.1	LIPOPOLYSACCHARIDES (LPS) STIMULATE SAA3 EXPRESSION IN NIH3T3 CELLS.....	122
6.2.2	VIPER INHIBITS LPS/TLR4 INDUCED SAA3 EXPRESSION IN NIH3T3 CELLS.....	124
6.2.3	THE EFFECTS OF VIPER AND CP7 ON P37-INDUCED GENE EXPRESSION IN NIH3T3 CELLS.....	128
6.2.4	MYCOPLASMA LIPOPROTEINS AND TLR RECEPTORS.....	134
6.2.5	GENES ACTIVATED VIA TLR4 ARE ALSO INDUCED BY P37-TREATMENT	136
7.	EFFECTS OF CHANGING THE THIAMINE PYROPHOSPHATE BINDING SITES OR TRUNCATION ON P37-INDUCED GENE EXPRESSION.....	138
7.1	INTRODUCTION	138
7.2	RESULTS & DISCUSSION.....	140
7.2.1	SITE DIRECTED MUTAGENESIS OF THE SFSK AMINO ACID SEQUENCE OF P37	140
7.2.2	MUTANT P37 PROTEIN PURIFICATION	145
7.2.3	MUTATED P37 DOES NOT INDUCE GENE EXPRESSION TO THE SAME DEGREE AS NATIVE P37	147
7.2.4	EFFECTS OF TRUNCATING P37 ON ITS CAPACITY TO INDUCE GENE EXPRESSION	149
	ISOLATION OF THE FUNCTIONAL PEPTIDE	149
	GUANIDINE HYDROCHLORIDE PURIFICATION OF THE INSOLUBLE TRUNCATED P37 PEPTIDES.....	151
	ARGININE PURIFICATION OF THE INSOLUBLE TRUNCATED P37 PEPTIDES.....	152
7.2.5	BLAST ALIGNMENT OF THE <i>M. HYORHINIS</i> P37 PROTEIN TO RELATED PROTEINS IN MYCOPLASMA.....	155
7.2.6	BLAST ALIGNMENT OF THE 20AA C-TERMINUS OF THE <i>M. HYORHINIS</i> P37 WITH OTHER PROTEINS...	157
7.3	CONCLUSION	160
8.	THE EFFECTS OF P37 ON WOUND HEALING AND CELL MIGRATION	161
8.1	INTRODUCTION	161
8.2	RESULTS	164
8.2.1	LIPOFECTION OF NIH3T3 CELLS WITH THE PSTP37 CONSTRUCT.....	164
8.2.2	P37 TRANSFECTION INFLUENCES NIH3T3 CELLULAR MORPHOLOGY	167
8.2.3	THE P37 PROTEIN PROMOTES CELL MOTILITY AND MIGRATION	169
8.2.4	RHOA IS ACTIVATED IN P37-TREATED NIH3T3 CELLS	172
8.2.5	EXPRESSION OF TWENTY SELECTED GENES IN P37-TRANSFECTED NIH3T3 CELLS	173
8.3	DISCUSSION.....	174
9.	FINAL DISCUSSION	177
9.1	GENES UP-REGULATED BY P37	177
9.2	MYCOPLASMA INFECTION: ARTHRITIS AND CANCER	181
9.3	THE EFFECTS ON P37-INDUCED GENE EXPRESSION OF BLOCKING IL6R OR STAT3.....	183
9.4	INTERACTION OF P37 WITH THE TOLL-LIKE 4 RECEPTOR.....	185
9.5	FUTURE WORK.....	187
10.	APPENDICES	189
	Appendix I.....	189
	Appendix II.....	190
	Appendix III.....	197
	Appendix IV.....	206
	Appendix V.....	206
	Appendix VI.....	207

Appendix VII.....	208
Appendix VIII.....	208
Appendix IX.....	209
Appendix X.....	209
Appendix XI.....	210
Appendix XII.....	214
Appendix XIII.....	214
Appendix XIV.....	214
Appendix XV.....	214
Appendix XVI.....	214
Appendix XVII.....	214
Appendix XVIII.....	215
Appendix XIX.....	216
Appendix XX.....	217
Appendix XXI.....	218
Appendix XXII.....	220
Appendix XXIII.....	221
Appendix XXIV.....	221
Appendix XXV.....	224
Appendix XXVI.....	227
Appendix XXVII.....	229
Appendix XXVIII.....	230
Appendix XXIX.....	230
Appendix XXX.....	230
Appendix XXXI.....	231

BIBLIOGRAPHY	232
---------------------------	------------

LIST OF FIGURES

Figure 1.1: Effects of Fab directed against plasma membrane antigens on the invasiveness of FS9 and chicken heart cells.	3
Figure 1.2: Nucleotide sequence of the 5.2kb genomic DNA fragment and the presumed amino acid sequence of p37, p29 and p69..	6
Figure 1.3: SDS-polyacrylamide gel and Western blot analysis of total protein preparations from <i>M. arginini</i> , <i>M. hyorhina</i> and <i>M. orale</i>	6
Figure 1.4: Architecture of ATP-binding cassette transport systems.....	7
Figure 1.5: Comparison of p29 and bacterial permease proteins.....	9
Figure 1.6: Sequence similarities between the N-terminal and C-terminal halves of p69..	10
Figure 1.7: Overall structure of <i>Mycoplasma hyorhina</i> p37.	12
Figure 1.8: Structural similarity of p37 to <i>E. coli</i> TbpA.....	13
Figure 1.9: Confocal micrographs demonstrating the binding and invasion of melanoma cells by <i>M. hyorhina</i> strain MCLD..	15
Figure 1.10: Influence of p37 on the migration and invasion of prostate cell lines PC-3 and DU145.	20
Figure 1.11: Morphological change of AGS cells transfected by the <i>p37</i> gene.	23
Figure 1.12: G-L Homotypic contact inhibition of locomotion in Neural Crest (NC) cells <i>in vitro</i> and <i>in vivo</i>	24
Figure 1.13: Heterotypic CIL in normal and cancer cells.....	25
Figure 1.14: (A) Schematic of Abercrombie's confronted explants invasion assay. (B) Homotypic contact inhibition in isolated cells.	27
Figure 1.15: Rho protein crosstalk during cell migration.	30
Figure 2.1: Standard curve for the Pierce® BSA Protein Assay Kit.	53
Figure 2.2: Kill curve of NIH3T3 cell confluence at various hygromycin concentrations at day 18.	55
Figure 2.3: Time line for time treatment of NIH3T3 cells.	57
Figure 2.4: Location of the images captured per wound.....	59
Figure 3.1: Sequence alignment of the <i>Mycoplasma hyorhina</i> p37 (<i>M. hyorhina</i> p37) gene to the p37 gene containing seven nucleotide mutations from TGA to TGG (p37 (7x TGG mut))..	63

Figure 3.2: Western blot of IPTG induced p37 protein expression.....	65
Figure 3.3: Purification of (His) ₆ -p37 protein using Ni-affinity chromatography.	66
Figure 3.4: Gene Ontology (GO) assignments of significantly up-regulated ($p \leq 0.001$, $f_c \geq 3$) genes identified in the microarray at the protein level.	69
Figure 3.5: Microarray validation by qPCR.	77
Figure 3.6: Correlation of qPCR and Microarray results.	79
Figure 3.7: Gene expression of NIH3T3 (mouse) fibroblasts treated with different concentrations of purified p37 (0.5, 1, 5 and 25 μ g/ml).....	81
Figure 3.8: Correlation between biological replicates for the inflammatory response and autoimmunity RT ² Profiler Array.	87
Figure 3.9: Overview of the cycle threshold for the inflammatory response and autoimmunity RT ² Profiler Array.	88
Figure 4.1: Interleukin 6 family cytokine signalling cascade.	94
Figure 4.2: Gene expression in NIH3T3 (mouse) fibroblasts treated with 0.1 μ g/ml Il6R antibody inhibitor for 25 hours.	97
Figure 4.3 Gene expression of NIH3T3 (mouse) fibroblasts treated with 0.1 μ g/ml Il6R <i>i</i> and 5 μ g/ml or 25 μ g/ml p37.	100
Figure 4.4: Correlation between Il6R <i>i</i> +25 μ g/ml p37 and Il6R <i>i</i> +5 μ g/ml p37 treatments..	101
Figure 5.1: <i>STAT3</i> expression in p37-treated NIH3T3 cells at different concentrations, at different times and the effect of Il6R inhibition.....	106
Figure 5.2: Chemical backbone of the STAT3 Inhibitor VI, S31-201 (NSC74859).....	107
Figure 5.3: Gene expression in STAT3 inhibited NIH3T3 (mouse) fibroblasts. NIH3T3 (mouse) fibroblasts were treated with 100 μ M S31-201 for 48hrs.	108
Figure 5.4: STAT3 inhibition effect on p37-induced gene expression in NIH3T3 cells.....	110
Figure 5.5: Correlation between biological replicates for the inflammatory response and autoimmunity RT ² Profiler Array.	112
Figure 5.6: Overview of the threshold cycle values for the RT ² Profiler Array of the inflammatory response and autoimmunity.	113
Figure 5.7: Volcano plot of RT ² Profiler Array of the Inflammatory Response and Autoimmunity.....	114
Figure 6.1: Lipopolysaccharide activation of Toll-like receptor 4 signalling pathway. domain-containing adaptor inducing IFN- β (TRIF).	120

Figure 6.2: <i>Il6</i> , <i>Saa3</i> and <i>TNFAip6</i> gene expression in Ultrapure LPS treated NIH3T3 (mouse) fibroblasts.....	123
Figure 6.3: <i>Saa3</i> gene expression of NIH3T3 cells treated with CP7 or VIPER.....	125
Figure 6.4: Dose-dependent effect of VIPER and CP7 on LPS-stimulated <i>Saa3</i> gene expression in NIH3T3 cells.....	126
Figure 6.5: Effect of VIPER and CP7 on expression of selected genes in NIH3T3 cells.	128
Figure 6.6: The effect of 1µM VIPER/CP7 effect on p37-induced gene expression in NIH3T3 cells.	130
Figure 6.7: NIH3T3 cells treated with 0.5uM VIPER or CP7.	131
Figure 6.8: The effect of 0.5µM VIPER/CP7 on p37-induced gene expression in NIH3T3 cells.	133
Figure 7.1: Thiamine pyrophosphate binding sites.	138
Figure 7.2: Sequence alignment of p37 and other mycoplasma p37-like proteins.	139
Figure 7.3: Schematic analysis of Thiamine pyrophosphate (TPP) binding in p37..	140
Figure 7.4: Secondary Structure of p37.....	140
Figure 7.5: Gradient PCR following the QuikChange™ Site-Directed Mutagenesis Protocol using varying concentrations of plasmid DNA..	142
Figure 7.6: Gradient PCR of 10ng pRA:p37 using primers Mutp37_F1/R1 and Mutp37_F2/R2.....	144
Figure 7.7: Western blot analysis showing the induction of the mutp37 protein.....	145
Figure 7.8: Coomassie blue staining and Western Blot of p37 and mutp37 purified from One Shot®BL21(DE3) cells.	146
Figure 7.9: Mutant p37 (mutp37) affect on gene expression of NIH3T3 cells.....	148
Figure 7.10: Schematic diagram of the p37 gene C-terminus truncations cloned into pRSET A.....	149
Figure 7.11: Western blot analysis of IPTG-induced truncated p37 expression.....	150
Figure 7.12: Coomassie Blue staining and Western Blot of truncated p37 as well as the wild type p37.	152
Figure 7.13: Effect of arginine soak purified truncated p37 on gene expression.	153
Figure 7.14: Schematic analysis of the p37 protein N and C-termini.....	154
Figure 7.15: Conservation analysis of the <i>Mycoplasma hyorhinis</i> p37 C-terminus aligned to several other mycoplasma proteins identified by BLASTp (Section 7.2.5).	157

Figure 7.16: Sequence alignment of LMP1 homologues and p37.....	159
Figure 8.1: Rho GTPase indirect activation of the NF-κB transcription factor.....	162
Figure 8.2: The pSTp37 construct.....	164
Figure 8.3: PCR confirmation of pST and pSTp37 transfected NIH3T3 clones.....	166
Figure 8.4: Morphology of pST and pSTp37 transfected NIH3T3 cells compared to wild type NIH3T3 cells.....	168
Figure 8.5: p37 enhances wound healing of NIH3T3 cells.....	169
Figure 8.6: Bridge formation of NIH3T3 cells.....	170
Figure 8.7: p37 increases the surface area (μm^2) covered by migrating cells.....	171
Figure 8.8: Levels of active RhoA in p37-treated and non-treated NIH3T3 (mouse) fibroblasts. NIH3T3 cells were either treated or not treated with 25 $\mu\text{g}/\text{ml}$ p37 and active and total RhoA was determined at 30min, 2, 4 and 24hrs.....	172
Figure 8.9: Gene expression in p37-transfected NIH3T3 cells.....	173
Figure 9.1: Inflammatory pathway initiated via activation of the Toll-like receptor 4.....	180
Figure 10.1: Affect of gudHCl purified native and truncated p37 protein on gene expression.....	220

LIST OF TABLES

Table 1.1: Proteins with structural similarity to p37.....	13
Table 1.2: The effect of neuraminidase treatment on the binding of p37 to PC-3 prostate carcinoma cells.	16
Table 2.1: Ligation DNA ratio.....	41
Table 2.2: Appropriate volumes of media required for tissue culture plates.....	54
Table 3.1: Number of genes identified in the microarray that were significantly up- and down-regulated ($p\text{-value}\leq 0.001$, $f_c \leq$ or ≥ 3).....	67
Table 3.2: Genes significantly up-regulated within the microarray chosen for further analysis.	73
Table 3.3: Gene fold changes at different times following p37 (5 μ g/ml) addition to NIH3T3 cells.	83
Table 3.4: Comparison of fold changes in gene expression obtained in the different experiments.....	85
Table 3.5: 84 genes of the mouse inflammatory response and autoimmunity pathways covered by the RT ² Profiler PCR array designed by SABiosciences.....	86
Table 3.6: Genes identified in the inflammatory response and autoimmunity RT ² Profiler Array.	89
Table 3.7: First 20 genes significantly down-regulated within the microarray.....	92
Table 5.1: Genes identified in the inflammatory response and autoimmunity RT ² Profiler Array.	116
Table 6.1: Peptide sequences of VIPER and CP7 synthesised by Lysakova-Devine et al. (2010) from the vaccinia virus A46 protein.....	124
Table 7.1: p37 primers designed based on the QuickChange™ Site-Directed Mutagenesis Protocol.	141
Table 7.2: Mutation of amino acids from native protein to mutated protein.....	141
Table 7.3: Primers based on Zheng et al. (2004) design.	143
Table 7.4: Two step PCR reaction introducing the mutation of amino acids from native protein to mutated protein.....	143
Table 7.5: Primer sequences for amplification of C-terminal truncated mutants by PCR.. ..	149

Table 7.6: Top ten BLASTp hits of the full-length <i>Mycoplasma hyorhinis</i> p37 protein sequence.....	156
Table 7.7: Top ten BLASTp results of the p37 C-terminal 20aa (excluding <i>Mycoplasma hyorhinis</i>).	158
Table 8.1: Rate of cell migration ($\mu\text{m}^2/\text{hr}$) increases due to p37.....	171

ABBREVIATIONS

GENERAL ABBREVIATIONS

%	percent
&	and
µg	microgram
µl	micro litre
µM	micromole
Å	Ångström
aa	amino acid
APP	acute phase proteins
ATP	adenosine triphosphate
ATPase	ATP hydrolase
bp	base pair
BSA	bovine serum albumin
cDNA	complementary deoxyribonucleic acid
CIL	contact inhibition of locomotion
Ct	cycle threshold
C-terminal	carboxyl-terminal
DNA	deoxyribonucleic acid
DNase	deoxyribonuclease
<i>E. coli</i>	<i>Escherichia coli</i>
EGFP	enhanced green fluorescent protein
Fab	fragmented antibody
g	grams
gDNA	genomic deoxyribonucleic acid
GDP	guanosine-5'-diphosphate
GTP	guanosine-5'-triphosphate
GTPases	guanine nucleotide guanosine-5'-triphosphate binding proteins
hr	hour
hrs	hours
kb	kilo base
kDa	kilodalton
L	litre
LB	Luria-bertani broth
M	molar
<i>M. hyorhinis</i>	<i>Mycoplasma hyorhinis</i>
mAb	monoclonal antibody
mg	milligram
min	minute

ml	millilitre
mM	millimolar
mmol	millimole
MQ	milli-Q
mRNA	messenger RNA
n/a	not applicable
nM	nanomolar
nmol	nanomol
No.	number
nt	nucleotide
N-terminal	amino-terminal
°C	degrees Celsius
OD	optical density
Oligo	oligonucleotide
ORF	open reading frame
PAGE	polyacrylamide gel by electrophoresis
PCR	polymerase chain reaction
PFA	paraformaldehyde
pM	picomolar
Pmol	picomol
qPCR	quantitative PCR
RNA	ribonucleic acid
RNase	ribonuclease
rpm	revolutions per minute
RT-PCR	reverse transcriptase polymerase chain reaction
SDS	sodium dodecyl sulphate
sec	seconds
UV	ultraviolet
V	volts
Vol	volume
WT	wild type

ABBREVIATIONS OF DIFFERENT CELL LINES

16HBE	human bronchial epithelial cells
A2780	ovarian carcinoma cells
AGS	stomach adenocarcinoma cells
BPH-1	benign human prostate cells
C3H/HeJ	common research mouse
CHF	chicken heart fibroblasts
CMT-93	mouse colonic epithelial cells
Colon-26	mouse colon carcinoma cell line 26
COS-7	ape kidney fibroblasts
D2F2	mouse mammary tumour cells
DU145	human prostate cells
EHS	Engelbreth-Holm-Swarm mouse sarcoma cells
FS9	mouse sarcoma cells
HEK-293	human embryonic kidney cells
L929	mouse fibrosarcoma cells
LB33mel	melanoma cell lines derived from patient LB33
NIH3T3	embryonic mouse fibroblasts
PBMC	human peripheral blood mononuclear cells
PC-3	human prostate cells (highly metastatic)
RAW 264.7	macrophage cells
RPMI 4788	human colon cancer cells
SH-SY5Y	neuroblastoma cells
U251-MG	human neuronal glioblastoma cells

Abbreviations for the main gene names used in this thesis are presented in Table 3.2, Table 3.6, Table 3.7 and Table 5.1.

ABSTRACT

The p37 protein is a lipoprotein associated with the plasma membrane of *Mycoplasma hyorhinis*. Cell lines treated with the purified p37 protein exhibit reduced heterotypic contact inhibition of locomotion in the Abercrombie confronted explant invasion assay. In addition p37-treated and *p37*-transformed cells show increased migration through transwell chambers and increased invasivity through a Matrigel matrix. However, the molecular mechanisms underlying these responses are not known.

This thesis identifies and characterizes the changes in gene expression of the NIH3T3 (mouse) fibroblast cell line in response to added p37 protein. A microarray analysis of p37-treated and untreated NIH3T3 cells identified many genes that were up or down-regulated. The most strongly up-regulated genes encoded cytokines and acute phase proteins which play a major role in the inflammatory response. Quantitative PCR was used to determine the temporal expression pattern of the p37-induced gene expression over 24hr. The cytokine interleukin 6 (Il6) was identified as a primary response gene. Possible explanations for this response are discussed. The Il6 protein, via the Il6 receptor, activates STAT3 transcription of secondary response genes. Unexpectedly, inhibition of the Il6 receptor and of STAT3 activation increased the potency of p37-induced gene expression. Inhibition of the Toll-like receptor 4 inhibited p37-induced gene expression in NIH3T3 cells.

NIH3T3 cells were transfected with the *p37* gene. The transfected cells lifted readily from the tissue culture plate and were smaller than the wild type NIH3T3 cells. Expression levels of eight of the twenty genes selected based on the microarray data were higher in *p37*-transfected cells than p37-treated NIH3T3 cells. p37-treated NIH3T3 cells exhibited increased migration rates in wound healing assays and rapid activation of RhoA.

Mutating the four amino acids required for thiamine pyrophosphate binding by p37 reduced the capacity of the protein to up-regulate gene expression. *Angptl4* was an exception, the mutated p37 protein further stimulated expression of the gene. The removal of the 20 C-terminal amino acids of p37 greatly reduced the proteins capacity for

stimulating gene expression. However, the stimulation of *Angptl4* was again the exception and induction was only affected when 40 C-terminal amino acids were removed from p37.

Finally, the amino acid sequence of p37 was compared with proteins from other mycoplasma species. Several homologues were observed.

STATEMENT OF AUTHORSHIP

Except where reference is made in the text of the thesis, this thesis contains no material published elsewhere or extracted in whole or in part from a thesis submitted for the award of any other degree or diploma.

No other person's work has been used without due acknowledgment in the main text of the thesis.

This thesis has not been submitted for the award of any degree or diploma in any other tertiary institution.

Amber Cathie Gomersall

3rd July 2013

ACKNOWLEDGEMENTS

First and foremost, I would like to express my sincere gratitude to Prof. Roger Parish – my supervisor and mentor - whose encouragement, advice and support over the past few years has been steadfast. Roger’s passion for knowledge, enthusiasm and dedication to research has been a great source of inspiration. His commitment to me and this project has left an indelible mark on my life.

I am greatly indebted to Dr. Kim Plummer and Dr. Tony Gendall for their encouragement, constructive advice and interest in my research and for taking the time to help me despite their busy schedules. I am also extremely grateful to Dr. Song Li for his guidance within the lab, continual support and conferring knowledge to help me achieve my goals.

I would like to thank all the past and present members of the RWP, KP and TG labs for their support, friendship and many morning coffees; Erica Wright, Barbara Dinsdale, Dr. Adrian Dinsdale, Reg Seyit, Ross Napoli, Brett Ford, Yue Xu, Amila Avdic, Sonia Fiorito, Jason Shiller, Dr. Menelaos Trapalis, Dr. Sylvana Iacuone, Jo Ernest, Alicia Greenhill as well as Hahn and Dr. Huy Phan. I also extend thanks to the entire Botany Department, particularly Ron Clarke, Serena Belvedere, June McIntosh and Edgar Pelcmanis-Sakers for your untiring support.

I am immensely grateful to my dearest friends Erica Wright, Barbara Dinsdale and Reg Seyit. Thank you for always being there; giving me strength during my kitchen floor resets, laughing at my not so funny jokes and encouraging me to persevere. Thank you for the shoulders to lean on and the endless supply of Turkish delight.

Finally, I wish to dedicate this thesis to my Grandmother and in loving memory of my Grandfather; Coral and Ronald Downie. Without their presence in my life I would not have been able to achieve this. From the very depth of my heart thank you to my Grandmother for her love and support over the past four years. Thank you also to my big brother, Stephen Gomersall, for his love and support.

1. INTRODUCTION

1.1 MYCOPLASMA AND CANCER

Mycoplasmas (Class *Mollicutes*) are descendants of gram positive bacteria distinguished by their minute size, lack of a cell wall, reduced genome and simplified metabolic pathways (Razin et al., 1998; Nir-Paz et al., 2002; Obara and Harasawa, 2008). They are amongst the smallest and simplest self-replicating organisms (Sirand-Pugnet et al., 2007). Species of mycoplasmas have been established on a molecular level by the comparison of 16S rRNA, heat shock Hsp70 family proteins, conserved gene sequences and genomic restriction patterns (Razin et al., 1998).

Mycoplasmas are bacterial pathogens of plants, reptiles, fish, arthropods and mammals and are widely known for being common contaminants of cell cultures (Nir-Paz et al., 2002; Obara and Harasawa, 2008). *Mycoplasma hyorhinis* has commonly been associated with polyserositis and arthritis of swine, however, it is also a natural component of the respiratory tract microflora of piglets. To be associated with disease in swine the mycoplasmas must be observed in serous membrane lesions causing secretion of fibrin and pus (Kim et al., 2010). A serous membrane is the tissue that lines the internal cavities of the body. A study of twenty pigs presenting with polyserositis but negative for *Streptococcus suis* and *Haemophilus parasuis* infections were tested specifically for *Mycoplasma hyorhinis* using polymerase chain reaction (PCR). Eighty percent of the pigs were *M. hyorhinis* positive (Kim et al., 2010).

Murine embryonic C3H cells infected with *M. penetrans* and *M. fermentans* exhibit multiple stages of malignant transformation, abnormal karyotypes and some genetic regulation associated with carcinogenesis. This suggests that mycoplasmas may play a role in cancer establishment and metastasis (Tsai et al., 1995; Ning et al., 2003b). Mycoplasma-infected cells have a higher ability to metastasize *in vivo*. Ushio et al. (1995) identified a 47kDa *M. arginini* protein (AG243-5) that promoted experimental metastasis in human RPMI 4788 and mouse Colon-26 colon cancer cell lines. PCR analysis identified a homologous gene in *M. hyorhinis*. More recently mycoplasma infections have been

observed in human cancer tissues. Huang et al. (2001) used the monoclonal antibody PD4, targeting *M. hyorhinis*, to identify the mycoplasmas presence in paraffin embedded carcinoma sections. Some 56% of gastric carcinomas, 55.1% of colon carcinomas and 45.5% of other carcinomas (oesophagus, lung, breast and glioma) examined were positive for *M. hyorhinis* infection. In a separate study using PCR, 63.9% of gastric cancer tissues were found positive for *M. hyorhinis* infection with 31.3% also positive for *M. fermentans* (Yang et al., 2010a). The same group also observed *M. hyorhinis* infections associated with ovarian cancer. *In situ* hybridization (22/109 specimens) and immunohistochemistry (47/109 specimens) were used (Yang et al., 2010b).

Yang et al. (2010a) also identified a relationship between *Mycoplasma hyorhinis* infection and lymph node metastasis ($p > 0.05$). Patients with *M. hyorhinis* infections showed a greater incidence of lymph node metastasis than non-infected patients. *M. hyorhinis* antibodies were detected in 52% of (N=105/209) prostate cancer patients and 36% of (N=144/209) benign prostate cancer patients in a case study of 209 patients (Urbanek et al., 2011).

1.2 THE DISCOVERY OF THE P37 PROTEIN

Steinemann et al. (1984a) first identified a 37kDa (p37) protein associated with the plasma membranes of FS9 mouse fibrosarcoma cells. Using Abercrombie's confronted explants technique (Section 1.7), Steinemann et al. (1984a) established that the FS9 cells were highly invasive when confronted with chicken heart fibroblasts (Figure 1.1a) compared to the control mouse fibrosarcoma L929 cell line. Polyclonal antibodies directed against the plasma membranes of the mouse cell lines were prepared and Western blotting identified a 37kDa protein (p37) in FS9 but not L929 plasma membrane preparations (Steinemann et al., 1984a). A monoclonal antibody (Fab, DD9) specific for p37 was isolated and when incubated with FS9 cells completely inhibited FS9 invasivity in the confronted explants assays (Figure 1.1b and c) (Steinemann et al., 1984a).

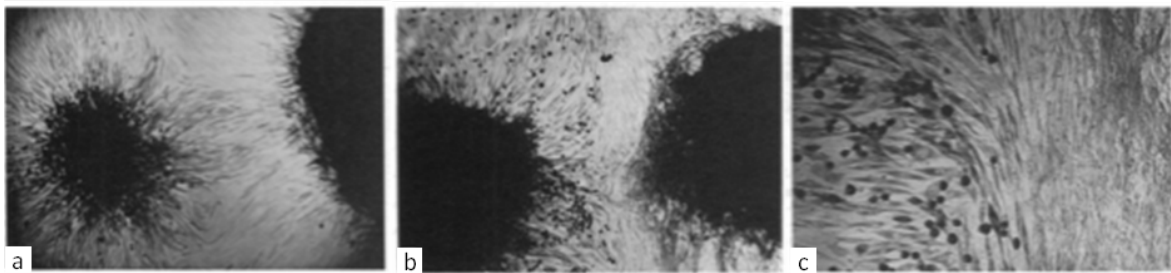


Figure 1.1: Effects of Fab directed against plasma membrane antigens on the invasiveness of FS9 and chicken heart cells. The FS9 explant is on the left and the chicken heart explant on the right-hand side of each image. **(a)** Control, no Fab added. FS9 cells moving in a direct line between the two explants can be seen to displace the chicken heart cells, which move out of the way. The FS9 cells actually reach the chicken heart explant. Outside the area directly between the explants invasivity did not occur. (x80) **(b)** Effect of Fab (1mg/ml) prepared from anti-FS9 plasma membrane antiserum that had been pre-absorbed with L929 cells. Invasivity of chicken heart cells by FS9 cells in the area between the explants is inhibited. (x70) **(c)** Same treatment as b, showing obstructed migration of FS9 cells (left) and chicken heart cells (right) in the area between the explants. (x150) (From Steinemann et al., 1984a).

Following p37 purification using the monoclonal antibody DD9 (Steinemann et al., 1984a), the N-terminus of p37 was sequenced (Dudler et al., 1988) (Figure 1.2: dashed line above sequence) and used to design an oligonucleotide. The oligonucleotide was used to screen a FS9 cDNA library; no positive matches could be isolated. However, a 5.2kb DNA fragment was isolated from the cytoplasmic fraction of the contaminated FS9 cells (Figure 1.2). Based on the sequence, the p37 protein was hypothesised to be a mycoplasma protein. Dudler et al. (1988) found purified p37 ran at a molecular weight of

approximately 42 kDa; Steinemann et al. (1984a, b) had underestimated the size using mass markers. Further analysis of the 380 amino acid sequence of p37 determined a molecular weight of 43.5 kDa, however the protein remained named p37 (Dudler et al., 1988).

Figure 1.2: Nucleotide sequence of the 5.2kb genomic DNA fragment and the presumed amino acid sequence of p37, p29 and p69. The proposed initiator codon TTG for p37 at position 758 is marked with a filled square above the sequence. The TGA codon at position 881, most likely read as tryptophan, is labelled with a filled triangle below the sequence. The hypothetical Shine-Dalgarno sequence from position 743 to 750 is boxed. The dashed line indicates the N-terminal protein sequence obtained by microsequencing techniques. The vertical arrow labels the site of processing of the p37 precursor protein. The first in-frame upstream stop-codons of Open Reading Frames 1, 2 and 3 are labelled with broad horizontal bars. A potential promoter region is marked by two bars beneath the -10 and -35 boxes. Position 625, assigned to be the potential initiator site of transcription, is labelled by an open circle. The horizontal arrows at bases 573-609 and 4522-4565 indicate the regions of dyad symmetry (From Dudler et al., 1988).

Three mycoplasma species were identified as contaminants of the FS9 cell line, namely *M. arginini*, *M. orale* and *M. hyorhinis*. Western blot analysis, using the Fab DD9 against total protein preparations, determined p37 to be associated with *M. hyorhinis* (Figure 1.3). Furthermore, when mycoplasma-free FS9 cells were incubated with either *M. arginini*, *M. orale* or *M. hyorhinis*, only the *M. hyorhinis* treated FS9 cells became p37 positive (Dudler et al., 1988).

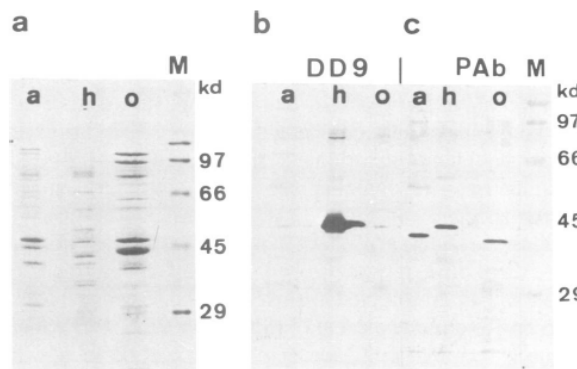


Figure 1.3: SDS-polyacrylamide gel and Western blot analysis of total protein preparations from *M. arginini*, *M. hyorhinis* and *M. orale*. (a) Coomassie blue stained proteins from *M. arginini* (a), *M. hyorhinis* (h) and *M. orale* (o), separated on a 12% SDS-polyacrylamide gel. (b & c) Identical Western blots of proteins of the three mycoplasma species. Probing the transferred proteins with the monoclonal antibody DD9, only p37 from *M. hyorhinis* was detected (panel b, lane h). An affinity-purified rabbit antiserum directed against a synthetic N-terminal peptide of p37 (Pab), recognized individual proteins from *M. arginini* and *M. orale* as well as p37 in *M. hyorhinis* (panel c). (From Dudler et al., 1988).

The p37 protein was also identified by Fareed et al. (1988) when analysing the immune response in a group of cancer patients immunized intralymphatically with tumour cell extracts. Those patients showing tumour regression had a measurable titre of antigens including one against a 38kDa protein. Ilantzis et al. (1993) confirmed this protein was p37, identical to that first described by Steinemann et al. (1984a; 1984b).

1.3 THE p37 OPERON HAS STRUCTURAL SIMILARITIES TO PERIPLASMIC BINDING-PROTEIN DEPENDENT TRANSPORT SYSTEMS

Sequence analysis indicated that the *p37* gene was part of an operon that codes for two additional proteins, p29 and p69 (Dudler et al., 1988). These proteins possess structural similarities to the periplasmic binding-protein dependent transport systems (permeases) found in gram negative bacteria (Dudler et al., 1988). In gram negative bacteria, periplasmic binding proteins (substrate binding protein; SBP) allow the delivery of ions and molecules to an ATP-binding cassette (ABC) transporter which also includes a transmembrane domain (TMD) permease and an ATPase, nucleotide binding domain (NBD) (Figure 1.4) (Geertsma et al., 2008; Soriano et al., 2008; Jurgenson et al., 2009). As *Mycoplasma hyorhinitis* has a single membrane and contains no periplasmic region, p37 would act as an extra-cytoplasmic binding lipoprotein dependent transport system (Gilson et al., 1988).

The p37 N-terminus contains the C-S-N amino acid sequence required for an N-terminal glyceride-cysteine lipid extension. Modification of the N-terminal cysteine (C) to a lipo-amino acid would allow p37 to anchor to the external leaflet of the *M. hyorhinitis* membrane (Figure 1.4c) (Dudler et al., 1988; Gilson et al., 1988; Tam and Saier, 1993).

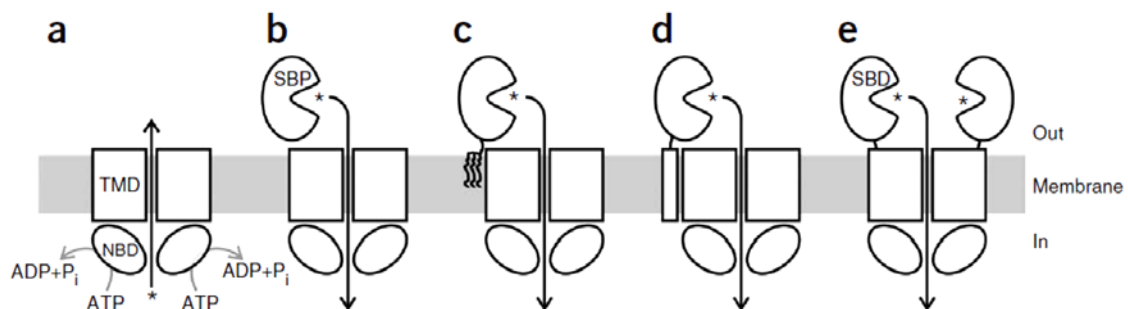


Figure 1.4: Architecture of ATP-binding cassette transport systems. TMD, NBD and SBP indicate the transmembrane domain, nucleotide-binding domain and substrate binding protein, respectively. **(a)** Efflux system; **(b)** uptake system with periplasmic SBP; **(c)** uptake system with lipid-anchored SBP; **(d)** uptake system with transmembrane peptide-anchored SBP; and **(e)** uptake system with covalently linked substrate-binding domains (SBDs) (From Geertsma et al., 2008).

The p29 protein sequence has sequence similarities with several bacterial permease ATPase proteins, namely *Salmonella typhimurium* hisP, *Escherichia coli* malk, *S. typhimurium* oppD and *E. coli* pstB (Figure 1.5) (Dudler et al., 1988). These proteins interact with both the periplasmic substrate binding proteins and the hydrophobic transmembrane proteins which comprise the other components of high-affinity transport systems (Hiles et al., 1987; Chan and Torriani, 1996; Nikaido et al., 1997; Bacac and Stamenkovic, 2008; Oldham and Chen, 2011). ATP binding by these proteins energises the permease protein complex. Hydrophilic similarities of the proteins hisP, malk, oppD and pstB to p29 suggest a similar function for p29 (Dudler et al., 1988).

P29	2		:: : : : : :::: ::::: :::::	
OppD	12	KKPLNKLEIK	NL--TFKNKN	DDYIILKNLN
Malk	1	QPANVLLLEV	DLRVTFTPDP	GDVTAVNDLN
HisP	1	-----MAS	VQLQNVTKAW	GEVVVSKDIN
PstB	1	----MMSENK	LHVIDLHKRY	GGHEVLKGV
		MSMVETAPSK	IQVRNLFYF	GKFHALKNIN
		:	: . .	: . .:::
				: : : : :
P29	49	-SSL--LK--	---TILKQT-	DVIEGTILF-
OppD	62	QSRLR-LM--	---GLLATN-	GRIGGSATF-
Malk	44	-TLLRMIA--	---GLETITS	GDLFI-GEK-
HisP	47	-TFLRCIN--	---FLEKPS	GAIIVNGQNI
PstB	51	-TLLRTFNKM	FELYPEQRAE	GEILLDGDNI
		: ↓ :	. :	: : .
				: : : : :
P29	84	--FLKEVSFL	NQTTTSIPFE	TVFTNIVRSL
OppD	102	--EQISMIFQ	DPMTSLNPYM	RVGEQLMEVL
Malk	76	--G-VGMVFQ	SYA--LYPHL	SVAEN-MSFG
HisP	91	LRTRLTMVFQ	HFN--LWSHM	TVLENVMEAP
PstB	89	LRAKVG MVFQ	KPT--PPF-M	SIYDNIAFGV
	 ↓ :	: : : .
				: : : : :
P29	132	EIT-SVLKEL	NILDKIYHRV	DSLGGGQQQR
OppD	148	LDA-VKMPEA	RKRKMYPH-	-EFGGMRQR
Malk	117	V-A--EVLQL	AHLLDRKPK-	-ALSGGQRQR
HisP	137	L-A--KVGID	ERAQGYKPV-	-HLSGGGQQQR
PstB	134	LTKAALWNET	KDKLHQSGY-	-SLSGGQQQR
	 : : : .
				: : : : :
P29	181	NFLDPN--IS	-KNI-IELII	KMAKKFNSIL
OppD	195	TALDVT--VQ	-AQI-MTLLN	ELKREFNTAI
Malk	162	SNLDAALRVQ	-MRIEISRLH	KRLGR--TMI
HisP	182	SALDPELVGE	VLRI-MQQLA	EE-GK--TMV
PstB	182	SALDPI-STG	RIEE-LITEL	KQ-DY--TMV
		: : ↓ : .	. . :	: :
				: : : : :
P29	227	KNQEYHFYKS	NKEI-N-SNI	LDQVFKND
OppD	241	YAGRTMEYGK	ARDV-F-YQP	VHPYSIGL
Malk	208	DAGRVAQVGK	PLAVPLSGRP	FCRRIYRF
HisP	227	HQGKIEEEGD	PEQV-F-GNP	QSPRLQQF
PstB	226	YLGELIEFSN	TDDL-F-TKP	AKKQTEDY
	

Figure 1.5: Comparison of p29 and bacterial permease proteins. Protein sequences are aligned to demonstrate similarities between p29 and the peripheral membrane components of the bacterial transport systems for oligopeptides (oppD), maltose (malk), histidine (hisP) and phosphate (pstB). Sequences are from the sources indicated in the text. Gaps were introduced to optimize similarities. Above the alignment the similarity between p29 and oppD is shown. Identical residues and conservative substitutions are indicated by bars and double dots respectively. Similarities between all five sequences are visualized below the sequence alignment. Identical and conserved residues, appearing in all five sequences, are indicated by vertical arrow heads and double dots respectively. Positions with identical residues and conserved substitutions present in four of the five sequences are labelled by a single dot. Amino acid substitution scoring 0 and higher in the log odd matrix of 250 PAMs (Dayhoff et al., 1978) were assigned to be conserved (From Dudler et al., 1988).

The p69 protein has a hydrophilic region in the N-terminal (residues 13-280) which is duplicated in the C-terminal (residues 281-547) sequence (Figure 1.6a) (Dudler et al., 1988). Sequence similarity between the N- and C-terminal halves is a common feature of integral membrane components of bacterial transport systems. Similarities were identified in the alignment of p69 and the conserved sequences of eight hydrophobic transport proteins (Figure 1.6b) (Dudler et al., 1988).

a

13	KNNK	KLK	LKW	KIL	LL	LS	LL	LF	IF	SF	YS	LF	QP	IN	YG	ST	RI	FT	KN	LK	EL	FT	
	
281	QNTS	FL	WI	KL	NFR	RIF	KW	FF	VL	FF	VG	LN	IY	SI	IK	IS	FT	LP	NY	IK	NF	WN	
63	-FS	NYS	KK	YP	SW	TL	WQ	LS	WY	YM	FL	TIR	YCA	LG	TL	GF	FIFA	FF	TS	FS	VSS	NF	
		
331	HFFS	FQ	NE	VF	SH	NK	EN	NP	FY	WI	LI	LI	YQ	CI	VS	IT	II	AI	IS	LV	FS	IL	GN
112	QKYK	FIR	YII	NIII	IF	FK	AF	PIS	LF	VY	FF	FS	---	IG	FD	KEL	AAT	LIL	FW	FS			
	
381	LNNV	TQ	WI	PL	RFL	N	TL	FR	II	PT	II	FI	YL	FS	IF	WI	GN	IF	LV	AV	IT	AL	
159	WL	WM	HK	YFL	FL	NN	LD	KT	NY	KIM	H	M	KT	NEN	FAS	FR	KT	LFP	YIV	N	K	Y	
		
431	ST	SL	VK	QL	NE	SIN	SIN	WE	IY	KT	LE	IQ	GK	SK	FQ	RI	IK	FV	FP	SI	KK	DY	
209	VYS	LES	NIR	W	TTI	INA	AG	VI	GIG	---	LL	LN	DAR	DF	SL	GW	SV	VG	IP	LL	VIL		
	
481	LF	YF	EN	QV	QT	LIL	LG	SV	GG	LL	GS	KI	SI	VG	QAG	ER	TEN	IL	EL	NT	YS	WI	
256	VT	II	FF	FL	T	LFL	NK	VI															
																	
531	VF	IA	II	QL	LQ	FY	FN	LIV															

b

MalF	406	<u>EAS</u> AMDGAGP	FQNFFKITLP
MalG	190	<u>AAA</u> ALDGATP	WQAFRLVLLP
HisQ	125	<u>EA</u> ATAFGFTH	GQTFRRIMRP
HisM	134	<u>EA</u> ARAYGFSS	FKMYRCIILP
PstC	202	<u>ES</u> AYGIGCTT	WEVIWRIVLP
PstA	185	<u>EA</u> AYALGTPK	WKMISAITLK
OppC	197	<u>EA</u> AQVGGVST	ASIVIRHIVP
OppB	207	RTA <u>RA</u> KGLPM	RRIIFRHALK
P69	179	KIMH <u>N</u> KTNEN	FASFRKTLP
P69	451	KTLE <u>I</u> QGKSK	FQRIIKFVFP

Figure 1.6: Sequence similarities between the N-terminal and C-terminal halves of p69. (a) Sequence similarity between p69 (13-272) and p69 (281-547). Identical amino acids are indicated by vertical bars; dots indicate conserved residues. For the assignment of conserved substitutions see Figure 3 Dudler et al., (1988). (b) Alignment of the conserved hydrophilic sequences of the integral membrane components of bacterial transport systems and the relatively hydrophilic stretches of p69. Conserved residues identified by Dassa and Hofnung (1985) are underlined (From Dudler et al., 1988).

1.4 P37 PROTEIN STRUCTURE

Sippel et al. (2008) determined the crystal structure of p37 refined to 1.9 Å resolutions. The p37 protein is an α/β class protein made up of two domains (Figure 1.7a). Domain I consists of six stranded β -sheets flanked by eight helices (39-140, 342-403 residues). Domain II consists of five β -strands and five helices (141-342 residues) (Figure 1.7b). The domains are separated by a cleft which modelling indicated bound thiamine pyrophosphate (TPP) (Figure 1.7c). Thiamine pyrophosphate binds to both domains with a methyl amino pyrimidine ring interacting with Asn200, Val201, Glu308, Trp314 and Leu379. The thiazole ring interacts with Leu379, Tyr343, Asp344, and Tyr215 and the pyrophosphate interacts with Lys258, Lys129, Tyr215, Ser255, Phe256 and Ser257. The p37 protein was also found to bind two calcium molecules at the distal ends of the domains. Sippel et al. (2009) designated p37 a thiamine pyrophosphate (TPP)-binding protein (CypI).

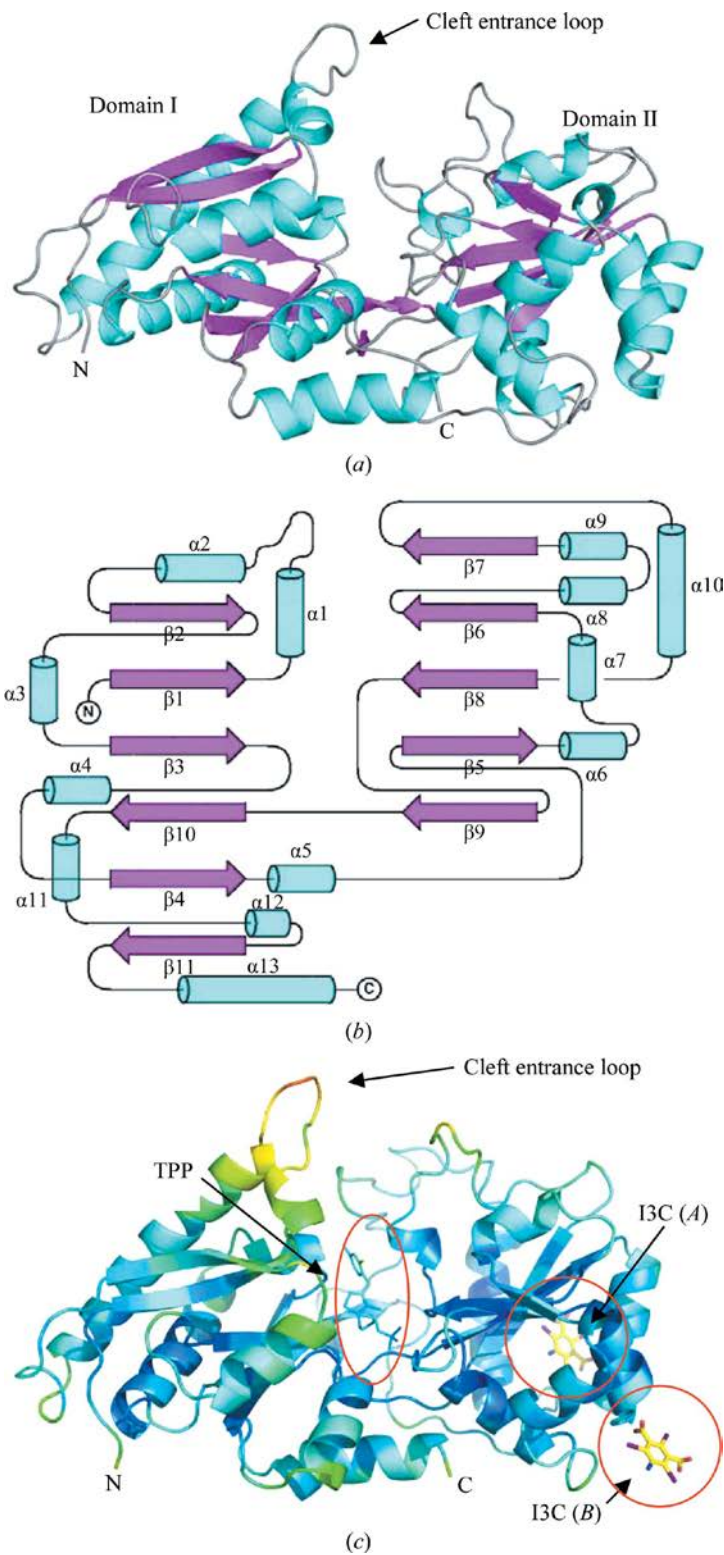


Figure 1.7: Overall structure of *Mycoplasma hyorhinis* p37. (a) C α ribbon trace showing the secondary-structural elements (α -helices, cyan; β -strands, magenta). **(b)** Structural topology of p37, defining domain I and II, coloured as above. **(c)** C α ribbon trace coloured from low to high (blue to red) temperature factor. Also shown (open red circles) are the binding sites for TPP and I3C (sites A and B). **(a)** and **(c)** were generated using PyMOL (Schrodinger, 2010); **(b)** was generated using TopDraw (Bond, 2003) (From Sippel et al., 2008).

Based on the crystal structure, the DALI server identified several binding proteins with structural homologies to that of the p37 structure (Table 1.1) (Sippel et al., 2009). The p37 protein had strong similarities to the N-lobe of human transferrin, however, not to the whole transferrin protein. The periplasmic thiamine binding protein, TbpA (2QRY), of *Escherichia coli* has significant structural similarities with p37 (Z-score>2) (Table 1.1) (Sippel et al., 2009). TbpA is known to bind three different forms of thiamine, including pyrophosphate, possibly delivering them to the ABC transporters to which TbpA is bound (Soriano et al., 2008; Jurgenson et al., 2009). Crystallographic Object-Oriented Toolkit (COOT) computer software was used to superimpose the TbpA protein 2QRY(C) and p37 (Figure 1.8) (Sippel et al., 2009). The structural topology showed that p37 is similar to Type II periplasmic thiamine binding proteins, however, unlike TbpA, p37 does not contain the conserved sequence allowing for the loading of thiamine as a cofactor (Sippel et al., 2009). This suggests that the p37 protein binds TPP but does not transport TPP like TbpA (Sippel et al., 2009).

Table 1.1: Proteins with structural similarity to p37 (Sippel et al., 2009)

PDB ID (chain ID)	Description	Z score	Root mean square deviation (Å) (no. of Cα)	No. of residues	% Identity	Reference
1JQF(A)	Human transferrin N-lobe mutant H249Q	16.1	4.1 (250)	329	13	(Baker et al., 2001)
3B7D(H)	GLUR2 ligand binding core (HS1S2J) in complex with CNQX	8.9	4.3 (210)	258	10	(Maniloff et al., 1992)
2QRY(C)	Periplasmic thiamine binding protein (TbpA)	6.9	4.3 (190)	318	10	(Soriano et al., 2008)
1Z7N(G)	ATP phosphoribosyl transferase (HisZG ATP-PRTase) from <i>Lactococcus lactis</i> with bound PRPP _a substrate	7.7	3.6 (164)	203	9	(Champagne et al., 2005)

^aPRPP, 5-phosphoribosyl-1-pyrophosphate.

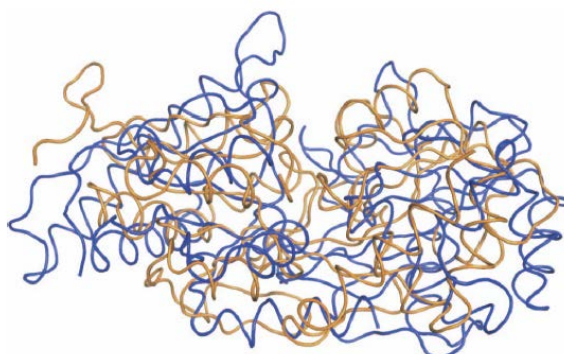


Figure 1.8: Structural similarity of p37 to *E. coli* TbpA. Coil C-alpha tracing of p37 (blue), with TbpA (PDB code 2QRY chain C; colour, orange). The figure was generated using PyMOL (Bond, 2003). (From Sippel et al., 2009).

1.5 P37 BINDING AND LOCALISATION ON MAMMALIAN CELLS

As mycoplasma lack an external cell wall, they rely on surface proteins that act as adhesives for direct interaction with host cells. Mycoplasmas, being wall-less bacteria, lack lipopolysaccharides (LPS), lipoteichoic acid and peptidoglycan (Henderson et al., 1996). However the surface lipoproteins of mycoplasma species are variable and differ from normal bacterial lipoproteins. Mycoplasma lipoproteins lack the N-acyl long chain fatty acid (lipid) extension and contain only two ester links (Kostyal et al., 1995; Razin et al., 1998; Sacht et al., 1998; Zuo et al., 2009). These lipoproteins have antigenic variation, increasing the ability of the bacteria to infect and evade the immune system. They are also believed to play a role in the adhesion of mycoplasmas to specific receptors of targeted tissues (Razin et al., 1998). The variable lipoprotein (*Vlp*) gene set encoded by *Mycoplasma hyorhinis* allows it to be a successful pathogen of swine (Razin et al., 1998).

Kornspan et al. (2010) hypothesised that the full native tertiary structure of mycoplasma surface proteins is required for the invasion of mammalian cells. *Mycoplasma hyorhinis* (strain MCLD) is able to bind and invade the melanoma cell line LB33mel (melanoma cell line derived from patient LB33) (Figure 1.9A) (Kornspan et al., 2010). Four percent paraformaldehyde (PFA) was used to alter the surface proteins of either the melanoma cells or the mycoplasma (Helander, 1994). Binding of *M. hyorhinis* (MCLD) to non-treated melanoma (LB33mel) cells was reduced by 80% if the mycoplasma had been pre-treated with 4% PFA. Pre-treatment of the LB33mel cells with 4% PFA decreased the ability of non-treated *M. hyorhinis* to bind by 20% (Figure 1.9B). Therefore it was proposed that the full native tertiary structure of mycoplasma surface proteins is required for binding and invasion of LB33mel cells (Kornspan et al., 2010).

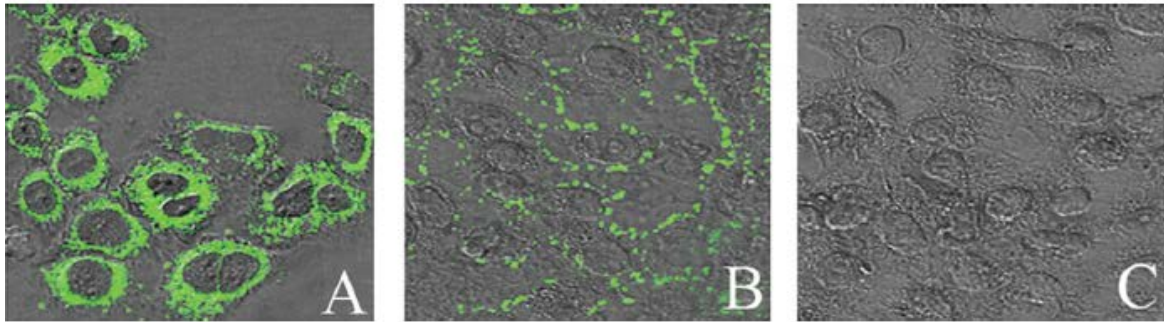


Figure 1.9: Confocal micrographs demonstrating the binding and invasion of melanoma cells by *M. hyorhinis* strain MCLD. Following infection of untreated (A) or PFA (4%)-pre-treated (B) melanoma cells with *M. hyorhinis* MCLD for 3hr, the infected melanoma cells were washed, fixed, permeabilised, and immunostained with anti-*M. hyorhinis* specific antibodies. *M. hyorhinis* (green fluorescence) bound and invaded untreated melanoma cells, however, only bound PFA (4%)-pre-treated melanoma cells. (C) Control uninfected melanoma cells (From Kornspan et al., 2010).

Plasminogen is a plasma glycoprotein that produces plasmin, a serine protease, following proteolysis. Plasmin cleaves peptide bonds activating other proteins such as matrix metalloproteinase 3 (Mmp3) (Ramos-DeSimone et al., 1999). Plasminogen promotes the binding and invasion of *M. fermentans* to HeLa cells and more so in its active form, plasmin (Yavlovich et al., 2001; Yavlovich et al., 2004). The pre-treatment of *M. hyorhinis* with plasminogen had no effect on its ability to bind or invade LB33mel cells. However, pre-treatment of *M. hyorhinis* with proteinase K, a broad spectrum serine protease, enhanced binding and invasion of the LB33mel cells (Kornspan et al., 2010). Protease treatment of *M. hyorhinis* may activate or enhance the exposure of surface receptors responsible for cell adhesion and allowing for increased binding and invasion of the melanoma cells (Kornspan et al., 2010).

A BLAST search identified a partial pair wise sequence alignment between p37 and the Avian influenza virus distal head domain of haemagglutinin A (residues 186-343 & 153-254) (Ketcham et al., 2005). There is a 41% similarity between the DNA sequences. Ketcham et al. (2005) used the software programs O7 (34), CNS (35) and BOBSCRIPT (36) to predict a model of the p37 protein. The modelling of a highly conserved hydrophobic pocket at the C-terminal domain of p37 was similar to that of the distal head domain of haemagglutinin A. However, the p37 protein possesses a tyrosine amino acid at position 202 that is not present in human or avian haemagglutinin Ketcham et al. (2005) suggested that the location of the tyrosine at the opening of the hydrophobic pocket may act as a

selective agent for receptor recognition (Ketcham et al., 2005). This model greatly differs from that determined by Sippel et al. (2008) (Section 1.4).

Haemagglutinin A is known to bind sialic acid surface receptors of mammalian cell membranes (Ketcham et al., 2005). The binding of the p37 protein to sialic acid receptors was tested by treating the metastatic human prostate cell line PC-3 with a broad spectrum neuraminidase prior to addition of p37. Neuraminidase removes the sialic acid from surface receptors, preventing recognition by haemagglutinin A. Neuraminidase treatment prevented the binding of p37 to the surface of the PC-3 prostate cells (Table 1.2) (Ketcham et al., 2005). The addition of free sialic acid and fetuin, a sialic acid containing molecule, to p37 enhanced binding of p37 to the neuraminidase treated PC-3 prostate cells (Table 1.2) (Ketcham et al., 2005). Hence, p37 may bind sialic acid surface receptors, allowing cell surface docking and subsequently via a conformational change of the p37 hydrophobic pocket, bind to a second cell surface receptor (Ketcham et al., 2005). However, Kornspan et al. (2010) found that pre-treatment of the LB33mel (melanoma) cells with neuraminidase (subtype not classified) did not affect *M. hyorhinis* binding, suggesting that *M. hyorhinis* binding to mammalian cells is independent of p37 and sialic acid surface receptors.

Table 1.2: The effect of neuraminidase treatment on the binding of p37 to PC-3 prostate carcinoma cells.
(From Ketcham et al., 2005).

Addition	% Binding
No addition	100 ± 4
α2,3 Neuraminidase	49 ± 11
α2-3,6,8 Neuraminidase	49 ± 15
Sialic acid	127 ± 8
Fetuin	194 ± 15

NOTE: PC-3 cells were treated with neuraminidase from either *A. ureafaciens* (removes terminal α2-3,6,8-linked sialic acid residues) or *M. decora* (removes only terminal α2,3-linked sialic acid residues), for 4hrs followed by 50µg/ml p37. For the conditions with sialic acid (2.5mmol/L) or fetuin (100µg/ml), the compounds were mixed with p37 before addition to the cells. The two-antibody sandwich ELISA assay was employed for the detection of bound p37. Values are averages of triplicate results and SDs are reported.

Yang et al. (2010a) found *M. hyorhina* was mainly localised in the cytoplasm of gastric cancer tissues. Using indirect immunofluorescence, Steinemann et al. (1984b) established that the *M. hyorhina* p37 protein was located in the cytoplasm as well as on the surface of FS9 (mouse sarcoma) cells. Using immunofluorescent staining, Ketcham et al. (2005) found that p37 bound to the plasma membrane of the prostate cell lines (PC-3). Ning et al. (2003b) used a monoclonal antibody (mAb) PD4 which targets 16 amino acids at the N-terminus of the p37 protein to demonstrate that purified p37 bound to the surface of the human stomach adenocarcinoma cell line (AGS).

COS-7 (ape kidney fibroblasts) cells were transfected with a p37 construct that included an N-terminal sequence encoding a plasma membrane localisation signal peptide. The construct was fused with the gene encoding the enhanced green fluorescent protein (EGFP) at either the 5' (N-terminal) or the 3' (C-terminal) end of the gene (EGFP-p37, p37-EGFP respectively) (Liu et al., 2006). The p37-EGFP localised to the Golgi of COS-7 cells whereas the EGFP-p37 was secreted to the supernatant (Liu et al., 2006). The retention of the p37-EGFP in the Golgi suggests that the EGFP prevented further processing of p37 and that the C-terminus of p37 possesses functional importance.

1.6 P37 AND CANCER

Schmidhauser et al. (1990) reported that L929 mouse fibroblasts, FS9 mouse sarcoma cells, NIH3T3 embryonic mouse fibroblasts and Rat-1 cells infected with *Mycoplasma hyorhinis* became invasive *in vitro* (i.e. exhibited reduced contact inhibition of locomotion in the Abercrombie confronted explant assay (Section 1.7)). DD9, a fragment (Fab) of the monoclonal antibody (mAb) directed against p37, inhibited the invasive behaviour of *M. hyorhinis* infected FS9 (mouse) sarcoma cells (Steinemann et al., 1984a; Schmidhauser et al., 1990). The decrease in the invasion index supported the hypothesis that the p37 protein was responsible for the invasive behaviour (i.e. loss of heterotypic contact inhibition of locomotion) of the *M. hyorhinis* infected cells.

Namiki et al. (2009) investigated the *in vitro* and *in vivo* effects of chronic mycoplasma infection on a benign human prostate cell line, BPH-1. Prolonged infection by *M. hyorhinis* or *M. genitalium* caused karyotypic entropy. The most noticeable change was the accumulation of multiple copies of apparently normal chromosomes (Namiki et al., 2009). p37-treatment of highly metastatic (PC-3) and a less metastatic (DU143) prostate cancer cell lines resulted in macronucleoli, double nucleoli and increased nuclear area. Goodison et al. (2007) proposed that the increased protein synthesis was the likely cause of macronucleoli and double nucleoli, a key indicator of cancer progression. Increased cell proliferation, vacuolation and protein synthesis was also observed in both cell lines following p37-treatment (Goodison et al., 2007). Anchorage independent growth was observed in BPH-1 cells that had been infected with both *M. hyorhinis* and *M. genitalium* (Namiki et al., 2009; Urbanek et al., 2011). Anchorage independent growth is the ability of cells to grow without a solid substratum, observed in aggressive tumours with metastatic potentials (Cifone and Fidler, 1980; Mori et al., 2009).

Using a transwell migration assay and a Matrigel assay, BPH-1 cells infected with *M. hyorhinis* or *M. genitalium* for 19 weeks exhibited increased migration and invasion. No changes were detected at 7 weeks (Namiki et al., 2009). The transwell migration assay involves placing cells on the upper layer of a cell permeable membrane. The number of cells migrating through the membrane is then determined. A Matrigel assay involves

addition of Matrigel onto the permeable membrane of a transwell migration assay. The Matrigel assay determines the ability of cells to degrade and migrate through the Matrigel, which is characterized as a basement membrane mixture secreted by Engelbreth-Holm-Swarm (EHS) mouse sarcoma cells. Matrigel contains extracellular matrix proteins, growth factors and collagenases (BD Biosciences). It is well established that the invasion of tumour cells through the Matrigel involves extracellular matrix receptors and matrix degrading enzymes, all of which play a role in tumour progression.

The prostate cancer cell lines PC-3 and DU145 were both found invasive in a Matrigel assay following treatment with p37 (Ketcham et al., 2005). The level of invasivity was p37 dose dependent. 1F6, a monoclonal antibody (mAb) directed against p37, inhibited the invasiveness of the p37-treated prostate cancer cell lines in the Matrigel assay (Ketcham et al., 2005). Goodison et al. (2007) also found that p37 increased the invasivity of PC-3 and DU145 cell lines in the Matrigel assay. However, a transwell assay revealed that the prostate cancer cell lines exhibited a greater migration rate following p37-treatment rather than an increased capacity to degrade the Matrigel (Figure 1.10) (Goodison et al., 2007).

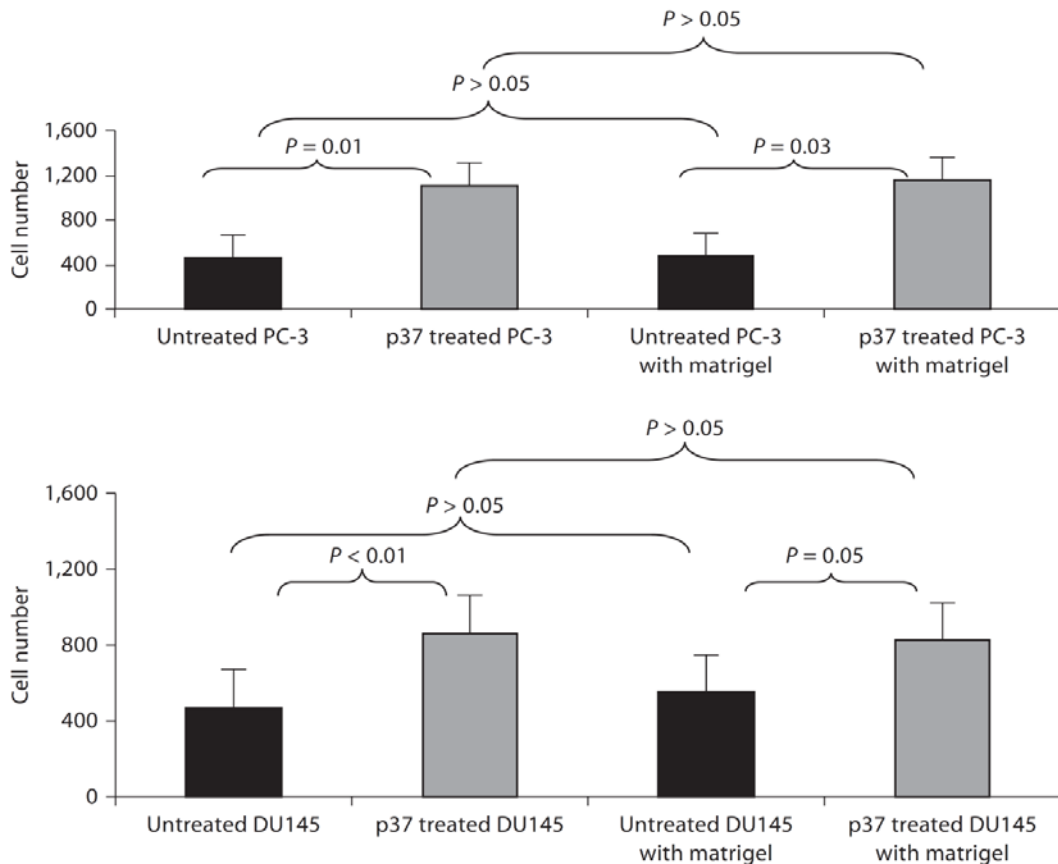


Figure 1.10: Influence of p37 on the migration and invasion of prostate cell lines PC-3 and DU145. Cells in serum-free medium supplemented with or without p37 (25µg/ml) were seeded onto 8µm pore membranes, with or without a pre-coating of Matrigel, in a modified Boyden chamber assay. The rate of cell migration was assessed by induction of movement toward serum through an uncoated membrane. Cell invasiveness was assessed by the movement toward serum through Matrigel-coated membranes. Cells that had migrated through the membranes after 24hrs were detached by trypsin and counted. Each value represents the mean of the triplicate results, and the error bars represent the standard error of the mean (From Goodison et al., 2007).

Microarray analysis of human prostate cancer cell lines PC-3 (highly metastatic) and DU145 (metastatic) treated with purified p37 established that expression of genes involved in proliferation and metabolic pathways were altered (Goodison et al., 2007). Genes involved in controlling the cell cycle were found to be down-regulated (namely cyclin D1 cyclin-dependent kinase inhibitors *CDKN1B*, *CDC25B* and *CDC25C*) in both p37 treated prostate cell lines. Down-regulation of these genes are common in cancer progression, facilitating increased proliferation. An increase was observed in the transcript expression levels of several Ras superfamily proteins (not specified), the cytokines interleukin (Il) 8, Il6 and tumour necrosis factors (TNF) (not specified) and some chemokines (not specified). These increases were detected in the highly metastatic human prostate cancer cell line PC-3 but not in DU145 (Goodison et al., 2007).

The Ras superfamily consists of monomeric GTP binding proteins that function as molecular switches activating cell proliferation, migration, gene expression and many other common cellular functions (Bishop and Hall, 2000). Ras proteins are often activated by the binding of an extracellular ligand to a tyrosine kinase receptor such as the epidermal growth factor receptor (EGFR). Active Ras binds and activates the Raf serine/threonine kinase which phosphorylates protein kinases 1/2 (MEK1/2). MEK1/2 phosphorylates the extracellular-signal-regulated kinases 1/2 (ERK1/2) which in turn activates transcription of proteins involved in many cellular functions including cell division (Wennerberg et al., 2005; Gong et al., 2008). The phosphorylation cascade is designated the Ras/Raf/MEK/ERK signalling pathway.

Human gastric carcinoma (AGS) cells either p37-treated or p37-transformed, show significantly increased migration in the transwell migration assay (which includes a layer of Matrigel) when compared with non-treated AGS controls (Gong et al., 2008). The level of the 72kDa matrix metalloproteinase 2 (Mmp2) protein increased significantly in the medium of p37-transfected and p37-treated AGS (human) gastric carcinoma cells (Gong et al., 2008). Tumour establishment, progression and angiogenesis relies on the secretion of matrix-degrading enzymes, such as matrix metalloproteinases (Mmps) (Klein et al., 2004; Mantovani, 2009). Mmp2 and Mmp9 are well known matrix metalloproteinases enhancing angiogenesis and the invasivity of tumour cells (Klein et al., 2004; Bekes et al., 2011). *Mmp2* transcription is activated through the Ras/Raf/MEK/ERK signalling pathway (Kolch, 2000). Phosphorylation of EGFR and ERK1/2 increased in p37-treated AGS cells in a dose-dependent manner (Gong et al., 2008). Inhibitors of MEK1/2 (U0126) and EGFR (AG1478) had little or no effect on the p37-induction of Mmp2 in AGS cells. However, the Mmp inhibitor (GM6001), which completely inhibits Mmp2 activity, also inhibited phosphorylation of MEK1/2 and EGFR. Hence, phosphorylation is occurring downstream of Mmp2 activation (Gong et al., 2008). Although the inhibitors of MEK1/2 and EGFR had little to no effect on the expression of *Mmp2*, they significantly suppressed p37-induced invasiveness of AGS cells through Matrigel (Gong et al., 2008). Hence, p37-induced invasion of AGS cells may be due to stimulation of EGFR phosphorylation (Gong et al., 2008).

Cytokines and small cytokines, known as chemokines, are important regulators of biological pathways that control the proliferation and migration of various cells, regulation of the innate and adaptive immune response, angiogenesis and tissue repair programs (Germano et al., 2011). The over-expression of cytokines and chemokines can increase a tumour cell's ability to metastasize by affecting cell dissemination and implantation at secondary sites (Colotta et al., 2009; Mantovani, 2009). Tumour necrosis factor α (TNF α) is a cytokine involved in regulation of the inflammatory response, however, overexpression of TNF α is also known to increase the metastatic potential of cell lines (Szlosarek et al., 2006; Cui et al., 2008). Ning et al. (2003a) investigated the expression and secretion of TNF α in p37-treated human peripheral blood mononuclear cells (PBMC). Increased levels of *TNF α* transcript were detected by reverse transcription - polymerase chain reaction (RT-PCR) and the TNF α protein was detected in the medium of p37-treated PBMC. Incubation of p37 with PD4, a monoclonal antibody targeting p37, prior to treatment of PBMC prevented the increased production of TNF α (Ning et al., 2003a). Therefore, p37-induced *TNF α* transcription and TNF α secretion may be responsible for the metastatic behaviour of p37-treated cell lines (Ning et al., 2003a).

Cytokines such as TNF α and Interleukin 1 (Il1) are known to regulate the transcription and activation of Intracellular Adhesion Molecule 1 (ICAM-1) and Integrin β 1 (Hashimoto et al., 1994; Shain et al., 2009). ICAM-1 is involved in vascular endothelium cell adhesion and Integrin- β 1 mediates cell adhesion and regulates cell proliferation and survival. Liu et al. (2006) found that AGS cells stably transfected with *p37* were smaller than control AGS cells and readily detached from each other and the culture plates (Figure 1.11). Western analysis found reduced levels of ICAM-1 and Integrin- β 1 in *p37*-transfected human gastric cancer cells (AGS) (Liu et al., 2006). The down-regulation of these genes may be responsible for the weakened adhesion between *p37*-transfected AGS cells and facilitate tumour cell dissemination and metastasis (Liu et al., 2006). Significant inhibition of cell adhesion was also observed in p37-treated D2F2 (mouse mammary tumour) cells. However p37-treated D2F2 cell lines that also contained the human epidermal growth factor receptor related 2 (*Her2*) gene, showed greater inhibition of cell adhesion. The Her2 receptor, once activated, regulates cell migration, adhesion and proliferation phenotypes. The p37 protein may interact with HER2 regulating adhesion and

proliferation (Liu et al., 2007). Anchorage independent growth and a decrease in senescence (cells cease to divide) was also observed in the *p37*-transfected AGS cells and in *p37*-transfected human embryonic kidney 293 cells (HEK-293) (Liu et al., 2007). Antisenescence is a property of malignant cells allowing them to proliferate for prolonged periods by avoiding cell death. Liu et al. (2007) transfected AGS cells with an N-terminal truncated *p37* (1-29aa removed) or a C-terminal truncated *p37* (319-403aa removed). Antisenescence behaviour significantly decreased, similar to control levels, in the N-terminal deletion however only slightly decreased in the C-terminal deletion of *p37*. Therefore it was suggested that the entire 403 amino acids of *p37* is required for the antisenescence behaviour of mammalian cells (Liu et al., 2007).

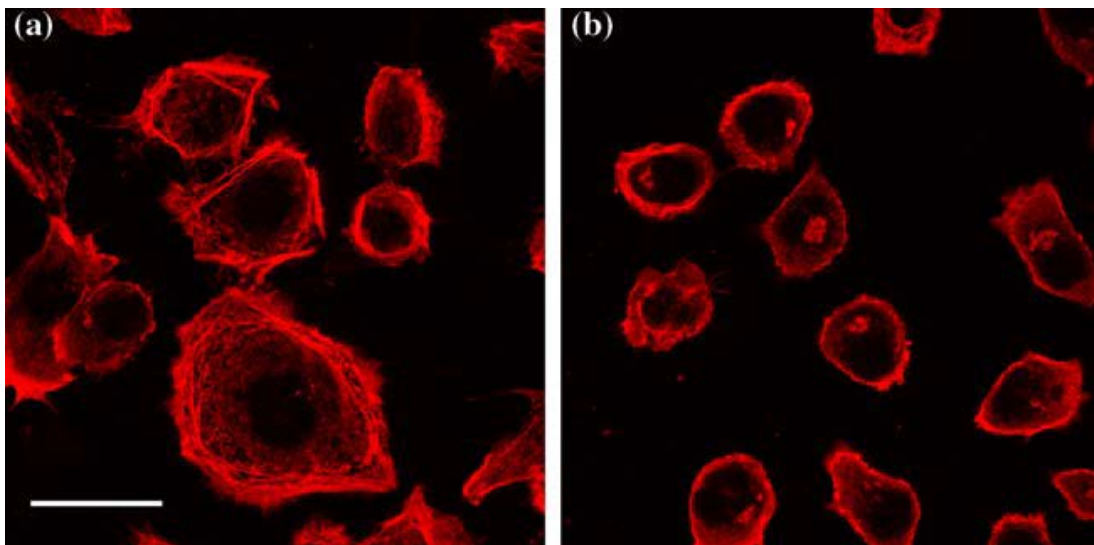


Figure 1.11: Morphological change of AGS cells transfected by the *p37* gene. (a) AGS cells transfected by an empty vector, and **(b)** transfected with *p37*. All data represents three independent experiments. Scale bar represents 20 μ m (From Liu et al., 2006).

1.7 HETEROTYPIC CONTACT INHIBITION OF LOCOMOTION

Contact inhibition of locomotion (CIL) is observed when migrating cells collide and change direction (Carmona-Fontaine et al., 2008; Mayor and Carmona-Fontaine, 2010). The characteristic sequence of events of CIL are: cell-cell contact, inhibition of cell protrusion activation at the site of contact, generation of new protrusions away from the site of contact and finally migration in direction of new protrusions (Figure 1.12) (Carmona-Fontaine et al., 2008).

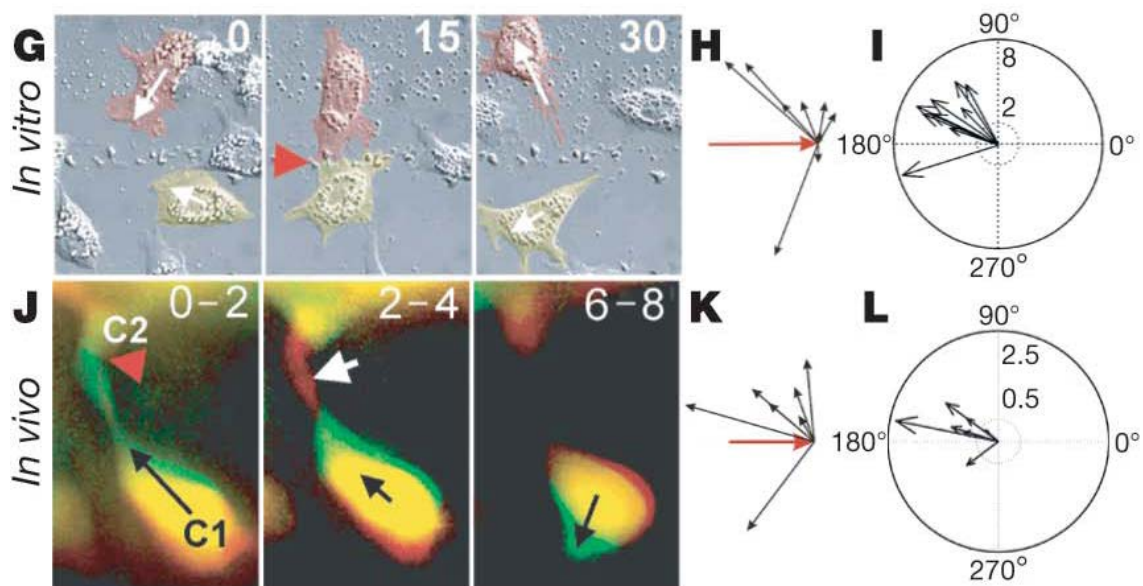


Figure 1.12: G-L Homotypic contact inhibition of locomotion in Neural Crest (NC) cells *in vitro* and *in vivo*. (G) Collision between two pseudocoloured neural crest (NC) cells *in vitro*. Time is shown in minutes. White arrows indicate direction of migration; the red arrow indicates collision. (H) Velocity vectors for NC *in vitro*; the red arrow indicates the initial velocity vector. (I) Acceleration vectors for NC collisions *in vitro*. They are clustered after collision ($P > 0.005$, $n = 10$). (J) Collision of two NC cells (C1 and C2) *in vivo* shown as the difference between two consecutive 2-min frames. Green, new area; red, collapsing area; black arrow, direction of migration; red arrowhead, cell contact; white arrow, collapsing protrusion. (K) *In vivo* velocity vector. (L) *In vivo* acceleration. They are clustered after the collision ($P > 0.01$, $n = 10$) (From Carmona-Fontaine et al., 2008).

Heterotypic (different cell types) and homotypic (same cell types) are two forms of contact inhibition of locomotion. Heterotypic contact inhibition plays an important role in tissue organization, development and repair, cell sorting, ordered migration and organogenesis (Omelchenko et al., 2001; Minami et al., 2007). Loss of heterotypic contact inhibition is related to the metastatic potential of cells (Figure 1.13) (Abercrombie and

Heaysman, 1953). However, contact inhibition of locomotion and contact inhibition of cell division probably involves different mechanisms. Cells that have been transformed with V12H-Ras, for example, lose their homotypic contact inhibition of growth (cell division) and multilayered cultures result (Minami et al., 2007). V12H-Ras stimulates Ras-like guanine nucleotide dissociation stimulators.

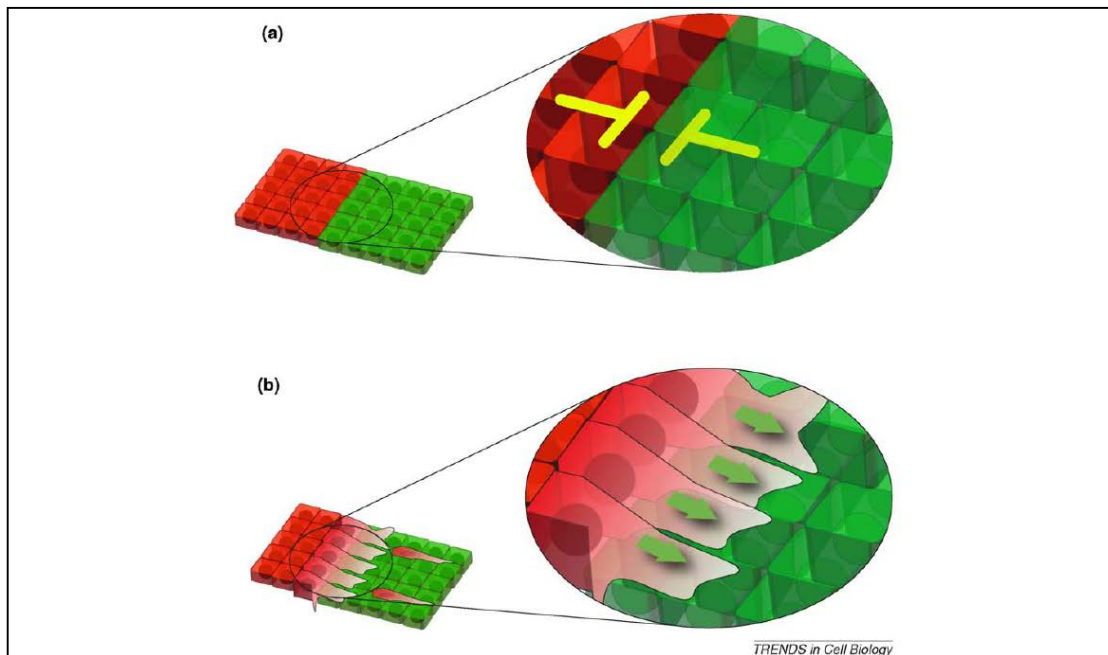


Figure 1.13: Heterotypic CIL in normal and cancer cells. (a) Two cell populations (indicated by two different colours) exhibit mutual CIL (yellow inhibitory arrows). This prevents the mixing of cells from these two populations. This kind of behaviour can be found in normal tissues. **(b)** Two cell populations are confronted and one of them (red cells) has lost CIL with the other (green cells). As a consequence the first group invades the second one. This invasive behaviour can be found in many cancer cells and has been proposed as the basis for metastasis (From Mayor and Carmona-Fontaine, 2010).

Heterotypic CIL was first described with fibroblasts (Abercrombie and Heaysman, 1953; Abercrombie and Heaysman, 1976; Abercrombie, 1979). Time-lapse recordings were used to observe heterotypic contact between invasive FS9 cells and chicken heart fibroblasts (CHF). Ruffling of the CHF leading lamellae ceased immediately on contact with the FS9 cells. The inhibition of ruffling was localized to the point of contact and the region of paralysis retracted, making room for the invading FS9 cells (Paddock and Dunn, 1986). However, the FS9 cells did not retract their lamellae and consequently invaded the CHF.

The confronted explant assay (Figure 1.14A) developed by Abercrombie and colleagues uses heterotypic contact inhibition of locomotion to determine cellular invasion *in vitro* (Abercrombie and Heaysman, 1976; Abercrombie, 1979). The confronted explant assay involves placing two explants approximately 1mm apart (Figure 1.14A). CHF₁ are used as the standard explant as their behaviour is well known and they are readily distinguishable from mouse fibroblasts. The CHF₁ provide a compact cell 'out wandering', ensuring collision with the confronting explant which may migrate at a different rate or density (Abercrombie and Heaysman, 1976). Cell 'out wandering' is the radial movement of the cells from the explants sides due to mutual homotypic contact inhibition directing the cells to un-inhabited space (Figure 1.14B). Contact inhibition between individual fibroblasts has been studied to determine overall collision behaviour (Paddock and Dunn, 1986).

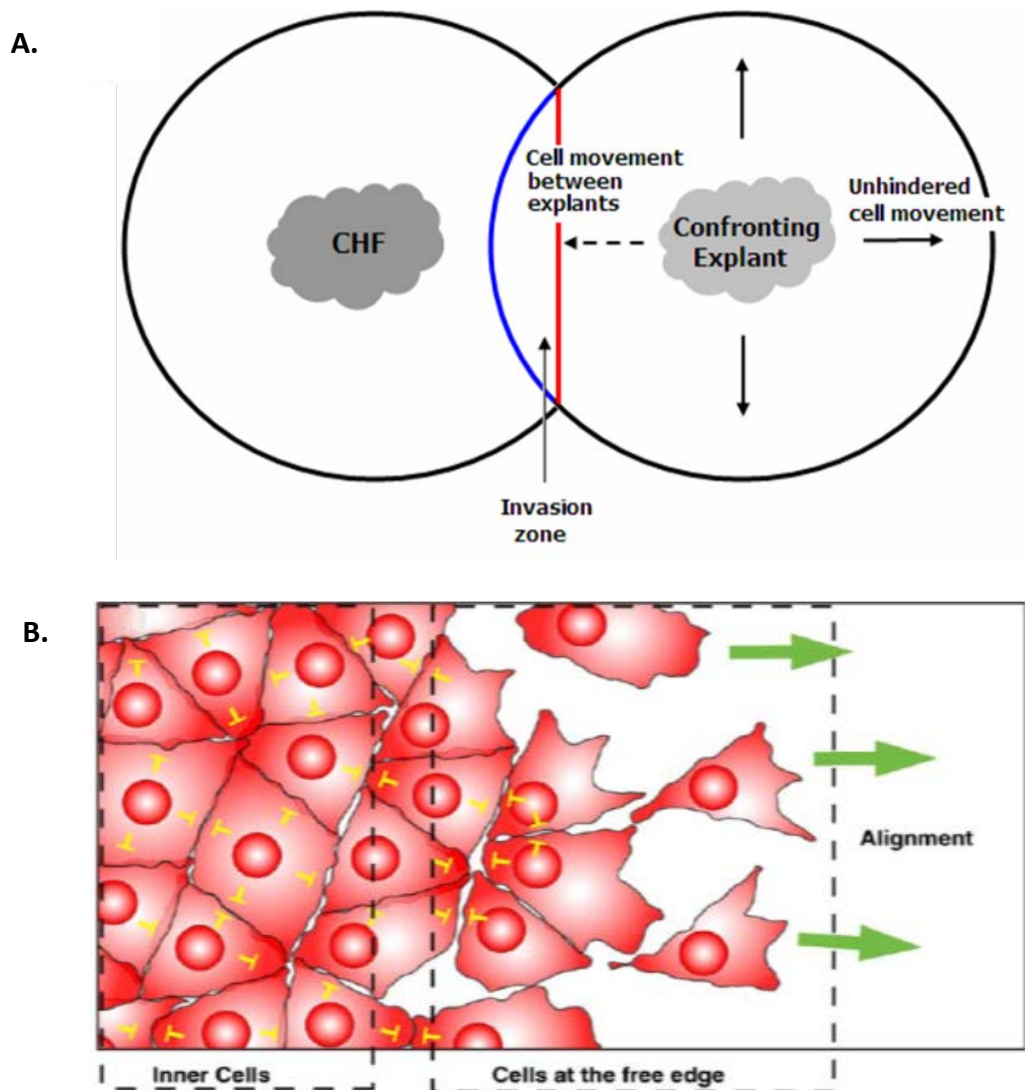


Figure 1.14: (A) Schematic of Abercrombie's confronted explants invasion assay. Chick embryo heart fibroblasts (CHF) and a confronting explant are inoculated approximately 1mm apart. The calculation of invasive indices is established by the comparison of the distance of cell movement between explants (dashed arrow) and the mean difference of the unhindered cell movement (solid arrows). Invasive confronting explants exhibiting no heterotypic contact inhibition will invade (blue line) the outgrowth of the CHF explant, whereas non-invasive (red line) cells will paralyse on contact and contract, a clear separation of the two population resulting. **(B) Homotypic contact inhibition in isolated cells.** CIL (represented by yellow inhibitory arrows in a group of cells). CIL between inner cells leads to inhibition of protrusions, whereas CIL between the leader cells, at the free edge, can lead to cell polarisation of the leaders (green arrows) and directional migration (Image b from Mayor and Carmona-Fontaine, 2010).

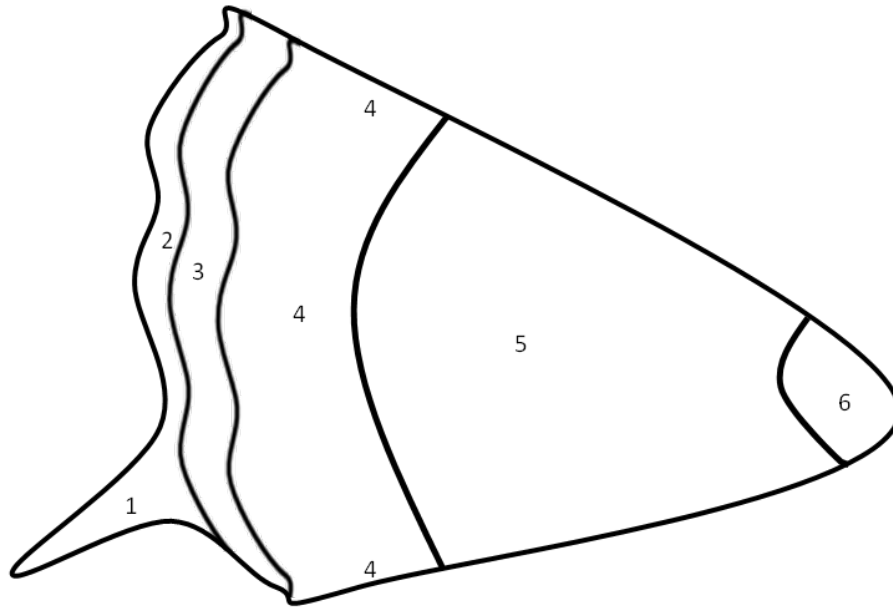
If the confronting explant is non-invasive, when two explants collide the cells become paralysed at the point of contact and a junction is formed (Figure 1.14A). If the confronting explant is invasive then paralysis does not occur and the cells invade the chicken heart fibroblasts (Figure 1.14A) (Abercrombie, 1979). The invasiveness of cells can be quantified using the invasion index. The invasion index is calculated by comparing the migration between the cell explants and the mean difference of unhindered cell movement on the outer sides of the explants confronting the CHF (Figure 1.14A) (Abercrombie, 1979). The invasion index ranges from 0 to 1; non-invasive to invasive. A value of 1.0 indicates a complete absence of contact inhibition of locomotion. Values of 0.2 to 0.3 are typical of non-invasive cells, while values between 0.5 and 0.8 indicate significant loss of contact inhibition (Abercrombie and Heaysman, 1976). Non-reciprocal invasion occurs when the invasive cells invade the territory of the non-invasive cells. Reciprocal invasion occurs when there is no contact inhibition of either explant (Abercrombie, 1979).

Contaminated FS9 cells were highly invasive in the Abercrombie assays with an invasion index of 0.8 (Steinemann et al., 1984a; Schmidhauser et al., 1990). When a monoclonal antibody specific for p37 was included in the assay, FS9 invasivity was completely inhibited and subsequently decreased the invasion index to 0.35. It was consequently shown that p37 was a *M. hyorhinis* surface protein and removal of *M. hyorhinis* from the cells resulted in heterotypic CIL (i.e. invasion index of <0.3) (Schmidhauser et al., 1990).

1.8 THE ROLE OF RAC1 AND RHOA IN HETEROTYPIC CONTACT INHIBITION OF LOCOMOTION

Rho GTPases (guanine nucleotide GTP-binding proteins) are members of the Ras superfamily of monomeric GTP binding proteins that play a major role in cell proliferation, apoptosis, gene expression and many other common cellular functions (Bishop and Hall, 2000). Ten different mammalian Rho GTPases, with multiple isoforms, have been identified. The most extensively characterised members are Rho (A, B, C isoforms), Rac (1, 2, 3, isoforms) and Cdc42 (Cdc42Hs, G25K isoforms) (Bishop and Hall, 2000). RhoA, Rac1 and Cdc42 are well known for their role in regulating the actin cytoskeleton and in controlling cell motility, adhesion and promoting lamellipodia and filopodia (thin protrusions similar to lamellipodia) formation (Wennerberg et al., 2005; Arulanandam et al., 2009). These GTPases act as molecular switches by cycling between an active GTP-bound state, and an inactive GDP-bound state. Conformational changes occur with the binding of GTP allowing for initiation of many downstream effector proteins (Bishop and Hall, 2000; Raftopoulou and Hall, 2004).

The Rho GTPases are regulated by receptors such as growth factor receptors (GFR), tyrosine kinase receptors, integrins and cadherin adhesion molecules (Etienne-Manneville and Hall, 2002). Cadherins are a major family of transmembrane receptors that mediate cell-cell, cell-matrix and contact inhibition of cell growth through their interactions with Rac1 and RhoA (Wildenburg et al., 2006). Engaged cadherins activate p120-catenins which in turn mediate cross-talk between Rac1 and RhoA, influencing cell motility (Niessen and Yap, 2006). The 'cross-talk' between Rac and Rho allows lamellipodial extension, adhesion and translocation to be regulated in accordance with cell movement (Figure 1.15) (Guilluy et al., 2011).



1. \uparrow Cdc42 (filopodia extension)
2. \uparrow RhoA \rightarrow mDia \rightarrow Rac1 (actin polymerization)
3. \uparrow Rac1 \rightarrow p190RhoAGap \rightarrow RhoA (nascent adhesion formation)
4. \uparrow RhoA \rightarrow ROCK \rightarrow Rac1 (contraction, adhesion maturation and prevents lateral protrusion)
5. \uparrow RhoA (cell body contraction)
6. \uparrow Rac1 (unknown function)

Figure 1.15: Rho protein crosstalk during cell migration. A diagram of a migrating fibroblast is shown depicting zones of Rho protein activation and crosstalk. **(1)** Cdc42 controls formation of exploratory filopodia. **(2)** RhoA activity has been detected at the leading edge of lamellipodia where it may contribute to actin polymerization, directly via Diaphanous-related formin protein (mDia) or indirectly through mDia activating Rac1. **(3)** Behind the narrow zone of high RhoA activity, a wider zone of high Rac1 activity has been described. This may arise downstream from integrin engagement. Alternatively, Cdc42 may contribute to Rac1 activation. This, in turn, inhibits RhoA and promotes nascent adhesion formation associated with actin-based protrusion. **(4)** RhoA generates Rho-associated, coiled-coil containing protein kinase (ROCK)-mediated contractility and inhibits Rac1, leading to adhesion maturation. RhoA also prevents inappropriate lateral protrusion by inhibiting Rac1 through ROCK2. **(5)** RhoA promotes cell body retraction through ROCK1-mediated myosin II stimulation. **(6)** Rac1 activation at the tail has been described but its function in this area is unknown (Modified from Guilluy et al., 2011).

Abercrombie's confronted explants assay (Section 1.7) was used to study the effects of changing Rac1 and RhoA activities on heterotypic contact inhibition of locomotion (CIL) between NIH3T3 cells and chicken heart fibroblasts (CHF) (Anear and Parish, 2012). Expression of either dominant active (L61) or dominant negative (N17) Rac1 in NIH3T3 cells resulted in a loss of heterotypic CIL. Down-regulation of Rac1 resulted in RhoA activation (i.e. increased levels of RhoA-GTP). Increasing RhoA activity directly using dominant active V14 RhoA or indirectly by down-regulating N-cadherin or p120 catenin expression levels also gave rise to a loss of heterotypic CIL (Anear and Parish, 2012).

Mutual antagonism occurs between Rac1 and RhoA and interfering with this reciprocal control most probably leads to the loss of heterotypic CIL by disturbing the periodicity of RhoA/Rac1 dynamics in the protrusion-retraction cycle. Machacek et al. (2009) found that mouse embryo fibroblasts (NIH3T3), during spontaneous cell motility, cycled through protrusion and retraction at the cell edge approximately every 100sec. RhoA is activated during the protrusion phase while Rac1 and Cdc42 activation lags edge protrusion, achieving peak activation 40sec after the commencement of protrusions. Rac1 activity is still significant during the retraction phase. Thus, RhoA is apparently responsible for initiating actin polymerisation at the commencement of the protrusion-retraction cycle. Rac1 then acts as an antagonist to RhoA since rapid suppression of RhoA takes place and increased Rac1 activation occurs. Hence, increased RhoA activity in NIH3T3 cells would interfere with heterotypic CIL by disrupting the retraction phase of the cycle (Machacek et al., 2009).

Anear and Parish (2012) provide a model for heterotypic CIL consistent with Machacek et al. (2009) results. Cell-cell contact (collision) between NIH3T3 fibroblasts and CHF results in N-cadherin engagement (between molecules on both cells), inducing rapid Rac1 activation which inactivates RhoA at the site of contact via the Ros/p190RhoAGAP pathway. Initiation of protrusions (via formin induced actin polymerisation) is thus inhibited until Rac1 is down-regulated. RhoGEFs may then be recruited away from the site of contact and initiate adjacent protrusions via Rho effector Diaphanous-related formin protein (mDia) induced actin polymerisation. On the other hand, levels of activated Rac1 may decrease at the contact sites (Kitt and Nelson, 2011). The consequent increase in

RhoA activity could result in membrane retraction.

The presence of *Mycoplasma hyorhinis* leads to loss of heterotypic CIL between FS9 fibroblasts and CHFs (Steinemann et al., 1984a; Steinemann et al., 1984b) and the p37 protein was found responsible (Schmidhauser et al., 1990). The purified p37 protein also results in loss of heterotypic CIL between NIH3T3 fibroblasts and CHFs (Darren Lowen, PhD Thesis, La Trobe University, 1995; Megan Drew, Honours Thesis, La Trobe University 2006). Whether p37 influences RhoA or Rac1 activity is not known.

1.9 Aims

1. Identify genes whose expression is changed when NIH3T3 (mouse) fibroblasts are incubated with the purified p37 protein. Determine effects of various p37 concentrations and different treatment times on p37-induced gene expression.
2. Since Il6 and STAT3 signalling appeared to be involved, ascertain the effects of inhibiting STAT3 or blocking the Il6 receptor in p37-induced gene expression.
3. Test the hypothesis that the p37 protein is binding the TLR4 receptor.
4. Determine whether bound thiamine pyrophosphate associated with p37 is required for p37 activation of gene expression. Ascertain the effects of truncating the p37 protein on gene induction.
5. Analyse gene expression and morphology of *p37*-transfected NIH3T3 cells as well as the motility of p37-treated and *p37*-transfected cells. Determine whether exogenous p37 affects RhoA activity of NIH3T3 cells.

2. MATERIALS AND METHODS

2.1 REAGENTS

Reagents, materials and kits were purchased from the following companies.

Dulbecco-modified Eagle's medium, Ampicillin and Tris were supplied from Sigma. Plasmocin from Invitrogen (San Diego, California, USA). Fetal calf serum, trypsin-versene solution and penicillin streptomycin solution were from JRH Bioscience (Lenexa Kansas USA). DOTAP liposomal transfection reagent was supplied by Roche. Wizard™ Plus SV Minipreps DNA purification system, restriction enzymes, Go-Taq DNA polymerase, T4 DNA ligase, RNase Out and Shrimp Alkaline Phosphatase were purchased from Promega (Madison, WI, USA). SuperScript™ III Reverse transcriptase, RNaseOUT and DDT for cDNA synthesis and Hygromycin B were purchased from Invitrogen (Carlsbad, California, USA). UltraClean™ 15 DNA Purification Kit from MOBIO Laboratories, Inc (Solana Beach, CA, USA). Plasmid Miniprep Kit was from Bio-RAD (Hercules, CA, USA). Tissue culture flasks, petri dishes, 24 and 6 well plates were from Falcon (New Jersey, USA), cryovials from Nalgene (New Jersey, USA) and Falcon Tubes were from Greiner. Agarose and Hyperladder I and IV were from Biorline USA Inc. (Randolph, MA, USA). RNeasy and DNeasy Kits from Qiagen (Valencia, CA, USA). UltraClean™15 DNA Purification Kit purchased from MOBIO. Custom primers were purchased from Geneworks (Adelaide, Australia). Quickchange II XL Site-Directed Mutagenesis Kit and XL10-Gold Ultracompetent cells from Agilent Technologies.

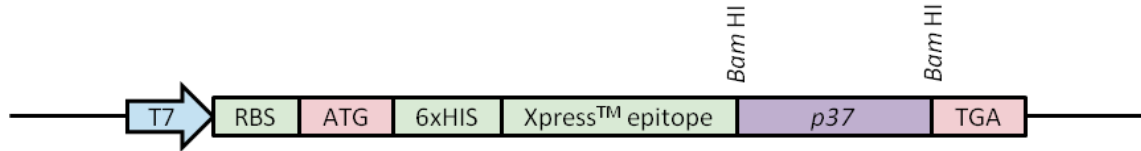
LEAF™ purified anti-mouse/rat CD126 (IL-6 R α chain) antibody purchased from BioLegend; Cat# 115807. STAT3 Inhibitor VI, S31-201, also known as NSC74859 purchased from Santa Cruz Biotechnology; Cat# sc-204304. Ultra pure lipopolysaccharide from *E. coli* 0111:B4 strain – TLR4 ligand purchased from Invivogen; Cat#tlrl-3pelps. TLR4 peptide inhibitor set (VIPER and CP7) purchased from IMGENEX; Cat#IMG-2011set.

Most analytical and Molecular biology grade chemicals were purchased from either Sigma (St Louis) or BDH chemicals (Melbourne, Australia).

2.2 CONSTRUCTS

2.2.1 pRAp37

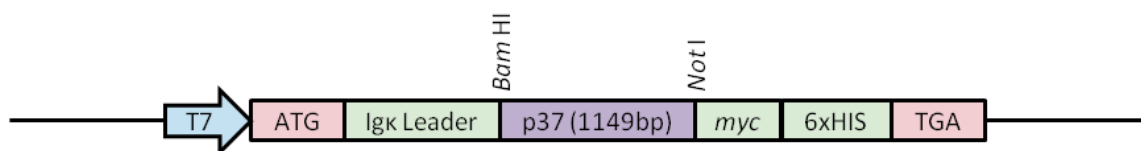
The pUC-derived pRSET A expression vector containing the mutated *p37* gene (pRAp37) was supplied by Megan Drew (Honours Thesis, La Trobe University, 2006).



The 2.9kb pRSET A (amp^r) vector (Invitrogen, Cat# V351-20) was designed to express high-levels of proteins from cloned genes in *Escherichia coli*. A T7 promoter (T7) allows high-expression of the inserted gene (*p37*) which was positioned in frame with a ribosomal binding site (RBS), the ATG initiation codon (ATG), an N-terminal polyhistidine tag (6xHIS) that allows protein purification, an Xpress™ epitope and the termination codon TGA. The multiple cloning site contains an array of restriction enzyme sites allowing the insertion of a gene. The *p37* gene was inserted at the *Bam*HI cut site. The pRSET A vector also contains a BLA promoter for transcription of the ampicillin resistance gene. The ampicillin resistance gene allows the selection of positively transformed *E. coli*. The purified p37 protein ran to the position of 48 kDa on an SDS-PAGE. The p37 protein was 43.5 kDa (Section 2.1) and the addition 4.5 kDa was due to the 6x HIS tag and the Xpress™ epitope.

2.2.2 pSTp37

The mammalian expression vector pSecTag2/HygroB (amp^r, hyg^r) vector was purchased from Invitrogen (Cat# V351-20 & V910-20). The *p37* gene was inserted into the multiple cloning site between restriction cut sites *Bam*HI and *Not*I. The construct was designated pSTp37.



The 5.7kb pSecTag2/HygroB vector was designed for propagation in *E. coli* cells and expression and secretion of the inserted gene (*p37*) in mammalian cells. A T7 promoter (T7) allows high-expression of the inserted gene (*p37*) which was positioned in frame with an ATG initiation codon (ATG) and the Murine Ig κ-chain leader sequence (Igκ Leader) the

signal sequence for the secretion of the p37 fusion protein. The *p37* gene is flanked with the *c-myc* epitope (*myc*) allowing detection of the fusion protein by the Anti-*myc* Antibody (Cat# R950-25), a C-terminal polyhistidine tag (6xHIS) that allows for protein purification and the termination codon TGA. The pSecTag2/HygroB vector also contains a BLA promoter for transcription of the ampicillin resistance gene and a SV40 early promoter/origin for efficient high-level expression of the hygromycin resistance gene. The ampicillin resistance gene allows the selection of positively transformed *E. coli* and the hygromycin resistance gene allows selection of stable transfectants in mammalian cells.

2.3 BACTERIAL STRAINS

Escherichia coli strain DH5 α (F- ϕ 80*lacZ* Δ M15 Δ (*lacZYA-argF*)U169 *recA1 endA1 hsdR17*(*r_K⁻, m_K⁺*) *phoA supE44 thi-1 gyrA96 relA1 λ*) for plasmid transformations and propagation was purchased from Invitrogen (Cat# 18265-017).

Escherichia coli strain One Shot[®]BL21(DE3) (F- *ompT hsdS_B* (*r_B⁻ m_B⁻*) *gal dcm* (DE3)) for plasmid transformation and IPTG induced expression of protein was purchased from Invitrogen (Cat# C6000-03).

Escherichia coli strain XL1-Blue Competent Cells (*recA1 endA1 gyrA96 thi-1 hsdR17 supE44 relA1 lac* [F' *proAB lacI^qZ* Δ M15 Tn10 (Tet^r)]; genes listed signify mutant alleles, genes on the F' episome, however, are wild-type unless indicated otherwise) for plasmid transformation and propagation was purchased from Stratagene (Cat# 2002249).

2.4 MAMMALIAN CELL LINE

NIH3T3 – embryonic mouse fibroblasts established from NIH Swiss mouse embryos

2.5 OLIGONUCLEOTIDES

2.5.1 General Oligonucleotides

Name	Anti/sense	Sequence 5'-3'
T7_F	sense	TAATACGACTCACTATAGGG
T7_R	antisense	CCTCGACTGTGCCTTCTA
p37 F	sense	ACCGAGCTCGGATCCTGTCTAATACAGGAGTAGTCAAG
p37 R	antisense	CCCTCCTCGAGCGCCGCTTTAATGGCTTTTTCATAAACTTC
Hyg ^R F	sense	CTCACCGCGACGTCTGTCGAGAAGTTTCTGATC
Hyg ^R R	antisense	TTCCTTTGCCCTCGGACGAGTGCTGGGGCGTCGGT
Mycp F1*	sense	CGCCTGAGTAGTACGTTCCGC
Mycp F2*	sense	CGCCTGAGTAGTACGTACGC
Mycp F3*	sense	TGCCTGAGTAGTACATTCCGC
Mycp F4*	sense	CGCCTGGGTAGTACATTCCGC
Mycp F5*	sense	CGCCTGAGTAGTATGCTCGC
Mycp F6*	sense	TGCCTGGGTAGTACATTCCGC
Mycp R1*	antisense	GCGGTGTGTACAAGACCCGA
Mycp R2*	antisense	GCGGTGTGTACAAAACCCGA
Mycp R3*	antisense	GCGGTGTGTACAAAACCCGA

^a mutated bases underlined

* Mycoplasma species covered by these primers have been described in (Wirth et al., 1994; Uphoff and Drexler, 2002)

2.5.2 PCR gene oligonucleotides

Gene (Accession N°)	Anti/sense	Sequence (5'-3')	Position	PCR size (bp)
Angptl4 (NM_020581)	sense	GGGACCAAGACCATGACCTCCGTGG	1112-1136	366
	antisense	TCTTTGTCCACAAGACGCAGATAGCC	1473-1448	
β-actin (NM_007393)	sense	TGACGGGGTCAACCCACTGTGCC	548-570	656
	antisense	GAAGCATTGCGGTGGACGATG	1204-1183	
C3 (NM_009778)	sense	CACTGGACCCAGAGAAGCTCGGTCA	2567-2591	1241
	antisense	GCGTAGGATGTGCCTCTACGTTGT	3808-3784	
GapDH (NM_008084)	sense	AGGCCGGTCTGAGTATGTC	315-334	529
	antisense	TGCCTGCTTACCACCTTCT	844-825	
Hp (NM_017370)	sense	GCCAAAGGCAGCTTTCCTTGGCAGGCC	376-402	819
	antisense	GCAGGGCTAGAACCATCAGAGTAT	1195-1171	
Il6 (NM_031168)	sense	GGTCTTCTGGAGTACCATAGCTACCTGG	377-404	295
	antisense	ACGCACTAGGTTTGCCGAGTAGATCTC	672-646	
Lcn2 (NM_008491)	sense	ACCAGGGCTGTGCTACTGGATCAGA	306-331	275
	antisense	TGTCGTCCTTGAGGCCAGAGACTT	581-557	
Lum (NM_008524)	sense	CATGTATGGGCAAATATCACCC	490-511	309
	antisense	GGACTCGGTCAGGTTGTTGT	799-780	
Saa3 (NM_011315)	sense	GCTGGTCAAGGTCTAGAGACATGT	116-140	394
	antisense	CAGCACATTGGGATGTTTAGGGATCCAG	510-484	
Vcam1 (NM_011693)	sense	AGCCCTCTCCTATACTAGAGGAGG	1876-1900	408
	antisense	TGGTGTACGACCATCCAGACTT	2284-2260	

Abbreviations are: Angptl4, Angiopoietin Like-4; β-actin, beta-actin; C3, Complement Component 3; GapDH, Glyceraldehyde 3-phosphate dehydrogenase; Hp, Haptoglobin; Il6, Interleukin 6; Lcn2, Lipocalin 2; Lum, Lumican; Saa3, Serum Amyloid A3; Vcam1, Vascular cell adhesion molecule 1.

2.5.3 qPCR oligonucleotides

Gene (Accession N°)	Anti/sense	Sequence (5' - 3')	Slope	R ²	E%
Angptl4 (NM_020581)	sense	TTGGGACCAAGACCATGACCTCCGTGG	-3.118	0.986	109.3
	antisense	CCGTGGGATAGAGTGGAAAGT			
β-actin (NM_007393)	sense	TTG CTG ACA GGA TGC AGA AGG	-3.343	0.999	99.1
	antisense	CACATCTGCTGGAAGGTGGA			
Cast (NM_009817)	sense	CCCATTGATGCCCTCTCAG	-3.381	0.996	97.6
	antisense	TCCTTTGTTTCTCTCCGTCC			
Cp (NM_001042611)	sense	CAAACCTAGAAATGTTTCCCC	-3.364	0.980	98.3
	antisense	GGTCATCCTGTAActCTGAGATG			
C3 (NM_009778)	sense	CTGACCTCTGGGGAGAAAAG	-3.313	0.989	100.4
	antisense	TAGATTCTGTGAATGCCCA			
Dcn (NM_007833)	sense	AACAGCATCACCGTTATGGAGAATGG	-3.288	0.973	101.4
	antisense	GTGAAGGTAGACGACCTGGAT			
Fkbp5 (NM_010220)	sense	AGGGCACCAGTAACAATGGA	-3.205	0.986	105.2
	antisense	CCCCACTCTTTTGACAATCTTT			
GapDH (NM_008084)	sense	CTGAGGACCAGTTGTGTCC	-3.55	0.991	91.3
	antisense	CCCTGTTGCTGTAGCCGTAT			
Hp (NM_017370)	sense	AAAACTCTTCTGAACCAC	-3.389	0.986	97.3
	antisense	AACGACCTTCTCAATCTCCAC			
Has2 (NM_008216)	sense	CTATGCTTGACCCTGCCTC	-3.455	1.000	94.7
	antisense	AAAGCCATCCAGTATCTCAGG			
Il6 (NM_031168)	sense	CAAAGCCAGAGTCCTTCAGAGAGATACAGAA ACTC	-3.147	0.989	107.9
	antisense	GTCCTTAGCCACTCCTTCTGTGACTCC			
LIF (NM_001039537)	sense	TTCCCATCACCCCTGTAAATG	-3.261	0.981	102.6
	antisense	GAAACGGCTCCCTTGAG			
Lcn2 (NM_008491)	sense	GAACGTTTCACCCGCTTTG	-3.152	0.977	107.6
	antisense	CATCCCAGTCAGCCACAC			
Lum (NM_008524)	sense	TTAGCTTAAGAGTATACCAACAGTTAATG	-3.52	0.982	92.4
	antisense	GCTTGATCTTGAGTAAGACAGT			
Mmp2 (NM_008610)	sense	TTGCTCGGGCCTTAAAAGTAT	-3.455	0.983	94.7
	antisense	CCATCAAATGGGTATCCATCTC			
Mmp9 (NM_013599)	sense	GTGCCCTGGAActCACACAAC	-3.478	0.981	93.9
	antisense	CCAGAAGAATTTGCCATGGCAGAA			
Saa3 (NM_011315)	sense	GTTACGGGACATGGAGCAGAGGA	-3.412	0.993	96.4
	antisense	GCAGGCCAGCAGTCCGGAAG			
STAT3 (NM_213659)	sense	ATAACGGTGAAGGTGCTGAG	-3.36	0.991	98.4
	antisense	GTGTCTCAAGTCACGTCTCTG			
Thbs1 (NM_011580)	sense	AGAAAATCATGGCTGACTCGG	-3.493	0.992	93.3
	antisense	GGTTATGATTGGCAGCTGATG			
Tm4sf1 (NM_008536)	sense	CTCTCGCCAACAGCAATATAA	-3.278	0.998	101.9
	antisense	GGTAGGATGTGGCACAAGGTG			
TNFAip6	anti/sense	QIAGEN; Cat#330001 PPM24986A			100

Vcam-1 (NM_011693)	sense	ACGAGTGTGAATCTAAGACTGAAG	-3.14	0.993	108.2
	antisense	CATCCCGATGGCAGGTATTAC			

Abbreviations are: Angptl4, Angiopoietin Like-4; β -actin, beta-actin; C3, Complement Component 3; Cast, Calpastatin; Cp, Ceruloplasmin; Dcn, Decorin; Fkbp5, FK506 binding protein 5; GapDH, Glyceraldehyde 3-phosphate dehydrogenase; Hp, Haptoglobin; Has2, Hyaluronan synthase 2; Il6, Interleukin 6; Lcn2, Lipocalin 2; LIF, leukemia inhibitory factor; Lum, Lumican; Mmp2, Matrix metalloproteinase 2, Mmp9, Matrix metalloproteinase 9; Saa3, Serum Amyloid A3; STAT3, Signal transducer and activator of transcription 3; Thbs1, thrombospondin type 1, domain containing 7a; Tm4sf1, Transmembrane 4 superfamily member 1; TNFaip6, tumor necrosis factor, alpha-induced protein 6; Vcam1, Vascular cell adhesion molecule 1.

2.6 CLONING

2.6.1 XL1-Blue Competent Cells (Stratagene) Heat Shock Transformation

XL1-Blue Competent Cells were heat shock transformed following the manufacturer's protocol (Stratagene; Cat# 2002249). In a 1.5ml centrifuge tube, 0.25 μ l of β -mercaptoethanol was added to 30 μ l of XL1-blue competent cells and incubated on ice for 30min. 2 μ l of DNA/ligation reaction was added and the reaction was incubated for a further 10min on ice. The reaction was then heat shocked for 40sec at 42°C and returned to ice for an additional 2min. 100 μ l of Luria Bertani (LB) media (1% Tryptone, 0.5% Yeast extract, 80mM NaCl, pH 7.0) was added and the reaction was incubated with agitation at 37°C for 30min. 10 μ l of the culture was spread onto LB agar plates (1% Tryptone, 0.5% Yeast extract, 80mM NaCl, 1.5% agar, pH 7.0) containing 50 μ g/ml ampicillin and the remainder on a second plate.

2.6.2 One Shot® BL21(DE3) (Invitrogen) Heat Shock Transformation

OneShot® BL21(DE3) Competent Cells were transformed by heat shock in accordance to the manufacturer's protocol (Invitrogen; Cat# 6000-03). A vial of OneShot cells were defrosted on ice and 30 μ l aliquots was placed into new microcentrifuge tubes. 10ng of DNA was added to the cells and mixed by gentle tapping on the bench. The OneShot/DNA mix was incubated on ice for 30min, followed by exactly 30sec incubation at 42°C. The cells were immediately returned to the ice and 250 μ l of 37°C 2YT (1.6% BactoTryptone, 1% BactoYeast Extract, 80mM NaCl, pH 7.0) was added. The cells were incubated at 37°C with agitation (225rpm) for 1hr. LB agar plates (1% Tryptone, 0.5% Yeast extract, 80mM NaCl, 1.5% agar, pH 7.0) containing 50 μ g/ml ampicillin were used to plate out 20 to 200 μ l of the transformation reaction. The plates were incubated overnight, inverted at 37°C.

2.6.3 Short Term Storage of Bacterial Transformations

The transformed cells plated on LB agar plates (1% Tryptone, 0.5% Yeast extract, 80mM NaCl, 1.5% agar, pH 7.0) containing 50µg/ml ampicillin were sealed with parafilm and placed in a clip lock plastic bag. Plates were kept at 4°C, inverted.

2.6.4 Long Term Storage of Bacterial Transformations

Transformed bacterial cell colonies were inoculated into 10ml of LB broth (1% Tryptone, 0.5% Yeast extract, 80mM NaCl, pH 7.0) containing 50µg/ml ampicillin and incubated at 37°C overnight with agitation. 500µl of the overnight culture and 500µl of 10% glycerol was placed into a 2ml cryovial and snap frozen in liquid nitrogen; stored at -80°C.

2.6.5 Isolation of plasmid DNA

LB media was inoculated with an *E. coli* strain containing the plasmid of interest and the selective antibiotic. The culture was incubated at 37°C, overnight, in a shaking incubator. Plasmid DNA was extracted from the culture using WizardTM Plus SV Minipreps DNA purification system (Promega; Cat# A1330) following the manufacturer's instructions.

2.6.6 Restriction Enzyme Digest

Restriction enzyme digest reactions were prepared to 50µl reactions. The reaction mix contained: 1µg DNA, 5µl of the appropriate 10x Buffer (Promega), 1µl of restriction enzyme(s) (Promega) and ddH₂O to the final volume of 50µl. The digest was incubated 3hrs - overnight at 37°C and run out on a 1% agarose gel (Section 2.7).

2.6.7 DNA Purification from Agarose Gel

DNA was purified from TBE buffered agarose gels (Section 2.7) following the UltraCleanTM15 DNA Purification Kit (MOBIO; Cat# 12100-300). The DNA bands were identified under UV light (Transluminator UVP Inc), excised from the gel using an Xtracta (Gene Works: Lab Tools), placed into sterile 1.5ml centrifuge tubes and weighed. Exceptions included 7µl of ULTRA BIND was added to each reaction, the pellet was allowed to air dry for 30min at room temperature and re-suspended in 14µl of nuclease-free H₂O. The reaction was incubated at room temperature for 5min, centrifuged for 1min at 10000rpm and the supernatant transferred into a fresh 1.5ml centrifuge tube without any silica traces.

2.6.8 Dephosphorylation using Shrimp Alkaline Phosphatase (Promega)

Dephosphorylation of vectors was carried out in accordance to the Standard Shrimp Alkaline Phosphatase (Promega; Cat# 9PIM820) protocol.

2.6.9 Ligation Reaction

The basic ligation reaction involved the addition of: 200ng vector DNA, 500ng gene insert DNA, 10% of the final volume of 10x ligase buffer, 1 μ l T4 DNA ligase (Promega; Cat# 9PIM180) and nuclease free water to a final volume of; 10 μ l if \leq 2 μ l vector or \leq 4 μ l of insert is used or 20 μ l if $>$ 2 μ l vector or $>$ 4 μ l of insert is used. The reaction is mixed by pipetting and incubated overnight at room temperature. The reaction was inactivated by heating to 65°C for 10min. Five different reactions with different ratios of vector DNA to gene insert DNA was implemented to establish a higher yield of ligation (Table 2.1). Two control ligations were also set up to determine efficiency of enzymatic digestion of the vector DNA and insert DNA. The vector only control contained vector DNA and the insert DNA was replaced with water. The insert only control contained insert DNA and the vector DNA was replaced with water. All ligations were incubated overnight at room temperature.

Table 2.1: Ligation DNA ratio

Ratio	Vector : insert (ng/ μ l)
3:1	525 : 175
2:1	467 : 233
1:1	350 : 350
1:2	233 : 467
1:3	175 : 525

2.6.10 QuikChange II XL Site-Directed Mutagenesis (Agilent Technologies)

Site-directed mutagenesis was performed using QuikChange II XL Site-Directed Mutagenesis kit as per the manufacturer's instructions (Agilent Technologies; Cat#200521). Exceptions include primer design, dsDNA concentration and annealing temperature discussed in Section 7.2.1.

2.7 AGAROSE GEL ELECTROPHORESIS

1-3% TBE (45 mM Tris-borate, 1 mM EDTA, pH 8.0) buffered agarose gels (Agarose 1, AMRESCO; Cat# 0710) stained with 0.5µg/ml ethidium bromide was used to separate DNA/RNA according to size. Gels were run at 90-100V for 60-90min in 1% TBE buffer (Bio-RAD PowerPac™ Basic power Supply).

The BioLine molecular weight markers Hyperladder I or IV were used for quantification and size determination of DNA. Hyperladder I produced a pattern of 14 regularly spaced bands ranging from 200 – 10000bp (Cat# BIO-33025). Hyperladder IV produced a pattern of 10 regularly spaced bands ranging from 100 to 1000bp (Cat# BIO-33029). 5µl Hyperladder was inoculated per well of a TBE agarose gel.

2.8 DNA SEQUENCING (AGRF)

2.8.1 Plasmid Sequencing

Plasmid DNA was sequenced by Australian Genome Research Facility (AGRF) standards with the reagents: 300ng of plasmid DNA, 1µl of a 6.4pmol primer and ddH₂O to prepare a 12µl volume. Individual reactions were completed for the forward and reverse primers and duplicates were prepared.

2.8.2 PCR Product Sequencing

PCR product DNA was sequenced by Australian Genome Research Facility (AGRF) standards with the reagents: 2-6ng of PCR product per 100bp, 1µl of a 6.4pmol primer and ddH₂O to prepare a 12µl volume. Individual reactions were completed for the forward and reverse primers and duplicates were made.

2.8.3 Sequence analyses

Sequence similarities were analyzed using BLAST analysis (Altschul et al., 1990; Altschul et al., 1997) at the National Centre for Biotechnology Information (NCBI; <http://www.ncbi.nlm.nih.gov/>). Basic sequence alignments and analysis was performed utilising the program CLC Sequence Viewer 6 (Version 6.8.1).

2.9 RNA PURIFICATION AND cDNA SYNTHESIS

2.9.1 RNA Extractions from Animal Cells

The RNeasy® Mini Kit (Qiagen; Cat# 74104) was used to extract RNA from animal cells as per the manufacturer's instructions. Tissue culture cells for RNA extraction were grown to ~70% confluence. Extracted RNA was eluted in 30µl of RNase-free water and stored at -80°C.

2.9.2 Removal of Genomic Contamination via DNase Treatment

Genomic contamination was eliminated using Deoxyribonuclease I, Amplification Grade (Invitrogen; Cat#18068-015) per the manufacturer's instructions. RNA samples (Section 2.9.1) were screened by PCR (Section 2.11). 1µl of extracted RNA was added to a PCR reaction including the B-actin primers (Section 2.5.2). Gel electrophoresis was used to analyse PCR reaction (Section 2.7). If genomic contamination was still evident after DNase treatment then a new aliquot of RNA would be treated.

2.9.3 RNA Integrity and Quantification

RNA extractions were performed following RNeasy® Mini Kit (Qiagen; Cat# 74104) (Section 2.9.1). Gel electrophoresis (Section 2.7) was used to check integrity. RNA samples had $A_{260}:A_{230}$ ratios greater than 1.7, $A_{260}:A_{280}$ ratios 1.8 to 2. Total RNA was quantified using a NanoDrop ND-1000 spectrophotometer according to the manufacturer's instructions (Labtech International, East Sussex, UK). RNA used for microarray analysis was also quantified using the Agilent 2100 Bioanalyzer (Agilent Technologies, Santa Clara, California, USA).

2.9.4 cDNA Synthesis using Reverse Transcription

Reverse transcription of mRNA was completed in accordance to the First-Strand cDNA using SuperScript™ III for RT-PCR (Invitrogen; Cat# 18080-044) protocol. The cDNA was diluted with an additional 20µl and stored at -20°C.

2.10 DNA PURIFICATION

2.10.1 Genomic DNA isolation

The DNeasy® Blood and Tissue Kit (Qiagen; Cat# 69504) were used to extract DNA from animal cells as per the manufacturer's instructions. Tissue culture cells for DNA extraction were grown to ~70% confluence. Extracted DNA was eluted in 30µl of Nuclease-free water and stored at -20°C.

2.11 POLYMERASE CHAIN REACTION (PCR)

2.11.1 PCR Mixture

GoTaq DNA polymerase reaction was set up in thin walled PCR microcentrifuge tubes. The following reagents were added: 9µl ddH₂O, 1µl of DNA, 1.25µl of 25pmol forward primer, 1.25µl of 25pmol reverse primer and last 12.5µl GoTaq® Green Master Mix (Promega; Cat#M7122) to each tube. In the case of more than one PCR reaction a master mix was prepared.

2.11.2 Proof Reading Taq (KAPA HiFi DNA polymerase)

The KAPA HiFi DNA polymerase reaction was prepared in a thin walled PCR microcentrifuge tubes following manufacturer's instructions (KAPABIOSYSTEMS; Cat#KK2102). In the case of more than on PCR reaction a master mix was prepared.

2.11.3 Colony PCR

A colony PCR was performed using PCR mixture (Section 2.11.1) however, instead of 1µl DNA a pipette tip was touched to the colony and swirled into the reaction mixture. The denaturing step of PCR amplification process (Section 2.11.4) is at 95°C for 5min.

2.11.4 PCR Amplification Process

The amplification process started with an initial denaturing step at 95°C for 2min. The amplification process then cycled through denaturation at 95°C for 30sec, primer annealing at the average melting temperature, 5°C lower than the primers for 30sec and then an extension at 72°C for a time allowing amplification of the length of the gene (~1min/1000bp). The amplification process ends with a final extension at 72°C for 5min and was held at 4°C until removed from the PCR machine (BioRad).

2.11.5 Semi-quantitative RT-PCR

The PCR reaction was performed according to Sections 2.11.1 and 2.11.4. Initial reactions were conducted for 25 cycles using the reference gene primer pairs, β -actin and GapDH (Section 2.5.2), to ensure equal input of cDNA in each reaction. cDNA template volumes were adjusted in subsequent PCR reactions until the intensity of each PCR product was similar. Once input cDNA levels were adjusted, semi-quantitative PCR was performed using gene-specific primers (Section 2.5.2).

2.12 QUANTITATIVE PCR (qPCR) ANALYSIS

2.12.1 Quantitative PCR (qPCR)

The quantitative PCR (qPCR) reaction was performed in 25 μ l reactions with 1 μ l cDNA, 12.5 μ l iQTM SYBR[®] Green Supermix (BioRad; Cat#170-3884), 5pmol of sense and antisense primers (Section 2.5.3). The qPCR reaction was performed in a 96-well iCycler iQ[®] PCR plate (BioRad; Cat#2239441) sealed with microseal 'B' film (BioRad; Cat#MSB1001). The same amplification conditions were used for all primer sets; initial denaturing at 95°C for 3min; amplification process cycled 40x through denaturation at 95°C for 10sec, primer annealing 60°C for 30sec and then an extension at 72°C for 30sec. Emitted fluorescence was measured during the cycled extension phase. A final extension of 95°C for 1min was completed before the melt (dissociation) curve. The melt curve began at 55°C with an increase of 0.5°C until the final temperature of 95°C was reached.

2.12.2 Primer Efficiency: Standard Curve

qPCR (Section 2.12.1) serial dilutions (1:10 or 1:2) of cDNA were performed for each of the gene of interest (GOI) primer sets. The Cycle Threshold (Ct) was plotted against the \log_{10} of gene copies in the template DNA to give the standard curve. Primers with a slope between -3.1 and -3.6, percent efficiencies between 90 - 110% and $R^2 \geq 0.985$ were deemed acceptable. The amplification efficiency of the exponential change per cycle per gene (E) of each primer was calculated by either the slope value (Equation 1) or by the percent efficiency (Equation 2). All primer pair efficiencies can be found in Section 2.5.

Equation 1: $E = 10^{-1/\text{slope}}$

Equation 2 : $E = E\% \times 0.01 + 1$

2.12.3 Primer efficiency: Contamination and Specificity

The negative controls were always checked to ensure there was no amplification and only a single peak was acceptable in the melt (dissociation) curve. All amplified products were sequenced (Section 2.8) to indicate the specificity of the primers to the GOI.

2.12.4 Normalised Cycle Threshold (ΔCt)

To normalise the different concentrations between samples all results were normalised to against two endogenous reference genes β -actin and GapDH (Section 2.5.3). ΔCt was calculated by subtracting the average Ct (\overline{Ct}) of the reference (ref.) gene from the average Ct (\overline{Ct}) of the gene of interest (GOI) (Equation 3). All Ct values were obtained from three biological replicates and three technical replicates of each biological replicate.

Equation 3:
$$\Delta Ct = \overline{Ct}_{GOI} - \overline{Ct}_{ref. genes}$$

2.12.5 Transcript Abundance

The transcript abundance is the quantity of the GOI transcript in relation to the reference gene transcript of a sample (Equation 4). This was calculated using the E value of Section 2.12.2.

Equation 4:
$$\text{Transcript abundance} = E^{-\Delta Ct}$$

2.12.6 Fold Change

Firstly, the difference between GOI ΔCt of a treated sample to a control sample ($\Delta \Delta Ct$) was calculated (Equation 5). Then the $\Delta \Delta Ct$ was used with the E value (Section 2.12.2) to calculate the relative fold change of gene expression due to a treatment (Equation 6).

Equation 5:
$$\Delta \Delta Ct = \Delta Ct_{Treated} - \Delta Ct_{Control}$$

Equation 6:
$$\text{Fold Change} = E^{-\Delta \Delta Ct}$$

2.12.7 Error Bars for Transcript Abundance

Equation 7:
$$\sigma = \sqrt{\frac{\sum (\Delta Ct - \overline{\Delta Ct})^2}{n}}$$

n = the number of the sample size (ΔCt)

Equation 8:
$$SE = \frac{\sigma}{\sqrt{n}}$$

n = the number of the sample size (ΔCt)

Equation 9:
$$\text{Upper} = \left[E^{-(\Delta\text{CT}-\text{SE})} \right] - \text{transcript abundance}$$

Equation 10:
$$\text{Lower} = \text{transcript abundance} - \left[E^{-(\Delta\text{CT}+\text{SE})} \right]$$

2.12.8 Error Bars for Fold Change

The standard deviation (σ) was calculated based on $\Delta\Delta\text{Ct}$ (Equation 11). The standard error (SE) was calculated from the standard deviation (Equation 12) and the upper (Equation 13) and lower error (Equation 14) bars were calculated using the standard error, E (Section 2.12.2) and the fold change (Section 2.12.6).

Equation 11:
$$\sigma = \sqrt{\frac{\sum (\Delta\Delta\text{Ct} - \overline{\Delta\Delta\text{Ct}})^2}{n}}$$

n = the number of the sample size ($\Delta\Delta\text{Ct}$)

Equation 12:
$$\text{SE} = \frac{\sigma}{\sqrt{n}}$$

n = the number of the sample size (ΔCt)

Equation 13:
$$\text{Upper} = \left[E^{-(\Delta\Delta\text{CT}-\text{SE})} \right] - \text{fold change}$$

Equation 14:
$$\text{Lower} = \text{fold change} - \left[E^{-(\Delta\Delta\text{CT}+\text{SE})} \right]$$

2.12.9 Analysis of Variance (ANOVA)

An ANOVA analysis was performed on all qPCR data comparing the normalized cycle threshold (ΔCt) (Section 2.12.4) of the treated samples to the controls or treated samples to their respective treated control. All experiments consisted of three biological replicates and three technical replicates of each biological replicate. All p-values are presented on data as * $p < 0.05$, ** $p < 0.01$, *** $p < 0.001$, unless otherwise stated.

2.13 MICROARRAY

2.13.1 Microarray

RNA was extracted (Section 2.9.1) from NIH3T3 cells which had been treated with purified protein p37 or non-treated NIH3T3 cells. Three biological replicates were taken of each treatment. Genomic contamination was analysed and removed (Section 2.9.2) and RNA integrity and quality checked (Section 2.9.3). RNA was amplified and cDNA synthesized

according to instructions in the Genechip® 3' IVT Express Kit User Manual (Affymetrix; Cat# P/N702646 Rev.8). Following biotin labelling of cDNA and fragmentation, samples were hybridized to Affymetrix Mouse Genome 430 2.0 Arrays, washed using a Genechip® Fluidics Station and scanned using the Genechip® Scanner 3000. Hybridization, washes and scanning was performed at Victorian AgriBiosciences Centre (VABC) (Bundoora, Australia).

2.13.2 Microarray Analysis

Microarray data was processed using the Affymetrix® Expression Console™ Software 1.2 (Affymetrix; Cat# P/N 702387 Rev. 2) and CLC Genomics Workbench 4.7 (CLC bio, <http://www.clcbio.com>; Vat#DK28305087).

2.14 RT²PROFILER™ PCR ARRAY SYSTEM

2.14.1 Sample Preparation

RNA was extracted (Section 2.9.1) from NIH3T3 cells which had been treated with purified protein p37, purified protein p37 and the STAT3 inhibitor (STAT3i), the STAT3i only or non-treated NIH3T3 cells. Three biological replicates were taken of each treatment. Genomic contamination was analysed and removed (Section 2.9.2) and RNA integrity and quality checked (Section 2.9.3).

2.14.2 RT² First Strand Synthesis (SABiosciences Cat#330401)

RNA Reverse Transcription for the RT²Profiler™PCR array System was performed following the User Manual/Handbook (SABiosciences; Part#1022A). The cDNA was diluted with 91µl of H₂O and kept on ice. The cDNA was stored at -20°C.

2.14.3 Real-Time PCR

RT²Profiler™PCR array System was performed following the User Manual/Handbook (SABioscience; Part#1022A). RT² qPCR SYBR Green/Fluor MasterMix was used with the Inflammatory Response & Autoimmunity PCR arrays (SABioscience; Cat# PAMM-077A-12) to analyse the cDNA from Section 2.14.2.

2.14.4 Analysis of data

An ANOVA analysis was performed comparing the cycle threshold (Ct) of the treated samples to the untreated control, unless otherwise stated. All p-values are presented on data as *p<0.05, **p<0.01, ***p<0.001, unless otherwise stated.

2.15 SOLUBLE PROTEIN EXPRESSION AND PURIFICATION

2.15.1 Protein Expression in OneShot®BL21 (DE3)

OneShot®BL21 (DE3) transformants (Section 2.6.2) were selected in accordance to the manufactures' protocol (Invitrogen; Cat#C6000-03). Colony PCR (Section 2.11.3) was used to confirm at least two transformants. The transformants were cultured in 50-100ml LB containing 100µg/ml ampicillin and incubated overnight at 37°C with agitation to saturation ($OD_{600} \geq 2$). The overnight culture was then inoculated into 500-1000ml of pre-warmed LB containing 100µg/ml ampicillin grown to a mid-log of $OD_{600} 0.4 < 0.35$. IPTG was added to a final concentration of 1mM and the cells cultured for an additional 4hrs at 37°C with agitation. The cells were harvested by centrifugation in 50ml Eppendorf tubes and the pellet stored at -80°C overnight, minimum.

2.15.2 Clarification of *E. coli* Lysate under Native Conditions

The cell pellet (Section 2.15.1) was allowed to defrost on ice before being resuspended in 50ml Lysis Buffer (50mM NaH_2PO_4 , 300mM NaCl, 10mM imidazole, pH 8.0). A Complete, Mini Protease Inhibitor Cocktail Tablet (Roche; Cat#11836153001) was added and Lysozyme (100mg/ml) was added to a final concentration of 1mg/ml and sonicated on ice for 30sec intervals for 6 cycles. The lysate was then agitated for 30min at 4°C before being transferred to 2ml microcentrifuge tubes (pre-chilled) and spun at 12000g for 10min at 4°C. The clear lysate was then pooled via filtering through a 25µm filter into a fresh 50ml falcon tube (pre-chilled).

2.15.3 Purification of 6x His Tag Proteins in Native Conditions

Protein purification was achieved through the use of Profinity™ IMAC Resin (BioRad; Cat#156-0123) with deviations from the manufactures protocol. 2ml of the Profinity™ IMAC Resin was added to the prepared cleared lysate (Section 2.15.2). The resin/lysate mixture was incubated for 1hr at 4°C to allow binding of the protein. The mixture was

then centrifuged for 1min at 3000g to pellet resin; supernatant was pipetted off the resin.

The IMAC resin was washed with 10ml Wash Buffer (50mM NaH₂PO₄, 300mM NaCl, 20mM imidazole, pH 8.0) by agitation for 5min at 4°C. The resin/wash mixture was then centrifuged for 1min at 3000g to pellet resin and the supernatant was pipetted off the resin. Protein absorbance readings at 280nm (A₂₈₀) were taken of the supernatant wash. The resin was repeatedly washed until the A₂₈₀ was >0.01. Elution was achieved by the addition of 7ml Elution Buffer (50mM NaH₂PO₄, 300mM NaCl, 500mM imidazole, pH 8.0). The his-tagged proteins were allowed to elute for an hour with agitation at 4°C. The mixture was then centrifuged for 1min at 3000g to pellet resin and 5x 1ml aliquots of the supernatant containing the eluted protein. The eluted protein was stored at -80°C.

2.16 INSOLUBLE PROTEIN EXPRESSION AND PURIFICATION

2.16.1 Isolation of Inclusion Bodies

The cell pellet (Section 2.15.1) was allowed to defrost on ice. The pellet was resuspended in 4ml Resuspension Buffer (20mM Tris-HCl, pH 8.0) for every 100ml culture. A Complete, Mini Protease Inhibitor Cocktail Tablet (Roche; Cat#11836153001) and Lysozyme (100mg/ml) (SIGMA; Cat#L6876) was added to a final concentration of 1mg/ml and sonicated on ice for 10sec intervals for 4 cycles. The lysate was centrifuged at 3000g for 20min at 4°C. Supernatant was discarded and pellet resuspended using a vortex in 3ml Isolation Buffer (20mM Tris-HCl, 0.5M NaCl, pH 8.0) with the assistance of 0.1g of glass beads. The lysate was then centrifuged again at 3000g for 20min. Pellet resuspension in Isolation buffer and centrifugation was repeated.

2.16.2 Solubilisation and Preparation of Inclusion Bodies

The isolated inclusion bodies (Section 2.16.1) pellet was resuspended in 5ml Binding Buffer (20mM Tris-HCl, 0.5M NaCl, 5mM imidazole, 1mM 2-mercaptoethanol, pH 8.0) with the addition of a detergent, discussed in Section 7.2.4, and incubated for 1hr at room temperature with agitation. The lysate was then centrifuged at high speed for 15min at 4°C before being passed through a 0.25µm filter.

2.16.3 Purification of 6x His Tag protein from Inclusion Bodies

The solubilised inclusion bodies (Section 2.16.2) were purified in the same manner as purification under native conditions (Section 2.15.3). However, the Wash buffer consisted of 2M urea, 20mM Tris-HCL, 0.5M NaCl, 5mM imidazole, 1mM 2-mercaptoethanol, pH 8.0 and the Elution buffer consisted of 20mM Tris-HCL, 0.5M NaCl, 5mM imidazole, 1mM 2-mercaptoethanol, pH 8.0.

2.17 PROTEIN ANALYSIS

2.17.1 SDS-PAGE Gels

SDS-PAGE gels were constructed following the Mini-PROTEAN[®] 3 Cell (BioRad; Cat#165-3301/165-3302) manufacturer's instructions. 10cm x 8cm glass Short Plate and a glass Spacer Place that gave 0.75mm thick gel was used to make a 12% acrylamide separating gel (2.5ml 1.5M Tris-HCL, 100 μ l 10% SDS, 3ml 40% acrylamide/bis, 50 μ l 10% ammonium persulfate, 5 μ l N,N,N',N'-tetramethylethane-1,2-diamine, 4.4ml ddH₂O) with a 4% acrylamide stacking gel (2.5ml 0.5M Tris-HCL, 100 μ l 10% SDS, 1ml 40% acrylamide/bis, 50 μ l 10% ammonium persulfate, 10 μ l N,N,N',N'-tetramethylethane-1,2-diamine, 6.4ml ddH₂O). The comb used allowed for 10 wells.

The Mini-PROTEAN 3 Cell Mini Tank (BioRad; Cat#165-3302) was assembled according to the manufacturer's instructions. Loading buffer (2.5ml 0.5M Tris-HCL, 0.4g 10% SDS, 2ml glycerol, 0.2ml β -mercaptoethanol, 0.1mg bromophenol blue, ddH₂O up to 10ml) was added to a selected amount of purified protein sample to give a total of 20 μ l. The samples were heated to 95°C for 10min and then loaded on the SDS-PAGE gel. The gels ran for 60min at 200 volts at 4°C (Bio-RAD PowerPac[™] Basic power Supply). The gel was removed from the glass plates using a wet spatula.

2.17.2 Coomassie Blue Staining of SDS-PAGE gels

To determine purification efficiency SDS-PAGE gels (Section 2.17.1) were stained with 0.1% Coomassie Blue Stain (0.1% Coomassie Blue R-250, 40% Methanol, 10% Acetic acid). The SDS-PAGE gel was placed into a clean square petri dish, covered with 10 ml Fixing Solution (50% Methanol, 10% Acetic acid) and incubated at room temperature for 10 min

with gentle agitation. The Fixing Solution was aspirated off and the gel covered in 0.1% Coomassie Blue Solution, incubated overnight at room temperature with gentle agitation. The following day the gel was covered with destaining solution (40% Methanol, 10% Acetic acid) for 2 hrs at room temperature with gentle agitation. The gel was then scanned onto the computer.

2.17.3 WESTERN

WESTERNS were constructed following the BIO-RAD Mini Trans-Blot® Electrophoretic protocol (Cat# 170-3930/170-3935) using the gels from Section 2.17.1. The BIO-RAD Mini Trans-Blot® Electrophoretic system ran either overnight at 30V or 2hrs at 200V.

2.17.4 Colorimetric Analysis of a WESTERN Membrane using Primary and Secondary Antibodies

The membrane was immersed in 10ml of 5% non-fat dried milk for 1hr with agitation at room temperature and washed twice for 5min with TBST buffer (137 mM NaCl, 20 mM Tris, 0.1% Tween-20). The membrane was incubated again for 1hr with the T7-Tag monoclonal antibody (Novagen; Cat#69522) diluted 1:10000 in 5% non-fat dried milk. After three washes with 10ml TBST buffer for 5min the membrane was incubated with goat anti-mouse IgG Horseradish Peroxide (HRP) conjugate (Invitrogen; Cat#G-21040) diluted 1:10000 in 5% non-fat dried milk for 1hr at room temp. The membrane was sequentially washed four more times with 10ml TBST buffer for 5min and all excess buffer removed. Alkaline Phosphatase Colourimetric development was then used (Section 2.17.5).

2.17.5 Alkaline Phosphatase Colorimetric development of a WESTERN Membrane

WESTERNS were developed following the manufacturers instructions using the Alkaline Phosphatase Conjugate Substrate Kit (BioRad; Cat#170-6432). The membrane was exposed to light for 10minutes with agitation except where longer exposure was required. Membranes were washed in ddH₂O to stop reaction before scanning.

2.17.6 Protein Size Analysis

The PageRuler Prestained Protein Ladder (Fermentas; Cat#SM0671) was used to determine the approximate size of the proteins.

2.17.7 Protein Quantification

A series of protein standards and the protein samples were assayed following Pierce® BCA Protein Assay Kit (ThermoScientific; Cat#23227). The data were imported into Excel and a standard curve produced (Figure 2.1). The concentration of the protein samples was calculated using the standard curve equation in addition to the concentrations produced by the BCA program of the Eppendorf BioPhotometer 6131.

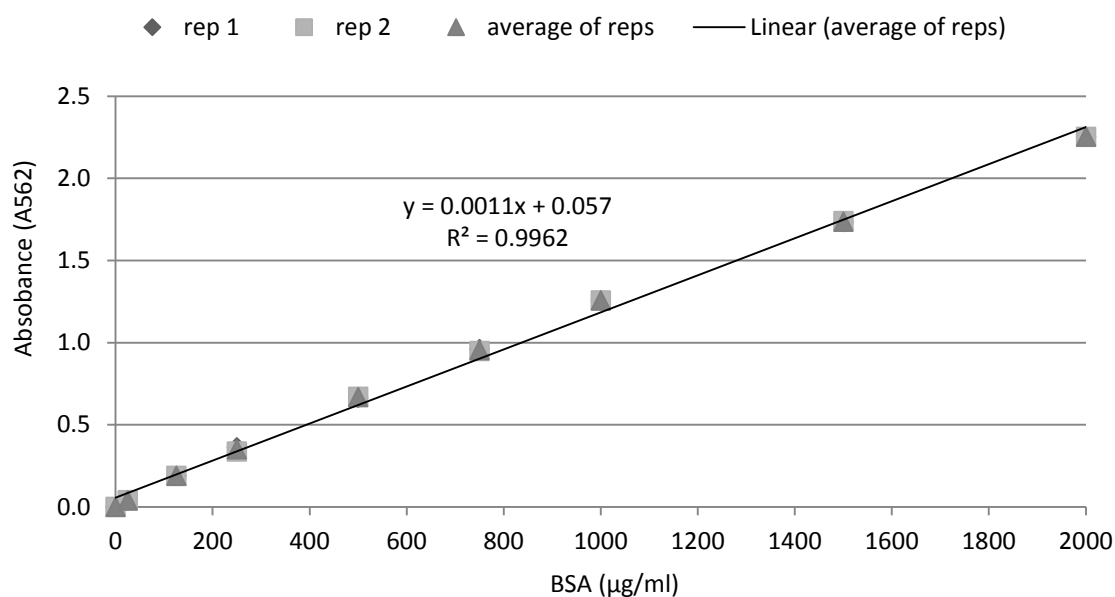


Figure 2.1: Standard curve for the Pierce® BSA Protein Assay Kit. Nine concentrations of the bovine serum albumin (BSA) were assayed in duplicate. The absorbances (A562) of the replicates (reps 1&2) and average of the reps were plotted. The line of best fit was drawn through the average of the reps and equation of the line determines ($y=0.0011x + 0.057$). The concentrations of unknown samples were determined by using the Pierce® BSA Assay to ascertain an absorbance and the line of best fit equation.

2.18 MAMMALIAN TISSUE CULTURE AND TRANSFORMATION

2.18.1 Passaging

Tissue culture cells were cultured in complete DMEM10%FCS medium (13.42g/L Dulbecco's Modified Eagle's Medium (DMEM), 100ml fetal calf serum (FCS), 3.7g/L NaHCO₃, 20ml/L penicillin/streptomycin, pH 7.2) and incubated in a Water-Jacketed Incubator (Forma Scientific). The incubator was automatically regulated at 37°C with 5% CO₂. Medium was changed every three days and the Mycoplasma antibiotic Plasmocin™ (InvivoGen; Cat# ant-mpt) was added to all culture media at a concentration of 5µg/ml.

Cells approaching 70% confluence were passaged; additionally cells were disposed of if they reached $\geq 80\%$ confluence. The DMEM10%FCS medium was aspirated from the

tissue culture dish and the cells rinsed twice with 5ml 1xPBS (137mM NaCl, 2.7mM KCl, 10mM Na₂HPO₄.2H₂O, 2mM KH₂PO₄. pH 7.4). 10% trypsin was added to the tissue culture dish at a volume of 1% of the original DMEM10%FCS medium. Tissue culture plates were then incubated for 5min allowing the cells to lift. The 10% trypsin was forcefully pipetted over the cell culture plate to assist in cell collection. The suspension was split into new tissue culture plates at desired concentrations or appropriate vessels for specific experiments. Each tissue culture plate contains the appropriate volume of medium (Table 2.2).

Table 2.2: Appropriate volumes of media required for tissue culture plates

Size of tissue culture plates	Media volume (ml)
Tissue culture plate (∅ 60mm)	10
6-well tissue culture plate (∅ 35mm)	2
12-well tissue culture plate (∅ 22.6mm)	1
24-well tissue culture plate (∅ 16mm)	0.5

2.18.2 Freezing Down

Selected cell cultures that had reached 70% confluence were frozen down. Lifted cells (Section 2.18.1) were diluted by 5ml DMEM10%FCS in a 15ml falcon tube and centrifuged for 10min at 11000rpm. The supernatant was aspirated and the cell pellet re-suspended in 1ml FCS and then 1ml 20%DMSO/FCS solution. Immediately 1ml aliquots were transferred to labelled cryovials and placed into a Nalgene™ Cryo1 1°C freezing container (Nalgene; Cat#5100-0001) known as 'Mr. Frosty'. The 'Mr. Frosty' allowed the cooling of the samples at a rate of -1°C/min. The 'Mr. Frosty' was stored at -80°C overnight and then the cryovials were transferred into liquid nitrogen dewars.

2.18.3 Defrosting Cell Cultures

A cryovial containing frozen cells (Section 2.18.2) was thawed rapidly. The cells were inoculated to one side of a ∅ 60mm tissue culture plate and 5ml of room temperature DMEM10%FCS to the other. Drop-wise 5ml of DMEM10%FCS was added gently to the cell suspension with continued mixing. Once the two inoculates were mixed the cells were gently rocked to assure even coverage over the plate and incubated (Section 2.18.1) overnight. The following day the medium was aspirated off along with any dead cells and replaced with fresh medium.

2.18.4 Kill Curve

Cells were grown to 20% confluence and passaged (Section 2.18.1) into 6-well plates with equal concentrations. Hygromycin B is an antibiotic that inhibits growth in both prokaryotic and eukaryotic cells. Hygromycin B (Invitrogen; SKU#10687-010) was added to each well in varying concentrations constructing a serial dilution. The DMEM10%FCS and antibiotic were changed every 3 days and die off recorded. The kill curve was terminated at day 18 and confluence recorded (Figure 2.2).

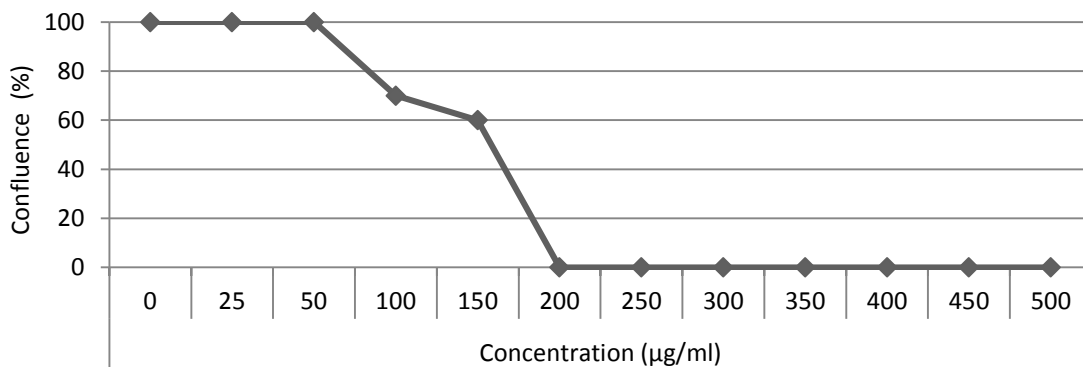


Figure 2.2: Kill curve of NIH3T3 cell confluence at various hygromycin concentrations at day 18. NIH3T3 cells were treated at concentrations ranging from 0 to 500µg/ml and the confluence determined at day 18.

2.18.5 Lipofection of NIH3T3 cells

Transformations of cells was carried out in accordance to the manufacturer's instructions of the DOTAP Liposomal Transfection Reagent (Roche; Cat#11202375001). 9µg of plasmid DNA was used and cells were incubated for 6hrs. After the 6hr period the DMEM10%FCS was replaced with fresh DMEM10%FCS with Hygromycin B. A concentration of 200µg/ml Hygromycin B over 18 days was required for the isolation of pSTp37 (Section 2.2.2) transfected NIH3T3 clones.

2.18.6 Isolating a Clone

After lipofection (Section 2.18.5) colonies were observed and their position marked on the bottom of the 6-well tissue culture plate. The medium was aspirated off and cells washed with 5ml 1x PBS. A scintillated glass ring coated in sterile silicone was placed around the marked cell colonies, 500µl of 10% trypsin placed into the ring and the plates incubated for 5min to allow cells to lift. The 10% trypsin was pipetted up and down several times and passaged into a new cell culture plate containing DMEM10%FCS with

Hygromycin B. A concentration of 100µg/ml Hygromycin B was used to maintain selection.

2.18.7 Mycoplasma Detection PCR

All cell cultures were tested for the contamination of over 30 Mycoplasma species, including *M. hyorhinis*. The Mycoplasma primers (Section 2.5.1) were selected from Wirth et al. (1994) and the PCR conditions of Uphoff and Drexler (2002) were followed.

2.18.8 Using a Haemocytometer

A haemocytometer was used to determine the concentration of cells in suspension following the protocol of Cascade Biologics™. Triplicates were done and an average taken of cell concentrations.

2.19 TREATING MAMMALIAN CELLS

2.19.1 Preparing NIH3T3 cells for treatment

NIH3T3 cells were passaged (Section 2.18.1) into the required amount of tissue culture plates to allow for three biological replicates per treatment. Cells were grown to 60% confluence. Before treatment, DMEM10%FCS medium was aspirated and cell cultures washed twice with 1xPBS. All NIH3T3 lines originated from the same freeze down batch at passage 10 and treatment occurred before passage 15.

Treatment was terminated by washing and lysis of cells for immediate RNA extractions (Section 2.9.1). Cells were observed post-treatment for toxicity levels, if there was an observable toxic effect the experiment was terminated.

2.19.2 Treating NIH3T3 cells with the purified p37 protein

DMEM10%FCS medium with the required concentration of purified p37 was added to the cells and the culture plates incubated in a Water-Jacketed Incubator (Forma Scientific) over 24hr. The incubator was automatically regulated at 37°C with 5% CO₂.

In the case of time trials, cell treatments were initiated at times that allowed for all treatment courses to be synchronised and ready for RNA extraction at T₀ (Figure 2.3). For

example at $-T_{24}$ 24hr treatment was initiated and at $-T_{12}$ 12hr treatment was initiated, however both treatments were terminated at T_0 . Therefore, all cells were in culture for the same amount of time but treatment was only for the required time.

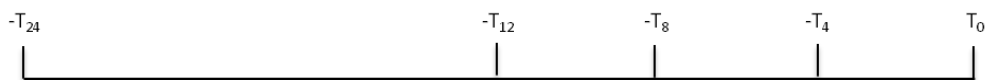


Figure 2.3: Time line for time treatment of NIH3T3 cells. NIH3T3 cell treatments based on time were initiated at times that allowed for termination at T_0 . The time the cells were to be treated was subtracted from T_0 ; for example 24hrs ($-T_{24}$), 12hrs ($-T_{12}$), 8hrs ($-T_8$) and 4hrs ($-T_4$).

2.19.3 IL6R α treatment

NIH3T3 cells were prepared (Section 2.19.1). The NIH3T3 cells were pre-incubated with DMEM10%FCS containing the required concentration of LEAFTM purified anti-mouse/rat CD126 (Biolegend; Cat#115809) inhibitor for an hour. Cultures were then 24hr-treated with or without p37. Purified p37 was added via pipetting into the DMEM10%FCS at the side of the tissue culture plate and mixing via gentle rocking. The cultures were incubated in a Water-Jacketed Incubator (Forma Scientific). The incubator was automatically regulated at 37°C with 5% CO₂.

2.19.4 STAT3 Inhibitor VI (S31-201) treatment

NIH3T3 cells were prepared (Section 2.19.1) for treatment, however, they were only grown to 50% confluence. The NIH3T3 cells were pre-incubated with DMEM10%FCS containing the required concentration of STAT3 Inhibitor VI (Santa Cruz Biotechnology; Cat#sc-204304) (S31-201) for 24hrs. Cultures were treated for a further 24hrs with or without p37. Purified p37 was added via pipetting into the DMEM10%FCS at the side of the tissue culture plate and mixing via gentle rocking. The cultures were incubated in a Water-Jacketed Incubator (Forma Scientific). The incubator was automatically regulated at 37°C with 5% CO₂.

2.19.5 LPS treatment

NIH3T3 cells were prepared (Section 2.19.1). The NIH3T3 cells were pre-incubated with DMEM10%FCS containing the required concentration of Ultra pure lipopolysaccharide from *E. coli* 0111:B4 strain – TLR4 ligand (Invivogen; Cat#tlrl-3pelps). The cultures were then incubated in a Water-Jacketed Incubator (Forma Scientific) for 24hr. The incubator

was automatically regulated at 37°C with 5% CO₂.

2.19.6 VIPER or CP7 treatment

NIH3T3 cells were prepared (Section 2.19.1). The NIH3T3 cells were pre-incubated with DMEM10%FCS containing the required concentration of VIPER or CP7 (IMGENEX; Cat# IMG-2011set) for 2hr. Cultures were then 24hr-treated with or without p37. Purified p37 was added via pipetting into the DMEM10%FCS at the side of the tissue culture plate and mixing via gentle rocking. The cultures were incubated in a Water-Jacketed Incubator (Forma Scientific). The incubator was automatically regulated at 37°C with 5% CO₂.

2.20 CYTOSKELETON: G-LISA™ RHOA ACTIVATION ASSAY BIOCHEM KIT (ABSORBANCE ASSAY)

RhoA activation was determined following the manufacturer's protocol (Cat#BK124). NIH3T3 fibroblasts were treated with p37 at selected time points (Sections 2.19.1) of 30min, 2, 4 and 24hrs. Biological and experimental triplicates were done. Normalised Active RhoA was calculated following the manufacturer's protocol (Cat#BK124).

2.21 WOUND HEALING ASSAYS

2.21.1 Wounding cell culture

Three horizontal lines were marked on the base of several tissue culture plates. NIH3T3 cells were grown to a 100% confluent monolayer and scratched using a sterile pipette tip, forming a wound of approximately 30µm. Cell debris was washed away with 1xPBS and DMEM10%FCS was added. All culture plates were incubated in a Water-Jacketed Incubator (Forma Scientific) for 38hr. The incubator was automatically regulated at 37°C with 5% CO₂. Images were captured at 0, 14, 19, 24 and 38hr. Six images were captured per time point per plate (Figure 2.4).

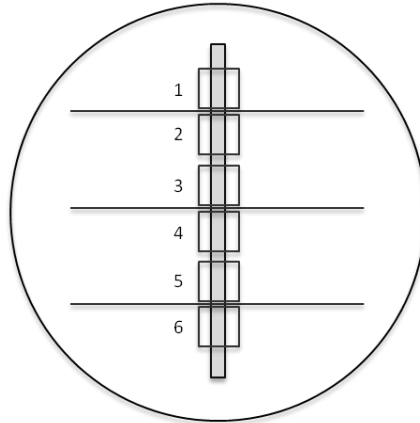
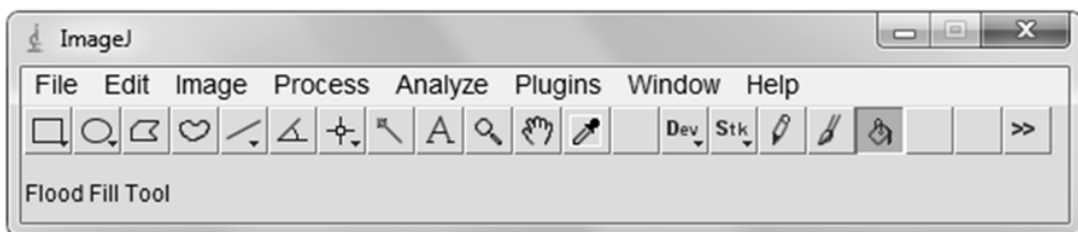


Figure 2.4: Location of the images captured per wound. NIH3T3 cells were grown to 100% confluence and a single wound was scratched (vertical grey line) and three horizontal lines were drawn on the base of the plate across the wound. Six images were captured (squares) of the wound on either side of the drawn lines.

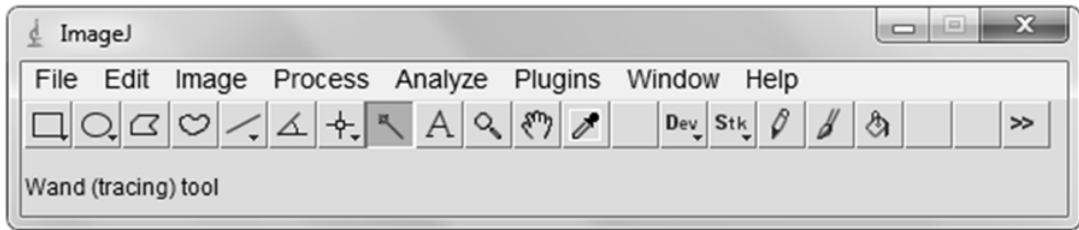
2.21.2 Analysis with ImageJ

The images captured (Section 2.21.1) were loaded onto the computer and printed; all images were printed at the same size. Outlines of the wounds were traced with a black marker onto overhead transparency sheets. The outlines were scanned into ImageJ and the following steps followed;

1. Process > Find edges
2. Image > Adjust > Threshold; Select B/W > untick dark background
3. Analyze > Set scale> Pixel Distance: 8.718, known dis: 1, Pixel aspect: 1; unit of length: um.
4. Select Flood Fill Tool and fill in wound area



5. Select Wand (tracing) Tool and select blacked out wound area (sometimes there was multiple blacked out areas therefore steps 5 & 6 are repeated for a single image).



6. Ctrl M to analyse
7. Analyse data using excel

2.21.3 Calculating the migration cell surface area

ImageJ calculated the area of the wound that was not closed. To establish the area to which the cells had migrated at each time point the area of the wound at time X was subtracted from the initial area of the wound.

3. GENE EXPRESSION PROFILING OF p37 TREATED NIH3T3 (MOUSE) FIBROBLASTS

3.1 INTRODUCTION

The addition of p37 to cells in culture has varied effects inducing loss of heterotypic contact inhibition (FS9 and NIH3T3 cells) (Steinemann et al., 1984a; Schmidhauser et al., 1990; Darren Lowen, PhD Thesis, La Trobe University, 1995) and increased rate of migration, proliferation, vacuolation and protein synthesis (prostatic cancer cells) (Goodison et al., 2007). Human gastric carcinoma (AGS) cells exhibited increased migration as determined using a transwell migration assay including a Matrigel layer (Gong et al., 2008). Cell-cell adhesion was reduced in p37-treated D2F2 mouse mammary cells and the reduction more severe in cells also expressing the HER2 receptor gene (Liu et al., 2006).

Microarray analysis has been used to identify genes whose expression is affected in the human prostate cancer cell line PC-3 (highly metastatic) and DU145 (metastatic) due to the addition of p37 (Goodison et al., 2007). The cyclin D1 cyclin-dependent kinase inhibitors *CDKN1B*, *CDC25B* and *CDC25C* were down-regulated, suggesting cell cycle control may be affected. Down-regulation of these genes is associated with cancer progression leading to cell proliferation. Treatment of the PC-3 cells with p37 resulted in increased expression levels of several Ras superfamily proteins (data no longer available), the cytokines IL8, IL6 and TNF (data no longer available) and chemokines (data no longer available) (Goodison et al., 2007).

The expression levels of selected genes were determined following p37 addition to human peripheral blood mononuclear cells (PBMC) and AGS cells transfected with the *p37* gene. Increased gene expression and secretion of TNF α resulted from p37-treatment of PBMCs (Ning et al., 2003a). TNF α over expression can increase the metastatic potential of cells (Szlosarek et al., 2006; Cui et al., 2008). AGS cells stably transfected with the *p37* gene down-regulated the expression levels of Intracellular Adhesion Molecule 1 (ICAM1) and Integrin- β 1 (Liu et al., 2006). AGS cells and embryonic kidney (HEK-293) cells

transfected with *p37* exhibited anchorage independent growth (easily detach from one another and the culture plate) and showed a reduced level of senescence (cell death) compared to AGS controls (Liu et al., 2007). The levels of the 72kDa matrix metalloproteinase 2 (Mmp2) protein increased in the media of both p37-treated and *p37*-transfected AGS cells (Gong et al., 2008). Changes in expression of other genes in these cells lines were not reported.

The aim of the work reported in this chapter was to determine the effect of p37-treatment on gene expression in NIH3T3 cells. A microarray analysis was carried out and quantitative (q) PCR used to validate the microarray data. Various concentrations of p37 were also tested, as were the effect of different treatment times.

3.2 RESULTS AND DISCUSSION

3.2.1 Purification of the p37 Protein

The *p37* gene contains several TGA termination codons which in *Mycoplasma* species are read as a tryptophan codon. To express the p37 protein in *Escherichia coli*, Darren Lowen (PhD Thesis, La Trobe University, 1995) implemented site directed mutagenesis to change all TGA to TGG codons, the tryptophan codon of *E. coli* (Figure 3.1).

M. hyorhinitis p37	CATGTTCTAA	TACAGGAGTA	GTCAAGCAAG	AGGATGTATC	AGTTAGTCAA	GGTCAA	TGAG	ATAAAAGTAT	AACATTTGGT	80
p37 (7x TGG mut)	CATGTTCTAA	TACAGGAGTA	GTCAAGCAAG	AGGATGTATC	AGTTAGTCAA	GGTCAA	TGGG	ATAAAAGTAT	AACATTTGGT	80
M. hyorhinitis p37	GTTTCAGAAG	CTTGGTTAAA	CAAGAAAAAA	GGAGGTGAAA	AAGTTAACAA	AGAAGTTATT		AATACATTTT	TAGAAAAATTT	160
p37 (7x TGG mut)	GTTTCAGAAG	CTTGGTTAAA	CAAGAAAAAA	GGAGGTGAAA	AAGTTAACAA	AGAAGTTATT		AATACATTTT	TAGAAAAATTT	160
M. hyorhinitis p37	CAAAAAAGAA	TTTAATAAAC	TCAAAAATGC	AAATGATAAA	ACCAAAAAC	TCGATGACGT		TGATTTTAAA	GTAACCTCAA	240
p37 (7x TGG mut)	CAAAAAAGAA	TTTAATAAAC	TCAAAAATGC	AAATGATAAA	ACCAAAAAC	TCGATGACGT		TGATTTTAAA	GTAACCTCAA	240
M. hyorhinitis p37	TTCAAGACTT	TACTGTGTTG	TAAACAATT	TATCTACTGA	CAATCCTGAA	TTAGATTTTG		GAATTAATGC	TTCAGGAAAA	320
p37 (7x TGG mut)	TTCAAGACTT	TACTGTGTTG	TAAACAATT	TATCTACTGA	CAATCCTGAA	TTAGATTTTG		GAATTAATGC	TTCAGGAAAA	320
M. hyorhinitis p37	TTGGTAGAAT	TTCTAAAAAA	TAATCCTGGT	ATAATAACTC	CAGCATTAGA	AACAACAAC		AATTCCTTTG	TATTTGACAA	400
p37 (7x TGG mut)	TTGGTAGAAT	TTCTAAAAAA	TAATCCTGGT	ATAATAACTC	CAGCATTAGA	AACAACAAC		AATTCCTTTG	TATTTGACAA	400
M. hyorhinitis p37	AGAAAAAGAT	AAATTTTATG	TTGATGGTAC	AGATTCAGAT	CCACTTGTA	AAATTGCTAA		AGAAATTAAT	AAAATTTTGG	480
p37 (7x TGG mut)	AGAAAAAGAT	AAATTTTATG	TTGATGGTAC	AGATTCAGAT	CCACTTGTA	AAATTGCTAA		AGAAATTAAT	AAAATTTTGG	480
M. hyorhinitis p37	TTGAAACTCC	ATATGCAAGT	TGA	ACTGATG	AAAATCATAA	GGA	ATGGT	AATGTTTATC	AAAGTGTTTA	560
p37 (7x TGG mut)	TTGAAACTCC	ATATGCAAGT	TGG	ACTGATG	AAAATCATAA	GGG	ATGGT	AATGTTTATC	AAAGTGTTTA	560
M. hyorhinitis p37	GTTCAAGCTA	ATTTTTATAG	AGGAATGATT	TGA	TAAAAAG	GTAATGATGA		AACCTAGCT	AAAATTAATA	640
p37 (7x TGG mut)	GTTCAAGCTA	ATTTTTATAG	AGGAATGATT	TGG	TAAAAAG	GTAATGATGA		AACCTAGCT	AAAATTAATA	640
M. hyorhinitis p37	TGATAAAGAT	TGA	TATACAT	TTAGAAATTT	TGGAATTTTA	CACGGTAAAG		ATAATTCCTT	TTCTAAATTC	720
p37 (7x TGG mut)	TGATAAAGAT	TGG	TATACAT	TTAGAAATTT	TGGAATTTTA	CACGGTAAAG		ATAATTCCTT	TTCTAAATTC	720
M. hyorhinitis p37	AAACTATATT	AAAAAACCCAC	TTTCAAATA	AATTTACAAC	ACTAAATGAA	GACAGAAGCG		CACATCCAAA	CGCATATAAA	800
p37 (7x TGG mut)	AAACTATATT	AAAAAACCCAC	TTTCAAATA	AATTTACAAC	ACTAAATGAA	GACAGAAGCG		CACATCCAAA	CGCATATAAA	800
M. hyorhinitis p37	CAAAAACTG	CAGATACATT	GGGAACTTTA	GATGATTTCC	ATATTGCTTT	TTCAGAAGAA		GGTCTTTTTG	CTTGAACACA	880
p37 (7x TGG mut)	CAAAAACTG	CAGATACATT	GGGAACTTTA	GATGATTTCC	ATATTGCTTT	TTCAGAAGAA		GGTCTTTTTG	CTTGGACACA	880
M. hyorhinitis p37	TAACAAATCA	GCAACAAAAC	CTTTTGAAAC	TAAAGCAAAT	GAAAAGATGG	AAGCACTTAT		AGTAACTAAT	CCAATTCCTG	960
p37 (7x TGG mut)	TAACAAATCA	GCAACAAAAC	CTTTTGAAAC	TAAAGCAAAT	GAAAAGATGG	AAGCACTTAT		AGTAACTAAT	CCAATTCCTG	960
M. hyorhinitis p37	ATGATGTTGG	AGTGTTTGA	AAAAGTGTTA	ACCAATTAGA	ACAAAATTTA	ATTGTTCAA		CATTCATTA	TTTAGCTAAA	1040
p37 (7x TGG mut)	ATGATGTTGG	AGTGTTTGA	AAAAGTGTTA	ACCAATTAGA	ACAAAATTTA	ATTGTTCAA		CATTCATTA	TTTAGCTAAA	1040
M. hyorhinitis p37	AATAACAAG	ATACATATGG	CCCACTTTTA	GGGTATAATG	GTTATAAAAA	AATTGACAA		TTCCAAAAG	AGATTGTAGA	1120
p37 (7x TGG mut)	AATAACAAG	ATACATATGG	CCCACTTTTA	GGGTATAATG	GTTATAAAAA	AATTGACAA		TTCCAAAAG	AGATTGTAGA	1120
M. hyorhinitis p37	AGTTTATGAA	AAAGCCATTA	AATAA	1145						
p37 (7x TGG mut)	AGTTTATGAA	AAAGCCATTA	AATAA	1145						

Figure 3.1: Sequence alignment of the *Mycoplasma hyorhinitis p37* (*M. hyorhinitis p37*) gene to the *p37* gene containing seven nucleotide mutations from TGA to TGG (*p37 (7x TGG mut)*). Seven *Mycoplasma* TGA codons for tryptophan, within the *p37* gene, were mutated to the *E. coli* TGG codon for tryptophan allowing expression within *E. coli*. The seven TGA to TGG mutations are boxed.

The mutated 1.1kb *p37* gene was cloned into the pUC-derived pRSET A expression vector (pRAp37) (Section 2.2.1; Figure 3.1), and sequenced (Section 2.8.1) using T7 primers (Section 2.5.1; T7_F/R). The pRAp37 construct was transformed into BL2(DE3) *E. coli* cells via heat shock (Section 2.6.2) and plated onto 2YT Amp⁺ plates. Colonies were screened via colony PCR (Section 2.11.3) using T7 primers (Section 2.5.1; T7_F/R). The colonies exhibiting the highest transformation efficiency were used for further protein expression studies.

Recombinant p37 protein expression was induced in BL2(DE3) *E. coli* cultures by a 4hr IPTG treatment (Section 2.15.1). Aliquots of 10µl culture were collected every hour and cells lysed by heating to 95°C for 10min. The fourth hour aliquot was pelleted, lysed and centrifuged separating soluble and insoluble fractions. The proteins were reduced with an equal volume of SDS-loading buffer and run on 12% sodium dodecyl sulfate (SDS) polyacrylamide gel by electrophoresis (PAGE) (Section 2.17). The proteins were transferred to a nitrocellulose membrane for expression evaluation by Western blot analysis (Figure 3.2). The p37 protein was detected using a T7-Tag monoclonal primary antibody and a goat anti-mouse-AP conjugated secondary antibody (Section 2.17). The Western blot analysis showed that the p37 protein was stably expressed during the 4hrs of IPTG induction and present within both the insoluble and soluble fractions (although at higher concentrations in the latter) of the *E. coli* lysate (Figure 3.2). The purified p37 protein gave a single band at the predicted 48kDa size on the SDS gel (Section 2.2.1).

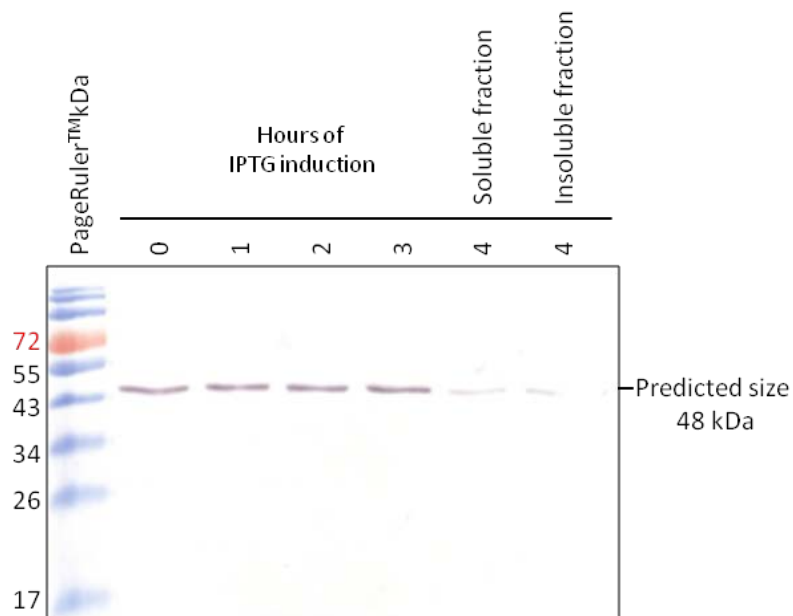


Figure 3.2: Western blot of IPTG induced p37 protein expression. *E. coli* cultures were IPTG treated over 4hrs and 10 μ l aliquots taken every hour. The 4th hour aliquot was separated into soluble and insoluble fractions. The 10 μ l aliquots of 1, 2 and 3hrs and the soluble and insoluble fractions of 4hrs were run on a 12% SDS-PAGE and transferred to a nitrocellulose membrane (Section 2.17.3). The p37 protein was detected by Western blot using a T7-Tag monoclonal primary antibody and a goat anti-mouse-AP conjugated secondary antibody producing a band at the predicted 48kDa (Section 2.17.4). The PageRuler Prestained Protein Ladder (Fermentas; Cat#SM0671) was used to analyse protein size.

Soluble p37 protein, expressed by *E. coli* cells treated with IPTG for 4hrs, was purified by Ni-affinity chromatography (Section 2.15.3). The protein from three eluted fractions was analyzed on a 12% SDS-PAGE by Coomassie Blue staining (Section 2.17.2) (Figure 3.3A). The three eluted fractions were also analyzed by Western blotting (Section 2.17.4) (Figure 3.3B). Elutions 1 and 2 were pooled and the concentration of the purified p37 protein was established, using the standard curve of a BSA assay, as 170.5 μ g/ml (Section 2.17.7). The identity of the p37 protein was further confirmed using protein sequencing (Appendix I).

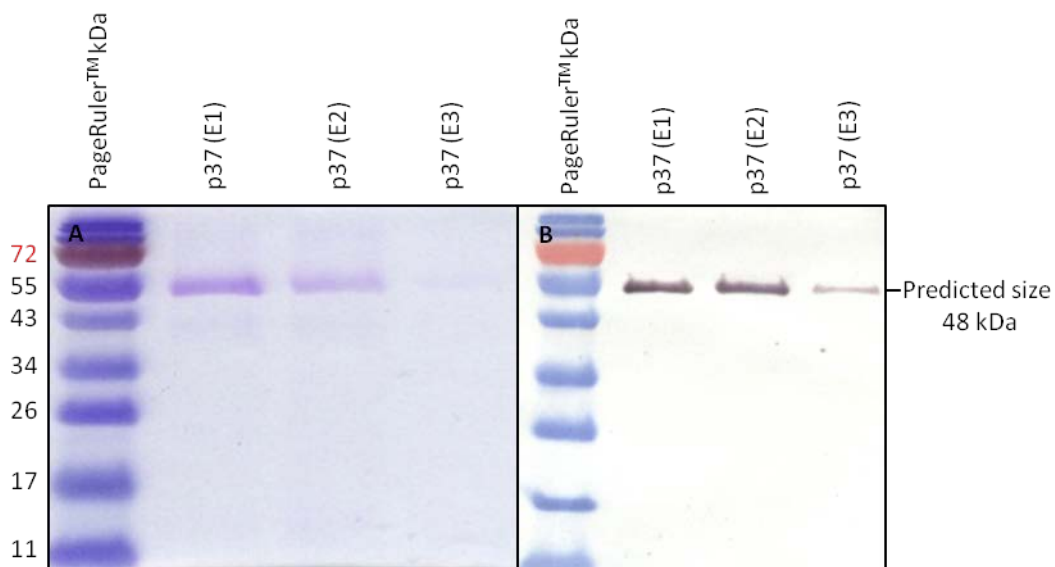


Figure 3.3: Purification of (His)₆-p37 protein using Ni-affinity chromatography. Three 5ml aliquots (E1,2&3) of purified p37 protein were collected (Section 0). **(A)** Coomassie blue stained gel; 10 μ l of each elution (E1-3) of purified p37 were run on a 12% SDS-PAGE (Section 2.17.2). **(B)** Western blot analysis; 10 μ l of each elution (E1-3) of purified p37 were run on a 12% SDS-PAGE and transferred to a nitrocellulose membrane (Section 2.17.3). A T7-Tag monoclonal primary antibody and a goat anti-mouse-AP conjugated secondary antibody was used to identify the p37 protein (Section 2.17.4). The PageRuler Prestained Protein Ladder (Fermentas; Cat#SM0671) was used to analyse protein size.

3.2.2 Gene Expression profiling of p37-treated NIH3T3 fibroblasts

Gene expression profiling of embryonic NIH3T3 (mouse) fibroblasts treated with the purified p37 protein (15µg/ml) was carried out using microarray technology. Messenger RNA (mRNA) was extracted from triplicate, 24hr p37-treated and non-treated NIH3T3 cell cultures and hybridized to Affymetrix Gene Chip® Mouse Genome 430A 2.0 Arrays (Section 2.19.2, 2.13). Megan Drew (Honours, LTU, 2006) provided the purified p37 for this microarray and total RNA was extracted after a 24hr p37-treatment. Sylvana Iacone and Huy Phan assisted with the first microarray experiment. Expression levels of 537 genes were significantly ($p \leq 0.001$) affected in 24hr p37-treated NIH3T3 fibroblasts; 288 genes were up-regulated (fold-change ≥ 3) and 249 down-regulated (fold-change ≤ 3) (Table 3.1). The lists of the genes significantly up and down-regulated are included in Appendix II and Appendix III.

Table 3.1: Number of genes identified in the microarray that were significantly up- and down-regulated (p -value ≤ 0.001 , $fc \leq$ or ≥ 3). The lists of genes up- and down-regulated are provided in Appendix II and Appendix III.

Total N° of genes detected on the array	537
Genes Up-regulated ($fc \geq 3$)	288
Genes Down-regulated ($fc \leq 3$)	249

Gene Ontology (GO), via the Mouse Genome Informatics Database, was used to assign GO terms to the 288 up-regulated genes, on a protein level, and separated into three classes: Cellular Components, Molecular Processes and Biological Processes (Figure 3.4). Cellular Components are either parts of the cell or its extracellular environment (e.g. nucleus or cytoskeleton), Molecular Processes are the activities of the gene products (e.g. nucleic acid binding or enzyme regulator activity) and Biological Processes are the proteins involved in molecular events regulating a cellular function (e.g. cell cycle proliferation or apoptosis). Since individual proteins can be responsible for a variety of molecular and biological processes and be located in different cellular components, a single protein can be associated with more than one GO term.

GO 'Cellular Component' classification assigned the majority of the 288 proteins up-regulated by p37 to the nucleus (91/288) (

Figure 3.4A) and under GO 'Molecular Processes' 36/288 proteins were assigned to nucleic acid binding and 29/288 to signal transduction activity (Figure 3.4B). GO 'Biological Process' classification assigned 60/288 proteins to cell cycle proliferation, 59/288 to cell organisation and biogenesis and 56/288 to developmental processes (Figure 3.4C).

Under the 'Cellular Component' classification, the 10 genes identified as most strongly up-regulated in the microarray were found to locate to the extracellular matrix and plasma membrane (7/10 and 3/10, respectively). These genes were involved in signal transduction (2/10) and enzyme regulation (2/10) under the 'Molecular Process' classification and mainly stress response (5/10) under the 'Biological Process' classification.

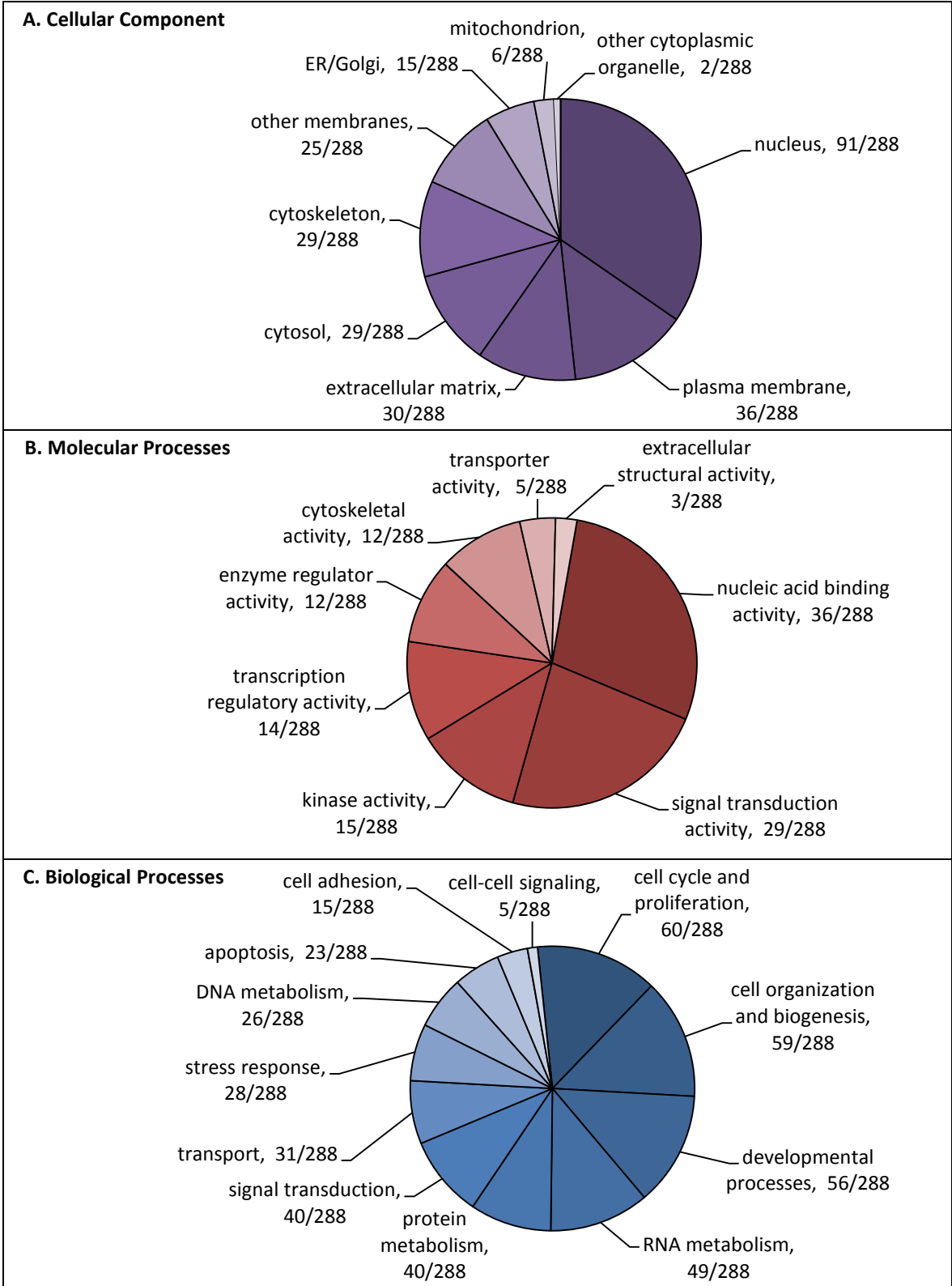


Figure 3.4: Gene Ontology (GO) assignments of significantly up-regulated ($p \leq 0.001$, $fc \geq 3$) genes identified in the microarray at the protein level. (A) Cellular components. (B) Molecular Processes. (C) Biological Processes. GO classifications were extracted from the Mouse Genome Informatics Database. Note: An individual protein can be associated with more than one GOterm.

Eighteen of the 288 genes significantly ($p \leq 0.001$) up-regulated (fold change ≥ 3) in the 24hr, p37-treated NIH3T3 fibroblasts were chosen for further analysis. The first ten genes were selected primarily due to their high fold-change. These genes were *Lipocalin 2 (Lcn2)*, *Haptoglobin (Hp)*, *Serum amyloid A3 (Saa3)*, *Angiopoietin-like-4 (Angptl4)*, *Complement component 3 (C3)*, *Interleukin 6 (Il6)*, *Lumican (Lum)*, *Transmembrane 4 superfamily member 1 (Tm4sf1)*, *Decorin (Dcn)* and *Hyaluronan synthase 2 (Has2)*. These genes are associated with cancer establishment and progression as well as being acute phase proteins (Table 3.2). Acute phase proteins (APPs), also known as acute phase reactants, are inflammatory mediator proteins whose plasma serum levels increase (positive APPs) or decrease (negative APPs) during an inflammatory response. The remaining eight genes selected were *Thrombospondin type 1 (Thbs1)*, *Ceruloplasmin (Cp)*, *Vascular cell adhesion molecule 1 (Vcam1)*, *Leukemia Inhibitory Factor (LIF)*, *Calpastatin (Cast)*, *FK506 binding protein 5 (Fkbp5)*, *Tumour necrosis factor alpha-induced protein 6 (TNFaip6)* and *Matrix metalloproteinase 9 (Mmp9)*. These eight genes were selected because of their role in cancer establishment and progression and/or because they are acute phase proteins. Some genes such as *LIF* and *TNFaip6*, which are cytokines like *Il6*, were selected for their similarities or associations to the first ten genes (Table 3.2).

The majority of the genes selected encode positive acute phase proteins (APPs) namely *Lcn2*, *Saa3*, *C3*, *Il6*, *Has2*, *Vcam1*, *LIF*, *Cast*, *Fkbp5* and *TNFaip6*. These APPs are involved in biological pathways controlling proliferation and migration, regulation of the innate and adaptive immune response, angiogenesis and tissue repair programs (Germano et al., 2011). Recently it has been established that the expression of acute phase proteins assists in establishing and maintaining the microenvironment required for tumour metastasis and progression (Pollard, 2004; Kopfstein and Christofori, 2006; Kim et al., 2009). Chronic non-resolving inflammation of selected organs can increase the potential of cancer development due to APPs giving rise to genetic instability (Colotta et al., 2009; Solinas et al., 2010).

The key regulatory APP molecules of the inflammatory response include transcription factors, cytokines and chemokines. Cytokines such as Interleukin (Il) 6, Leukemia Inhibitory Factor (LIF) and Tumour necrosis factor alpha induced protein 6 (TNFaip6) are

cell-signalling APPs that activate the expression of other APPs as a response to inflammation (Colotta et al., 2009; Mantovani, 2009). Chemokines are small cytokines secreted by cells inducing chemotaxis. Chemokines were identified in the microarray and will be discussed in Section 3.2.7 and Section 5.2.3. Il6 is a member of the Il6 family of cytokines, known to regulate transcription of acute phase proteins via Signal Transduction and Activator of Transcription 3 (STAT3) (Kisseleva et al., 2002; Linker et al., 2008). LIF and TNF α ip6 were selected for further analysis as they are also a part of the Il6 family of cytokines. Like Il6, TNF α ip6 and LIF initiate a cell signalling cascade through the glycoprotein (gp) 130 subunit, which forms a membrane bound receptor complex with a cytokine specific receptor.

Thbs1 was of interest due to its ability to assist in the formation of protein complexes such as cytokine receptors, membrane receptors, growth factors and matrix components, therefore regulating proliferation, migration and apoptosis in response to wound healing and inflammation (Chen et al., 2000; Firlej et al., 2011). Tm4sf1 also mediates signal transduction involved in the regulation of cell development and migration (Zukauskas et al., 2011). Cp is primarily a copper transport protein of the blood but also known to be an APP expressed in response to wound healing and inflammation (Marques et al., 2012).

Lcn2 is the gene most strongly induced by p37 (Table 3.2). *Lcn2* expression is up-regulated in epithelial cells under inflammatory conditions and the gene is over expressed in a number of cancer types including pancreatic, thyroid, ovary, breast, lung and oesophageal (Iacobuzio-Donahue et al., 2003; Fernandez et al., 2005; Lim et al., 2007; Zhang et al., 2007; Iannetti et al., 2008). The covalent complex between *Lcn2* and *Mmp9* is associated with enhancing invasion and metastasis in gastric, breast and oesophageal cancers (Leung et al., 2012). *Lcn2* can regulate *Mmp9* activity (Kubben et al., 2007).

Dcn and *Lum* are a part of the small leucine-rich proteoglycan (SLRP) family as they share the characteristic leucine rich repeats. They are present within the extracellular matrix, interacting with collagen fibres and soluble growth factors, facilitating cellular adhesion, proliferation and migration. They also regulate growth factors and cytokine activity required to re-structure the extracellular matrix and regulate the inflammatory response

(Naito, 2005; Kao et al., 2006; He et al., 2008; Ferdous et al., 2009; Williams et al., 2011; Bi et al., 2012).

Tumour establishment, progression and angiogenesis relies on the secretion of matrix-degrading enzymes, such as matrix metalloproteinases (Klein et al., 2004; Mantovani, 2009). Mmp2 and Mmp9 are well known matrix metalloproteinases (Mmp) enhancing angiogenesis and the invasivity of tumour cells (Klein et al., 2004; Bekes et al., 2011). Mmp9 but not Mmp2 was up-regulated by p37-treatment. Brief summaries of the functions of the eighteen selected genes are provided in Table 3.2.

Table 3.2: Genes significantly up-regulated within the microarray chosen for further analysis.

Gene Title	Gene Symbol	NCBI	Fold Change	Functions/Properties & relation to cancer/disease
Lipocalin 2	Lcn2	NM_008491	64	Lcn2 is a protein that binds small molecules and cell surface receptors to form macromolecular complexes (Mannelqvist et al., 2012). Elevated levels of plasma Lcn2 have been seen in the occurrence of stress and inflammation therefore known as an acute phase protein (Flower, 1996). It regulates breast cancer angiogenesis (Yang et al., 2012) by binding and sustaining the activation of matrix metalloproteinase 9 (Reilly et al., 2012).
Haptoglobin	Hp	NM_017370	54.9	Hp is an acute phase protein that binds loose haemoglobin preventing liver failure, incorrect degradation and iron loss from haemolysis (Sadrazadeh and Bozorgmehr, 2004). Hp also stimulates angiogenesis in chronic inflammatory conditions (Cid et al., 1993). Hp is been shown to be produced due to malignant diseases as well as several cancers including lung carcinomas (Kang et al., 2011).
Serum amyloid A3	Saa3	NM_011315	34	Saa proteins are involved in the transport of cholesterol and metabolism (Gutfeld et al., 2006). Saa3 increases in concentration following acute inflammation due to infection, trauma and stress (Huang and Liao, 1999; Gutfeld et al., 2006). The inhibition of Saa3 prevents mobilization and colonization of tumour cells (Spano and Zollo, 2012).
Angiopoietin-like-4	Angptl4	NM_020581	31.5	Angptl4 is a serum hormone involved in angiogenesis, metabolism regulation and is an apoptotic survival factor (Cazes et al., 2006; Zhu et al., 2011). Angptl4 has been observed to cause vascular metastasis of hypoxic breast cancer and also has been found to enhance growth and apoptotic survival of tumours (Zhu et al., 2011; Zhang et al., 2012).
Complement component 3	C3	NM_009778	19	C3 activates the complement component system initiating the innate immune system against bacterial infections (Sahu and Lambris, 2001). High levels of C3 are found in acute inflammatory diseases; promotes growth and metastasis of tumour cells and is necessary for the induction of arthritis (Monach et al., 2007; Rutkowski et al., 2010; Wang et al., 2011b).
Interleukin 6	Il6	NM_031168	15.9	Il6 is a cytokine that initiates transcription of acute phase proteins in response to infection and inflammation as well as regulating metabolic, regenerative and neural processes (Nishimoto, 2010; Scheller et al., 2011). Overproduction of Il6 underlies autoimmune and inflammatory diseases as well as playing an important role in the aggression of breast cancer migration (Gao et al., 2007; Sansone et al., 2007).

Lumican	Lum	NM_008524	12.7	Lum is a part of the small leucine-rich proteoglycan (SLRP) family class II and plays an important role in regulating stromal collagen matrix assembly and possibly regulates other cellular functions (Kao et al., 2006; Williams et al., 2011). High expression level of Lum is correlated with a significant decrease in survival rate of colorectal cancer patients with nodal metastasis (Seya et al., 2006).
Transmembrane 4 superfamily member 1	Tm4sf1	NM_008536	11.6	Tm4sf1 is a cell-surface protein that mediates signal transduction involved in the regulation of cell development and migration (Zukauskas et al., 2011). Tm4sf1 transcript levels are higher in cancer patients compared to benign prostatic hyperplasia (BPH) (Allioli et al., 2011). Tm4sf1 has also been found at high levels within the endothelial cells of angiogenic blood vessels supplying human cancer (Zukauskas et al., 2011).
Decorin	Dcn	NM_007833	11.5	Dcn is a part of the small leucine-rich proteoglycan (SLRP) family class I regulating collagen fibrillogenesis to organise the extracellular matrix, muscular development, wound healing and inflammation (He et al., 2008; Ferdous et al., 2009; Bi et al., 2012). Dcn suppresses tumour formation and migration via the epidermal growth factor receptor (EGFR), however, decorin expression and secretion is from cells surrounding the cancer cells (Dil and Banerjee, 2011; Bi et al., 2012).
Hyaluronan synthase 2	Has2	NM_008216	9.3	Has2 is a major constituent of the extracellular matrix allowing for cell migration in the processes of wound healing, tissue repair and angiogenesis. Has2 has been found in abundance within the stroma of many cancers and enhances the migration of melanoma cells (Kultti et al., 2012).
Thrombospondin 1	Thbs1	NM_011580	8	Thbs1 forms multi-protein complexes with cytokines and receptors that initiate signal transduction regulating cell proliferation, migration and apoptosis in response to wound healing and inflammation (Chen et al., 2000; Lawler, 2000). Thbsp1 is known to inhibit angiogenesis of xenografted tumours, however, expression is correlated with the invasiveness of prostate cancers (Firlej et al., 2011).
Ceruloplasmin	Cp	NM_001042611	6.8	Cp is mainly for copper transport in the blood, however, it is also an acute phase protein expressed in response to inflammation for the purposes of host defence and tissue repair processes (Marques et al., 2012). Increased levels of Cp have been detected in the malignant conditions of advanced prostate cancer compared to healthy controls (Aldemir et al., 2010; Kanoh et al., 2011).
Vascular cell adhesion molecule 1	Vcam1	NM_011693	5.9	Vcam1 is stimulated by cytokines via the NF-κB (nuclear factor-kappa B) transcription factor. Vcam1 mediates adhesion functions and leukocyte-endothelial cell signal transduction (Marui et al., 1993; Ley and Huo, 2001). Over-expression of Vcam1 in bone cancer promotes the transition to aggressive metastasis (Lu et al., 2011). Vcam1 expression has also been observed in pro-atherosclerotic conditions (Marui et al., 1993; Ley and Huo, 2001). Vcam1 is an adhesion molecule involved in the

				migration and recruitment of inflammatory cells through its interactions with an integrin present on infiltrating leukocytes.
Leukemia Inhibitory Factor	LIF	NM_001039537	5.6	LIF is a cytokine of the Interleukin-6 family involved in signal pathways promoting differentiation and growth of stem cells, bone homeostasis and cytokine expression in immune cells (Barnes et al., 2011). Increased LIF in mouse mammary tumour cells has been found to increase cell viability (Quaglino et al., 2007).
Calpastatin	Cast	NM_009817	5.2	Cast is an endogenous inhibitor of the ubiquitous Ca ²⁺ -dependent proteases known as calpains which regulate cytoskeleton remodelling, cell cycle progression, gene expression and apoptotic cell death (Hanna et al., 2008; Elkind et al., 2012). Increased mRNA and protein levels of Cast have been linked to the initial metastatic dissemination of breast cancer (Storr et al., 2011).
FK506 binding protein 5	Fkbp5	NM_010220	5.2	Fkbp5 is a member of the immunophilin protein family which interacts with corticoid receptor heterocomplexes and regulates steroid receptor functions as well as immunoregulation (Feng et al., 2011). Fkbp5 mRNA expression was increased within the bone marrow-derived mononuclear cells of rheumatoid arthritis patients (Nakamura et al., 2006).
Tumour necrosis factor alpha induced protein 6	TNF α ip6/ TNFip6/ TSG6	NM_009398	3	TNF α ip6 is a secreted protein involved in Extracellular Matrix (ECM) stability and cell migration. The gene can be induced by proinflammatory cytokines and assists in regulation of protease activity of the inflammatory response. Enhanced levels are found in the synovial fluid of patients with osteoarthritis and rheumatoid arthritis (Lee et al., 1992; Nagyeri et al., 2011).
Matrix metalloproteinase 9	Mmp9	NM_013599	3	Mmp9 is a key effector involved in the breakdown and synthesis of the ECM, assisting in normal physiological processes including; tissue remodelling, cell proliferation, migration as well as tissue remodelling and re-absorption (Nagase and Woessner, 1999; Lee et al., 2012). The over expression of Mmp9 in cancer cells allows for angiogenesis, tumour growth and metastasis with the level of TIMP-free proMmp9 determining the aggressive ability of tumour growth and dissemination (Klein et al., 2004; Bekes et al., 2011).

3.2.3 Validation of the 18 selected genes induced by p37 treatment of NIH3T3 cells

Semi-quantitative validation of the genes identified in the microarray was carried out using Reverse Transcription (RT) - PCR (Section 2.11.5). Six genes were selected for RT-PCR analysis and strong up-regulation was confirmed (results shown in Appendix IV). Quantitative (q) PCR (Section 2.12) was then used to validate all eighteen genes. Fold change ($2^{-\Delta\Delta Ct}$) of mRNA expression was calculated relative to untreated controls, normalised to the reference genes *Glyceraldehyde 3-phosphate dehydrogenase (GAPDH)* and *βactin*, as described in Section 2.12. In the presence of p37, qPCR expression levels of fifteen of the eighteen selected genes were found significantly up-regulated when compared to untreated controls (Figure 3.5). These included all ten genes with the highest fold changes in the microarray as well as *Thbsp1*, *LIF*, *Cast* and *Fkbp5*. However, *Cp*, *Vcam1*, *TNFaip6*, and *Mmp9* expression levels did not differ from the untreated controls.

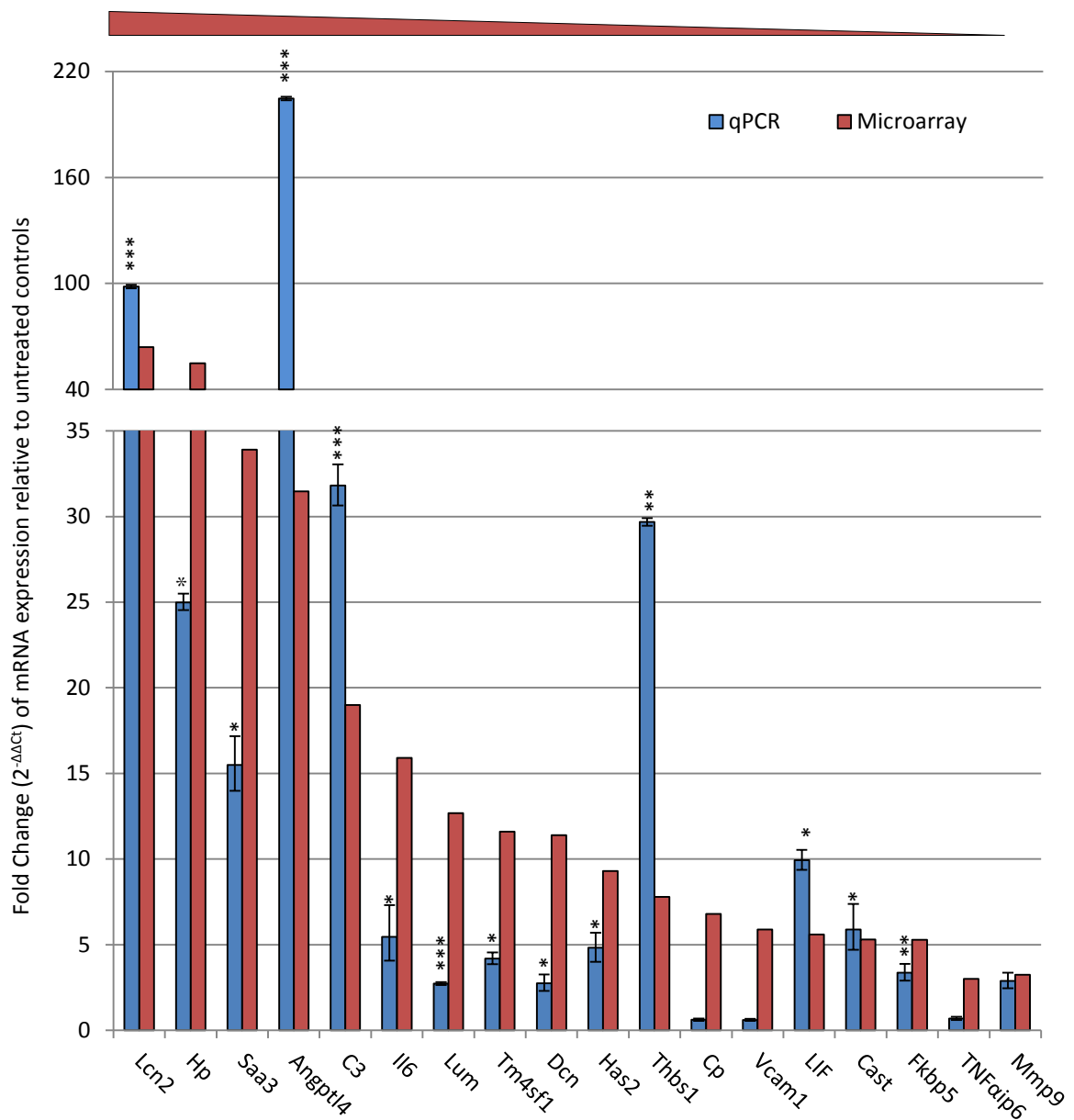


Figure 3.5: Microarray validation by qPCR. qPCR was used to validate the expression of 18 genes with $p < 0.001$ and fold change ≥ 3 . qPCR results were obtained from three biological replicates of the unamplified RNA used in the original microarray samples. Genes are in order of highest to lowest fold change based on the microarray data. The qPCR messenger RNA levels are expressed as fold change ($2^{-\Delta\Delta C_t}$) in relation to untreated controls (Section 2.12). Significant differences between treated and untreated were calculated by ANOVA analysis (* $p < 0.05$, ** $p < 0.01$, *** $p < 0.001$). Error bars depict \pm SE in relation to fold change (Section 2.12.8). Microarray mRNA levels are expressed as absolute fold change (treated vs. untreated), all p-values are $p < 0.001$. Raw data presented in Appendix V.

A positive correlation was achieved between the qPCR and microarray results; however, the association was weak with a Pearson correlation coefficient, r , of 0.53 (Figure 3.6A). The closer the Pearson correlation coefficient, r , is to 1, the stronger the positive association of the two variables. The difference between the fold change values of the microarray and qPCR were calculated and distribution evaluated using a histogram (Figure 3.6B). The histogram identified a single outlier with a fold change difference of 173. This outlier was identified as *Lcn2*. The outlier was removed and a strong positive correlation was achieved between the qPCR and microarray results with a Pearson correlation coefficient, r , of 0.79 (Figure 3.6C).

Microarray analysis is useful in gene expression profiling of whole genomes whereas qPCR is often used for quantifying the expression of a smaller number of genes. qPCR is more commonly used to validate gene expression data from microarrays, however, low correlation between the two techniques seems to be a re-occurring issue (Morey et al., 2006). Reasons for differences in variation are outlined within Appendix VI.

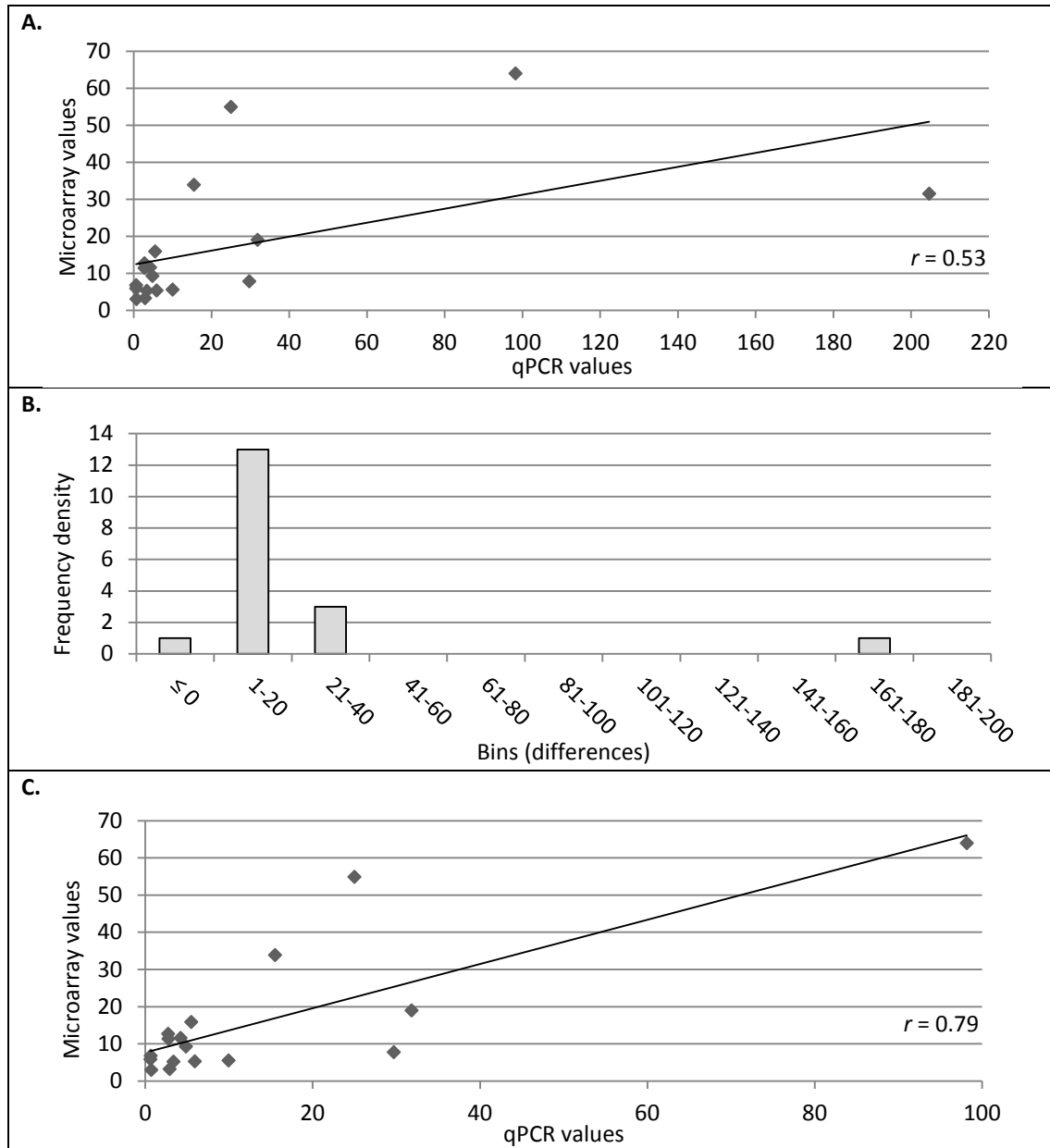


Figure 3.6: (A) Correlation of qPCR and Microarray results. Correlation indicates fold change values as determined by qPCR and Microarray for 18 genes regulated by 24hr p37-treatment. The positive correlation, indicative of the treadline, has a low Pearson correlation coefficient (r) of 0.53. **(B) Histograms indicating the frequency distribution of the difference between the microarray and qPCR results.** The difference between the fold changes were calculated (highest value – lowest value) for each gene and their frequency assigned to a bin category (differences). Majority of differences ranged between 0 and 40 with a single outlier in the bin category 161-180. **(C) Correlation of qPCR and Microarray results excluding an outlier.** Correlation indicates fold change values as determined by qPCR and Microarray for 17 genes regulated by 24hr p37-treatment. A single outlier identified in the histogram, C. was removed. The positive correlation, indicative of the treadline, has a strong Pearson correlation coefficient (r) of 0.79. Raw data presented in Appendix VII.

3.2.4 The effect of p37 concentrations on gene expression in NIH3T3 cells

To determine the effect of varying p37 concentrations on gene expression in NIH3T3 fibroblasts, triplicate cultures were treated for 24hrs with four different concentrations of purified p37 (0.5, 1, 5 or 25µg/ml) (Section 2.19.2). Quantitative (q) PCR was then used to calculate fold change ($2^{-\Delta\Delta Ct}$) of mRNA expression relative to untreated controls (Section 2.12).

A direct relationship between p37 concentration and the effect on gene expression (fold change) was observed in seven of the eighteen genes previously found up-regulated (Section 3.2.2; Figure 3.7). All seven genes, namely *Lcn2*, *Hp*, *Saa3*, *C3*, *Dcn* and *Has2*, were among the ten genes with the highest transcript expression in the microarray analysis. Of the eighteen genes selected *Lcn2*, *Hp*, *Angptl4*, *C3*, *Il6* and *Cast* showed a significant change in gene expression at the lowest p37 concentration (0.5µg/ml). *TNFaip6* also showed a 2-fold change in gene expression at the lowest concentration of 0.5µg/ml p37 but expression levels returned to control levels (1-fold) and stayed constant across the other three p37 concentrations (1, 5 and 25µg/ml). *Mmp9* expression first increased with 1µg/ml p37 and did not change with higher concentrations. However, *LIF* expression increased approximately 2-fold at 0.5µg and 1µg/ml p37 and then to approximately 5-fold at 5µg and 25µg/ml p37. Four of the eighteen genes selected showed no significant change in gene expression at any of the p37 concentrations tested.

Gong et al., (2008) found that *Mmp2* levels increased in the media of both 20µg/ml p37-treated and p37-transfected AGS cells. We found *Mmp2* expression increased only by 2.5-fold at 5µg and 25µg/ml p37.

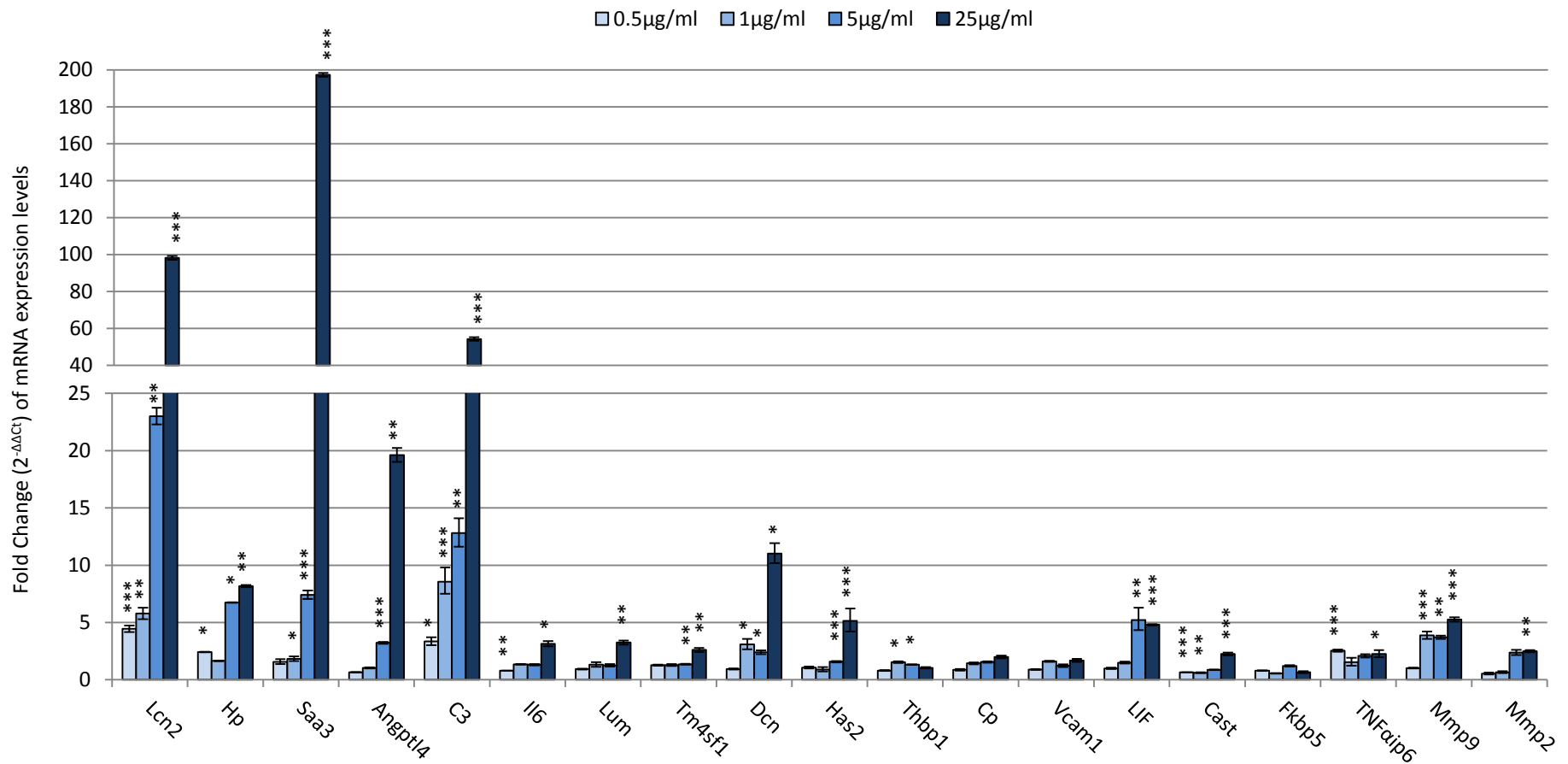


Figure 3.7: Gene expression of NIH3T3 (mouse) fibroblasts treated with different concentrations of purified p37 (0.5, 1, 5 and 25µg/ml). NIH3T3 cells were treated with purified p37 for 24 hours. qPCR results were obtained from the RNA extracted from NIH3T3 fibroblasts treated with purified p37. The messenger RNA levels are expressed as fold change ($2^{-\Delta\Delta C_t}$) in relation to untreated controls (Section 2.12.6). Genes are in order of highest to lowest fold change based on the microarray results (Section 3.2.2). Significant differences between treated and untreated cells were calculated by ANOVA analysis (* $p < 0.05$, ** $p < 0.01$, *** $p < 0.001$). Error bars depict \pm SE of three biological and three technical replicates (Section 2.12.8). Raw data presented in Appendix VIII.

3.2.5 Temporal induction patterns of gene induction due to 24hr p37 treatment

NIH3T3 fibroblasts, in triplicate, were treated with 5µg/ml p37 and RNA was extracted at 2, 4, 8, 12 and 24hr time points. Controls were un-treated fibroblasts. The lowest p37 concentration, namely 5µg/ml, inducing the majority of the genes of interest was used (Figure 3.7). Quantitative (q) PCR was employed to calculate fold change ($2^{-\Delta\Delta Ct}$) of mRNA expression relative to untreated controls (Section 2.12). The expression levels of the eighteen selected genes, plus *Mmp2*, were determined at each time point (Table 3.3).

Significant increases in the expression of *Saa3*, *Angptl4*, *Il6* and *Vcam1* occurred after 2hr treatment and reached a maximum at 4hrs, subsequently decreasing over the remaining 24hrs. A strong decrease occurred in *Il6* and *Vcam1* expression after 4hrs. *Dcn* was induced 8-fold after 2hrs but slightly decreased to 5-fold after 4hrs and was not induced at 8 and 12hrs. A steady increase in gene expression of *Hp* occurred between 2 and 12hrs of p37-treatment and was maintained at 24hr (7-fold). *Lcn2* induction was strongest between 12 and 24hr (4-fold increasing to 23-fold). Increased *C3* gene expression (13-fold) was detected only at 24hrs. *Tm4sf1* expression significantly increased reaching a maximum of 4-fold at 8hrs after which it decreased at 12 and 24hrs. *LIF* gene expression was detected at 2 and 4hrs and then again at 24hrs, with a maximum 5-fold change at 4 and 24hrs. No increased gene expression was detected at 8 and 12hrs. *Has2* expression followed a similar trend, however, the maximum was only 2-fold and limited to 2 and 24hrs. *Cp* maintained a 2-fold increase across all time points. *Thbs1* expression was variable with a maximum of 2-fold. No increase in *Lum* and *Fkbp5* was detected.

Table 3.3: Gene fold changes at different times following p37 (5µg/ml) addition to NIH3T3 cells. NIH3T3 cells were treated with 5µg/ml p37 and RNA extracted at 2, 4, 8, 12 and 24hr time points. The messenger RNA levels are expressed as fold change ($2^{-\Delta\Delta Ct}$) in relation to untreated controls. Genes are in order of highest to lowest fold change based on the microarray results (Section 3.2.2). Significant differences between treated and untreated cells were calculated by ANOVA analysis; p-value ≤ 0.05 are shown in bold. All standard errors are below ± 1 . Raw data presented in Appendix IX.

	Time					KEY
	2hr	4hr	8hr	12hr	24hr	
Lcn2	2	2	3	4	23	1
Hp	2	2	5	7	7	3
Saa3	46	80	66	15	7	5
Angptl4	108	202	68	35	3	10
C3	2	1	1	1	13	50
Il6	42	98	7	4	1	200
Lum	1	1	1	1	1	
Tm4sf1	3	3	4	2	1	
Dcn	8	5	1	1	2	
Has2	2	1	1	1	2	
Thbp1	2	2	1	2	1	
Cp	2	2	2	2	2	
Vcam1	17	21	3	1	1	
LIF	3	5	1	1	5	
Cast	1	1	1	1	1	
Fkbp5	1	1	1	1	1	
TNFaip6	1	1	1	2	2	
Mmp9	2	2	2	2	4	
Mmp2	1	1	1	3	2	

3.2.6 Comparison of p37-induced gene expression over the different experiments

The fold changes of the nineteen genes, selected from the microarray plus *Mmp2*, in the different experiments of this chapter are shown in Table 3.4. At 25µg/ml p37, expression levels of twelve genes increased by more than 3-fold over 24hrs. At 5µg/ml this drops to six genes. *Il6* and *Vcam1* exhibited strong expression at 4hr 5µg/ml p37 treatment however subsequently decreased (Table 3.3). *Tm4sf1* and *Dcn* are also induced early (3-fold and 8-fold, respectively at 2hrs). *Saa3*, *Angptl4*, *Il6* and *Vcam1* are all strongly induced after 2hrs of 5µg/ml p37 treatment. Considerable variation in the levels of expression occurred across the experiments, but it appears that fourteen of the nineteen genes selected for study, based on the original microarray data, consistently respond to p37.

The 'primary round' of inductions (5µg/ml p37) occurring between 0 and 4hrs involved *Saa3*, *Angptl4*, *Il6*, *Vcam1* and *LIF*. The 'secondary round' of inductions (5µg/ml p37, fold change>3) occurring between 4 and 24hrs involved *Lcn2*, *Hp*, *Saa3*, *C3* and *Mmp2*. The genes *Has2*, *Cp*, *TNFaip6* and *Mmp9* were also a part of the 'secondary round' of induction however induction was not as strong (fold change=2). The genes *Lum*, *Tm4sf1*, *Has2* and *Cast* cannot be ruled out of the 'second round' of inductions due to significant fold changes at 25µg/ml p37, 24hr treatment.

The pro-inflammatory cytokine *Il6* is known to induce the expression of acute phase proteins (APPs) such as *Hp*, *Has2* and *Cp*. Therefore the primary induction of *Il6* and secondary induction of these APPs indicates that p37 might initiate an inflammatory response via the increased expression of *Il6*.

Table 3.4: Comparison of fold changes in gene expression obtained in the different experiments. Fold changes ($2^{-\Delta\Delta Ct}$) represent mRNA expression relative to untreated controls (Section 2.12.6). Genes are in order of highest to lowest fold change based on the microarray results. Microarray mRNA levels are expressed as absolute fold change (treated vs. untreated), all p-values are $p < 0.001$. *Mmp2* expression was not detected in the microarray analysis therefore fold change is not applicable (n/a). Significant differences between treated and untreated cells for the different experiments were calculated by ANOVA analysis and can be found within the indicated sections.

	Microarray (Section 3.2.2)	qPCR validation of microarray (Section 3.2.3)	Various p37 concentrations (Section 3.2.4)				Various treatment times (Section 3.2.5)			
Concentration p37 ($\mu\text{g/ml}$)	15	15	0.1	1	5	25	5			
Time (hr)	24	24	24				2	4	8	12
Lcn2	64	98	4	6	23	96	2	2	3	4
Hp	55	25	2	2	7	8	2	2	5	7
Saa3	34	15	2	2	7	197	46	80	66	15
Angptl4	31	205	1	1	3	20	108	202	68	35
C3	19	32	3	9	13	54	2	1	1	1
Il6	16	5	1	1	1	3	42	98	7	4
Lum	13	3	1	1	1	3	1	1	1	1
Tm4sf1	12	4	1	1	1	3	3	3	4	2
Dcn	11	3	1	3	2	11	8	5	1	1
Has2	9	5	1	1	2	5	2	1	1	1
Thbp1	8	30	1	2	1	1	2	2	1	2
Cp	7	1	1	1	2	2	2	2	2	2
Vcam1	6	1	1	2	1	2	17	21	3	1
LIF	6	10	1	1	5	5	3	5	1	1
Cast	5	6	1	1	1	2	1	1	1	1
Fkbp5	5	3	1	1	1	1	1	1	1	1
TNF α ip6	3	1	3	2	2	2	1	1	1	2
Mmp9	3	3	1	1	2	2	2	2	2	2
Mmp2	n/a	2	1	4	4	5	1	1	1	3

3.2.7 The effect of p37 in the inflammatory response and autoimmunity pathways: an RT²Profiler PCR array study.

An RT²Profiler PCR array designed by SABiosciences was used to analyze 84 genes of the mouse inflammatory response and autoimmunity pathways (PAM-077A) plus 5 reference genes (Table 3.5). PCR arrays are a quick way of performing quantitative (q) PCR. Oligonucleotides for 96 genes are already wet lab tested by the company and placed, in powder form, at the bottom of each well of a 96-well PCR plate. The PCR array plate also contains oligonucleotides that detect genomic contamination controls, reverse transcription controls and positive PCR controls.

Table 3.5: 84 genes of the mouse inflammatory response and autoimmunity pathways covered by the RT²Profiler PCR array designed by SABiosciences. All gene names corresponding to the Gene IDs presented in Appendix XI. NOTE: Some genes are located in two categories; the second and consecutive appearances of a gene are in italics.

Categories:	Gene ID:
Cytokines	Cxcl1, Cxcl10, Cxcl11, Cxcl2, Cxcl3, Cxcl5, Cxcl9, Fasl, Flt3l, Ifng, Il10, Il18, Il1a, Il1b, Il1f10, Il1rn, Il22, Il23a, Il6, Il7, Il9, Lta, Ltb, TNF, TNFsf14.
Chemokines	Ccl1, Ccl11, Ccl12, Ccl17, Ccl19, Ccl2, Ccl20, Ccl22, Ccl24, Ccl25, Ccl3, Ccl4, Ccl5, Ccl7, Ccl8.
Cytokine Receptors	Il10rb, Il18rap, Il1r1, Il1rap, <i>Il1rn</i> , Il22ra2, Il23r, Il6ra, Cxcr1, Cxcr2, Ccr1, Cd40
Chemokine Receptors	<i>Ccr1</i> , Ccr2, Ccr3, Ccr4, Ccr7, Cxcr4, <i>Cxcr1</i> , <i>Cxcr2</i>
Cytokine Metabolism	<i>Il10</i> , <i>Il18</i> , TLR1, TLR3, TLR4, TLR6
Acute-Phase Response	Cebpb, Crp, <i>Il22</i> , <i>Il6</i>
Inflammatory Response	Bcl6, C3, C3ar1, C4b, <i>Ccl1</i> , <i>Ccl11</i> , <i>Ccl12</i> , <i>Ccl17</i> , <i>Ccl19</i> , <i>Ccl2</i> , <i>Ccl20</i> , <i>Ccl22</i> , <i>Ccl24</i> , <i>Ccl25</i> , <i>Ccl3</i> , <i>Ccl4</i> , <i>Ccl5</i> , <i>Ccl7</i> , <i>Ccl8</i> , <i>Ccr1</i> , <i>Ccr2</i> , <i>Ccr3</i> , <i>Ccr4</i> , <i>Ccr7</i> , <i>Cd40</i> , <i>Cd40lg</i> , <i>Cebpb</i> , <i>Crp</i> , <i>Csf1</i> , <i>Cxcl1</i> , <i>Cxcl10</i> , <i>Cxcl11</i> , <i>Cxcl2</i> , <i>Cxcl3</i> , <i>Cxcl5</i> , <i>Cxcl9</i> , <i>Cxcr4</i> , <i>Fos</i> , <i>Hdac4</i> , <i>Il10</i> , <i>Il10rb</i> , <i>Il18rap</i> , <i>Il1a</i> , <i>Il1b</i> , <i>Il1f10</i> , <i>Il1r1</i> , <i>Il1rap</i> , <i>Il1rn</i> , <i>Il22</i> , <i>Cxcr1</i> , <i>Cxcr2</i> , <i>Il9</i> , <i>Itgb2</i> , <i>Kng1</i> , <i>Ly96</i> , <i>Myd88</i> , <i>Nfatc3</i> , <i>Nfkb1</i> , <i>Nos2</i> , <i>Nr3c1</i> , <i>Ripk2</i> , <i>Tirap</i> , <i>TLR1</i> , <i>TLR2</i> , <i>TLR3</i> , <i>TLR4</i> , <i>TLR5</i> , <i>TLR6</i> , <i>TLR7</i> , <i>TNF</i> , <i>Tollip</i>
Humoral Immune Response	<i>C3</i> , <i>C4b</i> , <i>Ccl2</i> , <i>Ccl22</i> , <i>Ccl3</i> , <i>Ccl7</i> , <i>Ccr2</i> , <i>Ccr7</i> , <i>Cd40</i> , <i>Il10</i> , <i>Il1b</i> , <i>Il6</i> , <i>Itgb2</i> , <i>Ly96</i> , <i>Nfkb1</i>
Reference genes	GusB, Hpvt, Hsp90ab1, GapDH, Actb

NIH3T3 cell cultures were treated with 25µg/ml purified p37 for 24hrs and the PCR arrays performed on cDNA as described in Section 2.14. Three biological replicates were completed for un-treated controls and for 25µg/ml p37-treated NIH3T3 cells (24hr). Strong positive correlations of the cycle threshold (Ct) values were found between the PCR array biological replicates of each treatment, indicating reliable qPCR detection of gene expression (Figure 3.8). The triplicate un-treated NIH3T3 cells gave strong Pearson correlation coefficients, r , of 0.95, 0.93 and 0.96 (Figure 3.8A). The triplicate 25µg/ml p37-treated NIH3T3 cells (24hr) also produced strong Pearson correlation coefficients, r , of 0.99, 0.99 and 0.97 (Figure 3.8B). The closer the Pearson correlation coefficient, r , is to 1, the stronger the positive association of the two variables. No outliers were observed.

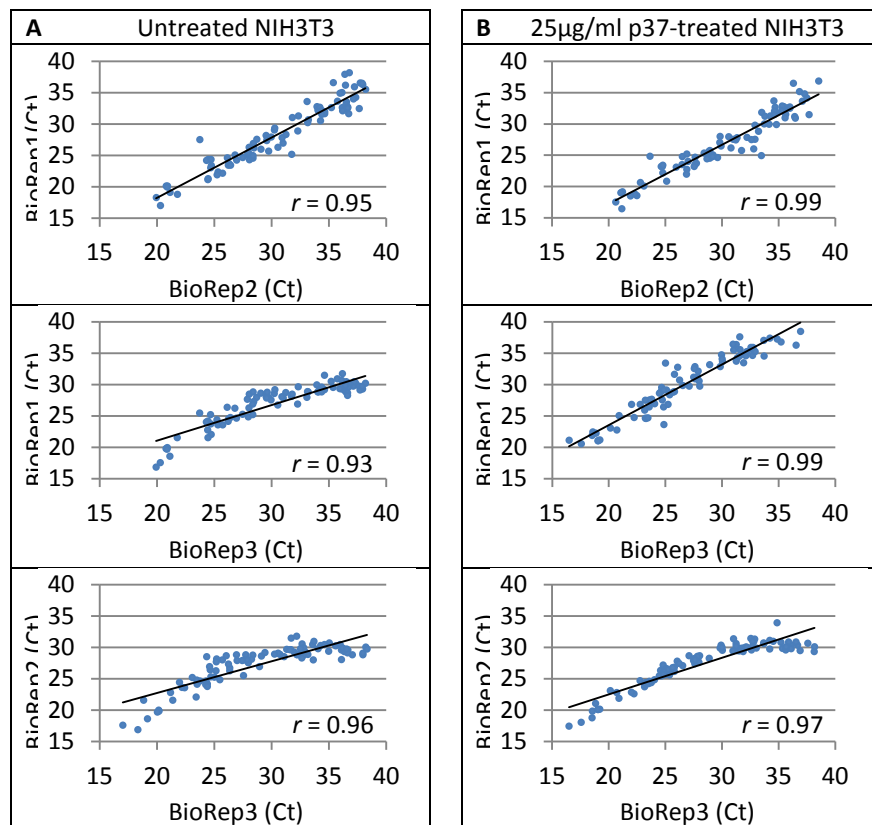


Figure 3.8: Correlation between biological replicates for the inflammatory response and autoimmunity RT²Profiler Array. Graphs indicate the Ct value correlation strength between each replicate of a treatment. **(A)** Strong positive correlations, indicated by the treadline, were observed between the three biological replicates (BioRep) of untreated control cells with Pearson correlation coefficients (r) of 95, 93 and 96. **(B)** Strong positive correlations, indicated by the treadline, were also observed between the three biological replicates of 25µg/ml p37-treated cells with Pearson correlation coefficients (r) of 99, 99 and 97. Raw data presented in Appendix X.

Cycle threshold (Ct) values greater than 35 (Ct>35) were not considered reliable and the relative genes were excluded from further analysis. Only 17% of the un-treated control genes and 19% of the p37-treated (25µg/ml, 24hrs) genes had Ct values > 35, averaged across the three biological replicates (Figure 3.9).

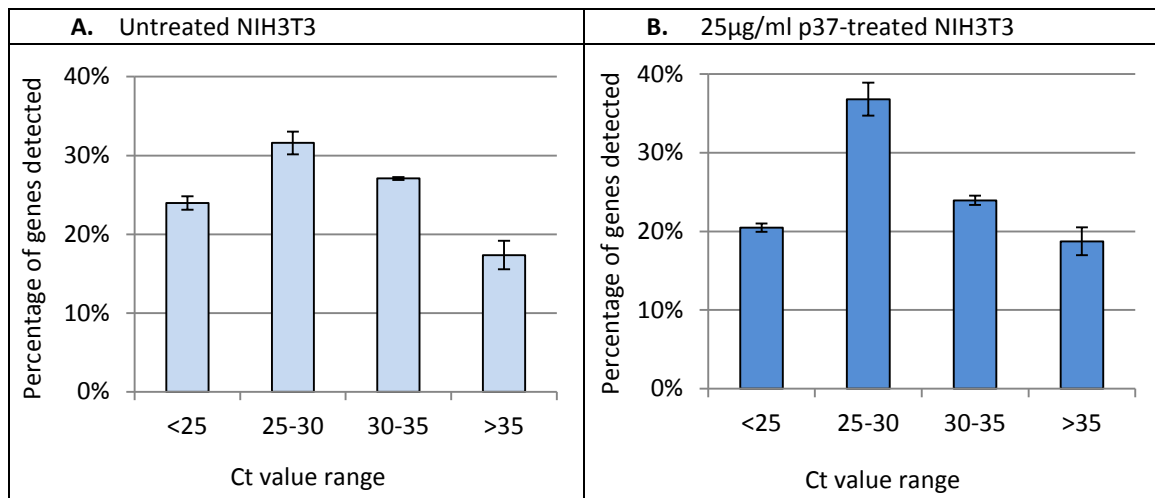


Figure 3.9: Overview of the cycle threshold for the inflammatory response and autoimmunity RT²Profiler Array. (A) Overview of Ct values for the biological replicates of the untreated controls (B) Overview of Ct values for the biological replicates of 25µg/ml p37-treated cells. The mean percentage of the cycle threshold (Ct) values were classified into four ranges; <25, 25-30, 30-35 and >35. Low Ct values (< 25) represent genes with high transcript copy numbers. Ct values of greater than 35 (> 35) were considered outside the detection threshold system. Error bars depict ±SE of the three biological reps of each treatment. Raw data presented in Appendix X.

Fold change ($2^{-\Delta\Delta Ct}$) of mRNA expression was calculated relative to the untreated controls and normalised to the reference genes *GAPDH* and *βactin* as described in Section 2.12.6. Although 5 reference genes are present on the PCR array only *GAPDH* and *βactin* were shown not to be regulated by p37-treatment and therefore used as reference genes. Of the eighty four genes analysed on the PCR array, only ten genes were up-regulated by 25µg/ml p37-treatment of NIH3T3 cells and one down-regulated however, they were not found to be significant (Table 3.6). A reason for the high p-values seen in the PCR array compared to previous qPCR data is sampling size. The Ct values of the PCR array are from three biological replicates whereas the Ct values of the qPCR experiments of this thesis are from three biological replicates and three technical replicates for each biological replicate.

Table 3.6: Genes identified in the inflammatory response and autoimmunity RT²Profiler Array. NIH3T3 cells were treated with 25µg/ml purified p37 for 24hr and the mouse inflammatory response and autoimmunity pathways (SABiosciences; PAM-077A) RT² Profiler PCR array was used to determine mRNA expression levels. Fold changes ($2^{-\Delta\Delta Ct}$) represent mRNA expression relative to untreated controls (Section 2.12.5). Significant differences were calculated by ANOVA. Fold changes of all Profiler Array genes presented in Appendix XI.

Gene Title	Gene ID	Fold Change	p-value	Categories
Complement component 3	C3	10	0.178	IR, HIR,
Chemokine (C-X-C motif) ligand 1	Cxcl1	10	0.064	IR, Cytokine
Chemokine (C-C motif) ligand 5	Ccl5	6	0.192	IR, Chemokine
Chemokine (C-X-C motif) ligand 5	Cxcl5	5	0.084	IR, Cytokine
Chemokine (C-C motif) ligand 2	Ccl2	4	0.192	IR, HIR, Chemokine
Chemokine (C-C motif) ligand 7	Ccl7	4	0.175	IR, HIR, Chemokine
C-reactive protein, pentraxin-related	Crp	3	0.255	APR
Chemokine (C-X-C motif) ligand 10	Cxcl10	3	0.085	IR, Cytokine
Interleukin 6	Il6	2	0.171	IR, APR, Cytokine
Toll-like receptor 2	TLR2	2	0.286	IR
Chemokine (C-X-C motif) receptor 1	Cxcr1	0.5	0.477	Cyto/Chemokine receptor

Abbreviations are: IR, inflammatory response; HIR, humoral immune response and APR, acute-phase response.

Increased *C3* and *Il6* expression were identified in the PCR array as in the original microarray and subsequent qPCRs previously described in this chapter. The fold changes observed in the PCR array are a lot lower compared to the previous qPCR (Section 3.2.4). *C3* had a fold change of 10- compared to 54-fold and 2- compared to 3-fold for *Il6*. The three chemokines *Cxcl1*, *Ccl2* and *Ccl7* were also identified within the original microarray with increased gene expression of 5-, 6- and 5-fold respectively (Appendix II). The remaining genes identified using the PCR array were not identified in the original

microarray. However, all genes, except TLR2, are present on the Affymetrix Gene Chip® Mouse Genome 430A 2.0 Arrays. The major differences between the two qPCRs are the oligonucleotides used. However, the oligonucleotides used in both experiments were tested for efficiency as described in Sections 2.12.2 and 2.12.3. Two separate kits and protocols were also used for RNA processing; Invitrogen for the microarray and Qiagen for the PCR array.

3.2.8 Genes Down-Regulated by p37

The microarray analysis identified 249 significantly down-regulated genes (fold-change \leq 3, $p\leq$ 0.001) in 24hr p37-treated NIH3T3 fibroblasts. A list of these genes is provided in Appendix III. The three most strongly down-regulated genes encode proteins involved in plasma membrane transport (Table 3.7). The proteins encoded include solute carrier family 6 (neurotransmitter transporter, betaine/GABA) member 12 (Slc6a12), chloride channel calcium activated 5 (Clca5) and PDZK1 interacting protein 1 (PDZK1). An ATPase, Na⁺/K⁺ transporting, beta 1 polypeptide (ATP1 β 1) encoding gene was also down-regulated.

Slc6a12 is a gene encoding a Na⁺ and Cl⁻ dependent membrane transporter protein of betaine (Zhou et al., 2012). *Mycoplasma pulmonis* infection has been directly linked to a decrease in epithelial cell Na⁺ and Cl⁻ transport (Lambert et al., 1998). The increased consumption of choline and betaine (a derivative of choline) reduces plasma serum levels of the cytokines interleukin 6 (Il6) and tumour necrosis factor-alpha (TNF α) and consequently reduces the inflammatory response (Detopoulou et al., 2008).

Rho/rac guanine nucleotide exchange factor (GEF) 18 (Arhgef18 or p114RhoGEF) was also significantly down regulated (12-fold) (Table 3.7). Arhgef18 is a guanine nucleotide exchange factor (GEF) which controls the activation of Rho GTPases. Rho GTPases are GTP binding proteins that regulate a wide spectrum of cellular functions, including motility (Section 1.8). Terry et al. (2011) have shown that Arhgef18 is required for activation of RhoA at cell-cell junctions. Reduced levels of Arhgef18 resulted in less active RhoA at the cell-cell junctions. Rac1 and Cdc42 levels were not affected by reduced levels of Arhgef18. Reduced active RhoA at cell-cell junctions would prevent the maturation of adhesions and lateral protrusions. Loss of heterotypic contact inhibition of locomotion is observed in *Mycoplasma hyorhinis* infected FS9 fibroblasts (Steinemann et al., 1984a; Steinemann et al., 1984b) and p37-treated NIH3T3 fibroblasts (Darren Lowen, PhD Thesis, La Trobe University, 1995; Megan Drew, Honours Thesis, La Trobe University, 2006).

Table 3.7: First 20 genes significantly down-regulated within the microarray. Microarray mRNA levels are expressed as absolute fold change (treated vs. untreated), all p-values are $p < 0.001$. A complete list of the down-regulated genes is provided in Appendix III.

Affymetrix Probe Set ID	Gene Symbol	Gene Title	Fold Change (Down)
1449382_at	Slc6a12	solute carrier family 6 (neurotransmitter transporter, betaine/GABA), member 12	47
1438109_at	Clca5	chloride channel calcium activated 5	32
1434195_at	Prss35	protease, serine, 35	27
1455477_s_at	Pdzk1ip1	PDZK1 interacting protein 1	21
1451322_at	Cmb1	carboxymethylenebutenolidase-like (Pseudomonas)	20
1419378_a_at	Fxyd2	FXYP domain-containing ion transport regulator 2	19
1422478_a_at	Acss2	acyl-CoA synthetase short-chain family member 2	18
1456601_x_at	Fxyd2	FXYP domain-containing ion transport regulator 2	17
1422479_at	Acss2	acyl-CoA synthetase short-chain family member 2	16
1421153_at	Loxl4	lysyl oxidase-like 4	16
1418925_at	Celsr1	cadherin EGF LAG seven-pass G-type receptor 1	14
1417689_a_at	Pdzk1ip1	PDZK1 interacting protein 1	13
1418595_at	S3-12	plasma membrane associated protein, S3-12	13
1443921_at	Ranbp3l	RAN binding protein 3-like	13
1419379_x_at	Fxyd2	FXYP domain-containing ion transport regulator 2	13
1439036_a_at	Atp1b1	ATPase, Na ⁺ /K ⁺ transporting, beta 1 polypeptide	12
1440700_a_at	Arhgef18	rho/rac guanine nucleotide exchange factor (GEF) 18	12
1452388_at	Hspa1a	heat shock protein 1A	12
1419872_at	Csf1r	colony stimulating factor 1 receptor	12
1452418_at	Rik	RIKEN cDNA 1200016E24 gene	12

4. THE ROLE OF THE INTERLEUKIN 6 PATHWAY IN ACTIVATION BY P37 OF GENES ENCODING ACUTE PHASE PROTEINS

4.1 INTRODUCTION

The interleukin 6 family of cytokines includes Interleukin (Il)6 , Il11, Oncostatin-M (OSM), Ciliary Neurotropic Factor (CNTF) and Leukemia Inhibitory Factor (LIF) (Heinrich et al., 2003; Nishimoto and Kishimoto, 2008; Cornelissen et al., 2011). These cytokines are multifunctional and responsible for the regulation of immune responses and haematopoietic systems (Taga and Kishimoto, 1997).

The interleukin 6 family of cytokines initiates cell signalling through a membrane bound receptor complex composed of a minimum of two different subunits. The cytokines initially bind to an alpha (α -) subunit (Il6R or LIFR) which subsequently activates the second subunit, a glycoprotein (gp) 130 subunit receptor (Figure 4.1) (Cornelissen et al., 2011). The Janus Kinase (JAK) family of kinases associate with the cytoplasmic region of the bound gp130 receptor complex as a consequence of a conformational change resulting from binding of the α -subunit cytokine receptor (Kisseleva et al., 2002). A tyrosine residue in JAK is phosphorylated which then recruits signal transducers and activators of transcription (STATs), which are subsequently also activated via phosphorylation (Kisseleva et al., 2002). The activated STAT dissociates from the receptor complex, forms a hetero- or homo-dimer with a second activated STAT and translocates to the nucleus where transcription is initiated (Kisseleva et al., 2002). The Il6 family of cytokines specifically activates STAT3 via gp130 (Figure 4.1) (Faruqi et al., 2001; Nishimoto and Kishimoto, 2008; Raptis et al., 2009). Constitutively active STAT3 has been observed in murine and human tumours and has also been shown to regulate Src dependent transformation of fibroblasts (Kisseleva et al., 2002).

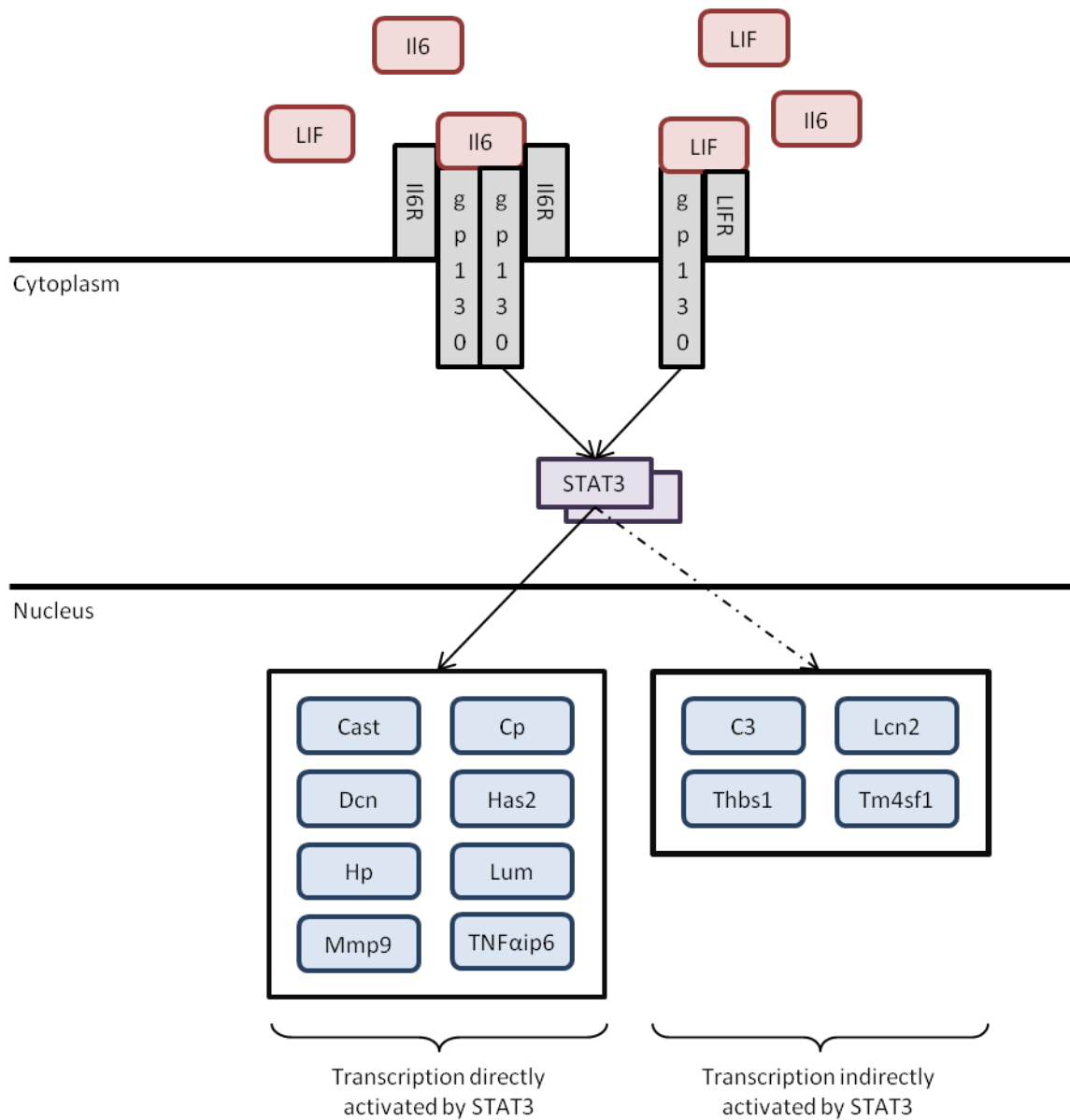


Figure 4.1: Interleukin 6 family cytokine signalling cascade. After the binding of cytokines (IL6 or LIF) to their specific α -subunit receptors (IL6R or LIFR), the activated α -subunit receptor binds to the shared glycoprotein 130 subunit receptor (gp130) (Cornelissen et al., 2011). The cytoplasmic region of gp130 is phosphorylated and in turn activates STAT3 (Kisseleva et al., 2002). Active STAT3 dimerises and translocates to the nucleus to directly transcribe acute phase protein genes such as *Cast*, *Cp*, *Dcn*, *Has2*, *Hp*, *Lum*, *Mmp9* and *TNFaip6*. Transcription of other acute phase protein genes are indirectly regulated by STAT3 transcription, namely *C3*, *Lcn2*, *Thbs1* and *Tm4sf1*.

Interleukin 6 (Il6) is a pro-inflammatory cytokine known to regulate the transcription of acute phase protein genes as a part of the innate immune system and the inflammatory response, collectively known as the acute phase response (Kisseleva et al., 2002; Linker et al., 2008). Acute phase proteins (APPs), also designated acute phase reactants, are proteins whose plasma serum levels increase (positive APPs) or decrease (negative APPs) in response to inflammation. Il6 can bind two types of receptors, membrane bound Il6 receptor (Il6R α) or a soluble Il6 receptor (sIl6R) (Nishimoto and Kishimoto, 2008). All cells of the body express the gp130 receptor (Jones and Rose-John, 2002; Linker et al., 2008). However, cells such as endothelial cells that lack IL6R can still initiate the Il6 signalling pathway via gp130 and sIl6R (Boulanger et al., 2003; Linker et al., 2008; Nishimoto and Kishimoto, 2008; Howlett et al., 2009). sIl6R present in human serum acts as a modulator of systemic response to circulating Il6 (Muller-Newen et al., 1998).

Overproduction of the Il6 cytokine has been shown to play a role in inflammatory autoimmune diseases such as rheumatoid arthritis (RA), juvenile idiopathic arthritis (JIA), inflammatory bowel disease, osteoporosis, multiple sclerosis and various types of cancer (Blay et al., 1992; Nishimoto, 2006; Yoshio-Hoshino et al., 2007; Howlett et al., 2009; Nishimoto, 2010). Wang et al. (2012) found that increased levels of Il6 in the human ovarian carcinoma (A2780) cell line resulted in increased anchorage independent growth, proliferation, adhesion to Matrigel coated plates and invasion of a transwell chamber assay coated with Matrigel. The A2780 cells exhibited increased Mmp9 activity, presumably in response to increased Il6 levels. Mmp9 may have been responsible for the increased invasivity. Gao et al. (2007) found blocking the transcription of the *Il6* gene inhibited cell-cycle progression, cell growth and tumourigenesis in adenocarcinomas.

As discussed in Chapter 3, NIH3T3 (mouse) fibroblasts treated with p37 showed increased expression of the *Il6* and *LIF* cytokine genes. *Il6* expression, in response to 5 μ g/ml p37-treatment, was highest at 2 and 4hr time points and subsequently decreased from 4 to 24hr (Table 3.3). The early induction of *Il6* indicates it may function as an initiator of the acute phase response seen in the p37-treated NIH3T3 cells.

The aim of the following experiments was to determine whether the p37-induced

expression of genes encoding acute phase proteins was due to an increase in Il6 levels. NIH3T3 fibroblasts possess the Il6 specific α -subunit receptor (Il6R) (Gyotoku et al., 2001; Peters et al., 2001). We used an Il6R specific antibody to block the Il6 receptor at the cell surface and determined if p37-induced gene expression was affected.

4.2 RESULTS AND DISCUSSION

4.2.1 Effect of the IL6Ri antibody on the expression of the nineteen selected genes

To test whether p37 functions via the IL6 pathway, an antibody (IL6Ri) directed against the interleukin 6 receptor α (IL6R) and its soluble counterpart (sIL6R) was employed. The IL6Ri antibody is a LEAFTM purified anti-mouse/rat CD126 (IL-6R α chain) purchased from BioLegend (Cat# 115809). The antibody binds the 80kDa IL6R chain and blocks binding of the gp130 receptor. The IL6 signalling cascade involving the phosphorylation of STAT3 is blocked and hence transcription of acute phase proteins (APP) is inhibited.

Initially, NIH3T3 fibroblasts were treated with 0.1 μ g/ml IL6Ri for 25hr (Figure 4.2). A 1hr treatment is required for IL6Ri to block all IL6R molecules. Quantitative (q) PCR (Section 2.12) was used to determine the transcript levels of the nineteen genes previously selected from the microarray analysis (Chapter 3). Eleven of the nineteen genes selected showed significant fold changes when IL6Ri (0.1 μ g/ml) was present. The fold changes ranged from 2 to 6-fold (Figure 4.2).

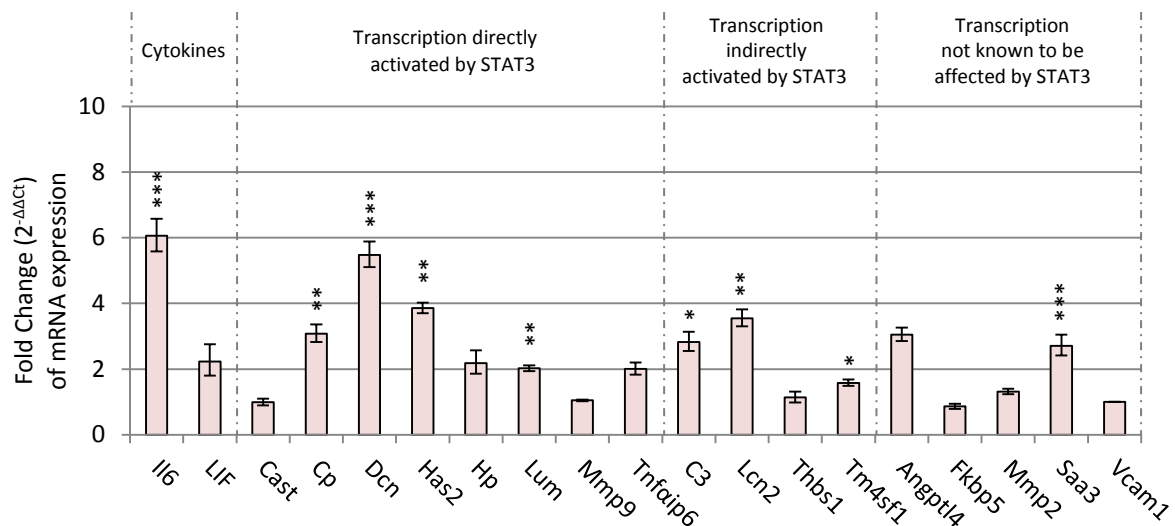


Figure 4.2: Gene expression in NIH3T3 (mouse) fibroblasts treated with 0.1 μ g/ml IL6R antibody inhibitor for 25 hours. NIH3T3 (mouse) fibroblasts were treated with 0.1 μ g/ml of the IL6R α inhibitor (IL6Ri) LEAFTM purified anti-mouse/rat CD126 (IL6R α chain) (BioLegend, Cat# 115809), for 25hrs (Section 2.19.3). The messenger RNA levels are expressed as fold change (2^{-ΔΔCt}) in relation to untreated controls (Section 2.12.6). Significant differences between treated and untreated were calculated by ANOVA analysis (* p<0.05, ** p<0.01, ***p<0.001). Error bars depict \pm SE in relation to fold change (Section 2.12.8). Raw data presented in Appendix XII.

Il6 expression increased 6-fold following *Il6Ri* treatment; however, expression of the *Il6* family cytokine *LIF* was unaffected. Genes directly activated by the *Il6* pathway, namely *Cp* (3-fold), *Dcn* (5-fold), *Has2* (4-fold) and *Lum* (2-fold), were significantly up-regulated following *Il6Ri* treatment while *Cast*, *Hp*, *Mmp9* and *TNFaip6* were not. *STAT3* may also increase serum levels of acute phase proteins indirectly by inducing other transcription factors or activating proteins. *C3* (3-fold), *Lcn2* (4-fold) and *Tm4sf1* (2-fold) are genes indirectly activated by the *Il6/STAT3* pathway (Liu et al., 2009; Sidhu et al., 2011). Genes not regulated by the *Il6/STAT3* pathway, namely *Angptl4* and *Saa3* also showed a 3-fold increase in expression.

Il6 expression is activated by an inflammatory stimulus, however, under normal conditions serum levels are stabilized between expression and elimination (Nishimoto et al., 2008). Elimination from the serum can be via receptor binding or degradation (Nishimoto et al., 2008). The marketed drug Tocilizumab is a humanized anti-*Il6* receptor antibody used to treat acute inflammation that causes rheumatoid arthritis and Castleman disease. The Tocilizumab antibody binds to the human *Il6* receptor inhibiting *Il6/STAT3* signalling, thereby preventing the progression of the structural joint damage associated with rheumatoid arthritis. Although Tocilizumab inhibits *Il6* signalling, Nishimoto et al. (2008) reported that the use of Tocilizumab significantly increased *Il6* levels in joint synovial fluid of healthy adults. The authors suggested the increased *Il6* levels were due to the inhibition of a negative feedback loop activated via the *Il6/STAT3* pathway. *NF-κB* is a transcriptional activator of *Il6* expression. If *Il6* activation of *STAT3* is required for the inhibition of *NF-κB* transcription then the inhibition of the *Il6R* would result in the increased activity of *NF-κB* and consequently increased *Il6* expression. The increased expression of *Il6* and genes encoding acute phase proteins following *Il6Ri* treatment we observed is possibly due to the disturbance of negative feedback loops which allow activation of alternative pathways. *NF-κB* is also responsible for the transcription of other acute phase genes such as *LIF*, *Angptl4*, *Saa3* and *Vcam1*.

4.2.2 The role of the Il6R in the activation of p37-induced gene expression

NIH3T3 fibroblasts were pre-treated with 0.1 μ g/ml Il6R α antibody inhibitor (Il6Ri) for an hour before the addition of 5 μ g/ml or 25 μ g/ml purified p37 and incubating for a further 24hr (Section 2.19.3). qPCR was used to determine the expression levels of the nineteen genes selected for further analysis from Chapter 3.

No reduction in p37-induced gene expression levels resulted from blocking the Il6R. On the contrary, both Il6Ri+5 μ g/ml p37 and Il6Ri+25 μ g/ml p37-treatments (24hr) caused an even greater increase in gene expression than the 5 μ g or 25 μ g/ml p37-treatments alone (Figure 4.3). *Il6* expression was significantly up-regulated in both the Il6Ri+5 μ g/ml p37 and Il6Ri+25 μ g/ml p37-treatments.

Thirteen of the nineteen genes examined exhibited significantly higher ($p < 0.05$) expression levels when Il6Ri was included with 5 μ g/ml p37 (Figure 4.3A). Some of the increases in expression were substantial, for example, an increase from 7- to 143-fold for *Hp*, 1- to 59-fold for *Lum*, 13- to 118-fold for *C3* and 23- to 437-fold for *Lcn2*. When the p37 concentration was increased to 25 μ g/ml, nine genes were significantly ($p < 0.05$) more highly expressed (Figure 4.3B). These increases again were also substantial; *Hp* expression increased from 8- to 180-fold, *Lum* from 3- to 68-fold, *C3* from 54- to 472-fold, *Lcn2* from 98- to 612-fold and *Fkbp5* from 1- to 39-fold (Figure 4.3B). Expression of *Cast*, *Vcam1* and *Mmp2* were not significantly affected by p37 or p37+Il6Ri treatments. Expression of the two cytokine genes *Il6* and *LIF* was stimulated 18-fold/26-fold and 15-fold/11-fold by including p37 (5 μ g or 25 μ g/ml, 24hr) with the Il6Ri pre-treatment (1hr).

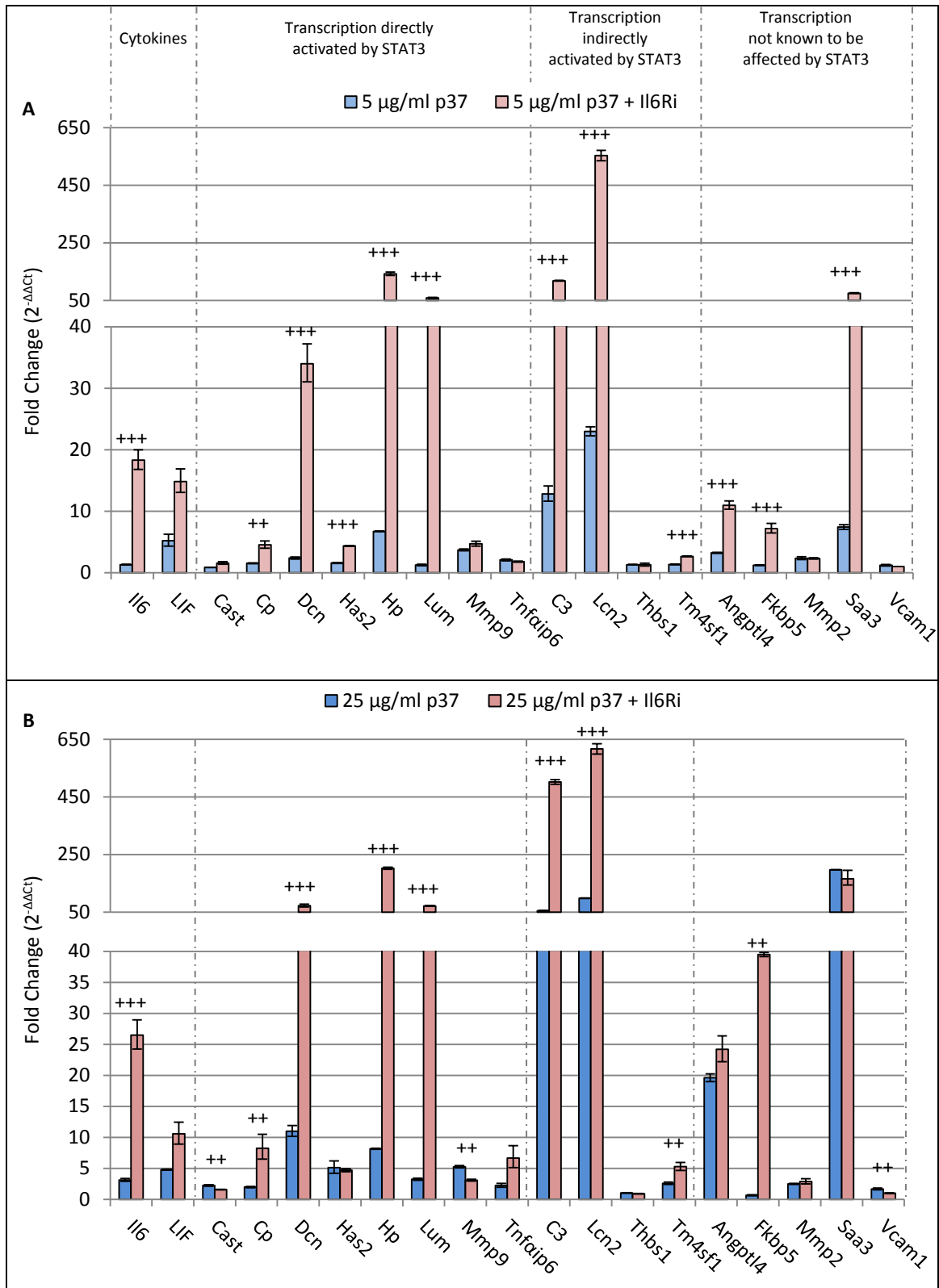


Figure 4.3 Gene expression of NIH3T3 (mouse) fibroblasts treated with 0.1µg/ml IL6Ri and 5µg/ml or 25µg/ml p37. NIH3T3 (mouse) fibroblasts were pre-treated with 0.1µg/ml IL6Ri for an hour before treatment with 5µg/ml (A) or 25µg/ml (B) p37 for an additional 24hrs. The messenger RNA levels are expressed as fold change ($2^{-\Delta\Delta C_t}$) in relation to untreated controls. Significant differences between p37 treated and p37+IL6Ri were calculated by ANOVA analysis (* $p < 0.05$, ** $p < 0.01$, *** $p < 0.001$). Error bars depict \pm SE in relation to fold change (Section 2.12.8). Raw data presented in Appendix XII.

A similar trend of increased gene expression resulted from the addition of Il6Ri at both 5 μ g and 25 μ g/ml p37 concentrations. A strong positive correlation between treatments was shown by a Pearson correlation coefficient, r , of 0.87 (Figure 4.4). No significant outliers were observed with the exception of *Lcn2*.

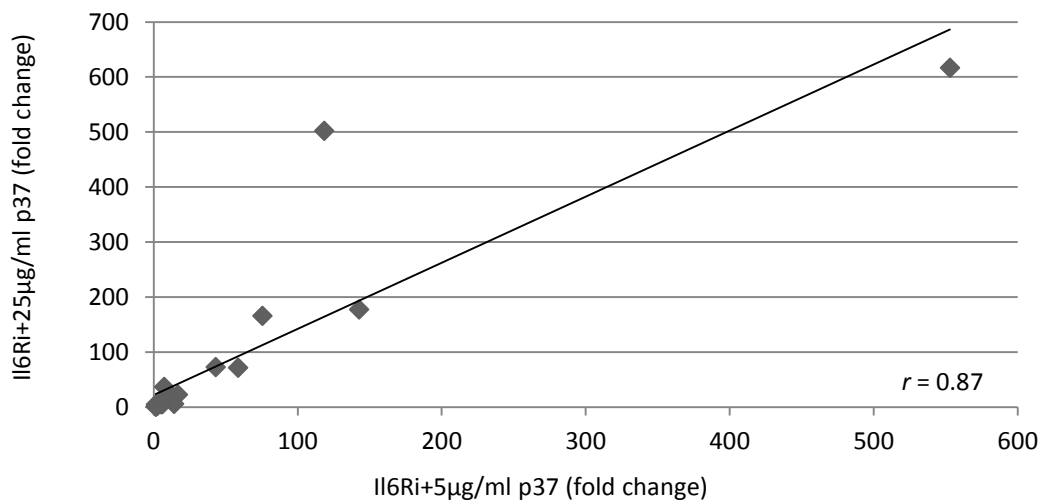


Figure 4.4: Correlation between Il6Ri+25 μ g/ml p37 and Il6Ri+5 μ g/ml p37 treatments. Correlation indicates fold change values of the two different treatments Il6Ri+25 μ g/ml p37 and Il6Ri+5 μ g/ml p37 for 19 genes regulated by 24hr p37 treatment. The positive correlation, indicative of the trend line, has a high Pearson correlation coefficient (r) of 0.87. Calculations for Pearson correlation coefficient presented in Appendix XII.

4.3 CONCLUSION

The aim of blocking the Il6 receptor (Il6R) was to ascertain whether p37-activation of acute phase proteins was at least in part a consequence of the observed increase in *Il6* expression. Il6R inhibition caused a 6-fold increase in *Il6* expression (Figure 4.2) suggesting a feedback effect was occurring (Section 4.2.1). However, blocking the Il6R resulted in a stronger increase in p37-induced acute phase protein genes normally activated by Il6. Il6 acts as both a pro- and anti-inflammatory cytokine (Tilg et al., 1994; Scheller et al., 2011). The anti-inflammatory effect of Il6 includes the inhibition of the pro-inflammatory cytokines TNF α and Il1 (Schindler et al., 1990). Il6 also activates STAT3 transcription of the anti-inflammatory cytokine Il10 (Steensberg et al., 2003). Expression levels of these genes were not determined in the Il6Ri-treated NIH3T3 cells.

A second possibility is that down-regulation of STAT3 signalling occurs as a consequence of blocking the Il6R. As discussed in the next chapter (Section 5.3), STAT3 inhibition appears to initiate the anti-inflammatory activity of Il10. Moreover, STAT3 inhibition over-activates both Toll-like receptor (TLR) and STAT1 signalling, resulting in increased pro-inflammatory signalling (Karim C. El Kasmi, University of Colorado, personal communication).

A neutralizing Il6R antibody has been found to increase rather than decrease gene transcription in Il6-treated macrophages (Karim C. El Kasmi, University of Colorado, personal communication). The reasons are not known but it is possible that the Il6 antibody promotes STAT signalling or up-regulates other surface receptor such as TLRs, Il6R or Il4R. The Il6Ri antibody pre-treatment may have blocked endogenous Il6/STAT3 pathways which are then compensated for by STAT1. Hence, aberrant and enhanced gene transcription would be induced by p37-treatment.

The complex cellular response to blocking Il6R means that we are unable to determine to what extent the activation of *Il6* expression by p37 is involved in subsequent gene activation. Using cells in which *Il6* is knocked out, for example using RNAi, is an option but again pleiotropic effects may render interpretation difficult.

5. THE EFFECT OF INHIBITING STAT3 ON P37-INDUCED GENE EXPRESSION

5.1 INTRODUCTION

Signal Transducers and Activators of Transcription (STATs) are transcription factors that are activated by phosphorylation in response to extracellular cytokines and growth factors (Kisseleva et al., 2002; Sherry et al., 2009; Cornelissen et al., 2011). STATs are phosphorylated by the Janus Kinases (JAK) family of kinases which associate with the intracellular domain of cytokine bound receptors. Unphosphorylated STAT3 is localized within the nucleus of cells and translocates to the cytoplasm for activation after the initiation of a cytokine or growth factor signalling pathways (Kisseleva et al., 2002; Sherry et al., 2009; Cornelissen et al., 2011). *STAT3* expression does not occur unless there is a depletion of unphosphorylated STAT3 within the cell. Phosphorylated active STAT forms homo- or hetero-dimers and translocates to the nucleus to initiate transcription (Kisseleva et al., 2002). The IL6 family of cytokines, such as IL6 and LIF, specifically activate STAT3 which subsequently activates transcription of acute phase proteins (Faruqi et al., 2001; Nishimoto and Kishimoto, 2008; Raptis et al., 2009). IL6 activated STAT3 also increases the transcription of genes encoding proteins responsible for cell cycle progression (Barre et al., 2003).

Murine and human inflammation associated tumourigenesis, malignancy and cancer progression have been linked to STAT3 activity (Mantovani et al., 2008; Rebouissou et al., 2009). Constitutively active STAT3 has been shown to regulate Src dependent transformation of fibroblasts and is also reported within the bone marrow mononuclear cells of patients with multiple myeloma (Catlett-Falcone et al., 1999; Kisseleva et al., 2002). Active STAT3 controls cell proliferation, survival, differentiation and development (Bowman et al., 2000). Inhibition of STAT3 signalling has been shown to arrest the cell cycle, induce apoptosis and inhibit tumour cell invasion in colorectal cancer cells (Xiong et al., 2008). Down-regulation of *STAT3* also induces apoptosis in vSrc-transformed NIH3T3 cells (Anagnostopoulou et al., 2006).

Expression of the genes encoding the cytokines Il6 and LIF increased in p37-treated NIH3T3 cells (Chapter 3). However, inhibition of the Il6 receptor resulted in continued and increased expression of genes encoding for acute phase proteins (Chapter 4), possibly as a result of STAT3 activation by other cytokines such as LIF. The aim of the experiments described in this chapter was to determine whether p37-induced gene expression of acute phase proteins was indeed via STAT3 activation. A chemical probe, S31-201, which binds the Src homology 2 (SH2) domain of STAT3 was used. The probe inhibits STAT3 phosphorylation and dimerisation preventing it from inducing transcription (Siddiquee et al., 2007).

5.2 RESULTS AND DISCUSSION

5.2.1 Effects of p37 on *STAT3* transcription in NIH3T3 cells

Quantitative (q) PCR (Section 2.12) was used to determine whether *STAT3* expression was induced by p37. Treatment of NIH3T3 cells with different concentrations of p37 (24hr) failed to significantly influence *STAT3* expression (Figure 5.1A). However, a p37 concentration of 5 μ g/ml caused an approximate 2-fold increase in *STAT3* expression at 4, 8 and 12hr of treatment (Figure 5.1B). Blocking the Il6 receptor resulted in a slight increase in *STAT3* expression (2-fold) and in the presence of 25 μ g/ml p37, *STAT3* expression increased 3-fold (Figure 5.1C).

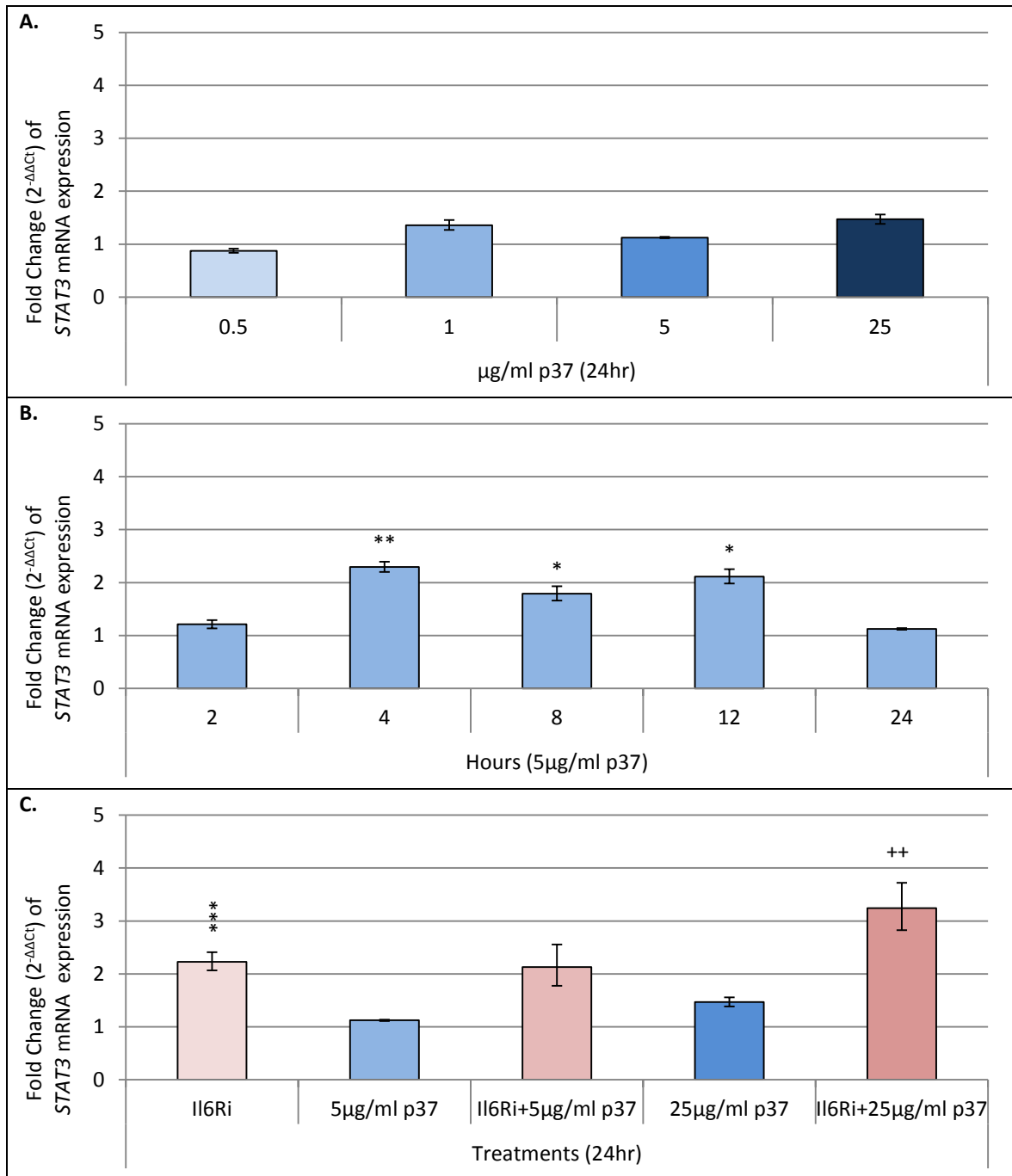


Figure 5.1: STAT3 expression in p37-treated NIH3T3 cells at different concentrations, at different times and the effect of IL6R inhibition. (A) NIH3T3 cells were treated with varied concentrations (0.5, 1, 5 and 25µg/ml) of p37 for 24hr. **(B)** NIH3T3 cells were treated with 5µg/ml p37 for 2, 4, 8, 12 and 24hr. **(C)** NIH3T3 cells were treated with 0.1µg/ml of the IL6Rα inhibitor (IL6i) LEAF™ purified anti-mouse/rat CD126 (IL6Rα chain) (BioLegend, Cat# 115809), for 25hrs or NIH3T3 were pre-treated with 0.1µg/ml IL6Ri for an hour before treatment with 5µg/ml or 25µg/ml p37 for an additional 24hrs. Messenger RNA levels are expressed as fold change ($2^{-\Delta\Delta Ct}$) in relation to untreated controls (Section 2.12.6). Significant differences between treated and untreated cells (* p<0.05, ** p<0.01, ***p<0.001) or p37-treated and p37+IL6Ri treated (*p<0.05, **p<0.01, ***p<0.001) were calculated by ANOVA analysis. Error bars depict ±SE in relation to fold change (Section 2.12.8). Raw data presented in Appendix XIII.

5.2.2 Effect of the STAT3 inhibitor S31-201 on p37-induced gene expression

STAT3 Inhibitor VI, S31-201, also known as NSC74859 (Figure 5.2), docks to the Src homology 2 (SH2) domain of STAT3, inhibiting its ability to phosphorylate and homo/heterodimerise (Siddiquee et al., 2007). Siddiquee et al. (2007) found that 100 μ M S31-201 completely inhibited STAT3 dimerisation in vSrc-transformed NIH3T3 cells after 24hr to 72hr treatments; vSrc-transformed NIH3T3 cells contain constitutively active STAT3. The growth and viability of normal NIH3T3 fibroblasts were not significantly altered by treatment with S31-201.

Consequently, a concentration of 100 μ M S31-201 was chosen and NIH3T3 fibroblasts treated for 48hrs (Section 2.19.4). Quantitative (q) PCR (Section 2.12) was used to calculate the transcript levels of the nineteen genes previously selected for further analysis based on the data presented in Chapter 3.

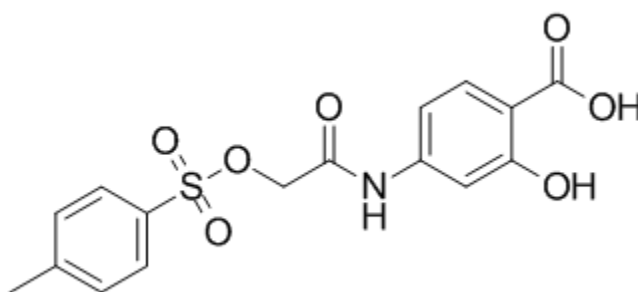


Figure 5.2: Chemical backbone of the STAT3 Inhibitor VI, S31-201 (NSC74859). The S31-201 molecular formula is C₁₆H₁₅NO₇S with an average molecular weight of 365 Daltons. (From Santa Cruz Biotechnology;sc-204304)

Inhibiting STAT3 activity in NIH3T3 cells resulted in slightly increased expression (2- to 3-fold) of *Il6*, *Has2*, *Hp*, *Lcn2* and *Saa3* while expression levels of *LIF*, *Fkbp5*, and *Mmp2* decreased (Figure 5.3).

Increase in *Il6* expression has been observed with the STAT3 inhibitor JS1-124 (cucurbitacin), a chemical compound similar to S31-201. STAT3 inhibition with JS1-124 (1 μ mol/L) increased *Il6* expression 5-fold after 1hr in human neuronal glioblastoma (U251-MG) cells (McFarland et al., 2013). The combined inhibition of NF- κ B and STAT3 inhibited the expression of *Il6*. The activation of NF- κ B may account for the increase in expression of *Il6*, *Has2*, *Hp* and *Saa3* when STAT3 activity is blocked by S31-201 in NIH3T3 cells (Figure 5.3). Although the expression of these four genes was significantly increased by S31-201 treatment, the fold changes were still significantly lower than the fold changes induced by p37-treatment (25 μ g/ml, 24hr) alone.

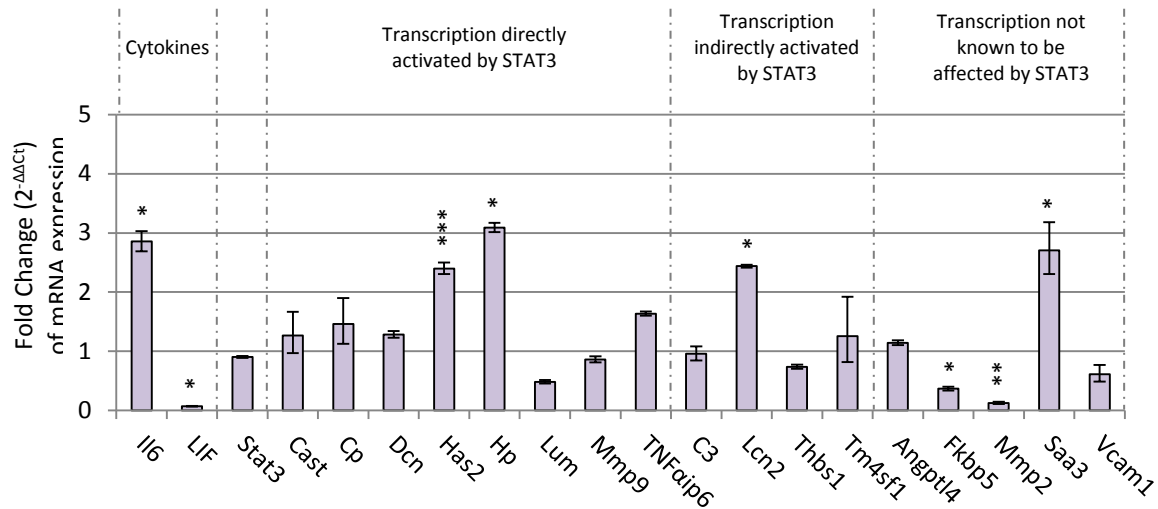


Figure 5.3: Gene expression in STAT3 inhibited NIH3T3 (mouse) fibroblasts. NIH3T3 (mouse) fibroblasts were treated with 100 μ M S31-201 for 48hrs. The messenger RNA levels are expressed as fold change (2^{-ΔΔCt}) in relation to untreated controls (Section 2.12). Significant differences between treated and untreated were calculated by ANOVA analysis (* p<0.05, ** p<0.01, ***p<0.001). Error bars depict \pm SE in relation to fold change (Section 2.12.8). Raw data presented in Appendix XIV.

NIH3T3 cells were pre-treated with 100 μ M S31-201 for 24hrs prior to treatment with 25 μ g/ml purified p37 for a further 24hrs (S31-201+25 μ g/ml p37) (Section 2.19.4). p37-induction of six of the twenty genes tested was greatly increased when the STAT3 inhibitor was present (Figure 5.4). These six genes and their approximate fold increases resulting from the addition of S31-201 are *Il6* (3- to 23-fold), *Hp* (8- to 180-fold), *Lum* (3- to 11-fold), *C3* (54- to 105-fold), *Lcn2* (95- to 3350-fold) and *Saa3* (197- to 1860-fold). The p37-induction of *LIF* expression was completely inhibited by S31-201 while the p37-induced expression of *Angptl4* was unaffected (Figure 5.4).

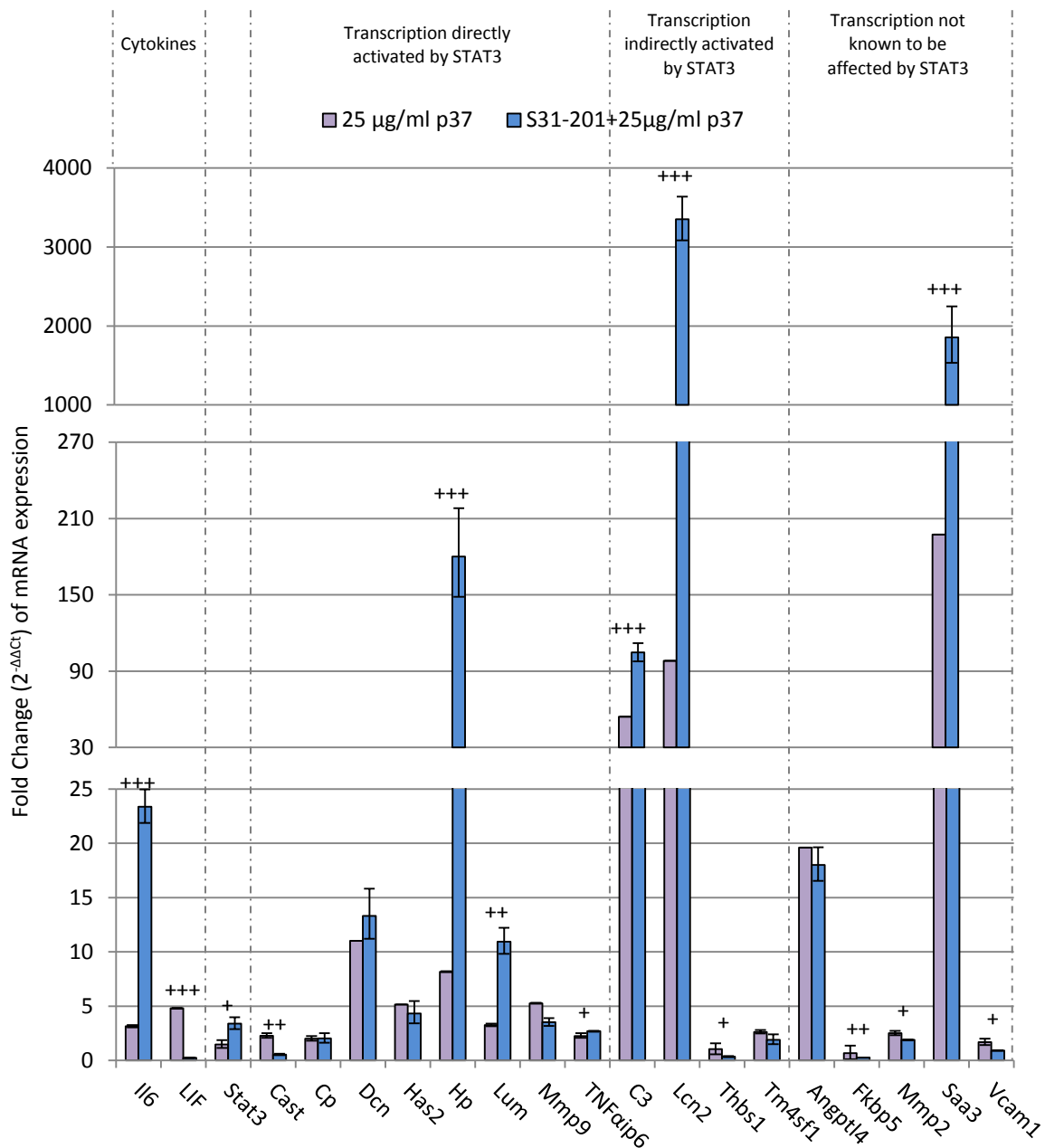


Figure 5.4: STAT3 inhibition effect on p37-induced gene expression in NIH3T3 cells. NIH3T3 (mouse) fibroblasts were pre-treated with 100μM of the STAT3 inhibitor S31-201 for 24hrs before treatment with 25μg/ml p37 for an additional 24hr. The messenger RNA levels are expressed as fold change ($2^{-\Delta\Delta C_t}$) in relation to untreated controls (Section 2.12). Significant differences between S31-201-treated and S31-201+25μg/ml p37 were calculated by ANOVA analysis (* $p < 0.05$, ** $p < 0.01$, *** $p < 0.001$). Error bars depict \pm SE in relation to fold change (Section 2.12.8). Raw data presented in Appendix XIV.

5.2.3 The effect of STAT3 inhibition on p37-induced expression of the inflammatory response and autoimmunity pathway: An RT²Profiler PCR array study

Mouse inflammatory response and autoimmunity pathway RT²Profiler PCR arrays (SABiosciences, PAM-077) were used to analyze the response of 84 genes in S31-201 treated and S31-201 pre-treated, 24hr 25µg/ml p37-treated (S31-201+25µg/ml p37) NIH3T3 cells (Sections 2.19.4 and 2.14). Strong positive correlations of the qPCR cycle threshold (Ct) values were found between the biological triplicates of the S31-201 treatments (Figure 5.5A) and the biological triplicates of the S31-201+25µg/ml p37-treatments (Figure 5.5B). Pearson correlation coefficients (*r*) of 0.99, 0.99 and 0.99 were obtained between S31-201 treatments and 0.98, 0.99 and 0.99 between S31-201+25ug/ml p37-treatment. The closer the Pearson correlation coefficient, *r*, is to 1, the stronger the positive association of two variables. Strong positive correlations between the PCR array biological triplicates of each treatment indicate reliable qPCR detection of gene expression (Figure 5.5). No outliers were observed.

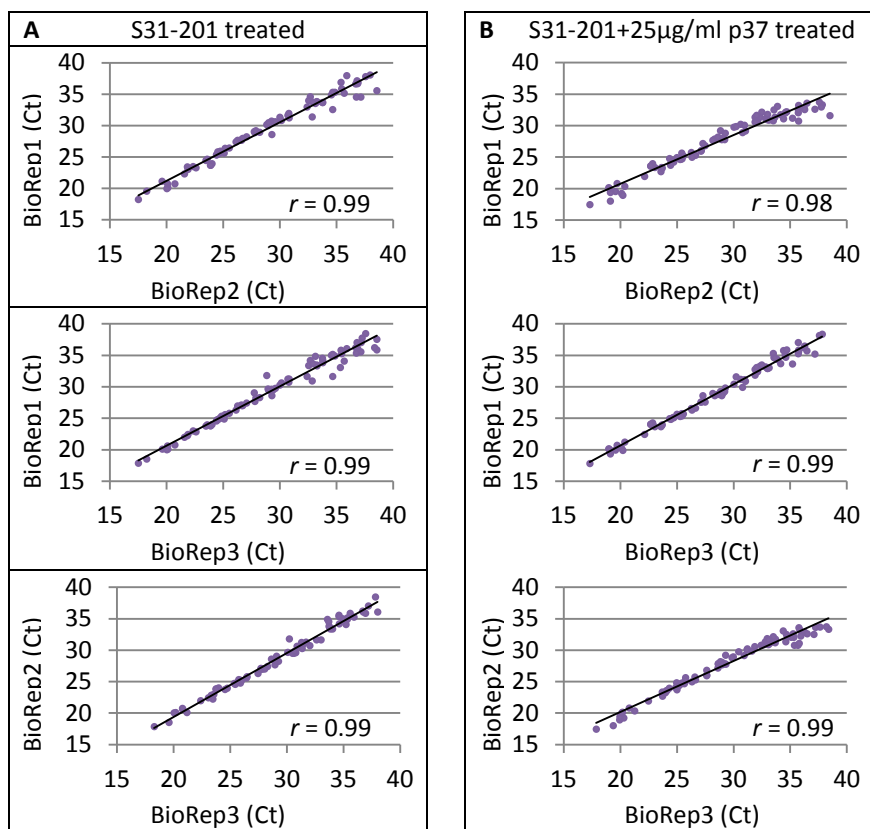


Figure 5.5: Correlation between biological replicates for the inflammatory response and autoimmunity RT²Profiler Array. Graphs indicate the Ct value correlation strength between each replicate (BioRep) of a treatment. **(A)** Strong positive correlations, indicated by the treadline, were observed between the three biological replicates of S31-201 treated NIH3T3 cells with Pearson correlation coefficients (r) of 0.99, 0.99 and 0.99. **(B)** Strong positive correlations, indicated by the treadline, were also observed between the three biological replicates of S31-201+25 μ g/ml p37-treated cells with Pearson correlation coefficients (r) of 0.98, 0.99 and 0.97. Raw data presented in Appendix XV.

Genes with Ct values greater than 35 (Ct>35) were excluded from further analysis as these were not considered reliable Ct expression values. Only 17% of the S31-201 treatments and 18% of the S31-201+25µg/ml p37-treatments had Ct>35, averaged across the three biological triplicates (Figure 5.6).

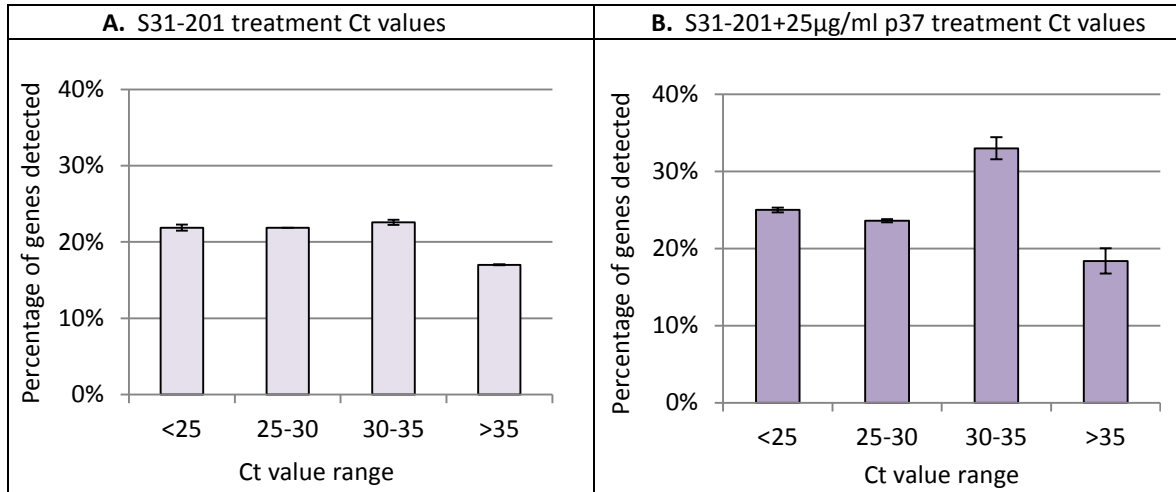


Figure 5.6: Overview of the threshold cycle values for the RT²Profiler Array of the inflammatory response and autoimmunity. (A) Overview of Ct values for biological triplicates of the S31-201 controls. **(B)** Overview of Ct values for biological triplicates of S31-201+25µg/ml p37-treated cells. The mean percentage of the cycle threshold (Ct) values were classified into four ranges; <25, 25-30, 30-35 and >35. Low Ct values (< 25) represent genes with high transcript copy numbers. Ct values of greater than 35 (> 35) were considered outside the detection threshold system. Error bars depict ±SE of the three biological reps of each treatment. Raw data presented in Appendix XV.

Fold change ($2^{-\Delta\Delta Ct}$) of mRNA expression was calculated relative to untreated controls and normalised to the reference genes *GAPDH* and *βactin* which are not affected by p37-treatment. Similar trends in fold changes due to S31-201 and S31-201+25µg/ml p37-treatments were obtained to those in Section 5.2.2 (Figure 5.3 & Figure 5.4). No significant increases in gene expression were detected in NIH3T3 cells treated with 25µg/ml p37 (Figure 5.7A). S31-201 treatment resulted in the up-regulation of six and down-regulation of two genes (Figure 5.7B). Combined p37 and S31-201 treatment increased the expression of nineteen genes while one gene was down-regulated (Figure 5.7C).

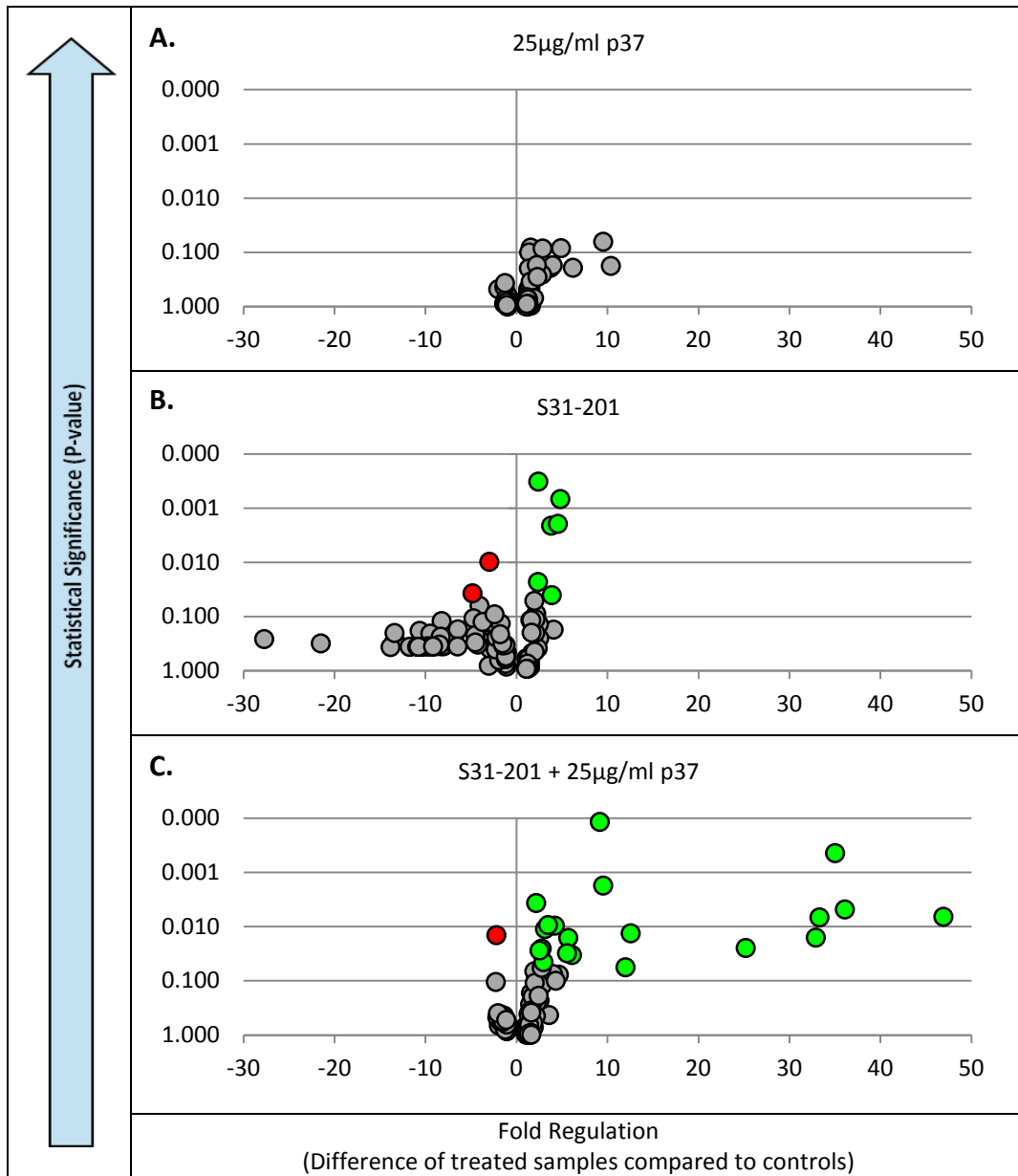


Figure 5.7: Volcano plot of RT²Profiler Array of the Inflammatory Response and Autoimmunity. Triplicate total RNA samples from NIH3T3 fibroblasts (either untreated or treated with 25µg/ml p37, 100µM S31-201, or both 25µg/ml p37 and 100µM S31-201 for 24hrs) were characterized using the inflammatory response and autoimmunity RT²Profiler Array. NIH3T3 cells treated with; **(A)** p37 showed up-regulation of 10 genes (none with p<0.05); **(B)** S31-201 showed up-regulation of 13 genes (5 with p<0.05) and down-regulation of 46 genes (2 with p<0.05); **(C)** p37 and S31-201 showed up-regulation of 36 genes (21 with p<0.05) and down-regulation of 8 genes (1 with p<0.05). Significant differences between treated and untreated were calculated by ANOVA analysis; significantly up-regulated are shown in green (●) and significantly down-regulated are red (●). Raw data presented in Appendix XI.

The genes whose expression was significantly induced following S31-201+25µg/ml p37-treatment are listed below in Table 5.1. The genes *C3*, *Cxcl1*, *Ccl7*, *Ccl2* and *Il6* activated following 25µg/ml p37-treatment (24hr) were identified in the microarray as well as in the RT²Profiler Array and previously discussed in Chapter 3, Section 3.2.7.

Differences occur in the extent to which genes such as *C3* and *Il6* are activated in the qPCR experiments (Figure 5.3 & Figure 5.4) and the PCR array (Table 5.1). The reasons for the discrepancies are not known. The major difference between the two experiments is the oligonucleotides, although the oligonucleotides used in both experiments were tested for efficiency as described in Sections 2.12.2 and 2.12.3. Two separate company kits and protocols were used for RNA processing; Invitrogen for the qPCR and Qiagen for the PCR array. Moreover, three biological replicates were employed in the PCR array whereas for all qPCR experiments three experimental replicates of three biological replicates were used. Nonetheless, the results consistently show that p37 and S31-201 significantly stimulate the expression of *C3* and *Il6*.

The PCR array identified a number of additional genes whose expression is strongly induced by the combination of p37 and STAT3 inhibition. These include the chemokines genes *Cxcl1*, *Cxcl5*, *Cxcl10*, *Ccl5*, *Ccl7* and *Ccl2*. Chemokines are a family of small cytokines, approx 8-10kDa, that function as pro-inflammatory proteins, inducing the immune response or controlling cell migration during normal processes of tissue maintenance and development.

Il10rβ and *Il1r1* expression were also activated (9-fold and 10-fold) as was *Il18* (6-fold) (Table 5.1). *Il10rβ* forms the *Il10* receptor complex with *Il10rα* and is activated by the *Il10* cytokine (Pletnev et al., 2005). *Il10rβ* is the signal transducer of the receptor complex and is known to activate STAT3 (Weber-Nordt et al., 1996). *Il1r1* is also a part of a cytokine receptor complex that initiates a signal cascade of acute phase proteins following the binding of the *Il1* family of cytokines including *Il1* and *Il18*. *Il1r* activates the transcription factor NF-κB which in turn initiates transcription of the *Il6* gene (Contassot et al., 2012). The transcription factor NF-κB was also found to be up-regulated 3-fold in response to S31-201+25µg/ml p37-treatment.

The gene encoding Lymphocyte antigen 96 (Ly96) was up-regulated 6-fold when p37 and the STAT3 inhibitor were present. Ly96 is an assistant protein that increases the binding ability of TLR4 to the PAMP lipopolysaccharide (LPS). Consequently, LPS will preferentially bind to TLR4 rather than TLR1 and TLR2 (Shimazu et al., 1999; Re and Strominger, 2002; DeMarco and Woods, 2011).

Table 5.1: Genes identified in the inflammatory response and autoimmunity RT²Profiler Array. NIH3T3 cells were treated with S31-201 or S31-201 and 25µg/ml p37 over 24hr. The mouse inflammatory response and autoimmunity pathway (SABiosciences; PAM-077A) RT² Profiler PCR arrays were used to determine mRNA expression levels. Fold change ($2^{-\Delta\Delta Ct}$) of mRNA expression was calculated relative to untreated controls and normalised to the reference genes *GAPDH* and *βactin*. Fold changes with a p-value < 0.05 are shown in bold. Genes chosen for further analysis are shown in bold (Gene title). Raw data presented in Appendix XI.

Gene Title	ID	Fold Change		
		25µg/ml p37 (Section 3.2.7)	S31-201	S31-201+ 25µg/ml p37
Complement component 3	C3	10	1	36
Chemokine (C-X-C motif) ligand	Cxcl1	10	3	47
Chemokine (C-C motif) ligand 5	Ccl5	6	2	13
Chemokine (C-X-C motif) ligand 5	Cxcl5	5	2	33
Chemokine (C-C motif) ligand 7	Ccl7	4	3	33
Chemokine (C-C motif) ligand 2	Ccl2	4	3	35
Chemokine (C-X-C motif) ligand 10	Cxcl10	3	1	6
C-reactive protein, pentraxin-related	Crp	3	1	3
Toll-like receptor 2	TLR2	2	0.3	2
Interleukin 6	Il6	2	5	25
Histone deacetylase 4	Hdac4	2	2	2
Interleukin 10 receptor, beta	Il10rβ	2	4	9
Colony stimulating factor 1	Csf1	1	3	2
Nuclear factor of kappa light	Nfkb	1	1	3
Lymphocyte antigen 96	Ly96	1	2	6
Nuclear factor of activated T-cells, cytoplasmic, calcineurin-dependent 3	Nfatc3	1	2	3
Interleukin 18	Il18	1	4	6
Heat shock protein 90 alpha (cytosolic), class B member 1	Hsp90ab1	1	2	3
Receptor (TNFRSF)-interacting serine-threonine kinase 2	Ripk2	1	3	4
Hypoxanthine guanine phosphoribosyl transferase	Hprt	1	2	3
Interleukin 1 receptor, type I	Il1r1	1	5	10
Interleukin 18 receptor accessory protein	Il18rap	1	0.3	0.5
Toll-like receptor 1	TLR1	1	2	3

5.3 CONCLUSION

Unexpectedly, the addition of p37 to STAT3-inhibited fibroblasts resulted in a greater increase in the gene expression induced by p37-treatment alone. The absence of *STAT3* activity in mouse embryonic fibroblasts (MEFs) has been shown to increase STAT1-dependent pro-inflammatory activation in response to Il6 (Costa-Pereira et al., 2002). It has been suggested that inhibition of STAT3 signalling prevents the anti-inflammatory activity of Il10, thereby promoting activation of alternative pro-inflammatory pathways (Riley et al., 1999). Il10 signals through the STAT3 pathway (Turner et al., 2010), however, the signals induced differ from those induced by Il6. Monocyte-derived macrophages exhibit potent STAT3 phosphorylation in response to Il10 (Turner et al., 2010). However the genes transcribed by Il10-activated STAT3 differ from the genes transcribed by Il6-activated STAT3. For example Il10/STAT3 signalling induces the expression of suppressor of cytokine signalling 3 (SOCS-3) which inhibits the phosphorylation of STAT1 (Driessler et al., 2004). Constitutively active STAT3 mimics the anti-inflammatory actions of Il10 (Williams et al., 2007).

The activation of genes by p37 encoding acute phase proteins resembles gene expression activated by lipopolysaccharides (LPS). LPS are major structural components of the outer wall of gram-negative bacteria that activate the toll-like receptor 4 (TLR4), eliciting a strong inflammatory response (Poltorak et al., 1998). When *STAT3* is knocked out in mice, the animals become extremely sensitive to LPS challenge. The mice exhibited a strong inflammatory response and subsequently died (Kano et al., 2003).

p37-treatment increased expression of some chemokine genes, suggesting enhanced NF- κ B signalling downstream of LPS/TLR4 pathways. Macrophages deficient in *STAT3* exhibited a strong increase in pro-inflammatory signalling and constitutively secreted the pro-inflammatory cytokines TNF α , Il1, Il6 and Il12 in response to inflammatory stimuli (Takeda et al., 1999). The authors suggested that this was due to increased STAT1 signalling, as STAT1 phosphorylation increased in *STAT3* deficient macrophages. Whether STAT1 signalling occurred in the p37-treated *STAT3* inhibited NIH3T3 cells is not known, however, expression of the STAT1 targeted genes *Cxcl10* and *Il1r1* were stimulated 6- and

10-fold, respectively (Table 5.1).

The increased expression of some chemokine genes by p37-treatment suggests greatly enhanced NF- κ B signalling downstream of TLR pathways. TLRs and STAT1 signalling are over-activated following STAT3 inhibition, resulting in increased pro-inflammatory signalling (Karim C. El Kasmi, University of Colorado, personal communication). The strong additional increase in chemokine expression when STAT3 inhibition is combined with p37-treatment could be due to increased activation of STAT1, STAT3 or NF- κ B signals or a combination of the three. The increased expression of the genes encoding the Il1r1 and Cxcl10 (Table 5.1), for example, is consistent with increased STAT1 signalling.

6. P37 ACTIVATES THE EXPRESSION OF ACUTE PHASE PROTEINS VIA TOLL LIKE RECEPTOR 4 PATHWAY

6.1 INTRODUCTION

Toll-like receptors (TLRs) are receptors that recognize pathogen associated molecular patterns (PAMPs) of gram positive and negative bacteria or damage-associated molecular patterns (DAMPs) of endogenously derived molecules released from necrotic cells (Medzhitov and Janeway, 2000; Takeda and Akira, 2005; Spirig et al., 2012). Toll-like receptor expression is constitutive in many immune cells allowing detection and elimination of pathogens as well as re-building the damage caused by pathogens via activation of the innate immune and adaptive immune systems.

The toll-like receptor 4 (TLR4) can be activated by lipopolysaccharides (LPS) from gram-negative bacteria, fusion proteins from the respiratory syncytial virus and envelope proteins from the mouse mammary tumour virus (Poltorak et al., 1998). A *TLR4* gene mutation in C3H/HeJ mice predisposes the animals to gram negative bacterial sepsis (Poltorak et al., 1998). Following activation of TLR4, adaptors containing Toll-interleukin-1 receptor (TIR) domains are recruited, including myeloid differentiation primary response 88 (MyD88) with its adaptor protein MyD88-adaptor-like (Mal) and TIR domain-containing adaptor inducing IFN- β (TRIF) with its adaptor protein TRIF-related adaptor molecule (TRAM) (Dunne et al., 2003; Oshiumi et al., 2003; Stack et al., 2005; Stack and Bowie, 2012). MyD88 and TRIF phosphorylate the inhibitory protein I kappa B ($\text{I}\kappa\text{B}$) bound to the transcription factor Nuclear Factor Kappa-light-chain-enhancer of activated B cells (NF- κB). Following phosphorylation $\text{I}\kappa\text{B}$ dissociates from NF- κB and is degraded. Dissociation of $\text{I}\kappa\text{B}$ activates NF- κB allowing for the transcription of genes encoding cytokines such as TNF α , IL1 β , IL6, IL12 and IL8, thereby initiating many signal pathways leading to the inflammatory response (Chi et al., 2006). MyD88 activates early NF- κB transcription of pro-inflammatory cytokines whereas TRIF activates late NF- κB transcription of Type 1 interferons (Figure 6.1) (Cirl et al., 2008; Lu et al., 2008).

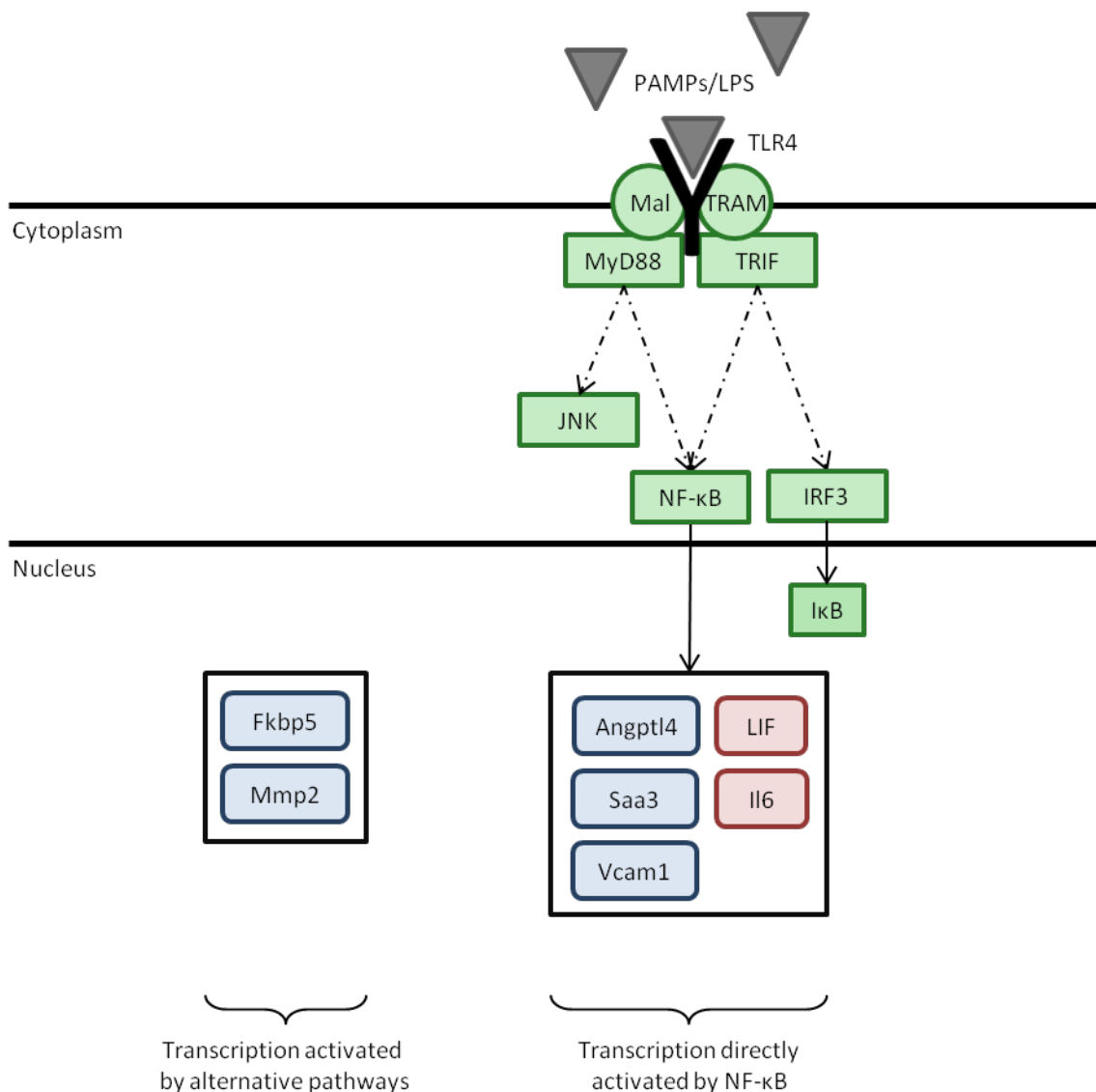


Figure 6.1: Lipopolysaccharide activation of Toll-like receptor 4 signalling pathway. Lipopolysaccharides (LPS) activate Toll-like receptor 4 (TLR4) inducing downstream signalling pathways; myeloid differentiation primary response 88 (MyD88) and TIR domain-containing adaptor inducing IFN- β (TRIF). MyD88 is recruited alongside its adaptor protein MyD88-adaptor-like (Mal) and TRIF with its adaptor protein TRIF-related adaptor molecule (TRAM). MyD88 is recruited to TLR4 in early phase indirect activation of Nuclear Factor Kappa-light-chain-enhancer of activated B cells (NF- κ B) which consequently induces transcription of acute phase proteins, cytokines and chemokines. MyD88 also activates c-Jun Kinase (JNK) which activates acute phase protein transcription. TRIF recruitment by TLR4 occurs in late phase indirect activation of NF- κ B. TRIF also activates Interferon regulatory factor 3 (IRF3) which is responsible for the activation of the NF- κ B inhibitor I kappa B (I κ B) (Chi et al., 2006). Active NF- κ B transcribes acute phase proteins such as *Angptl4*, *Saa3*, *Vcam1*, *LIF*, *IL6*.

Although TLR4 plays a positive role in the activation of an inflammatory response against pathogens, more recently TLR4 has been linked to the pathogenesis of chronic inflammatory diseases such as rheumatoid arthritis as well as tumour establishment and progression. Increased expression of TLR4 and the IL6 cytokine has been found in the peripheral blood mononuclear cells (PBMC) and synovial fluid monocytes of juvenile idiopathic arthritis patients (Myles and Aggarwal, 2011). Tumor aggressiveness in breast cancer has also been associated with increased *TLR4* expression (Gonzalez-Reyes et al., 2010). The inhibition of TLR4 signalling in experimental arthritis resulted in the protection of mice against cartilage and bone degradation initiated by *E. coli* LPS (Abdollahi-Roodsaz et al., 2007).

The aim of the following experiments was to determine whether p37-induced gene expression of acute phase proteins is via activation of Toll-like receptor 4 (TLR4).

6.2 RESULTS AND DISCUSSION

6.2.1 Lipopolysaccharides (LPS) stimulate *Saa3* expression in NIH3T3 cells

Toll-like receptor (TLR) gene expression is constitutive in many immune cells, however, Toll-like receptor 4 (TLR4) mRNA has been identified in a variety of other cell lines (Kurt-Jones et al., 2004). To test if NIH3T3 mouse fibroblasts express and signal via TLR4, lipopolysaccharides (LPS) were used. LPS are major structural components of the outer wall of gram-negative bacteria. *E. coli* 0111:B4 Ultrapure LPS is a preparation of LPS that binds and specifically activates TLR4 signalling (InvivoGen; Cat# tlrl-3pelps).

Triplicate NIH3T3 cell cultures were treated for 24hr with four different concentrations of LPS (0.01, 0.1, 1 or 10µg/ml) (Section 2.19.5). Quantitative (q) PCR was used to analyse the mRNA expression (Section 2.12) of the three genes *Il6*, *Saa3* and *TNFaip6*, as previous research has shown that the TLR4 pathway activates their expression (Litvak et al., 2009; Geurts et al., 2011).

A significant (12-fold) increase of *Saa3* expression was obtained after 24hr following 1µg and 10µg/ml LPS-treatment of NIH3T3 cells (Figure 6.2). At the lower concentrations of 0.01 and 0.1µg/ml, LPS did not induce significant *Saa3* expression. In 1µg/ml LPS-stimulated NIH3T3 cells, Geurts et al. (2011) reported a 36-fold increase of *Saa3* expression, however, this was at 6hr. In 5µg/ml p37-treated cells, *Saa3* expression rapidly increased to 46- and 80-fold after 2 and 4hr treatment, respectively (Table 3.3). Expression subsequently decreased to 66-fold at 8hr, 15-fold at 12hr and 7-fold at 24hr. We did not determine whether LPS change in *Saa3* expression follows a similar time course.

Il6 and *TNFaip6* expression were only slightly affected by 24hr LPS-treatment. Geurts et al. (2011) reported a 28-fold increase in *Il6* expression at 6hr in 1µg/ml LPS-stimulated NIH3T3 cells. The activation of *Il6* expression was strong at 2hr 5µg/ml p37-treatment (42-fold), reaching a maximum at 4hr (98-fold), but decreased drastically over the remaining 24hr (Table 3.3). We did not determine whether LPS-induced *Il6* expression responded similarly. *TNFaip6* expression significantly increased at all 2, 4, 8, 12 and 24hr

time points with 5µg/ml p37-treatment, however, 24hr LPS-treatment failed to increase expression (Figure 6.2).

Based on the induction of *Saa3* expression by LPS, we concluded that TLR4 signalling is occurring in NIH3T3 cell lines. The absence of changes in *Il6* and *TNFaip6* expression may reflect the 24hr treatment time.

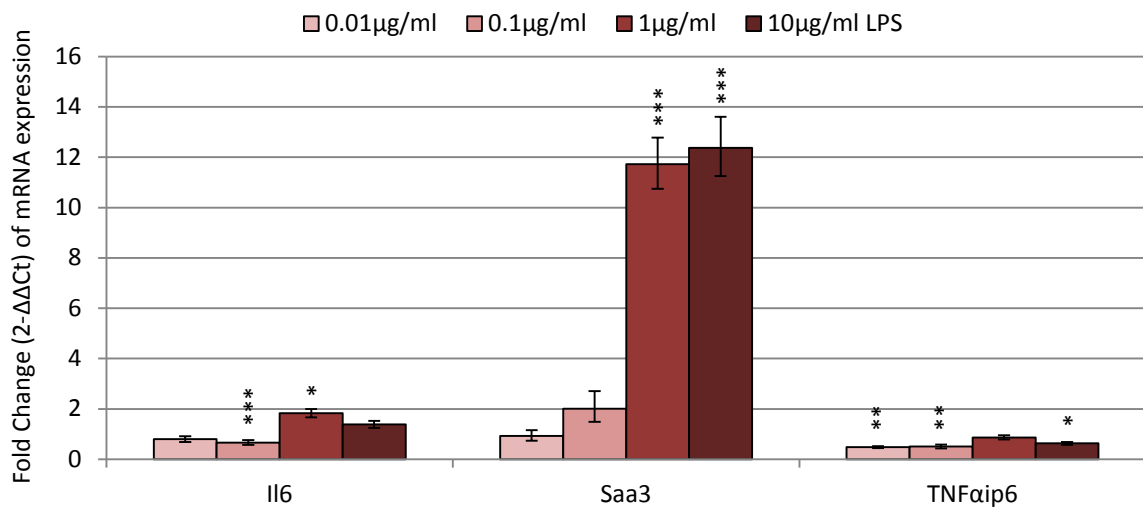


Figure 6.2: *Il6*, *Saa3* and *TNFaip6* gene expression in Ultrapure LPS treated NIH3T3 (mouse) fibroblasts. NIH3T3 cells were treated with varied concentrations (0.01, 0.1, 1 and 10µg/ml) of Ultrapure LPS for 24hr. The fold change ($2^{-\Delta\Delta C_t}$) of *Il6*, *Saa3* and *TNFaip6* mRNA is relative to untreated controls and normalised to reference genes *GAPDH* and *β actin* as described in Section 2.12. Significant differences between treated and untreated cells were calculated by ANOVA analysis (* $p < 0.05$, ** $p < 0.01$, *** $p < 0.001$) and the error bars depict \pm SE in relation to fold change (Section 2.12.8). Raw data presented in Appendix XVI.

6.2.2 VIPER inhibits LPS/TLR4 induced *Saa3* expression in NIH3T3 cells

To determine whether p37 activates transcription of acute phase proteins via the TLR4 signalling pathway, the TLR4 antagonist VIPER and its control peptide CP7 were used. Lysakova-Devine et al. (2010) synthesized fourteen peptides from the vaccinia virus A46 protein. The A46 protein is known to bind multiple cytokine/TLR domain containing proteins and block their signalling. Of the fourteen peptides tested only one peptide specifically inhibited the TLR4 pathway. The peptide was designated Viral Inhibitor Peptide of TLR4, abbreviated to VIPER (Table 6.1). Another of the fourteen peptides, that demonstrated no inhibition against TLR4 signalling, was designated a control peptide of VIPER, CP7 (Table 6.1). A 9 L-arginine (9R) peptide sequence was linked to the C-termini of the VIPER and CP7 peptides to increase cellular up-take (Wender et al., 2000; Siddiquee et al., 2007)

Table 6.1: Peptide sequences of VIPER and CP7 synthesised by Lysakova-Devine et al. (2010) from the vaccinia virus A46 protein. Viral Inhibitor Peptide of TLR4 (VIPER) inhibits the TLR4 signalling pathway. CP7 is the control peptide which does not inhibit TLR4 signalling. Peptides contain a 9 L-arginine (9R) peptide sequence

	Peptide Sequence
VIPER	KYSFKLILAEY-9R
CP7	RNTISGNIYSA-9R

VIPER has been shown to inhibit TLR4 signalling at various concentrations using a range of cell lines. TLR4 signalling was inhibited by VIPER in neuronal primary cell cultures extracted from embryo C57BL/6 mice (2µM), mouse leukemia monocyte-macrophage cell lines (RAW264.7) (1 and 5µM), immortalized bone marrow derived macrophages (iBMDMs) (5µM), human embryonic kidney cell line 293 (HEK293) (5 and 10µM), human peripheral blood mononuclear cells (PBMC) (5 and 25µM), and in BALB/c mice (0.1 and 0.3mg/kg) (Lysakova-Devine et al., 2010; Leow-Dyke et al., 2012). The peptide CP7 did not inhibit TLR4 signalling in the RAW264.7, iBMDMs, PBMC or HEK293 cells. Hence, CP7 was considered a control peptide to be used in experiments involving VIPER and at the same concentration.

VIPER was tested on triplicate non-stimulated NIH3T3 cell cultures at several different concentrations (0.25, 0.5, 0.75, 1, 5, 10 and 25 μ M) for 26hr (Section 2.19.6). In subsequent experiments 24hr LPS-stimulated NIH3T3 cells were pre-treated for 2hrs with VIPER or CP7. Hence, 26hr treatment was chosen for this control experiment. Quantitative (q) PCR was used to calculate the fold change ($2^{-\Delta\Delta Ct}$) of *Saa3* mRNA expression (Section 2.12). Neither peptide significantly (p -value <0.05) affected *Saa3* expression, with exception of an approximately 25% decrease with 10 μ M and 25 μ M CP7 and VIPER, respectively (Figure 6.3). An approximate 25% increase of *Saa3* expression was observed at 25 μ M CP7, however, this increase was not statistically significantly (p -value >0.05).

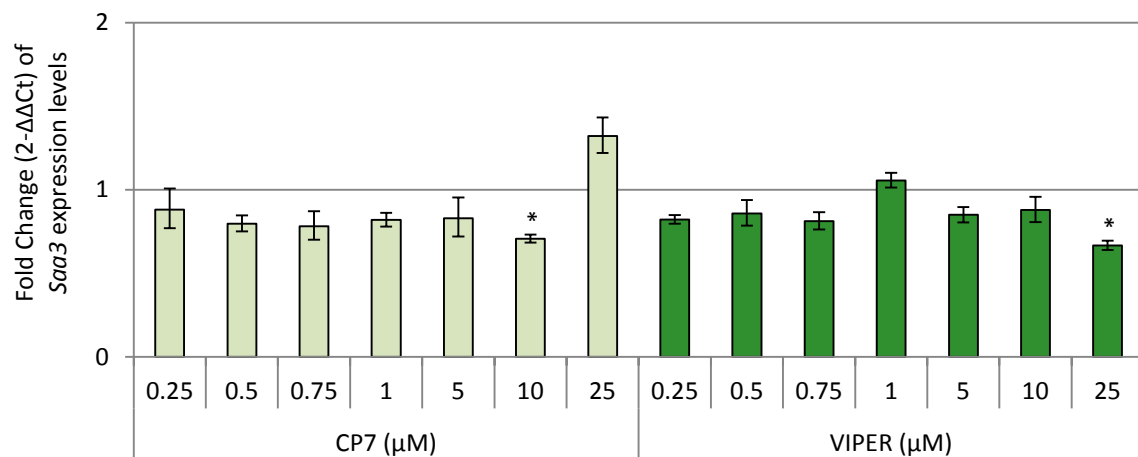


Figure 6.3: *Saa3* gene expression of NIH3T3 cells treated with CP7 or VIPER. NIH3T3 cells were treated with varied concentrations (0.25, 0.5, 0.75, 1, 5, 10 and 25 μ M) of either CP7 or VIPER for 26hr. Fold change ($2^{-\Delta\Delta Ct}$) of *Saa3* mRNA expression is relative to untreated controls, normalised to reference genes *GAPDH* and *β actin* (Section 2.12). Significant differences between treated and untreated cells were calculated by ANOVA analysis (* p <0.05 , ** p <0.01 , *** p <0.001) and error bars depict \pm SE in relation to fold change (Section 2.12.8). Raw data presented in Appendix XVI.

To determine to what extent blocking the TLR4 receptor affected LPS-induced gene expression, NIH3T3 cells were incubated with various concentrations of VIPER or CP7 for 2hr prior to 24hr LPS-stimulation (1µg/ml) (Figure 6.4). At low VIPER concentrations (0.25, 0.5 and 0.75µM), LPS-stimulation of *Saa3* expression was reduced from 11.7-fold to 5-, 4.7- and 2.5-fold respectively. CP7 at 0.25µM and 0.5µM slightly increased (13.5-fold) and decreased (11-fold), respectively, LPS-stimulated *Saa3* expression although the changes were not statistically significant from the 1µg/ml LPS control (12-fold). However, at 0.75µM and higher concentrations CP7 equally inhibited LPS-induction of *Saa3* expression. At 1µM and higher concentrations both CP7 and VIPER had completely inhibited LPS-induction of *Saa3* expression.

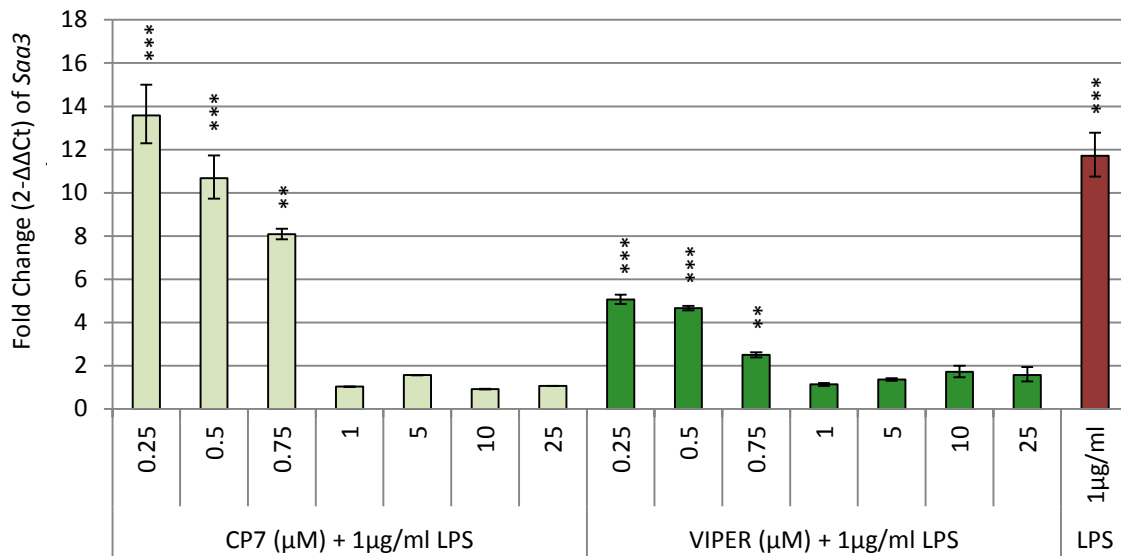


Figure 6.4: Dose-dependent effect of VIPER and CP7 on LPS-stimulated *Saa3* gene expression in NIH3T3 cells. 1µg/ml LPS-stimulated NIH3T3 cells were pre-treated for 2hrs with varied concentrations (0.25, 0.5, 0.75, 1, 5, 10 and 25µM) of either CP7 or VIPER. Fold change (2^{-ΔΔCt}) of *Saa3* mRNA expression is relative to untreated controls, normalised to reference genes *GAPDH* and *βactin* (Section 2.12). Data for 1µg/ml LPS-treatment is taken from Figure 6.2. Significant differences between treated (CP7 or VIPER with the addition of 1µg/ml LPS) and untreated cells were calculated by ANOVA analysis (* p<0.05, ** p<0.01, ***p<0.001) and error bars depict ±SE in relation to fold change (Section 2.12.8). Raw data presented in Appendix XVI.

The vaccinia virus A46 interacts with the TIR-domains of TLR4 and the TLR4 receptor complexes MyD88, Mal, TRAM and TRIF, preventing TLR4 complex formation and NF-κB activation (Figure 6.1) (Stack et al., 2005). VIPER, derived from the A46 protein, interacts with both Mal and TRAM adaptors preventing TLR4 signalling (Lysakova-Devine et al., 2010).

Mutation of the VIPER peptide sequence region of the A46 protein prevented binding of the TRAM adaptor protein but still bound Mal (Stack and Bowie, 2012). This suggests that the CP7 peptide may inhibit Mal LPS-induced TLR4 signalling. Inhibition of *Saa3* expression by CP7 at higher concentrations may be due to inhibition of Mal/TLR4 signalling (Figure 6.4).

6.2.3 The effects of VIPER and CP7 on p37-induced gene expression in NIH3T3 cells

Neither VIPER nor CP7 (1 μ M) significantly changed the endogenous expression of the fourteen genes selected for study (Figure 6.5).

VIPER was used to determine whether p37 activation of gene expression is at least in part via the TLR4 pathway. NIH3T3 cells were pre-treated with 1 μ M VIPER (2hr) and then treated with either 5 μ g or 25 μ g/ml p37 for 24hr. A concentration of 1 μ M VIPER was employed as it was the lowest concentration to completely inhibit *Saa3* expression in LPS-induced NIH3T3 cells (Figure 6.4). Quantitative (q) PCR was used to determine the expression levels of the fourteen genes of interest encoding APPs (Chapter 3). The expression of all fourteen genes chosen was significantly activated by 5 μ g or 25 μ g/ml p37 at 24hr.

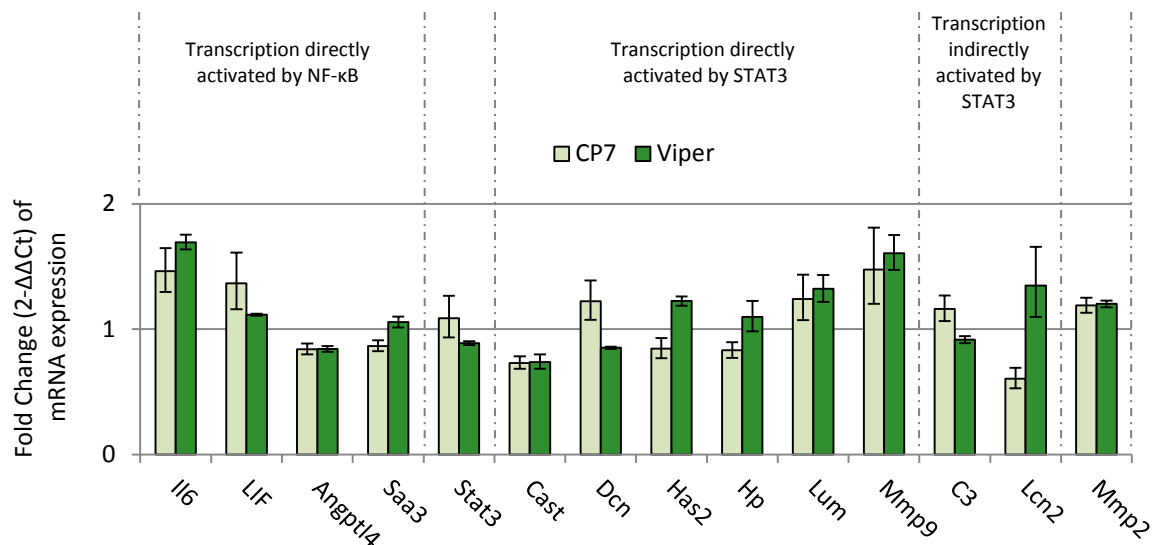


Figure 6.5: Effect of VIPER and CP7 on expression of selected genes in NIH3T3 cells. NIH3T3 cells were treated with either 1 μ M CP7 or VIPER for 26hr. Fold change ($2^{-\Delta\Delta C_t}$) is calculated relative to untreated controls, normalised to reference genes *GAPDH* and *β actin* (Section 2.12). Significant differences between treated and untreated cells were calculated by ANOVA analysis (* $p < 0.05$, ** $p < 0.01$, *** $p < 0.001$) and error bars depict \pm SE in relation to fold change (Section 2.12.8). Raw data presented in Appendix XVII.

Treatment with 5µg/ml p37 failed to significantly stimulate expression of seven out of nine genes when the cells had been pre-incubated with 1µM of VIPER (2hr) (Figure 6.6A). The control peptide CP7 (1µM) also blocked expression although *LIF* and *Lcn2* expression were not as strongly inhibited by CP7 as VIPER. Since the fourteen genes are more strongly activated by 25µg/ml then by 5µg/ml p37 (24hr) (Figure 3.7), the experiment was repeated using the higher p37 concentration.

Once again both VIPER and CP7 strongly inhibited p37-induced gene expression (Figure 6.6B). VIPER was also more effective than CP7 in inhibiting *C3*, *Cast*, *Dcn*, *Lum*, *Lcn2*, *Mmp2* and *Mmp9*. *Il6* expression levels were induced 3-fold by 25µg/ml p37 (24hr) and while VIPER inhibited this induction, CP7 had no effect. VIPER and CP7 at 1µM are equally effective at inhibiting p37-induced expression of *Angptl4*, *LIF*, *Saa3*, *STAT3*, *Has2* and *Hp*.

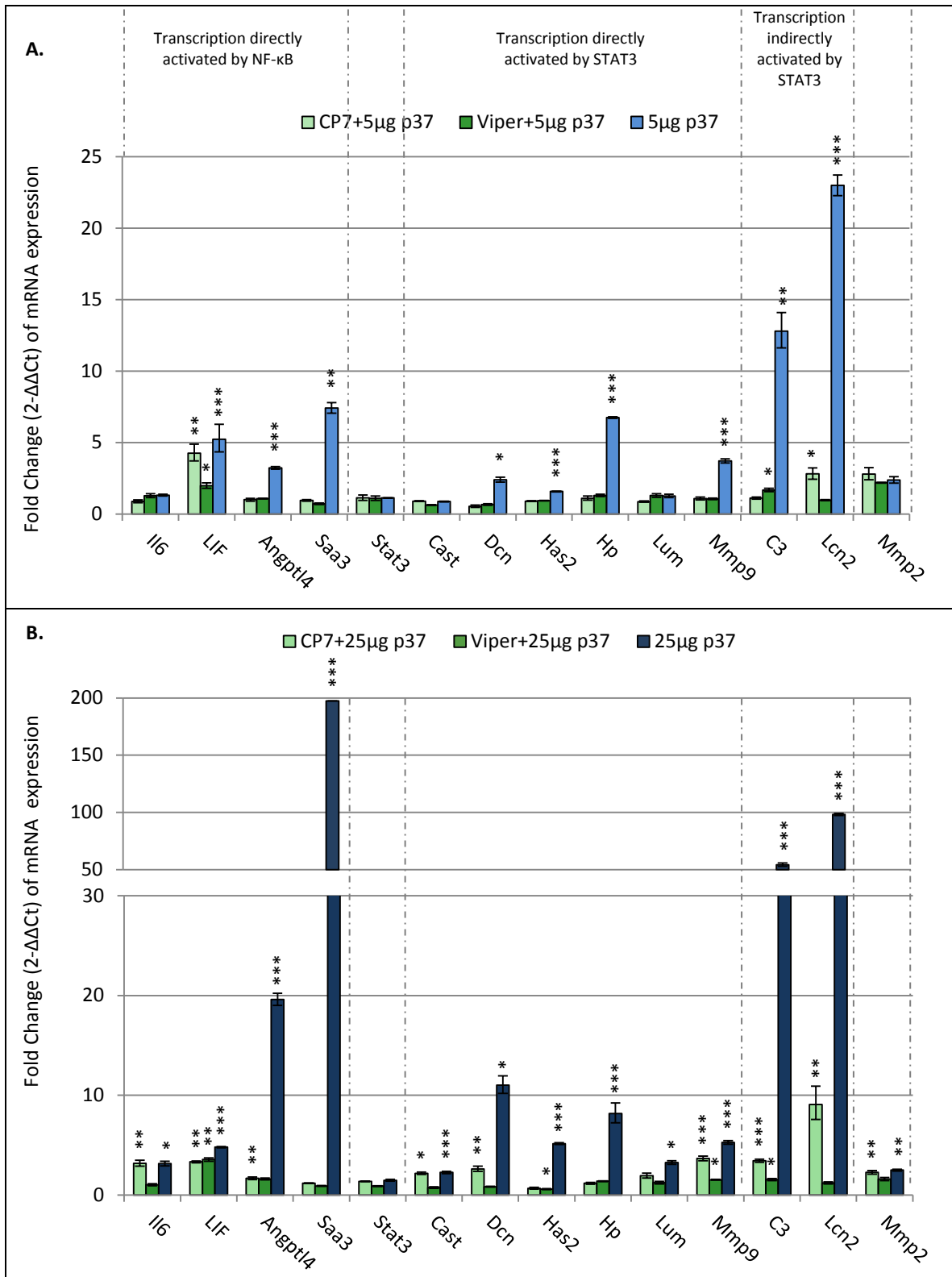


Figure 6.6: The effect of 1 μ M VIPER/CP7 effect on p37-induced gene expression in NIH3T3 cells. NIH3T3 cells treated with either 5 μ g/ml (A) or 25 μ g/ml (B) p37 for 24hr was pre-treated for 2hr with 1 μ M of VIPER or CP7. Fold change ($2^{-\Delta\Delta Ct}$) is relative to untreated controls, normalised to reference genes *GAPDH* and *β actin* (Section 2.12.4). Significant differences between treated and untreated cells were calculated by ANOVA analysis (* $p < 0.05$, ** $p < 0.01$, *** $p < 0.001$) and error bars depict \pm SE in relation to fold change (Section 2.12.8). Raw data presented in Appendix XVII. Fold change data of 24hr 5 μ g/ml and 25 μ g/ml p37-treated NIH3T3 cells is from Chapter 3.

The experiment was repeated using 0.5 μ M VIPER or CP7. At this concentration VIPER was more effective at inhibiting LPS-induced *Saa3* expression than CP7 (Figure 6.4). When the cells were treated with 0.5 μ M VIPER or CP7, no significant changes were found in gene expression with the exception of approximately 50% reduction in *Saa3* expression.

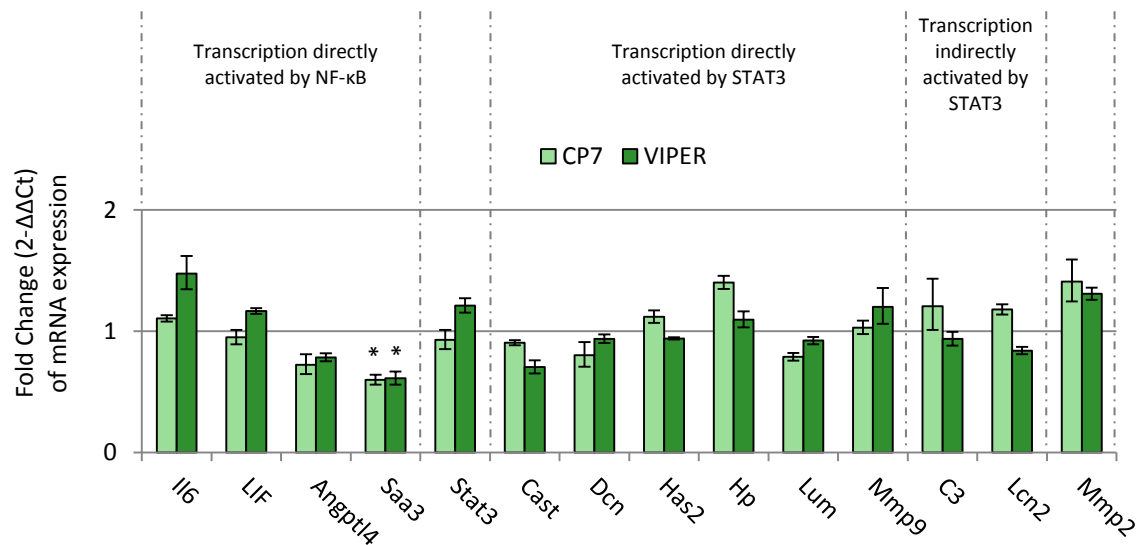


Figure 6.7: NIH3T3 cells treated with 0.5 μ M VIPER or CP7. NIH3T3 cells were treated with either 0.5 μ M CP7 or VIPER for 26hr. Fold change ($2^{-\Delta\Delta C_t}$) is calculated relative to untreated controls, normalised to reference genes *GAPDH* and *β actin* (Section 2.12). Significant differences between treated and untreated cells were calculated by ANOVA analysis (* $p < 0.05$, ** $p < 0.01$, *** $p < 0.001$) and error bars depict \pm SE in relation to fold change (Section 2.12.8). Raw data presented in Appendix XVIII.

The p37-induced (5µg/ml) expression of nine genes, namely *Angptl4*, *LIF*, *Saa3*, *Dcn*, *Has2*, *Hp*, *Mmp9*, *C3* and *Lcn2* was significantly inhibited by 0.5µM VIPER. CP7, as the control peptide, was less effective than VIPER in inhibiting their expression. When 25µg/ml p37 was used, VIPER inhibited the expression of six genes, *Il6*, *Cast*, *Has2*, *Lum*, *Mmp9* and *Lcn2* to untreated control levels (1-fold). CP7, again, was less affective then VIPER in inhibiting p37-induced gene expression.

Mmp2 expression was not inhibited by CP7 or VIPER in the presence of 5µg or 25µg/ml p37 (24hr). This was expected as *Mmp2* is not known to be regulated by the TLR4 pathway. Neither 5µg nor 25µg/ml p37 induced *STAT3* expression. *LIF* induction is inhibited by VIPER at the lower but not the higher p37 concentrations. The reason for this is unclear.

The results suggest p37 (25µg/ml) is signalling via TLR4 to activate the expression of eleven of the fourteen genes studied (Section 6.2.3).

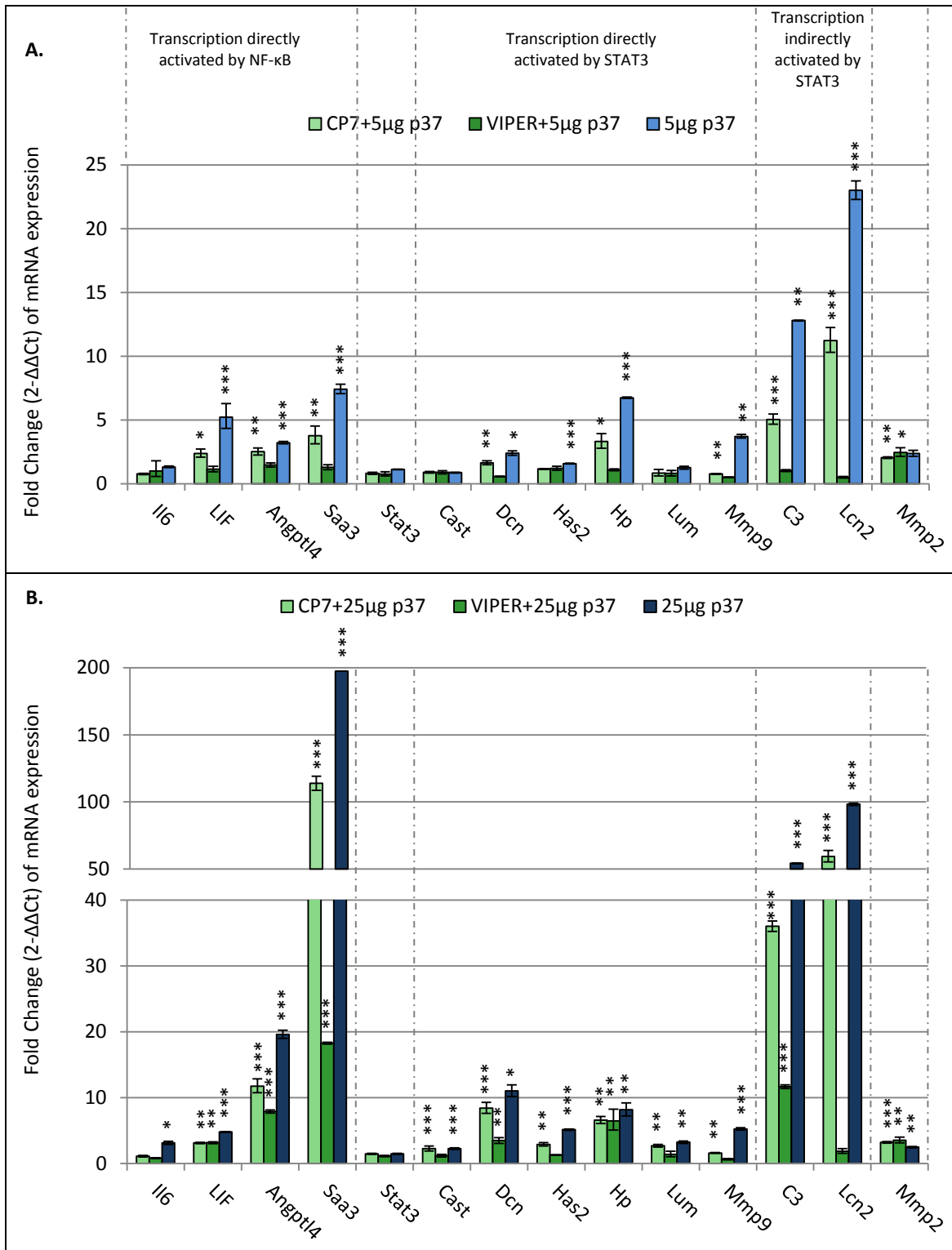


Figure 6.8: The effect of 0.5 μ M VIPER/CP7 on p37-induced gene expression in NIH3T3 cells. NIH3T3 cells treated with either 5 μ g/ml (A) or 25 μ g/ml (B) p37 for 24hr were pre-treated for 2hr with 0.5 μ M of VIPER or CP7. Fold change ($2^{-\Delta\Delta Ct}$) is relative to untreated controls, normalised to reference genes *GAPDH* and *β actin* (Section 2.12). Significant differences between treated and untreated cells were calculated by ANOVA analysis (* $p < 0.05$, ** $p < 0.01$, *** $p < 0.001$) and error bars depict \pm SE in relation to fold change (Section 2.12.8). Raw data presented in Appendix XVIII. Fold change data of 24hr 5 μ g/ml and 25 μ g/ml p37-treated NIH3T3 cells is from Chapter 3.

6.2.4 Mycoplasma lipoproteins and TLR receptors

M. pneumoniae infection-induced mucin expression in mice and human lung (A549) epithelial cells is dependent on the activation of TLR2 signalling (Chu et al., 2005). The macrophage-activating lipopeptide-2 (MALP-2) from *M. fermentans* binds TLR2 activating NF- κ B and the subsequent production of the pro-inflammatory cytokines TNF α , IL8 and MCP-1. Macrophages from TLR2 deficient mice failed to respond to the MALP-2 lipopeptide (Takeuchi et al., 2000).

At 4hr post infection cytoadherence of *M. hominis* to HeLa cells caused differential regulation of forty one host genes with a greater than 10-fold change in expression (Hopfe et al., 2013). Up-regulated genes included *Il6*, *Il11*, *Il20*, *Il7r* and the chemokines *Cxcl1* and *Cxcl2*. Chronic infection of HeLa cells (2 weeks) with *M. hominis* activated genes encoding the S100 calcium binding proteins A8 and A9 which are associated with inflammation (Hopfe et al., 2013). The *Saa1*, *Saa2* and *Lcn2* genes were also up-regulated.

M. arthritidis causes arthritis in specific mice strains. The mitogen (MAM) superantigen produced by *M. arthritidis* plays a major role. MAM activates T-cells and also interacts with TLR2 and 4 on cells of the innate immune system (Mu et al., 2005). In C3H/HeJ mice with hyperfunctional TLR4, MAM exposure results in the up-regulation of the number of surface TLR2 molecules. Macrophages from C3H/HeJ mice, when injected with MAM exhibited a type 1 cytokine profile of IL2, Interferon-1 and TNF α . However, mice with functional TLR4 and TLR2 have a type 1 cytokine profile of IL4, IL6 and IL10 (Mu et al., 2001).

Purified lipid-associated membrane proteins from *M. penetrans* activate NF- κ B through TLR1 and TLR2 (Shimizu et al., 2004). However, NF- κ B activation by lipoproteins from *M. fermentans* was induced through TLR2 and TLR6 but not TLR1. Human monocytes were used in these experiments. A lipoprotein, F₀F₁-ATPase from *M. pneumoniae* induced NF- κ B activation via TLR1, TLR2 and TLR6 in mouse peritoneal macrophages (Shimizu et al., 2005, 2007b). However, two other lipoproteins, N-ALP1 and N-ALP2, activated NF- κ B through TLR1 and TLR2 but not TLR6. In general, TLR1 and TLR2 are thought to recognise

triacylated lipoproteins while diacylated lipoproteins bind TLR2 and TLR6 (Kawai and Akira, 2007). Lipoproteins prepared from *M. genitalium* stimulated human monocytes to produce TNF α , IL1 β and IL6 in a dose-dependent manner (Wu et al., 2008). The expression of these three genes was up-regulated.

The active component of the mycoplasma lipoproteins is believed to be the lipid rather than the protein moieties. Proteinase K treatment has no effect on the activity of the lipoprotein from *M. fermentans* or *M. penetrans* whereas lipase decreased their ability to induce NF- κ B (Shimizu et al., 2004). The *M. genitalium* lipopeptide MG309 activates NF- κ B via TLR2 and TLR6 in human genital epithelial cells (McGowin et al., 2009). The C-terminus portion of MG309 (rMG309c) elicited the secretion of the pro-inflammatory cytokines IL6, IL8, G-CSF and GM-CSF from the genital epithelial cells. Proteinase K treatment reduced the capacity of rMG309c to bind TLR2/6 and elicit inflammation. A 90 amino acid subfragment was also active, indicating that the TLR activation is amino acid based.

Mycoplasma species lack a cell wall and do not contain LPS, therefore further studies are required to establish possible Mycoplasma TLR4 ligands (Shimizu et al., 2014). However, TLR4 has been shown to recognise viral proteins (Poltorak et al., 1998; Haynes et al., 2001), fungal proteins (Netea et al., 2004). The p37 data (Section 6.2.3) indicates that TLR4, like TLR2 and TLR6 in the case of MG309, can bind and be activated by the protein moiety of a lipoprotein.

6.2.5 Genes activated via TLR4 are also induced by p37-treatment

Gene expression induced by p37-treatment resembles that observed by LPS-treatment activating TLR4. TLR4 is known to recognise LPS (Figure 6.1) (Poltorak et al., 1998). LPS-induced *Il6* expression in human colorectal adenocarcinoma SW480 cells increased the migration and invasion of the SW480 cells through a Matrigel matrix (Rakhesh et al., 2012). When the TLR4 receptor was inhibited, *Il6* expression and invasion was reduced (Rakhesh et al., 2012).

LPS rapidly induces *Angptl4* expression in heart, liver, muscle and adipose tissues via TLR4 (Lu et al., 2010). *Saa3* and *TNF α* expression is activated by the TLR4/NF- κ B pathway in mouse colonic epithelial CMT-93 and macrophage RAW 264.7 cell lines (Reigstad et al., 2009) and *Cast* expression is rapidly regulated by LPS in bone marrow derived macrophage (BMDM) cells (Huang et al., 2011). LPS stimulates the expression of *Dcn* in mouse odontoblast-lineage cells (OLCs) (He et al., 2012). A 24hr treatment with 1 μ g/ml LPS, for example, resulted in a 16-fold increase in *Dcn* expression and blocking TLR4 reduced the increase to 2-fold.

The genes encoding the acute phase proteins *Lcn2* and *Hp* are also up-regulated by LPS (Glaros et al., 2012). *Lcn2* up-regulation by *E. coli* LPS requires TLR4 (Cowland et al., 2003) and *Hp* production in PBMC cells is induced by *Il6* which is consequently regulated via the TLR4 pathway (Arredouani et al., 2005).

Inhibition of the protein kinases MEK1/2 prevents *TLR4* expression in gastric carcinoma cell lines and *Helicobacter pylori* LPS was unable to stimulate TLR4 activity within these cells (Yokota et al., 2010). Gong et al. (2008) found that inhibiting MEK1/2 phosphorylation significantly suppressed p37-induced invasiveness of AGS cells through Matrigel. Since MEK1/2 phosphorylation has been linked to increased *TLR4* expression (Yokota et al., 2010), the increased activity of p37-treated cells may also involve TLR4.

LPS-stimulation induced *Mmp9* gene expression in human primary corneal fibroblasts and along with a number of cytokines (namely *Il6* and *TNF α*) and chemokines (*IFN γ*) (Wang et

al., 2011a). TLR4 activation has been linked to the LPS-stimulated up-regulation of Mmp9 (Li et al., 2011). The induction of Mmp9 by p37 may be responsible for the increased capacity of p37-treated PC-3 and p37-transfected AGS cell lines to migrate and invade Matrigel assays (Goodison et al., 2007; Gong et al., 2008).

Has2 interacts with TLR2 and TLR4 to induce chemokines and cytokines in peritoneal macrophages (Jiang et al., 2005a). Has2 induction of chemokines and cytokines is absent in *TLR2* and *TLR4* gene deficient peritoneal macrophages and the inhibition of NF- κ B blocked *Has2* transcription in human dermal fibroblasts (Li et al., 2007). Moreover, increased Has2 facilitates migration of melanoma cells (Kultti et al., 2012). The increased expression of *Has2* following p37-treatment may be due to TLR4 signalling and play a role in the increased cell motility observed in p37-treated and p37-transfected cells.

The expression of *Lum* in mouse embryonic fibroblasts (MEFs) is also increased by LPS-activation of TLR4 (Wu et al., 2007). The peritoneal macrophages of *Lum* deficient mice exhibit an impaired ability to produce *TNF α* and *Il6* in response to LPS (Wu et al., 2007). Lum also binds to Cluster of Differentiation 14 (CD14) in human embryonic kidney (HEK-239) cells. CD14 is a co-receptor that binds LPS, delivering it to TLR4 and activating NF- κ B via MyD88 (Wright et al., 1990; Jiang et al., 2005b; Wu et al., 2007; Zanoni et al., 2011).

7. EFFECTS OF CHANGING THE THIAMINE PYROPHOSPHATE BINDING SITES OR TRUNCATION ON p37-INDUCED GENE EXPRESSION

7.1 INTRODUCTION

The crystalline structure of p37 has been refined to 1.9 Å resolution (Sippel et al., 2008). p37 was found to be an α/β class protein made up of two domains. The domains are separated by a cleft which modelling indicated can bind thiamine pyrophosphate, Vitamin B1. Thiamine pyrophosphate consists of a pyrimidine ring, thiazolium ring and two phosphate groups (α and β) (Figure 7.1).

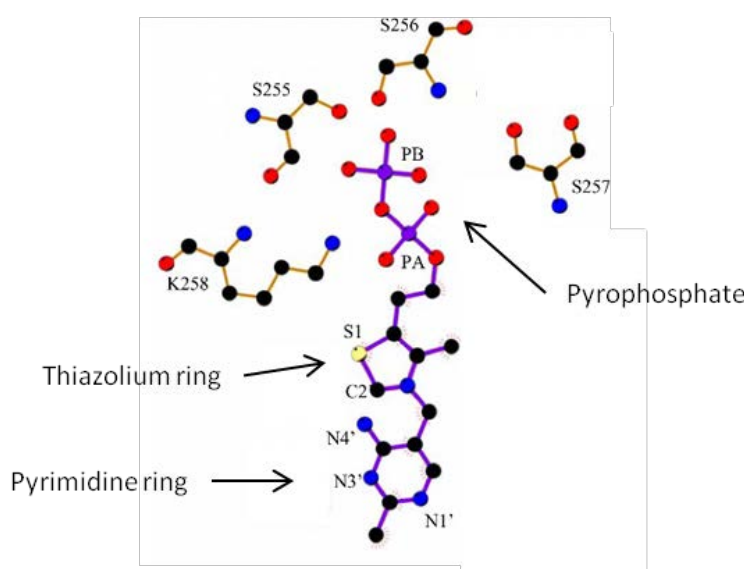


Figure 7.1: Thiamine pyrophosphate binding sites. Stereo image showing the thiazolium ring and pyrimidine ring of the thiamine pyrophosphate molecule as well as two bound phosphate groups α (PA) and β (PB). The image also demonstrates the positions of the consecutive amino acids Ser(S255), Ser(S256), Ser(S257) and Lys(K258) required by a protein to bind thiamine pyrophosphate. (Modified from Sippel et al., 2009).

Several residues involved in thiamine binding are conserved in p37-like proteins from five mycoplasma species (Figure 7.2). Four consecutive amino acids serine (S255), serine (S256), serine (S257) and lysine (K258) are specific to the hydrogen bonding of thiamine pyrophosphate (Figure 7.1). The 2nd serine (S256) in most mycoplasma p37-like proteins is replaced with an alanine and in the *Mycoplasma hyorhina* p37 protein a phenylalanine (F256).



Figure 7.2: Sequence alignment of p37 and other mycoplasma p37-like proteins. *M. hyorhinis* (hyor), *M. genitalium* (geni), *M. hyopneumoniae* (hyop), *M. pneumoniae* (pneu), *M. penetrans* (pene). Sequences are highlighted by percentage identity and consensus. Symbols above columns denote residues involved in TPP binding (*). Box indicates four amino acids specific to binding the alpha phosphate (PA) of TPP. Figure generated using Jalview. (Modified from Sippel et al., 2008)

Liu et al. (2007) transfected AGS cells with an N-terminal truncated (29-403aa) or a C-terminal truncated p37 (1-319aa). Upon the removal of 29 amino acids (aa) from the N-terminus or the removal of 84aa from the C-terminus, Liu et al. (2007) observed reduced antisenescence behaviour of p37-transfected cells. Antisenescence is a property of malignant cells in which the cells proliferate for prolonged periods and avoid cell death. Hence, it was suggested that the entire 403aa of p37 is required to induce antisenescence behaviour in mammalian cells (Liu et al., 2007).

Liu et al. (2006) transfected COS-7 (ape kidney fibroblasts) with a p37 gene construct fused with the enhanced green fluorescent protein (EGFP) gene at either the 5' (N-terminal) or the 3' (C-terminal) end of the gene (EGFP-p37, p37-EGFP, respectively). The p37-EGFP localised to the Golgi of COS-7 cells whereas the EGFP-p37 was secreted to the supernatant (Liu et al., 2006). Retention of the p37-EGFP in the Golgi suggested that the EGFP prevented further processing of the p37 protein and that the C-terminus of p37 possesses functional importance.

The aim of this chapter was firstly to determine whether bound thiamine pyrophosphate was required for p37 activation of gene expression in NIH3T3 cells and, secondly, whether the C-terminus played a role in the gene induction, by p37.

7.2 RESULTS & DISCUSSION

7.2.1 Site Directed Mutagenesis of the SFSK amino acid sequence of p37

To test the hypothesis that the bound thiamine pyrophosphate (TPP) is required for gene activation by exogenous p37 *in vitro*, site-directed mutagenesis of the p37 was carried out. The four amino acids S255, F256, S257 and K258 were all replaced by valine (Figure 7.2). Alanine is the usual amino acid of choice for point mutations due to its small size and short side chains. Short side chains make alanine non-reactive and hence not involved in protein function (Betts and Russel, 2003). However, as other p37-like proteins contain alanine within the four consecutive amino acids required for TPP binding, the amino acids were instead mutated to valine (Figure 7.3). Valine is similar to alanine being a small amino acid, non-reactive and rarely involved in protein function (Betts and Russel, 2003). The introduced point mutations are positioned between a β -strand (248-250) and a turn (256-259) of p37 (Figure 7.4).

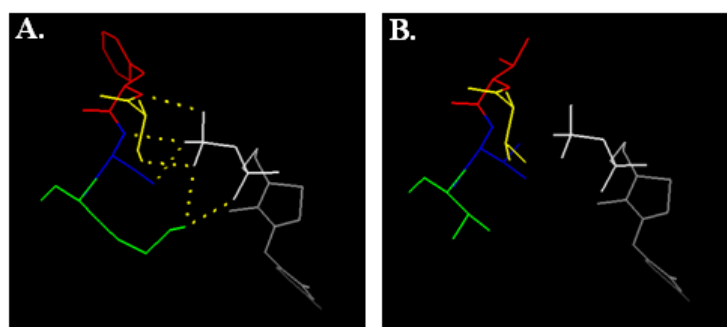


Figure 7.3: Schematic analysis of Thiamine pyrophosphate (TPP) binding in p37. Figures prepared using PyMOL. **(A)** Predicted structure of TPP (grey), binding via hydrogen bonds (yellow dashed lines), to Ser255 (yellow), Phe256 (red), Ser257 (blue) and Lys258 (green) of the p37 protein. **(B)** No hydrogen bonds are predicted between TPP and the valine amino acids 255 (yellow), 256 (red), 257 (blue) and 258 (green) of the mutated p37. (Designed using Pymol, Schrodinger, 2010).



Figure 7.4: Secondary Structure of p37. The p37 protein secondary structure contains several α -helices (blue), β -strands (green) and turns (pink). The point mutations, indicated by the arrow, were positioned between a β -strand (248-250) and a turn (256-259) (Modified from The UniProt Consortium, 2012).

The oligonucleotides originally used for mutagenesis were designed based on the QuikChange™ Site-Directed Mutagenesis Protocol developed by Agilent Technologies (Cat#200521) (Section 2.6.10). The conditions for oligonucleotide design included a set of 25 to 45 base pair primers that were complimentary and contained the mutations of interest with a melting temperature (T_m) $\geq 78^\circ\text{C}$. Due to the high AT% content in *p37*, longer primers were designed to reach a T_m of 78°C , although this introduced the probability of secondary structures forming (Table 7.1). The mutations were to be introduced in a single PCR using the 38QUIK_F1/R1 primers containing the seven points of mutation (Table 7.2).

Table 7.1: p37 primers designed based on the QuikChange™ Site-Directed Mutagenesis Protocol. Forward (38QUIK_F1) and Reverse (38QUIK_R1) primers were 37bp long with a melting temperature (T_m) of 78°C . The bold bases are those introducing the mutation.

Oligo Name:	Sequence (5'- 3')	T_m (°C)
38QUIK_F1	CAC GGT AAA GAT AAT GTG GTG GTG GTA TTC AAG TTA G	78
38QUIK_R1	C TAA CTT GAA TAC CAC CAC ATT ATC TTT ACC GTG	78

Table 7.2: Mutation of amino acids from native protein to mutated protein. The native protein amino acid sequence (SFSK) was mutated (VTVV) via a single PCR with primers containing 7 point mutation (highlighted in bold) present in the primers.

S T C T G T T V	F T T T G T T V	S T C T G T T V	K A A A G T A V	- Native protein amino acids - Original codon - Mutated codon - Mutated protein amino acids
---------------------------------	---------------------------------	---------------------------------	---------------------------------	--

Primer dimer formation was favoured using the QuikChange™ Site-Directed Mutagenesis protocol developed by Agilent Technologies (Cat#200521) (Figure 7.5).

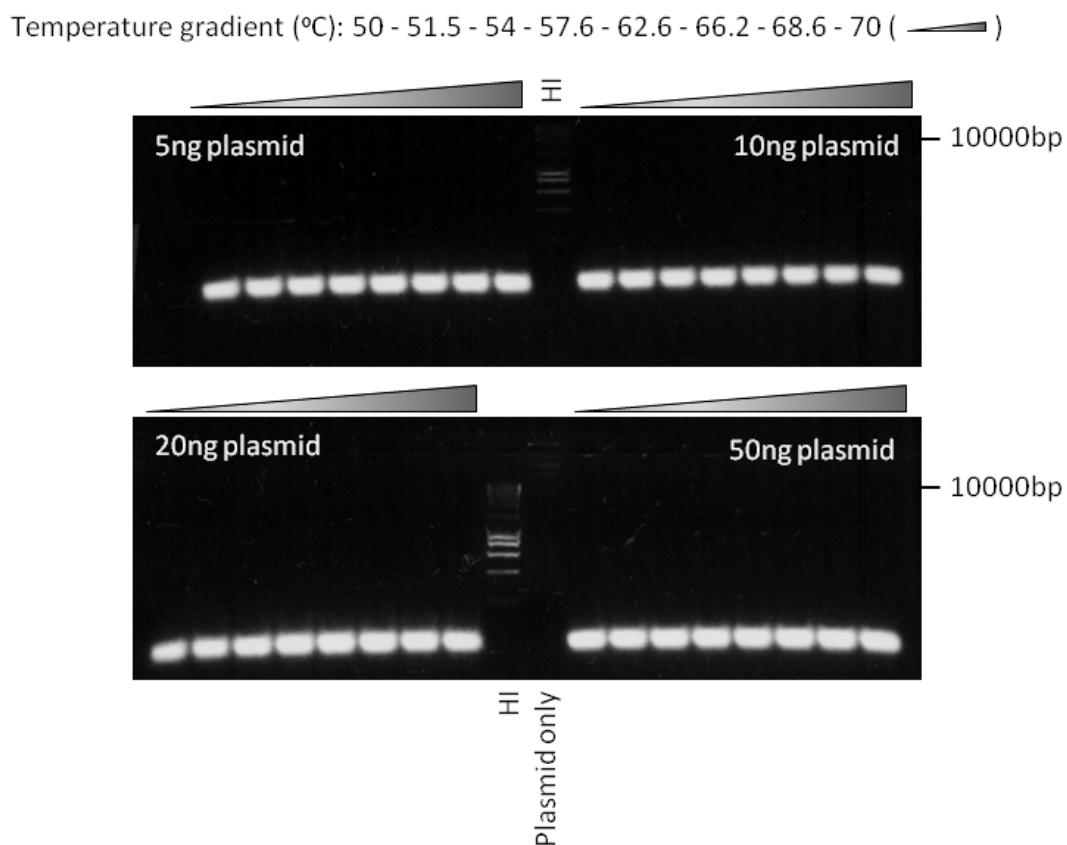



Figure 7.5: Gradient PCR following the QuikChange™ Site-Directed Mutagenesis Protocol using varying concentrations of plasmid DNA. Gradient PCR of pRA:p37 using complementary primers 38QUIK_F1/R1 (Table 7.1). These primers should amplify the pRA:p37 plasmid producing a band of 4kb. Four different plasmid pRA:p37 concentrations (5, 10, 20 and 50ng plasmid) were used and no bands produced. A negative control was setup containing all the PCR reagents and the plasmid pRA:p37 but without primers (Plasmid only). The PCR amplification process started with an initial denaturing step at 95°C for 1min. The PCR then cycled 18x through denaturation at 95°C for 50sec, primer annealing was at a gradient ranging from 50°C to 70°C () for 50sec and then an extension at 68°C for 5min. The amplification process ended with a final extension at 68°C for 7min and was held at 4°C. The PCR was run on an ethidium bromide stained 1% agarose gel. The PCR reactions were run out on a 1% agarose gel and Hyperladder I (HI) was used for size determination (Section 2.7).

A novel primer design method developed by Zheng et al. (2004) was employed. This method minimizes primer dimerisation by prioritizing primer to template annealing over primer self-pairing during PCR. The primer design properties require primer pairs that are complimentary at the 5'-terminus and overhanging at the 3'-terminus. The mutation must be present in both primers and G or C should terminate the primers. Mutations should be as close as 4 bases from the 5'-terminus and at least 6-8 bases from the 3'-terminus and the mutation content no greater than 17.5% of the primer (Zheng et al., 2004). Since these properties reduce the formation of primer dimerisation, they also remove the limitations of the melting temperature (T_m) $\geq 78^\circ\text{C}$ of the QuikChange™ Site-Directed Mutagenesis primers. Since seven point mutations were to be introduced, it was decided to design two sets of primers, the first set containing three and the second set containing four of the mutations (Table 7.3). Thus the mutation of SFSK to VVVV was carried out using two polymerase chain reactions (Table 7.4).

Table 7.3: Primers based on Zheng et al. (2004) design. The bold base pairs are those introducing the point mutations.

OligoName:	Seq (5'-3')	T_m
Mutp37_F1	AAT GCTGTTGCTGAA TTC AAG TTA GAA GAA ACT ATA TTA AAA AAC C	62
Mutp37_R1	CTT GAA TTCAGCAACAGC ATT ATC TTT ACC GTG TAA	63
Mutp37_F2	GAT AAT GTTGTTGTTGTA TTC AAG TTA GAA GAA ACT ATA TTA AAA AAC C	61
Mutp37_R2	CTT GAA TACAACAACAAC ATT ATC TTT ACC GTG TAA AAT TCC	62

Table 7.4: Two step PCR reaction introducing the mutation of amino acids from native protein to mutated protein. The native protein amino acid sequence (SFSK) was mutated (VVVV) two PCRs with primers containing seven point mutation (highlighted in bold) present in the primers.

S	F	S	K	- Native protein amino acid
T C T	T T T	T C T	A A A	- Original codon
G C T	G T T	G C T	G A A	- 1 st mutated codon
G T T	G T T	G T T	G T A	- 2 nd mutated codon
V	V	V	V	- Mutated protein amino acid

Gradient PCRs determined the optimum primer annealing temperatures for Mutp37_F1/R1 and Mutp37_F2/R2 as 56.4°C (Figure 7.6). The QuikChange™ Site-Directed Mutagenesis Protocol developed by Agilent Technologies was then followed using the newly designed primers with an annealing temperature of 56.4°C.

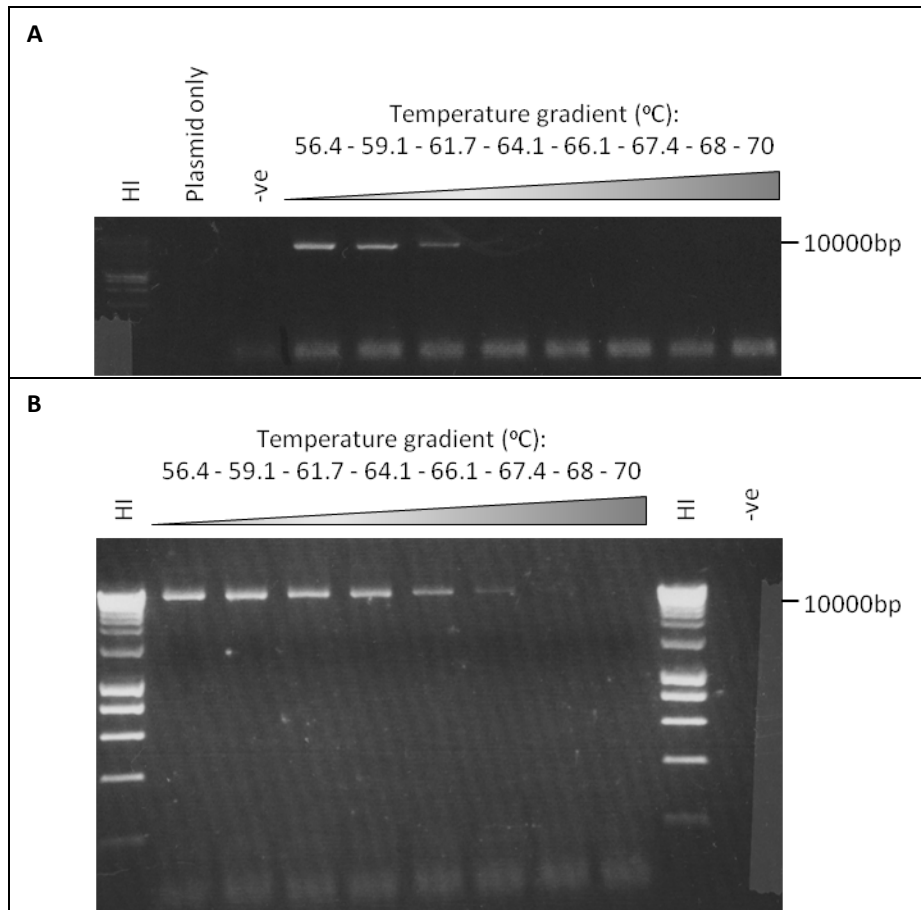


Figure 7.6: Gradient PCR of 10ng pRA:p37 using primers Mutp37_F1/R1 and Mutp37_F2/R2. (A) Mutp37_F1/R1 primers amplified 10ng of pRA:p37 plasmid at temperatures 56.4, 59.1 and 61.7°C. Two negative controls were set up; one with 10ng of plasmid only (Plasmid only) and the other containing all the PCR reagents and primers (-ve). **(B)** Mutp37_F2/R2 primers amplified 10ng of pRA:p37 plasmid at temperatures 56.4, 59.1, 61.7, 64.1, 66.1 and 67.4°C. A negative control containing all the PCR reagents and primers (-ve) was also included. The PCR amplification process started with an initial denaturing step at 95°C for 1min. The PCR then cycled 18x through denaturation at 95°C for 50sec, primer annealing was at a gradient ranging from 56.4°C to 70°C (—) for 50sec and then an extension at 68°C for 5min. The amplification process ended with a final extension at 68°C for 7min and was held at 4°C. The PCR reactions were run out on a 1% agarose gel and Hyperladder I (HI) was used for size determination (Section 2.7).

7.2.2 Mutant p37 protein purification

Several *E. coli* XL10-Gold Ultracompetent colonies obtained using the QuikChange™ Site-Directed Mutagenesis Protocol were cultured overnight and the plasmids purified (Section 2.6.5). The plasmids were sequenced (Section 2.8.1) and those containing the seven mutations were re-named pRA:mutp37 (Appendix XIX). The pRA:mutp37 construct was transformed into OneShot®BL21(DE3) (Section 2.6.2) and approximately equal concentrations of the mutated p37 protein were found in the soluble and insoluble fractions (Figure 7.7).

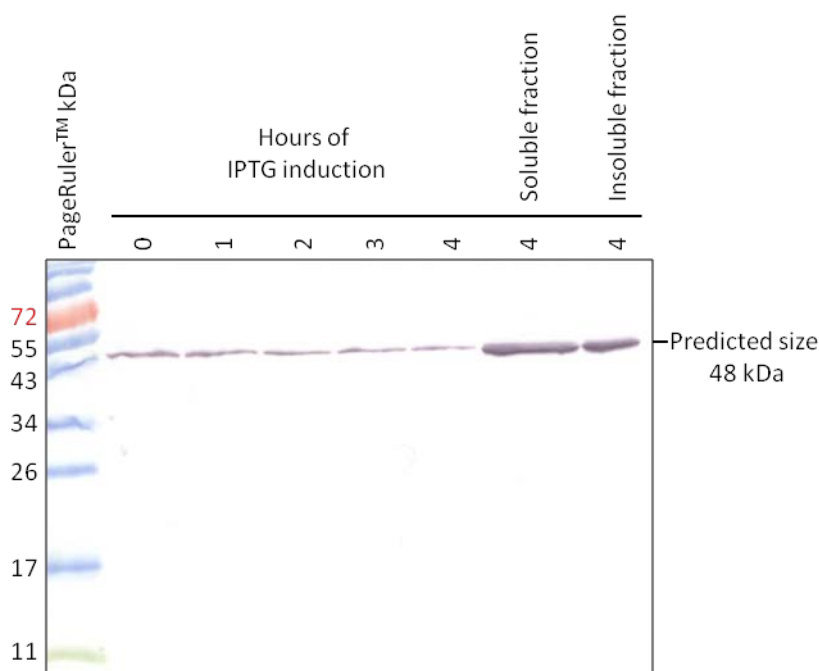


Figure 7.7: Western blot analysis showing the induction of the mutp37 protein. The pRA:mutp37 construct was transformed into One Shot®BL21(DE3) and the (His)₆-mutp37 protein was expressed over 4hrs after IPTG induction. 10µl aliquots were taken every hour and an additional 4th hour aliquot was separated into soluble and insoluble fractions. The 10µl aliquots of 1, 2, 3 and 4hrs and the soluble and insoluble fractions of 4hrs were run on a 12% SDS-PAGE and transferred to a nitrocellulose membrane (Section 2.17). The p37 protein was detected by Western blotting using a T7-Tag monoclonal primary antibody and the goat anti-mouse-AP conjugated secondary antibody producing a band at the predicted molecular weight 48kDa (Section 2.17). The PageRuler Prestained Protein Ladder (Fermentas; Cat#SM0671) was used to analyse protein size.

The mutant p37 (mutp37) gene was expressed and the protein product purified (Section 2.15). The mutp37 protein was shown to be pure using Coomassie Blue staining (Figure 7.8A). Western blotting confirmed the protein was mutp37 (Figure 7.8B).

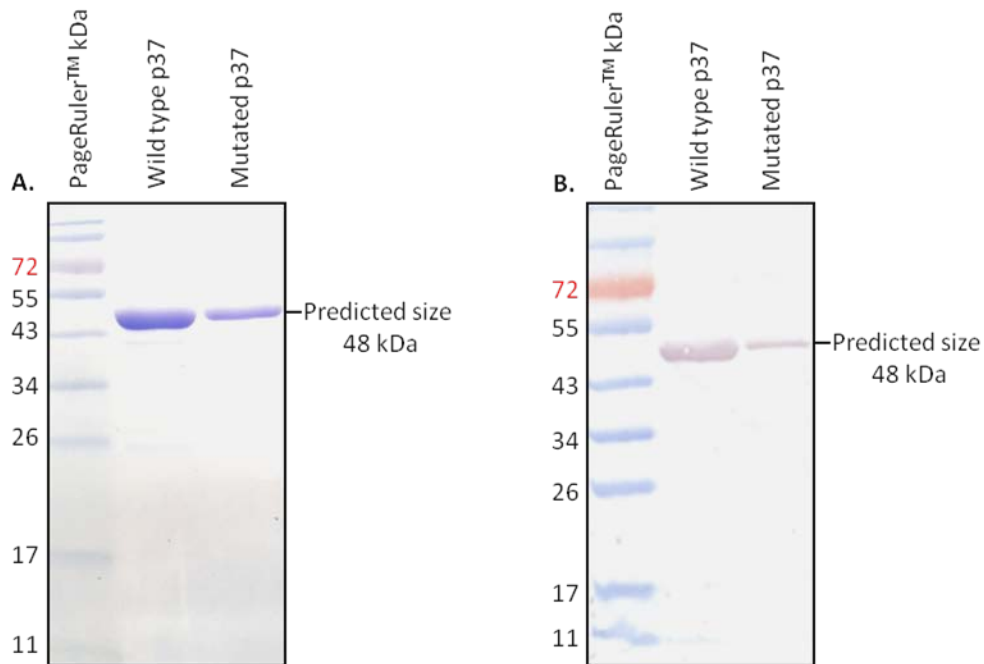


Figure 7.8: Coomassie blue staining and Western Blot of p37 and mutp37 purified from One Shot®BL21(DE3) cells. p37 and mutp37 were purified using Profinity™ IMAC Resin and 10µl of each sample were run on a 12% SDS-PAGE gel. **(A)** Coomassie blue staining (Section 2.17.2) verified purification of p37 and mutp37. **(B)** The proteins were transferred to a nitrocellulose membrane and the membrane incubated with a T7-Tag monoclonal primary antibody and the goat anti-mouse-AP conjugated secondary antibody (Section 2.17.3). Both, p37 and mutp37, produced a band at the predicted molecular weight of 48kDa (Section 2.17). The PageRuler Prestained Protein Ladder (Fermentas; Cat#SM0671) was used to analyse protein size.

7.2.3 Mutated p37 does not induce gene expression to the same degree as native p37

NIH3T3 (mouse) fibroblasts were treated with 25µg/ml purified mutp37 for 24hr. Quantitative (q) PCR was used to analyse the mRNA expression (Section 2.12) of seventeen genes whose expression levels were previously found to be significantly induced by p37 at the same concentration and treatment time (Chapter 3). Expression was significantly reduced in thirteen of the genes tested (Figure 7.9).

In the majority of genes tested, the mutated p37 failed to induce expression above control levels or the increase was considerably weaker than that obtained with native p37 (Figure 7.9). Nonetheless, mutant p37 did induce expression of *Angptl4* (5-fold), *Saa3* (17-fold), *C3* (5-fold) and *Lcn2* (15-fold). *LIF* expression was actually higher with mutant p37 (16-fold) than native p37 (5-fold). The data suggest that the presence of TPP modifies the p37 structure in such a way as to facilitate binding to and activation of the TLR4 and possibly other cell surface receptors. The strong induction of *LIF* by the mutant p37 could indicate that receptor(s) other than TLR4 are involved.

The four valine mutations are considered unlikely to change the secondary structure of the p37 protein (Figure 7.3). However, the exclusion of TPP from the p37 cleft may have modified the tertiary structure of the protein. Structural studies would be required to confirm if a change had occurred.

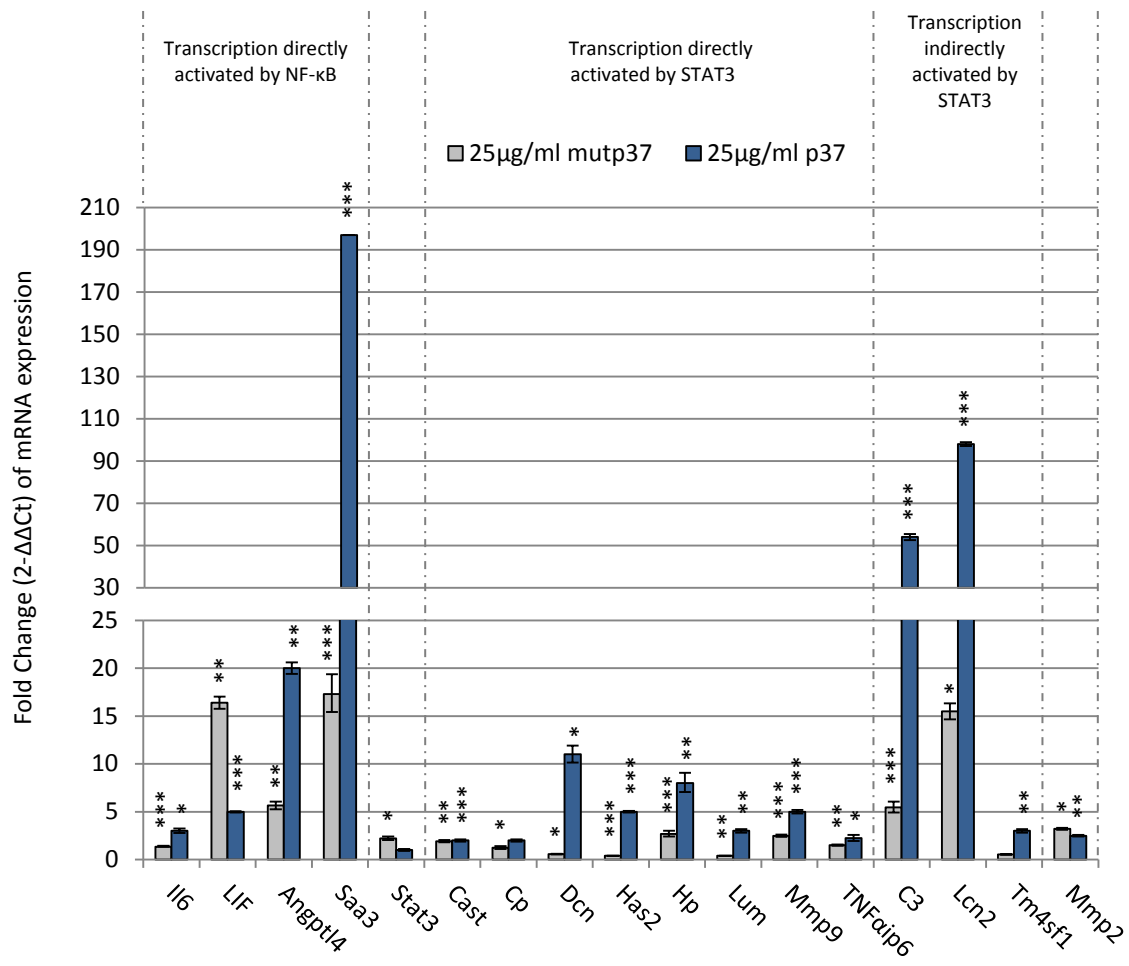


Figure 7.9: Mutant p37 (mutp37) affect on gene expression of NIH3T3 cells. NIH3T3 cells treated with either mutp37 or wild type p37 for 24hr. Fold change ($2^{-\Delta\Delta Ct}$) is relative to untreated controls, normalised to reference genes *GAPDH* and *β -actin* (Section 2.12). Significant differences between treated and untreated cells were calculated by ANOVA analysis (* $p < 0.05$, ** $p < 0.01$, *** $p < 0.001$) and error bars depict \pm SE in relation to fold change (Section 2.12.8). Raw data presented in Appendix XIX. Fold change data of 24hr 25µg/ml p37-treated NIH3T3 cells is from Chapter 3.

7.2.4 Effects of truncating p37 on its capacity to induce gene expression

Isolation of the functional peptide

To determine to what extent the carboxyl-terminus (C-terminus) region of the p37 protein is required for gene activation four truncated peptides were isolated. Using PCR (Section 2.11), *Bam*HI and *Nco*I restriction cut sites were introduced into the *p37* gene (Table 7.5). The reverse primers introduced an *Nco*I restriction cut site at several points which facilitated the production of DNA sequences that reduced the size of the p37 protein by 20, 60, 80 or 105aa. The PCR products were digested with the *Bam*HI and *Nco*I restriction enzymes and ligated into the pRSET A vector (Figure 7.10). Sequence analyses of the four constructs are presented in Appendix XXI.

Table 7.5: Primer sequences for amplification of C-terminal truncated mutants by PCR. The same forward primer was used for all truncated gene amplification (Trunc_F).

Truncation	Primer sequence (Reverse primer 5' – 3')
p37-20	TCAAGCTTCGAATTCTTAACCATTATACCCTAAAAG
p37-60	TCAAGCTTCGAATTCTTAATACGGAATTGGATTAG
p37-80	TCAAGCTTCGAATTCTTAAGTTTTGTTGCTGATT
p37-105	TCAAGCTTCGAATTCTTAATGGAAATCATCTAAAG
Trunc. F	GGATCGATGGGGATCCGCATGTTCTAATACAGGAGTA

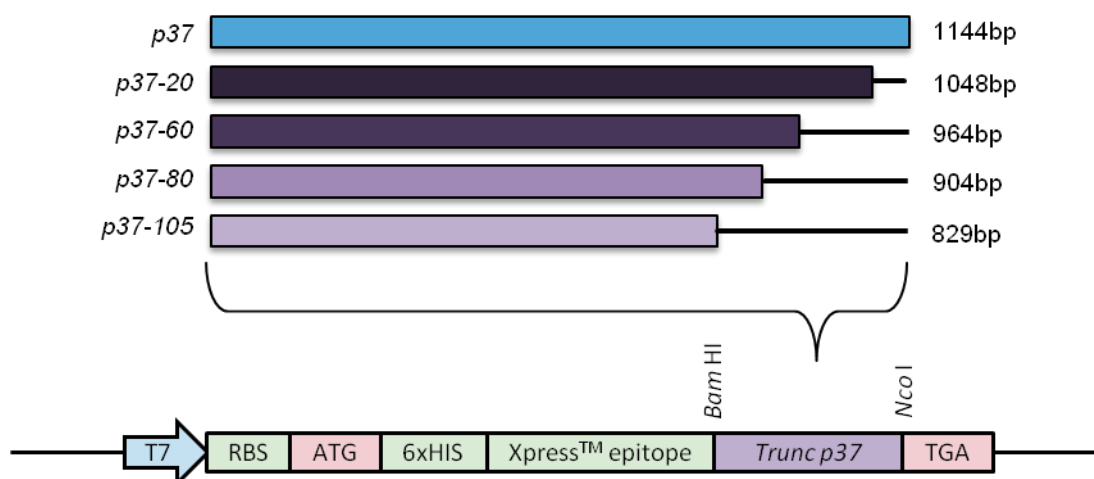


Figure 7.10: Schematic diagram of the p37 gene C-terminus truncations cloned into pRSET A. Numbers on the right indicate the base pair size of the gene insert. Names of each construct are indicated on the left. Closed boxes represent the truncated p37 gene inserted into the *Bam*HI and *Nco*I restriction enzyme sites of the pRSET A multiple cloning site. Unbroken lines represent the section of the C-terminus that has been deleted. Sequence analyses of the four constructs are presented in Appendix XXI.

Recombinant truncated p37 protein expression was induced in BL2(DE3) *E. coli* cultures by a 4hr IPTG treatment (Section 2.15.1). Aliquots of 10µl culture were pelleted, lysed and centrifuged separating the soluble and insoluble fractions. The proteins were reduced with an equal volume of SDS-loading buffer and run on 12% sodium dodecyl sulfate (SDS) polyacrylamide gel by electrophoresis (PAGE) (Section 2.17.1). The proteins were transferred to a nitrocellulose membrane for expression evaluation by Western blotting using a T7•Tag monoclonal antibody (Section 2.17.3) (Figure 7.11). Western blot analysis revealed that the truncated p37 proteins were stably expressed during the 4hr IPTG induction. However, higher concentrations of the truncated proteins were present in the insoluble rather than soluble fraction of the *E. coli* lysate. Purification using Ni-affinity (Section 2.15.3) of the truncated proteins from soluble fractions was unsuccessful due to the low concentration of soluble protein.

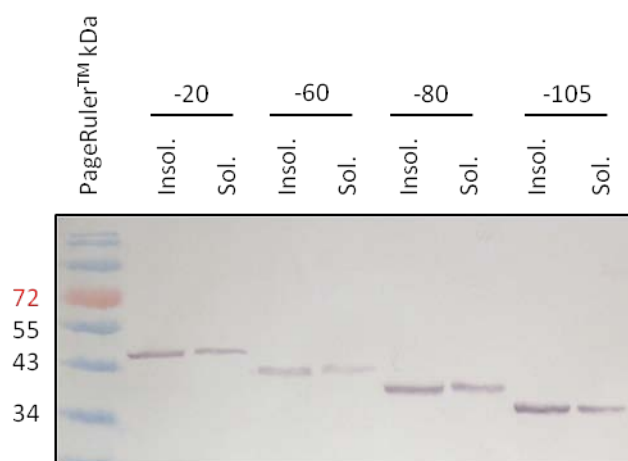


Figure 7.11: Western blot analysis of IPTG-induced truncated p37 expression. The pRAp37 truncated constructs were transformed into One Shot®BL21(DE3) and the proteins IPTG-induced over 4hrs. A 10µl aliquot of each truncated protein (-20, -60, -80 and -105) expressing *E. coli* BL21(DE3) was taken and separated into soluble and insoluble fractions. The soluble and insoluble fractions of each truncated p37 protein was run on a 12% SDS-PAGE and transferred to a nitrocellulose membrane (Section 2.17). The protein was detected by Western blot using a T7•Tag monoclonal primary antibody and the goat anti-mouse-AP conjugated secondary antibody producing a band at the predicted 48kDa (Section 2.17). The PageRuler Prestained Protein Ladder (Fermentas; Cat#SM0671) was used to analyse protein size.

Guanidine hydrochloride purification of the insoluble truncated p37 peptides

Expression of recombinant proteins usually gives rise to soluble and insoluble proteins. Insoluble proteins are either not completely folded or mis-folded and aggregate to form inclusion bodies. When insufficient soluble protein is obtained a purification method is required for the insoluble fraction. Lowering the temperature at which the transformed *E. coli* is cultured and lowering the concentrations of IPTG can reduce formation of inclusion bodies. Various temperatures and concentrations of IPTG were used; however, no truncated p37 peptide was detected in the Western blots.

One way to resolve the issue of inclusion bodies is to denature and solubilise insoluble proteins using detergents. The proteins are then refolded. Different detergents such as sodium dodecyl sulfate (SDS; an anionic detergent), CHAPS (Zwitterionic detergent) Triton X-100 and Tween 20 (nonionic detergents) as well as the organic solvents urea and guanidine hydrochloride (gudHCl) were used in an attempt to solubilise the insoluble proteins (Section 2.16). Only gudHCl was successful in solubilising the inclusion bodies and allowing subsequent purification using Ni-affinity chromatography (Section 2.16.3). Wild type p37 protein was also purified under the same gudHCl conditions to ensure the procedure had not affected the capacity of p37 to activate gene expression. GudHCl purified p37 did not induce expression of the eight genes tested (Appendix XXII).

Arginine purification of the insoluble truncated p37 peptides

The presence of free amino acids has been found to prevent protein aggregation and enhance protein stability. Arginine is a positively charged amino acid (at pH 7.0) that interacts with the outer polar environment of proteins, suppressing protein aggregation and allowing correct folding. Unlike detergents and guanidinium chloride, arginine does not denature proteins. Using the method described by Tsumoto et al. (2010), the truncated peptides were solubilised with a 1M arginine soak prior to purification by Ni-affinity chromatography (Section 2.16.3). Wild type p37 was also subjected to the 1M arginine soak. Aliquots of purified truncated peptides were reduced with an equal volume of SDS-loading buffer and run on 12% SDS-PAGE stained with Coomassie Blue (Section 2.17.1) (Figure 7.12A). A second SDS-PAGE gel of the reduced truncated peptides and wild type p37 were Western blotted using a T7•Tag monoclonal antibody (Section 2.17.3) (Figure 7.12B).

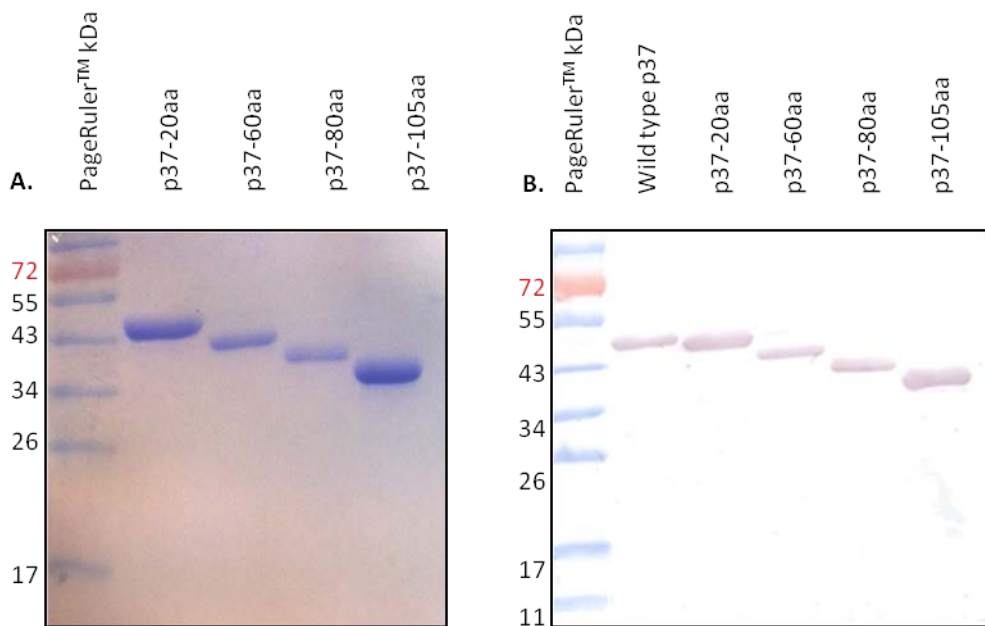


Figure 7.12: Coomassie Blue staining and Western Blot of truncated p37 as well as the wild type p37. Truncated p37-20, -60, -80 and -105 as well as wild type p37 was purified using Profinity™ IMAC Resin and 10µl of the samples were subjected to a 12% SDS-PAGE gel. **(A)** Coomassie Blue staining verifying purification and **(B)** Western Blotting using a T7-Tag monoclonal primary antibody and a goat anti-mouse-AP conjugated secondary antibody identified the p37 truncated proteins (Section 2.17). The PageRuler Prestained Protein Ladder (Fermentas; Cat#SM0671) was used to analyse protein size.

NIH3T3 cells were treated for 24hr with 25µg/ml arginine-purified p37-20, -60, -80 or -105 truncated proteins, as well as 25µg/ml arginine-purified wild type p37 protein. Quantitative (q) PCR was used to analyse the mRNA expression (Section 2.12) of the eight selected genes.

The arginine soak purified p37 induced slightly lower levels of gene expression than the purified native p37 (Figure 7.13). Hence, the purification method had not significantly affected p37 activity. The removal of 20 amino acids (aa) from the C-terminus of p37 (-20) significantly reduced expression in seven genes to control levels (1-fold) (Figure 7.13). However, *Angptl4* expression was still strongly enhanced. Removal of 60aa from p37 greatly reduced the *Angptl4* induction and removal of 80 and 105aa further reduced the induction.

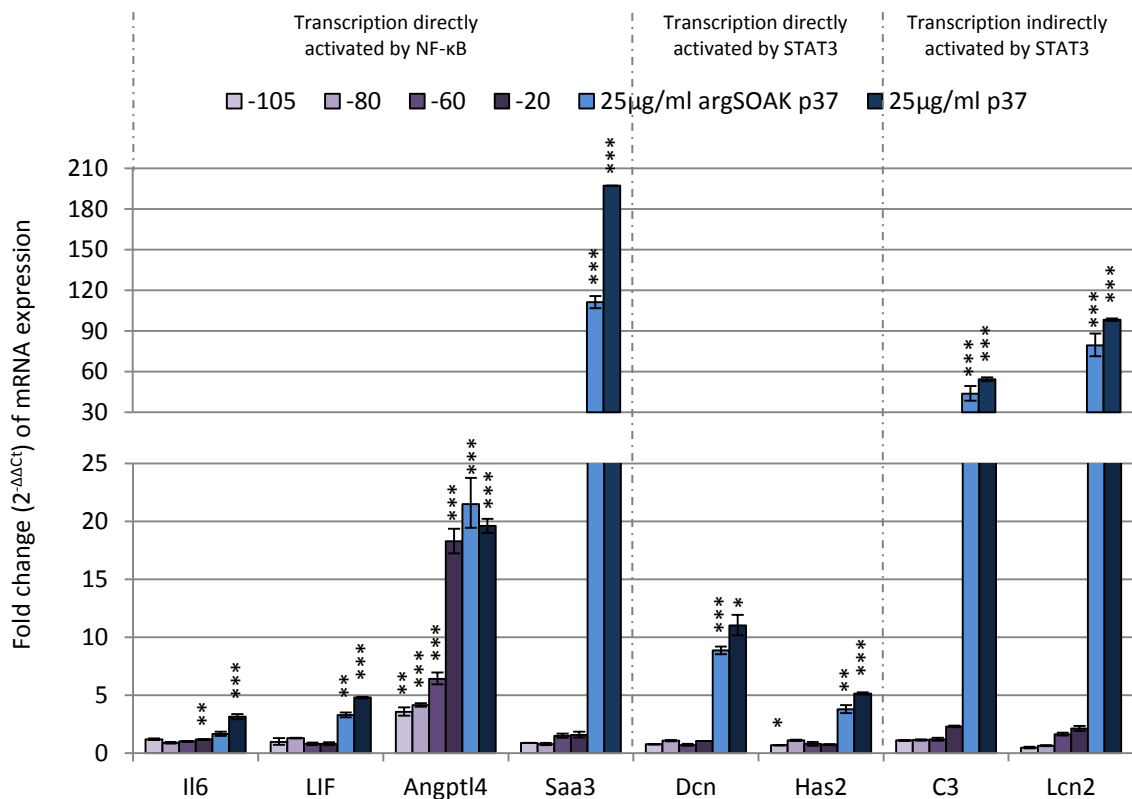


Figure 7.13: Effect of arginine soak purified truncated p37 on gene expression. NIH3T3 cells treated with arginine soak purified p37-20, -60, -80, -105 or p37 for 24hr. Fold change ($2^{-\Delta\Delta C_t}$) is relative to untreated controls, normalised to reference genes *GAPDH* and *βactin* (Section 2.12.4). Significant differences between treated and untreated cells were calculated by ANOVA analysis (* $p < 0.05$, ** $p < 0.01$, *** $p < 0.001$) and error bars depict \pm SE in relation to fold change (Section 2.12.8). Fold change data of 24hr 25µg/ml p37-treated NIH3T3 cells from Chapter 3. Raw data presented in Appendix XXIII.

The results suggest that the C-terminal of p37 is required for the activation of gene expression. However, the continued expression of *Angptl4*, in the absence of the C-terminal 20aa suggests that p37 may induce gene expression via an alternative receptor. *Angptl4* transcription is directly activated by NF- κ B. NF- κ B is activated by the TLR4 receptor but may also be activated by Tumour Necrosis Factor (TNF) receptors (TNFR) (Wan and Lenardo, 2010). It may be that the inhibition of TLR4 only resulted in a 50% decrease in 25 μ g/ml p37-induced *Angptl4* expression (Section 6.2.3).

It has previously been shown that both N- or C-termini truncations can reduce p37-induced antisenesence behaviour in varying degrees (Liu et al., 2006; Liu et al., 2007). This suggests that both the N- and C-termini of p37 contribute to the formation of the fully active p37 protein structure. Structural analysis determined that the p37 20aa C-terminus is exposed at the base of the two p37 domains, I and II (Figure 7.14, highlighted in red) (Sippel et al., 2008; Sippel et al., 2009). Based on the PyMOL schematic of p37 the 20aa removal from the C-termini should not affect conformation of the remaining p37 tertiary structure. The thiamine pyrophosphate (TPP) does not interact with the C-terminal of p37 and therefore the truncation would not prevent TPP binding. The N-terminal 6 to 18 positioned amino acids are located within Domain I of p37 and amino acids 19 to 24 form a folded loop at the domain I entrance of the central cleft (Figure 7.14, highlighted in yellow) (Sippel et al., 2008). This loop may be responsible for recognition and/or binding of receptors, different from those activated by the C-terminal.

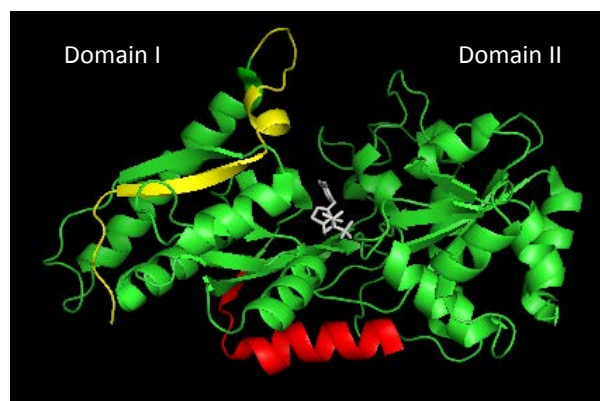


Figure 7.14: Schematic analysis of the p37 protein N and C-termini. The C-terminal 20aa (red) is exposed at the base of the p37 protein, the N-terminal 20aa (yellow) is located within Domain I looping above the cleft entrance and the thiamine pyrophosphate (grey) is located within the cleft. (Designed using Pymol, Schrodinger, 2010).

7.2.5 BLAST alignment of the *M. hyorhina* p37 protein to related proteins in mycoplasma

A BLASTp of the full *Mycoplasma hyorhina* p37 sequence against other mycoplasma species was performed (Section 2.8.3). BLASTp is a search of the NCBI protein databases using a protein query. Many mycoplasma proteins were identified and the top ten hits, representing different mycoplasma species, are tabulated in Table 7.6. The top ten hits are all transport proteins with the exception of the *M. conjunctivae* DNA repair protein HhH-GPD. Four proteins were identified as p37-like ABC transporter substrate-binding lipoproteins, another four are ABC transporter substrate-binding proteins and one was identified as a high affinity transport system protein. The expectation values (E-values) were very low between the alignments, ranging between $2e-92$ to $8e-59$. The E-value indicates statistical significance of a given alignment. A low E-value, approaching 0.0, implies that the alignment is statistically significant. The functions of other p37-like proteins have not been determined.

Table 7.6: Top ten BLASTp hits of the full-length *Mycoplasma hyorhinis* p37 protein sequence. The top ten BLASTp hits of the full-length *Mycoplasma hyorhinis* p37 protein query against other mycoplasma species. The e-values are low indicating statistical significance between the alignments. Alignment identity indicates the percentage of the same amino acids residues at the same position between the two alignments. Positives of an alignment indicate percentage of residues located in the same position that have similar properties. The gaps are the spaces introduced into a sequence to improve the alignment of two sequences. Sequence alignments and raw data of identity, positives and gaps are presented in Appendix XXIV.

Mycoplasma species	Protein (Accession Number)	E-value	Identity	Positives	Gaps
<i>M. hyorhinis</i>	p37 (CAA32357.1)	Query sequence			
<i>M. conjunctivae</i> HRC/581	putative P37-like ABC transporter substrate-bi (YP_002960563.1)	2e-92	44%	62%	7%
<i>M. ovipneumoniae</i>	DNA repair protein HhH-GPD (WP_010321138.1)	3e-86	38%	54%	5%
<i>M. flocculare</i>	p37-like ABC transporter substrate-binding lipoprotein (WP_002557691.1)	5e-86	39%	57%	5%
<i>M. pulmonis</i>	lipoprotein ABC transporter substrate-binding protein (WP_010925029.1)	1e-84	39%	57%	5%
<i>M. hyopneumoniae</i> (7448/J/232/168/168-L)*	p37-like ABC transporter substrate-binding lipoprotein (YP_287754.1)	6e-84	40%	58%	5%
<i>M. auris</i>	Alkylphosphonate ABC transporter, substrate-binding protein (PhnD) (WP_004423763.1)	5e-63	32%	51%	10%
<i>M. arthritidis</i> 158L3-1	p37-like ABC transporter substrate-binding lipoprotein (YP_001999750.1)	5e-60	34%	52%	12%
<i>M. genitalium</i> M6282	Alkylphosphonate ABC transporter substrate-binding protein (YP_006600321.1)	4e-59	39%	59%	3%
<i>M. arginini</i>	Alkylphosphonate ABC transporter, substrate-binding component (WP_004416279.1)	8e-59	40%	60%	4%
<i>M. genitalium</i>	Phosphonate substrate binding protein MG289, Chain A (3MYU)	8e-59	39%	59%	3%

*The p37 protein aligned to five homologues of the *M. hyopneumoniae* protein in five sub-types (7448/J/232/168/168-L) and therefore was counted as a single hit.

7.2.6 BLAST alignment of the 20aa C-terminus of the *M. hyorhinis* p37 with other proteins

The p37 truncation experiments (Section 7.2.4) suggested that the C-terminal 20 amino acids of p37 were required to induce gene expression in NIH3T3 cells. Analysis of the p37 C-terminal 20 amino acid (aa) against other p37-like proteins revealed three amino acids of p37 were 100% conserved across the eleven mycoplasma species identified in Section 7.2.5; Tyr384 (Y), Ile387 (I) and Glu393 (E) (Figure 7.15). Two other amino acids, namely Lys385 (K) and Lys386 (K) were 50 and 58% conserved, respectively.

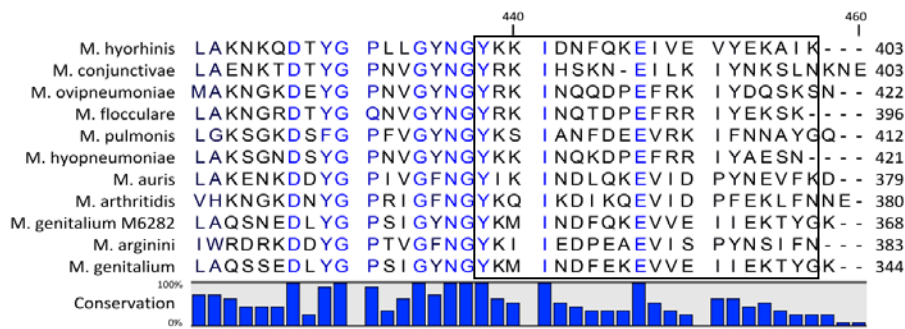


Figure 7.15: Conservation analysis of the *Mycoplasma hyorhinis* p37 C-terminus aligned to several other mycoplasma proteins identified by BLASTp (Section 7.2.5). The C-terminal Tyr384 (Y), Ile387 (I) and Glu393 (E) of the *Mycoplasma hyorhinis* p37 protein sequence was conserved 100% across all mycoplasma proteins. The amino acids Lys385 (K) and Lys386 (K) were conserved 50 and 58% across the mycoplasma species. Full sequence alignments presented in the Appendix XXIV.

A BLASTp search was conducted using only the C-terminal 20aa of *Mycoplasma hyorhinis* p37 (Section 2.8.3). The top 10 hits included proteins from four *Mycoplasma genitalium* strains, five *Borrelia garinii* strains and a single protein of *Borrelia burgdorferi* (Table 7.7). The E-values are high due to the short input sequence, however, the percentage of positives between the alignments was high. Positives indicate the percentage of residues located in the same position and with similar properties. The 20aa of *M. genitalium* strains aligned with 88% positives, except *M. genitalium* strain M2321 (76%). The *Borrelia* proteins aligned with 65% identity and 80% positives.

Table 7.7: Top ten BLASTp results of the p37 C-terminal 20aa (excluding *Mycoplasma hyorhinis*). The top ten BLASTp hits for the p37 C-terminal 20aa (excluding *Mycoplasma hyorhinis*) were *M. genitalium* proteins and the LMP1 homologue protein of *Borrelia*. Alignment identity indicates the percentage of the same amino acids residues at the same position between the two alignments. Positives of an alignment indicate percentage of residues located in the same position that have similar properties. The gaps are the spaces introduced into a sequence to improve the alignment of two sequences. Sequence alignments and raw data of identity, positives and gaps are presented in Appendix XXV.

Organism	Protein (Accession Number)	E-value	Identity	Positives	Gaps
<i>Mycoplasma genitalium</i> M6282	alkylphosphonate ABC transporter substrate-binding protein (YP_006600321.1)	0.013	65%	88%	0%
<i>Mycoplasma genitalium</i> M2321	alkylphosphonate ABC transporter substrate-binding protein (YP_006599832.1)	0.044	52%	76%	19%
<i>Borrelia garinii</i> PBi	surface-located membrane protein 1 (YP_072659.1)	0.086	65%	80%	5%
<i>Borrelia garinii</i> NMJW1	surface-located membrane protein 1 (YP_006870908.1)	0.086	65%	80%	5%
<i>Borrelia garinii</i> BgVir	LMP1 (YP_006202902.1)	0.086	65%	80%	5%
<i>Borrelia garinii</i> PBr	tetratricopeptide repeat domain protein (ZP_03539481.1)	0.086	65%	80%	5%
<i>Borrelia burgdorferi</i>	LMP1 (AAK18802)	0.086	65%	80%	5%
<i>Borrelia garinii</i>	hypothetical protein (WP_004793842.1)	0.086	65%	80%	5%
<i>Mycoplasma genitalium</i> MG289	Chain A (3MYU_A)	0.110	59%	88%	0%
<i>Mycoplasma genitalium</i> G37	phosphonate ABC transporter substrate-binding protein (NP_072955.1)	0.110	59%	88%	0%

The six proteins of *Borrelia burgdorferi* and the *Borrelia garinii* subtypes are homologues of surface-located membrane protein 1 (LMP1). *B. burgdorferi* is the common cause of Lyme disease in North America whereas *B. garinii* and *B. afzelii* cause Lyme disease in Eurasia (Norris, 2006). Lyme disease is a chronic inflammatory disease that results in skin lesions, neurological symptoms and arthritis (Norris, 2006; Yang et al., 2009; Yang et al., 2010c). The specific function of LMP1 is unknown, however, depletion of the protein impairs the pathogen's persistence within a healthy host (Yang et al., 2009). Alignment of the *M. hyorhinitis* p37 protein with LMP1 homologues located the p37 C-terminal 20aa approximately 100aa from the *Borrelia* protein C-terminus (Figure 7.16). Twelve of the twenty amino acids were conserved in the LMP1 proteins.

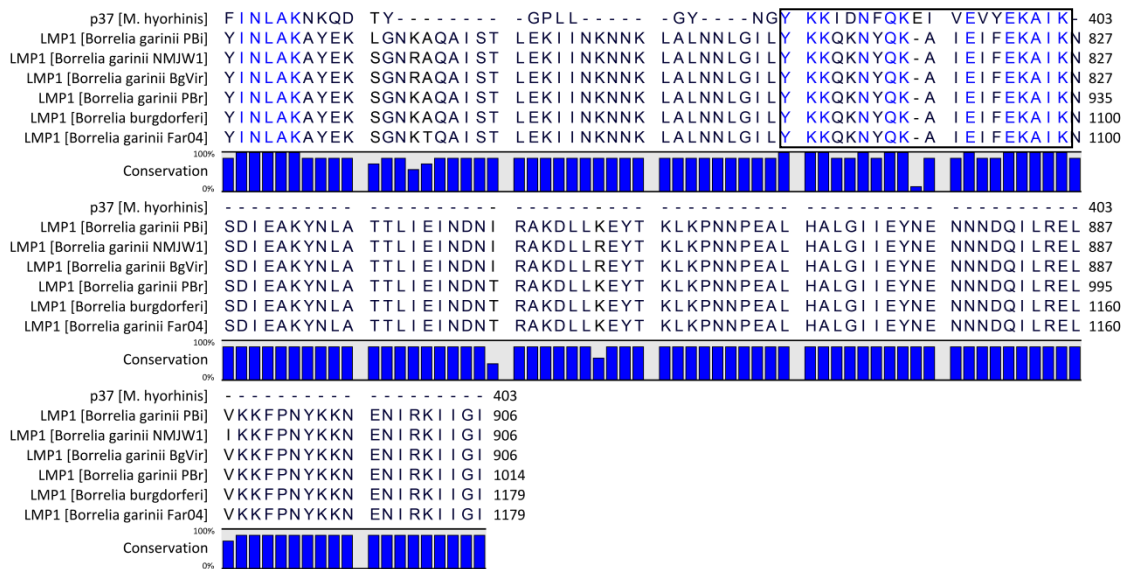


Figure 7.16: Sequence alignment of LMP1 homologues and p37. Full alignment presented in Appendix XXV.

Yang et al. (2010c) found that the LMP1 C-terminus was exposed at the surface of the *B. burgdorferi* plasma membrane. An antibody targeting the C-terminal 750-1119aa interfered with the bacteria's persistence within joints. The C-terminal of LMP1 is responsible for the evasion of the immune system by *B. burgdorferi*. Deletion of the LMP1 C-terminal decreased *B. burgdorferi* persistence in immunodeficient mice injected with anti-*B. burgdorferi* sera (Yang et al., 2009). The molecular mechanisms by which the LMP1 protein allows *B. burgdorferi* to evade the immune system as well as induce chronic inflammatory disease are not known.

7.3 CONCLUSION

Mutations that interfere with thiamine pyrophosphate binding by p37 reduce the gene induction levels of most genes tested (Figure 7.9). However, *Angptl4*, *STAT3* and *Mmp2* expression was higher with the mutated than the native p37 protein. *Angptl4* expression was 3.5-fold higher than stimulation obtained by native p37. The reasons are not known but suggest a receptor(s) other than TLR4 may be involved.

Removing the C-terminal 20 amino acids of p37 greatly reduced the protein's capacity to induce expression of seven of the eight genes studied (Figure 7.13). However, the level of induction of *Angptl4* was not affected by removal of 20 amino acids. When 60 amino acids were removed *Angptl4* induction by the truncated peptide was greatly reduced.

Receptors involved in activation of *Angptl4* are not known although its transcription can be induced by glucocorticoids (Koliwad et al., 2012) and viral G-protein-coupled receptor (GPCRs) up-regulated *Angptl4* expression, suggesting that G-protein-coupled receptors are involved (Ma et al., 2010). I κ B ϵ , an I κ B kinase, links GPCRs to NF- κ B activation (Wang et al., 2013).

8. THE EFFECTS OF P37 ON WOUND HEALING AND CELL MIGRATION

8.1 INTRODUCTION

Wound healing is a complex process that repairs damaged tissue. Injury initiates the inflammatory response with the production of cytokines and acute phase proteins (APPs) signalling migration of immune cells to prevent infection and to remove infectious agents. In response to cytokines, fibroblasts also migrate to the site of injury for the purposes of extracellular matrix remodelling and proliferation to structure and replace damaged tissue (Green et al., 2004; Arwert et al., 2012). *In vitro* wound healing assays are a simple method to observe cell migration, including spreading and proliferation. A cell monolayer is wounded (scratched) with a sterile pipette tip and images captured. Image capture is made at the beginning (0hr) and at regular intervals during cell migration until wound closure. The images are compared to quantify migration rates of treated/transformed cells with controls (Liang et al., 2007).

Cell migration involves protrusion of the leading edge, formation of new adhesions with the extracellular matrix (ECM), cell body contraction and rear detachment (Guilluy et al., 2011). The Rho GTPases RhoA, Rac1 and Cdc42 are well known for their role in regulating the actin cytoskeleton and controlling cell motility, adhesion and promoting lamellipodia and filopodia (thin protrusions similar to lamellipodia) as discussed in Section 1.8 (Wennerberg et al., 2005; Arulanandam et al., 2009). Desai et al. (2004) found that constitutively activated and dominant negative RhoA inhibited wound healing in human bronchial epithelial cells (16HBE) as did RhoA over-expression and dominant negative Rac1. The coordination of both Rho GTPases is required for efficient wound closure (Desai et al., 2004).

Rho GTPase activity has been linked to the activation of NF- κ B and consequent activation of STAT3 by Il6-family cytokines (Figure 8.1). In NIH3T3 cells, activated RhoA or Rac1 inhibits I κ B, an NF- κ B inhibitor, enabling activation of NF- κ B (Perona et al., 1997). Mouse mammary epithelial cell lines (HCII) with mutationally activated Rac1 (Rac^{V12}) have increased mRNA levels of the Il6 and LIF cytokines. Active gp130, a common receptor for

the IL6 family of cytokines, is required to maintain increased migration in comparison with control HCII cells (Raptis et al., 2011). In NIH3T3 cells, RhoA small interfering (si) RNA inhibited NF- κ B activation (Shimizu et al., 2007a). Inhibition of RhoA or GEF-H1 significantly reduces LPS-induced TLR4 activation of NF- κ B (Shibolet et al., 2007; Guo et al., 2012). GEF-H1 is a guanine-nucleotide exchange factor (GEF) that exhibits RhoA-specific GDP/GTP exchange activity (Ren et al., 1998; Zheng, 2001; Guo et al., 2012). Guo et al. (2012) established that LPS-induced NF- κ B activation, via TLR4, is due to interactions between TLR4 and GEF, however, GEF is transcriptionally regulated by NF- κ B. Therefore, RhoA activation strengthens TLR4 signalling and NF- κ B activation.

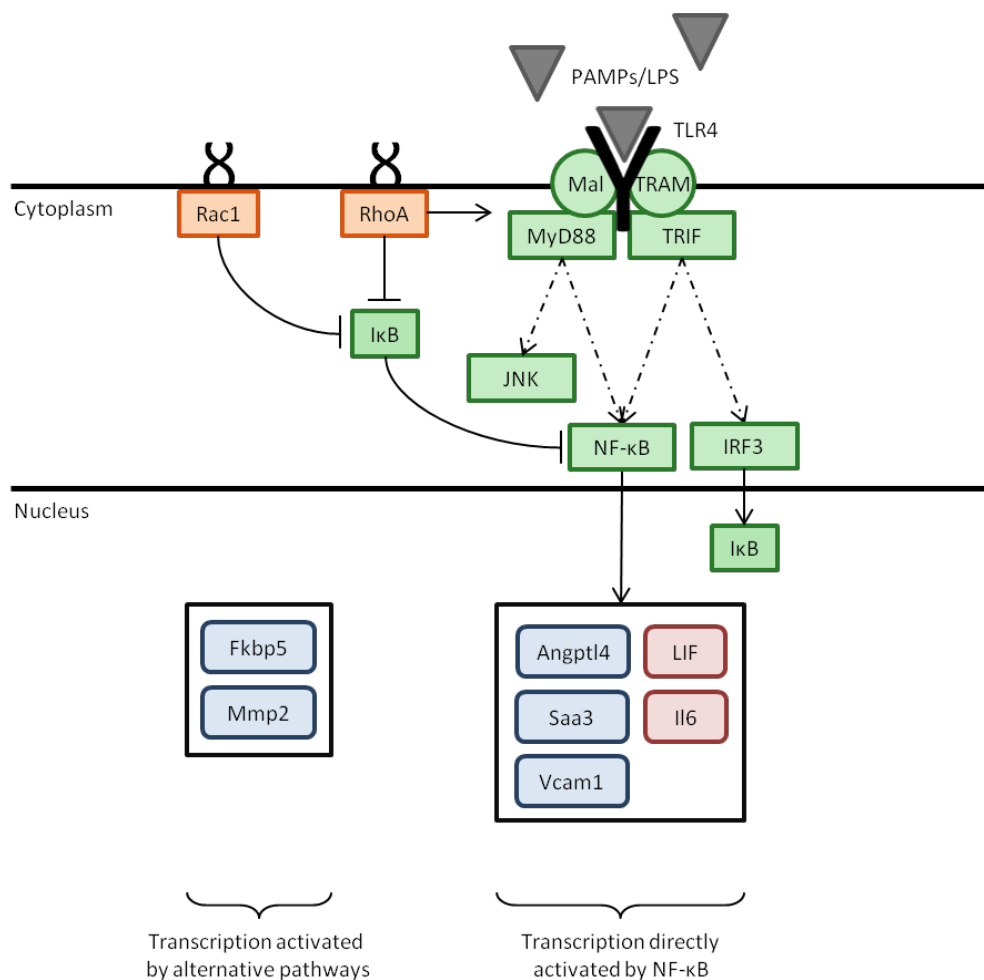


Figure 8.1: Rho GTPase indirect activation of the NF- κ B transcription factor. Active Rho GTPases, RhoA and Rac1, dissociate I κ B from the NF- κ B transcription factor (Perona et al., 1997). I κ B is an inhibitor of NF- κ B transcription. The dissociation of I κ B from NF- κ B allows the transcription of the cytokines *Il6* and *LIF* as well as the acute phase protein genes *Angptl4*, *Saa3* and *Vcam1*. RhoA has also been shown to strengthen LPS-induced TLR4 signalling (Guo et al., 2012).

The experiments described in this chapter were aimed at analysing the morphology of *p37*-transfected NIH3T3 cells and the motility of p37-treated and *p37*-transfected NIH3T3 cells. Quantitative (q) PCR was used to analyse the expression levels in *p37*-transfected NIH3T3 cells of the eighteen genes originally found to be activated by p37-treatment, plus *STAT3* and *Mmp2*, and selected for study (Chapter 3). The effect of p37 on RhoA activity was also determined.

8.2 RESULTS

8.2.1 Lipofection of NIH3T3 cells with the pSTp37 construct

Embryonic mouse fibroblasts (NIH3T3) were transfected (Section 2.18.5) with either the pSecTag (pST) empty vector or the pSTp37 construct (Figure 8.2) (Section 2.2.2). The pSecTag vector was selected due to its murine Ig κ -chain leader sequence and *c-myc* epitope allowing secretion and detection of the p37 fusion protein. Secretion of the p37 protein is required from the NIH3T3 cells, as our previous results suggest that it interacts with a receptor or receptors on the cell surface. This interaction is apparently necessary for gene induction. NIH3T3 cells were also transformed with the empty pST vector as a control. The effects of cytoplasmic located p37 are unknown, although ruptured cells would release cytoplasmic p37 and the surface receptor pathway would be activated. The pSTp37 construct was sequenced before lipofection into NIH3T3 cells (Appendix XXVI). The cells were transfected with the *p37* gene and Hygromycin B was used for the selections of stable transformants. Experiments were conducted before passage (P) 20 and PCR confirmed the presence of *p37* mRNA.

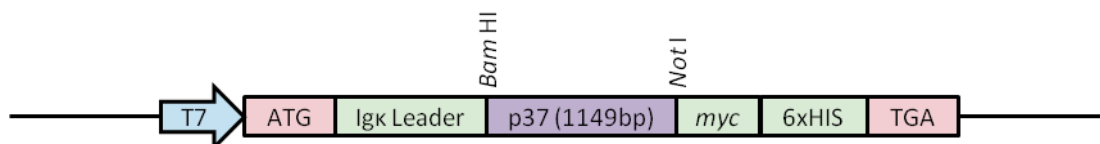


Figure 8.2: The pSTp37 construct. The pSTp37 construct consists of the 5.7 kb pSecTag2/Hygro B vector with a 1.2 kb *p37* open reading frame (ORF) insert (Section 2.2.2). The 1.2kb *p37* ORF consists of several point mutations changing TGA to TGG codons (Section 3.2.1) and excludes the *M. hyorhina* localization signal sequence and the start and stop codons. The start and stop codons were removed from the 1.2kb *p37* ORF to allow for fusion of the Murine Ig κ -chain leader sequence and a *c-myc* epitope. The Murine Ig κ -chain leader sequence (IgK secretion) fused at the N-terminus signals for secretion of the fusion protein.

During lipofection it was observed that the *p37*-transfected NIH3T3 cells at low confluence (<50%) lifted easily from the cell culture plates. Liu et al. (2006) has also reported *p37*-transfected AGS cells are easily detachable from culture plates in comparison to control cells. Disruptions of cell-cell junctions would reduce cell adhesion and increase the ability of a cell to migrate (Cavallaro and Christofori, 2004; Liu et al., 2007; Gong et al., 2008). Coating of the culture plates with 2, 10 or 50µg/ml bovine fibronectin increased petri-dish adhesion ability of *p37*-transfected AGS cells to resemble that of control cells (Liu et al., 2006). Bovine fibronectin (R&D; Cat# 1030-FN) is an extracellular matrix (ECM) component and one of the primary cell adhesion molecules. Clone selection of NIH3T3 cells with pSTp37 was achieved with 2.5µg/cm² fibronectin coating of the cell culture plates.

Three clones of pST (C1, C5 and C7) and pSTp37 (C1, C3 and C10) transfected NIH3T3 cells were selected using 200µg/ml Hygromycin B and maintained in 100µg/ml Hygromycin B (Section 2.18.4). Hygromycin B is an antibiotic that inhibits growth in both prokaryotic and eukaryotic cells. The pSecTag vector contains the Hygromycin resistance (*Hyg^R*) gene which encodes a kinase that phosphorylates and inactivates Hygromycin B. Lipofection of the NIH3T3 cells with the pST and pSTp37 vectors was confirmed by PCR (Figure 8.3A). Transcription of the vectors was also confirmed using PCR (Figure 8.3B). No mycoplasma contamination was found in the NIH3T3 cell cultures or the clones of the NIH:pSTp37 and NIH:pST cell cultures (Section 2.18.7).

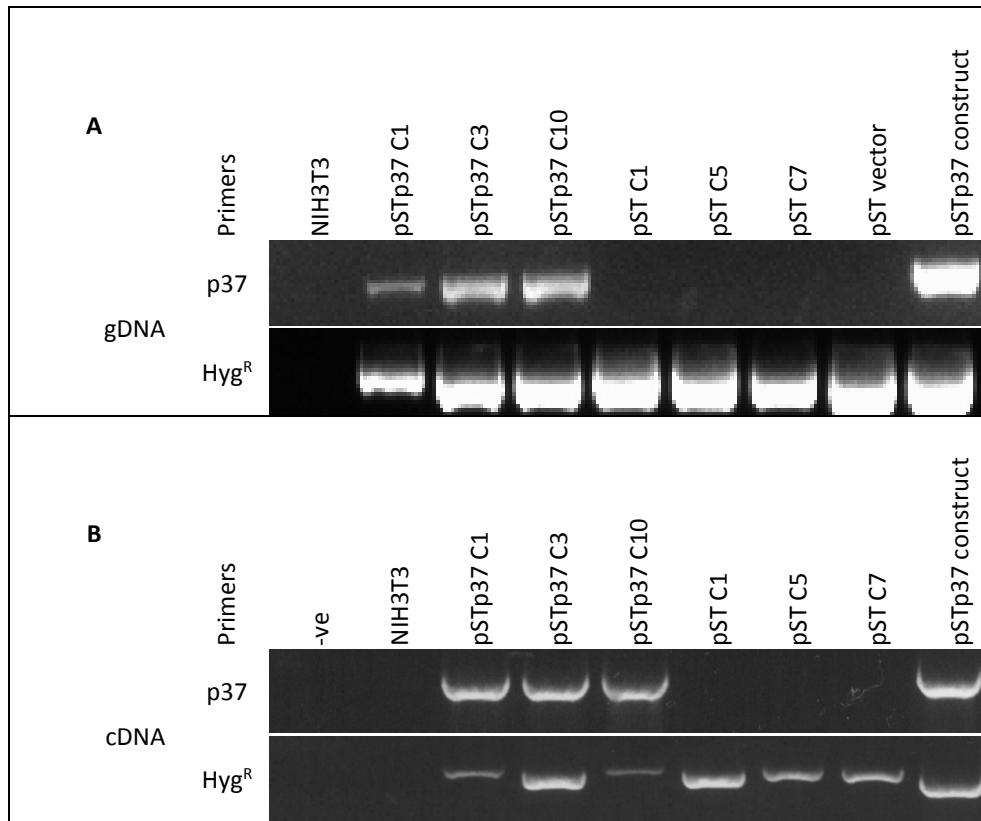


Figure 8.3: PCR confirmation of pST and pSTp37 transfected NIH3T3 clones. Genomic DNA and mRNA was extracted (Sections 2.9 and 2.10.1) from three clones (C1, C3 and C10) of pSTp37 transfected NIH3T3 cell cultures and three clones (C1, C5 and C7) of pST transfected cell cultures. **(A)** PCR (Section 2.11) was used to confirm lipofection of pSTp37 and pST NIH3T3 clones. As anticipated, using *p37* primers (Section 2.5.1; p37F/R), the pSTp37 transfected NIH3T3 cells produced a band whereas the pST empty vector did not. However, using *Hyg^R* primers (Section 2.5.1; Hyg^RF/R) a band was produced in all transfected NIH3T3 cells. **(B)** PCR (Section 2.11) confirmed transcription of the empty vector and pSTp37 construct within the NIH3T3 cells. Again, using *p37* primers (Section 2.5.1; p37F/R), only the pSTp37 transfected NIH3T3 cells produced a band and the *Hyg^R* primers (Section 2.5.1; Hyg^RF/R) produced a band in all the transfected NIH3T3 cells. Non-transfected NIH3T3 cells were used as a negative control (NIH3T3) and the pST and pSTp37 constructs as positive controls. A negative control (-ve control) was also setup containing all the reagents of a GoTaq PCR reaction except the DNA template. The PCR reactions was run out on a 2% agarose gel and observed under a UV light (Transilluminator UVP, inc) (Section 2.7).

8.2.2 *p37* transfection influences NIH3T3 cellular morphology

The *p37*-transfected NIH3T3 cells readily detached from the tissue culture plates at low confluence in the absence of fibronectin. NIH3T3:pSTp37 cells (Figure 8.4F,G&H) plated in the absence of fibronectin were more rounded when compared to the control empty vector lines (B,C&D) and wild type NIH3T3 cells (A&E). Liu et al. (2006) observed that *p37*-transfected AGS cells were also smaller and more spherical than the controls and detached readily from one another and the matrix.

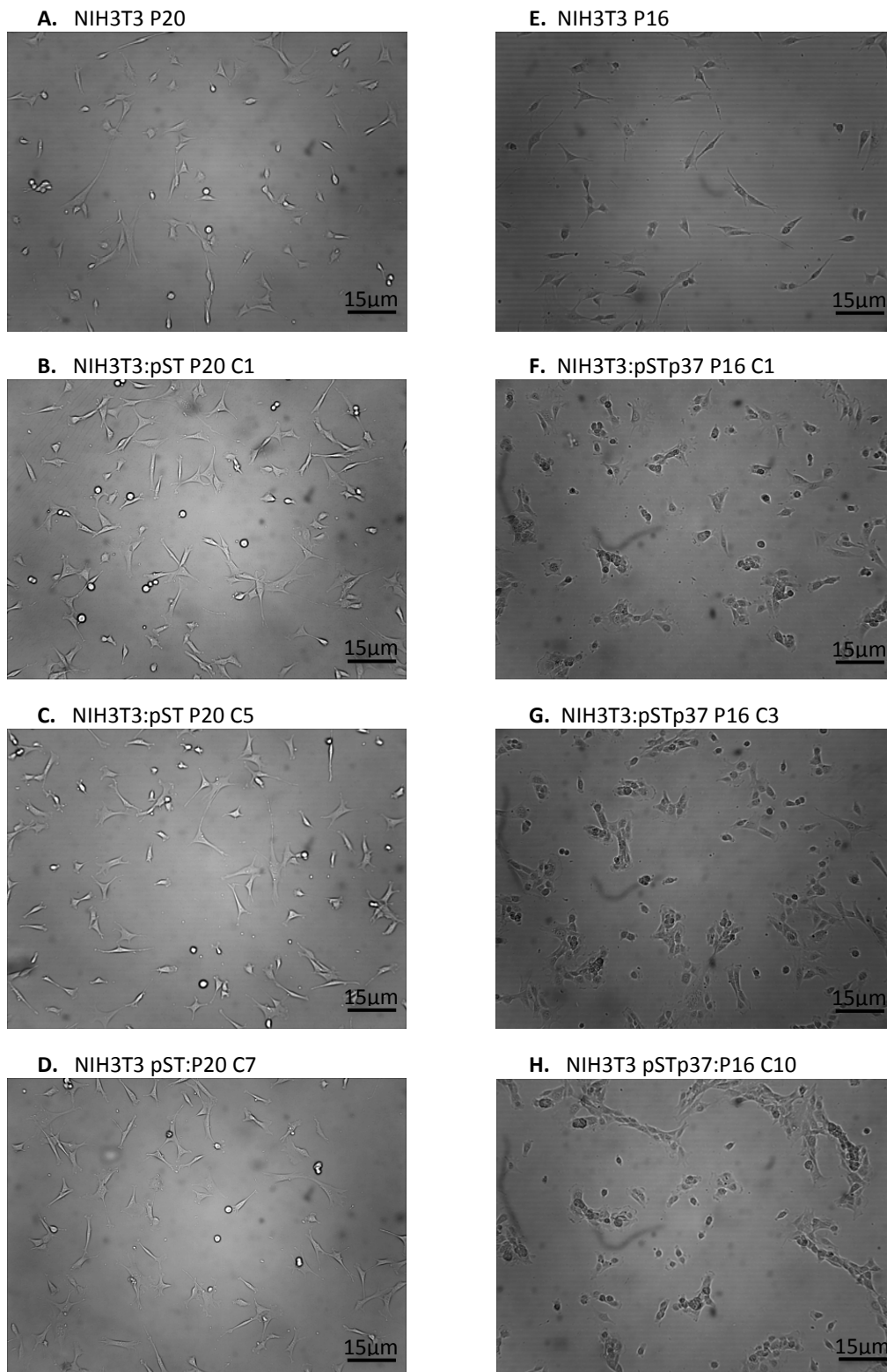


Figure 8.4: Morphology of pST and pSTp37 transfected NIH3T3 cells compared to wild type NIH3T3 cells. Wild type NIH3T3 cells (**A&E**) and NIH3T3:pST cells (**B, C&D**) are elongated compared to the NIH3T3:pSTp37 transformed cells (**F, G&H**) which are smaller and rounded. All cell cultures were passaged (Section 2.18.1) either 16 or 20 times (P16 and P20 respectively). Photos were captured of the pST and pSTp37 transfected NIH3T3 cells clones (C1, C5 and C7; C1, C3 and C10). Scale bar represents 15µm.

8.2.3 The p37 protein promotes cell motility and migration

A wound healing assay was used to determine the effects of p37 on cell motility using p37-treated and p37-transfected NIH3T3 cells. Un-treated and pST-transfected NIH3T3 cells were used as the controls. Confluent monolayers of the NIH3T3 cell lines were wounded (scratched) with a sterile pipette tip (Section 2.21). Images were captured at 0, 14, 19, 24 and 38hr.

Increased migration and wound closure was evident in the presence of 25µg/ml p37 (NIH+25µg/ml p37), and with p37-transfected NIH3T3 cells (NIH:pSTp37). The increase was more pronounced with NIH:pSTp37 cells than p37-treated cells. NIH:pST cells were less effective at wound healing than the NIH3T3 control.

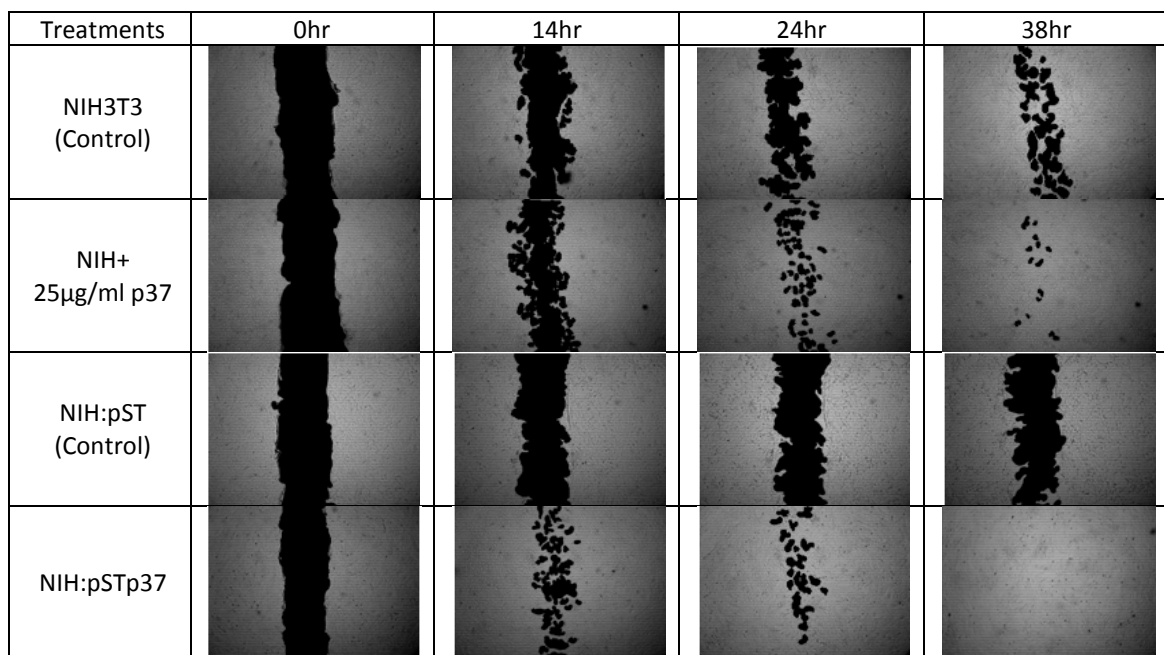


Figure 8.5: p37 enhances wound healing of NIH3T3 cells. NIH3T3 cells were grown to a confluent monolayer and wounded (scratched) with a sterile pipette tip (Section 2.21). The wound, absent of cells, was blacked out to better visualise migration of the NIH3T3 cells. Photographs were taken at 0, 14, 24 and 36hr after wounding. Increased migration and wound closure is seen in the p37-treated (NIH+25µg/ml p37) and p37-transfected (NIH:pSTp37) NIH3T3 cells compared to their controls.

The NIH3T3 fibroblasts did not exhibit the flattening and spreading characteristics seen by Gong et al. (2008) with AGS cell cultures. Green et al. (2004) details NIH3T3 cell wound healing by the formation of cell bridges at regular intervals along a wound before the subsequent closure. Fibroblasts flatten at the surface of a wound extending unidirectional filopodia into the wound (Figure 8.6). Single cells elongate into the wound until contact with similar stretching cells. These bridges are then used by other cells to move into the wound and form bridges between bridges. Cell migration, flattening and mitosis eventually close the wound. This is evident in our experiment by the patchy blacked out wounding that occurred for example in Figure 8.5, the NIH3T3 Control at 38hr.

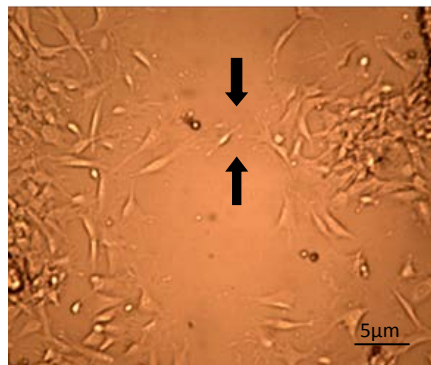


Figure 8.6: Bridge formation of NIH3T3 cells. Monolayers of NIH3T3 cells extend unidirectional filopodia into the wound (scratch) in search of other cells. Bridges of cells are then formed allowing closure of the wound (arrows point to the formation of a bridge).

As a consequence of the formation of cell bridges the standard method of calculating the rate of cell migration ($\mu\text{m}/\text{hr}$) is inadequate. Rate of cell migration ($\mu\text{m}/\text{hr}$) is usually calculated by measuring wound width at 0hr and during wound closure. The cell surface migration area (μm^2) of 5 wounds for each treatment at different time points was instead quantified using IMAGE J (Figure 8.7) and the rate of cell migration calculated (Section 2.21.3) (Table 8.1). The *p37*-transfected NIH3T3 cells migrated at a faster rate than the *p37*-treated NIH3T3 cells (Figure 8.7 & Table 8.1). Both treatments resulted in more rapid cell migration than the control NIH3T3 cells. Cells transfected with the empty vector migrated more slowly than control cells.

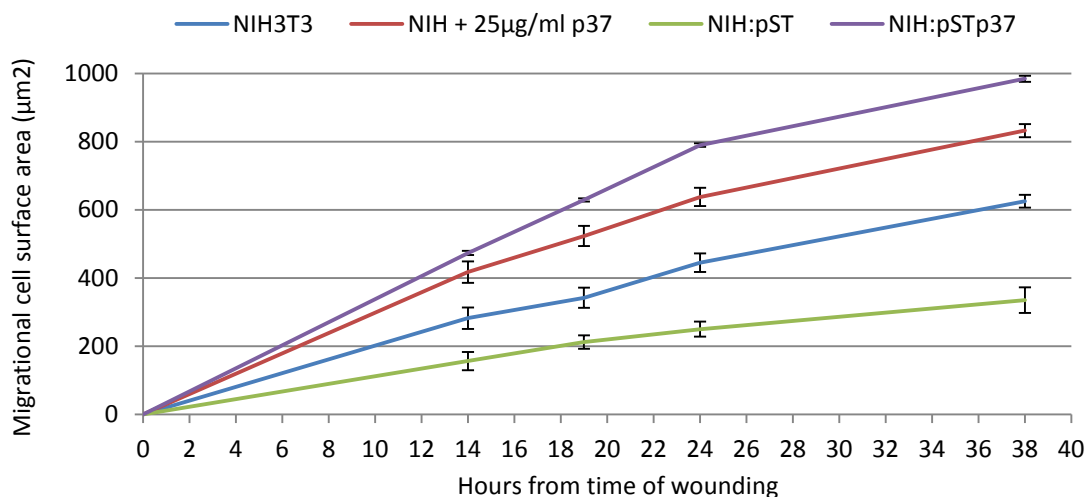


Figure 8.7: p37 increases the surface area (μm^2) covered by migrating cells. Using Image J the surface area (μm^2) covered by migrating cells during wound healing was calculated at 0, 14, 19, 24 and 38hrs was calculated (Section 2.21.3). p37-treated and p37-transfected NIH3T3 cells migrated further than the control cells. Raw data presented in Appendix XXVII.

Table 8.1: Rate of cell migration ($\mu\text{m}^2/\text{hr}$) increases due to p37. The rate of cell migration was calculated by the surface area (μm^2) covered by migrating cells divided by time (hr). The p37 protein increased the rate of cell migration compared to the controls. Raw data presented in Appendix XXVII.

Time (hr)	Rate of cell migration ($\mu\text{m}^2/\text{hr}$)				Rate of cell migration averaged over all four times ($\mu\text{m}^2/\text{hr}$)
	14	19	24	38	
NIH3T3	20	18	19	16	18
NIH+25µg/ml p37	30	28	27	22	26
NIH:pST	11	11	10	9	10
NIH:pSTp37	34	33	33	26	31

8.2.4 RhoA is activated in p37-treated NIH3T3 cells

NIH3T3 cells were treated with 25µg/ml p37, and the cell lysates of three biological replicates were collected at 30min, 2, 4 and 24hrs after initiation of treatment. Total and active RhoA was detected using the G-LISA® RhoA Total and Activation Assay Biochem Kit™ (Absorbance Based) (Cytoskeleton; Cat#BK124/BK150) (Section 2.20). Levels of total RhoA were no more than 12% different between the biological replicates and time points of the treated and control cells (Appendix XXVIII). The active RhoA (%) was normalized against total RhoA at each time point (Figure 8.8). RhoA was significantly activated after 2hrs 25µg/ml p37-treatment in NIH3T3 cells. The increase was still detected after 4hrs but was no longer present 24hrs after p37 addition.

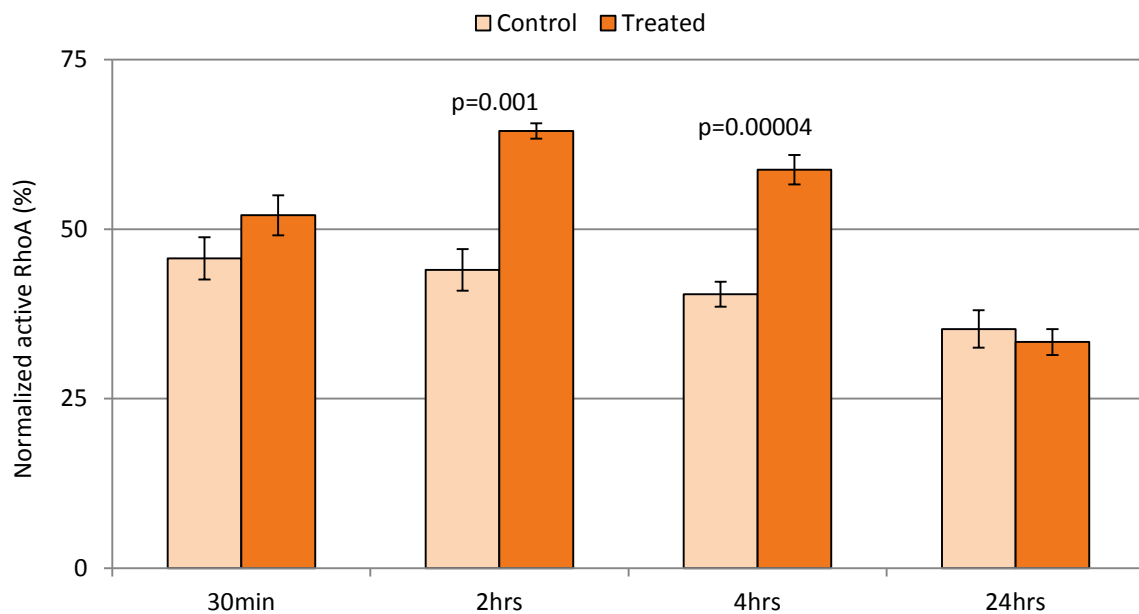


Figure 8.8: Levels of active RhoA in p37-treated and non-treated NIH3T3 (mouse) fibroblasts. NIH3T3 cells were either treated or not treated with 25µg/ml p37 and active and total RhoA was determined at 30min, 2, 4 and 24hrs. Normalised Active RhoA (%) was calculated as described in Section 2.20. The p37 protein significantly increased active RhoA at 2 and 4hrs after treatment. Significant differences between treated and untreated cells were calculated from three biological and three technical replicates by ANOVA analysis. Raw data presented in Appendix XXIX.

8.2.5 Expression of twenty selected genes in p37-transfected NIH3T3 cells

Fold change of the eighteen genes previously selected from the microarray analysis, plus STAT3 and Mmp2, were calculated relative to non-transfected controls. The eight genes encoding Il6, Angptl4, Cast, Dcn, Mmp9, TNFaip6, Lcn2 and Mmp2 were significantly up-regulated in p37-transfected NIH3T3 cells (Figure 8.9). The expression levels of *Angptl4*, *Cast*, *Dcn* and *Lcn2* were lower in the p37-transfected cells than the 25µg/ml p37-treated NIH3T3 cells (Chapter 3), however, expression of *Il6*, *Mmp9*, *TNFaip6* and *Mmp2* was higher.

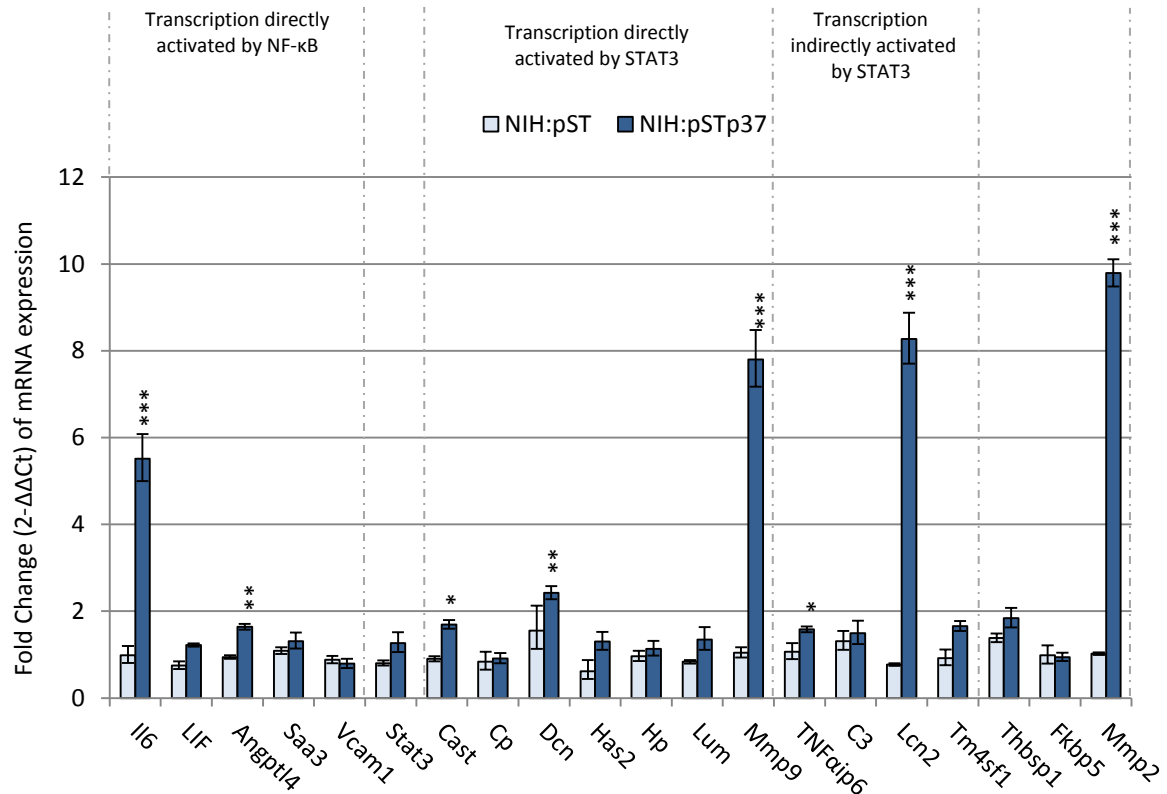


Figure 8.9: Gene expression in p37-transfected NIH3T3 cells. NIH3T3 cells were transfected with pST or pSTp37 and three clones of each were selected. Fold change ($2^{-\Delta\Delta C_t}$) is calculated relative to non transfected controls, normalised to reference genes *GAPDH* and *βactin* (Section 2.12.4). Significant differences were calculated by ANOVA analysis (* $p < 0.05$, ** $p < 0.01$, *** $p < 0.001$) and error bars depict \pm SE in relation to fold change (Section 2.12.8). Raw data presented in Appendix XXX.

8.3 DISCUSSION

The *p37*-transfected NIH3T3 cells detached readily from one another and from the surface of culture plates. When cultured in the absence of fibronectin they were smaller and more spherical than control cells. These results are consistent with those reported by Liu et al. (2006) who suggested that the morphological changes were due to the decreased production of ICAM-1 and integrin- β 1 identified by Western blot analysis. ICAM-1 plays an important role in cell adhesion of vascular endothelial cells to the extracellular matrix (ECM) (Kevil et al., 2004). Integrin mediated cell adhesion regulates a multitude of cellular responses, including proliferation, survival and cross-talk between different cellular signalling pathways (Lee et al., 2004). Down-regulation of *ICAM-1* and *integrin- β 1* was not observed in our microarray of *p37*-treated NIH3T3 cells (24hr). However, *integrin- β 2* expression was down-regulated 4-fold (Appendix III). Integrin- β 2 is a subunit of the complement component 3 receptor (C3R) whereas Integrin- β 1 is a fibronectin receptor.

The *p37* protein has been associated with invasion and may facilitate metastasis (Section 1.6). Metastatic cells exhibit reduced heterotypic contact inhibition of locomotion and cell-cell adhesion, facilitating separation and migration from a primary tumor (Cavallaro and Christofori, 2004). The *p37*-transfected NIH3T3 cells resemble metastatic cells with their reduced abilities to attach to tissue culture plates (Section 8.2.1). The addition of *p37* to cell monolayers increased cell migration rates and wound closure. The same effect was observed with *p37*-transfected cells. The increased production of *Il6* by *p37*-treated cells may be responsible for reduced cell-cell adhesion and cell motility. Cells of the human breast carcinoma line ZR-75-1-Tx round up and detach from other cells and the substratum in response to *Il6* (Tamm et al., 1994) resembling the *p37*-transfected NIH3T3 cells. The inhibition of *Il6* expression reversed the phenotype. The increased *Il6* expression was suggested to regulate the level of proteins that play integral roles in cell migration and adhesion.

Angiopoietin-like 4 (*Angptl4*) is an acute phase protein more commonly known as an apoptosis survival factor, therefore, increased levels would decrease apoptosis,

promoting cell antisenescence (immortality) (Padua et al., 2008). However, Angptl4 has also been linked to the cell junction disruption of vascular endothelial cells in breast cancer (Padua et al., 2008; Welm, 2008). The disruption of cell junctions would be expected to reduce cell-cell adhesion and favour invasion (Cavallaro and Christofori, 2004). Liu et al. (2006) observed that the human gastric cancer cells (AGS) stably transfected with the *p37* gene exhibited increased antisenescence and a decrease of cell-cell adhesion.

Expression levels of the twenty genes up-regulated by exogenously added p37 (Chapter 3) were determined in *p37*-transfected NIH3T3 cells. Expression of these genes was significantly better than in empty vector controls. The genes most strongly activated were *Il6* (5-fold), *Mmp9* (8-fold), *Lcn2* (8.5-fold) and *Mmp2* (9.5-fold). These are higher levels than those observed with 25µg/ml p37 (24hr) (Figure 3.7). The differences in gene expression levels between p37-treated and *p37*-transfected cells may reflect the length of time the latter cells have been exposed to p37. The expression changes are presumably due to p37 secreted into the medium but we have not attempted to quantify the amount of p37 released. To what extent intracellular p37 affects cell behaviour (including gene expression) is unclear. The increased expression of *Mmp9*, *Lcn2* and *Mmp2* is noteworthy as all these proteins play a role in cancer progression and metastasis (Leung et al., 2012). Genes specifically regulating cell motility and wound healing were not examined.

The NIH3T3 cells transfected with *p37* could be used for *in vivo* studies in mice. *In vivo* experiments may reveal if p37 promotes cell motility, migration and invasion contributing to tumor growth and metastasis. Migration of cells through the extracellular matrix requires secretion of proteases such as the matrix metalloproteinases (Mmps) that degrade the basement membrane facilitating invasion (Sledge Jr. and Miller, 2003). Increased serum levels of *Mmp2* and *9* have been found in patients with metastatic cancers (Ray and Stetler-Stevenson, 1994; Sledge Jr. and Miller, 2003; Visse and Nagase, 2003).

NIH3T3 cells treated with the p37 protein exhibit a loss of heterotypic contact inhibition of locomotion in Abercrombie's confronted explants (Steinemann et al., 1984a;

Schmidhauser et al., 1990). Constitutive activation of RhoA in NIH3T3 cells also resulted in a loss of heterotypic contact inhibition of locomotion (Anear and Parish, 2012). When p37 was added to NIH3T3 cells, we found a significant increase in levels of activated RhoA at 2 and 4hr. Hence, p37 may interfere with heterotypic CIL by activating RhoA. Activated RhoA inhibits I κ B which then permits the activation of NF- κ B (Figure 8.1). The increased expression levels of *I/6* and acute phase protein genes via the TLR4 pathways are a consequence of this NF- κ B activation.

9. FINAL DISCUSSION

9.1 GENES UP-REGULATED BY p37

The aim of the research discussed in this thesis was to determine the effect of short term (up to 24hr) p37-treatment on gene expression in mouse NIH3T3 fibroblasts. This cell line along with other fibroblast lines were used in the original work leading to the discovery of p37 (Steinemann et al., 1984a; Steinemann et al., 1984b).

The data presented in Chapter 6 indicates that p37 of *M. hyorhinis* is initially signalling via the Toll-like receptor 4 (TLR4) of NIH3T3 cells. This is consistent with the strong induction after only 2hr p37-treatment of the *Angptl4*, *Saa3*, *Vcam1*, *Il6* and genes (Table 3.3). *LIF* expression also increases, but to a lesser degree (Table 3.3). These genes are regulated by NF- κ B, which is activated by TLR4 (Figure 9.1).

Genes whose induction first became significant after 12hr p37-treatment, included *Dcn*, *Has2*, *Hp*, *Lum*, *C3*, *Lcn2* and *Mmp9* (Table 3.3). These genes are regulated by the STAT3 pathway. Their delayed induction is consistent with the early induction of a cytokine such as *Il6*. *Il6* regulates the transcription of many acute phase proteins via STAT3 phosphorylation (Figure 9.1) in response to injury and bacterial infection (Rokita et al., 1992; Heinrich et al., 2003; Monach et al., 2007). NIH3T3 cells transfected with the *p37* gene exhibited increased expression of fifteen of the twenty genes selected for study. The genes most strongly expressed were *Il6*, *Lcn2*, *Mmp2* and *Mmp9* (Figure 8.9).

LPS signals via the TLR4 receptor and consequently activates *Il6* expression (Figure 9.1). Inhibition of the TLR4 receptor prevents LPS-induced *Il6* expression in colon carcinoma SW480 cells (Reigstad et al., 2009). LPS increased the migration and invasion of SW480 cells through a Matrigel matrix. When the TLR4 receptor was inhibited, invasion was reduced (Rakhesh et al., 2012). In monocytes and macrophages, LPS binding to TLR4 rapidly induced the expression of *Il6*, *Il8*, *Il10* family, *Il12* family, *TNF α* and *TGF- β* genes (Rossol et al., 2011). We detected *Il6* induction by p37 but did not check the early treatment times for the expression of these other cytokines. Since the microarray analysis

used 24hr p37-treated cells, the expression of these genes may already have declined. The decline in p37-induced *Il6* expression after 4hr treatment (Table 3.3) may reflect a decrease in p37 levels (e.g. via proteolysis). However, we did not replenish p37 or determine whether p37 degradation had occurred.

The inflammatory pathway initiated by TLR4 via NF- κ B and the activation of STAT3 by Il6 and LIF which up-regulates the transcription of genes encoding acute phase proteins are depicted in Figure 9.1.

Previous studies reported that *TNF α* transcript and TNF α levels in the medium increased in human peripheral blood mononuclear (PBMC) cells following p37-treatment (Ning et al., 2003a). p37-induced increase of *Mmp2* levels has been observed in the medium of human gastric adenocarcinoma (AGS) cells (Gong et al., 2008), while Liu et al. (2006) described reduced levels of ICAM-1 and Integrin β 1 in p37-treated cells. The transcript levels of *Il8*, TNF (not specified) and some chemokines (not specified) were found in p37-treated PC-3 (highly metastatic) but not DU145 (metastatic) human prostate cell lines (Goodison et al., 2007). Our research with NIH3T3 cells provided different results with the exception of *Mmp2* induction. However, the microarray would not have detected genes that were rapidly up-regulated or down-regulated following p37 addition at the 24hr time point when mRNA was isolated for analysis. Increased *Il6* expression was detected at 24hr but subsequent analysis indicated the levels at 2 and 4hr of p37-treatment were much higher (Table 3.3).

Expression of *TNF α* , *TNF β* , *Il8*, *Il10* and *Il12* should be analysed at these earlier times as they are also activated by LPS via the TLR4 receptor. Cytokine genes activated by other mycoplasma lipoproteins such as *Il8*, *Il4* and *Il6* (Section 6.2.4) should also be checked.

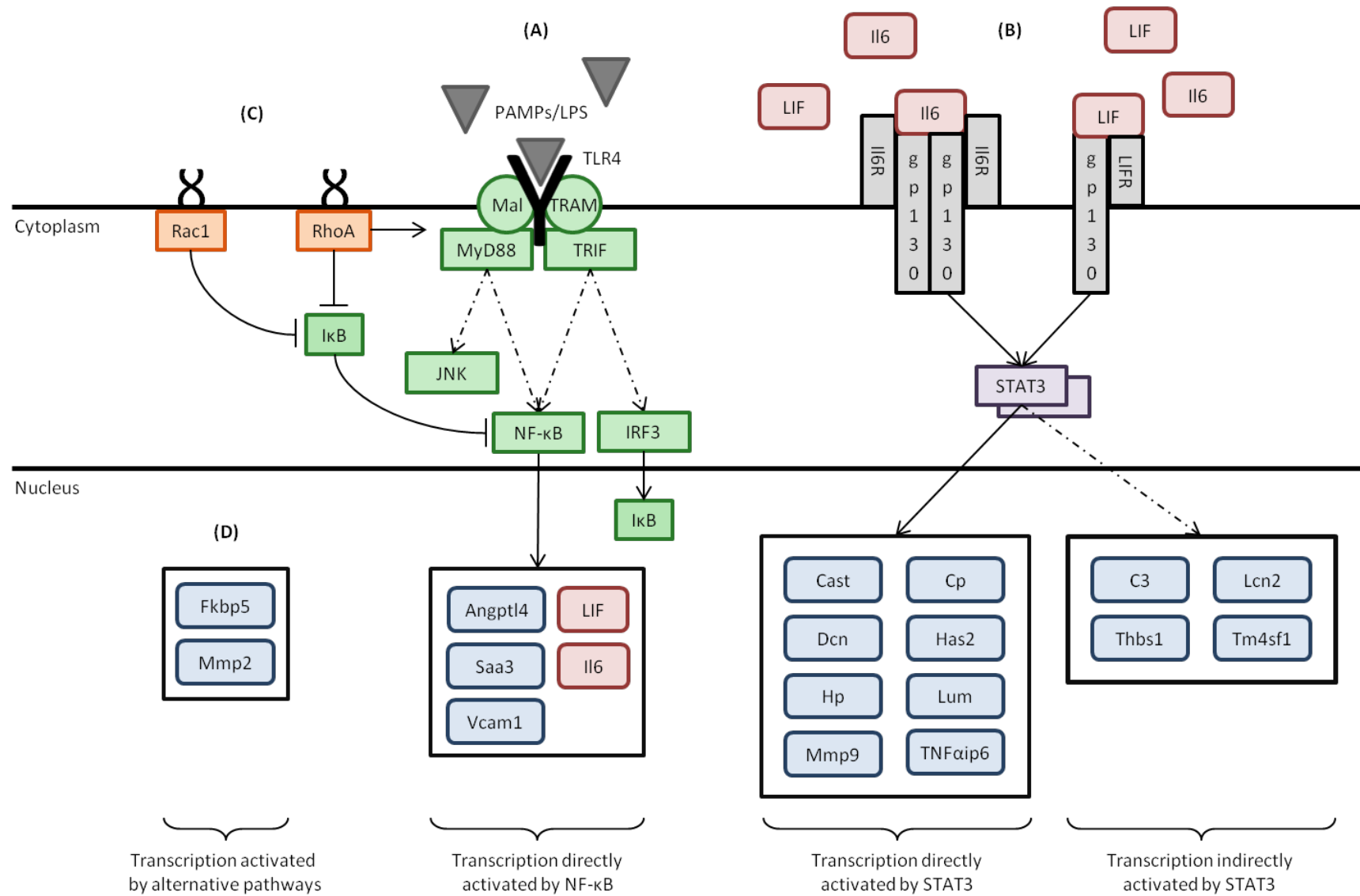


Figure 9.1: Inflammatory pathway initiated via activation of the Toll-like receptor 4. **(A)** Toll-like receptor 4 (TLR4) recognizes pathogen associated molecular patterns (PAMPs) and Lipopolysaccharides (LPS) inducing downstream signalling pathways. The myeloid differentiation primary response 88 (MyD88) is recruited to TLR4, alongside its adaptor protein MyD88-adaptor-like (Mal), in early phase indirect activation of Nuclear Factor Kappa-light-chain-enhancer of activated B cells (NF- κ B) consequently inducing transcription of the cytokines, *Il6* and *LIF* and the acute phase protein genes, *Angptl4*, *Saa3* and *Vcam1*. MyD88 also activates c-Jun Kinase (JNK). The TIR domain-containing adaptor inducing IFN- β (TRIF) is also recruited by TLR4, with the adaptor protein TRIF-related adaptor molecule (TRAM). TRIF recruitment by TLR4 occurs in late phase indirect activation of NF- κ B. TRIF also activates Interferon regulatory factor 3 (IRF3) which is responsible for the activation of the NF- κ B inhibitor I kappa B ($\text{I}\kappa\text{B}$). **(B)** The cytokines *Il6* and *LIF* bind to their specific α -subunit receptors (*Il6R* and *LIFR*) and the activated α -subunit receptor binds to the shared glycoprotein 130 subunit receptor (*gp130*). The cytoplasmic region of *gp130* is phosphorylated and in turn activates STAT3 by phosphorylation. Active STAT3 dimerises and translocates to the nucleus to directly transcribe acute phase protein genes such as *Cast*, *Cp*, *Dcn*, *Has2*, *Hp*, *Lum*, *Mmp9* and *TNFAip6*. Other acute phase proteins are indirectly regulated by STAT3 transcription, namely *C3*, *Lcn2*, *Thbs1* and *Tm4sf1*. **(C)** Active Rho GTPases, RhoA and Rac1, indirectly activate NF- κ B transcription by the inhibition of $\text{I}\kappa\text{B}$. RhoA has also been shown to strengthen LPS-induced TLR4 signalling. **(D)** Transcription of the acute phase protein genes *Fkbp5* and *Mmp2* are not known to be activated by the TLR4 pathway.

9.2 MYCOPLASMA INFECTION: ARTHRITIS AND CANCER

As well as *M. hyorhinis*, chronic inflammation with characteristics of rheumatoid arthritis can be produced by other mycoplasma species such as *M. capricolum* subsp. *capricolum*, *M. hyosynoviae*, *M. synoviae*, *M. fermentans* and *M. pneumoniae* (Ramirez et al., 2005; Kawahito et al., 2008). *M. bovis* causes a variety of diseases in cattle including arthritis (Maunsell et al., 2011). *M. hominis* is a facultative human pathogen and although mainly associated with bacterial vaginosis and pelvic inflammatory diseases can spread to other sites resulting in arthritis (Hopfe et al., 2013). *M. pneumoniae* can cause arthritis in humans with the infection associated with induction of pro-inflammatory cytokines (Ramirez et al., 2005). A glycolipid antigen of *M. fermentans* was detected in 38% of rheumatoid arthritis patients' tissues, but not in osteoarthritis or normal synovial tissues (Kawahito et al., 2008). The glycolipid induced TNF α and IL6 production from peripheral blood mononuclear cells.

M. hyorhinis affects the immune system by causing B- and T-cell proliferation, immunoglobulin secretion, T-cell cyto-toxicity suppression and the release of the cytokines IL1, IL6 and TNF α from monocytes (Kostyal et al., 1995; Razin et al., 1998; Sacht et al., 1998). *M. hyorhinis* is a known causative agent of arthritis in post-weaned swine (Kim et al., 2010; Gomes et al., 2012). Acute arthritis followed by chronic polyserositis occurs when pigs are given an intraperitoneal inoculation of *M. hyorhinis*. The pathogen is present in the affected joints and synovial fluid (Barden and Decker, 1971). When arthritis was induced in pigs with *M. hyorhinis*, increased mRNA frequency of *IL6*, *IL8*, *IL10* and *TNF α* was detected in mononuclear cells from the synovial membranes (with some differences between high and low response animals) (Jayagopala Reddy et al., 2000).

Thus, the evidence for mycoplasma as causative agents of arthritis is considerable. The p37 protein located on the surface of *M. hyorhinis* may be the molecule responsible for the signals leading to inflammation and eventually arthritis. Homologues might exist in other mycoplasmas associated with arthritis and, certainly, p37-like proteins have been identified (Table 7.6).

The role of mycoplasma in the development of cancers is less clear. Chronic non-resolving inflammation can increase the potential for cancer development and metastatic progression (Colotta et al., 2009; Solinas et al., 2010). Overproduction of the Il6 cytokine has been shown to play a role in various types of cancer as well as chronic inflammatory diseases such as rheumatoid arthritis (Blay et al., 1992; Nishimoto, 2006; Yoshio-Hoshino et al., 2007; Howlett et al., 2009; Nishimoto, 2010). The aggressive behaviour of renal cell carcinoma primary tumours has been linked to increased *Il6* expression (Blay et al., 1992).

Both purified and *M. hyorhinis* associated p37 give rise to increased cell invasiveness through Matrigel when added to prostate cancer and melanoma cell lines (Ketcham et al., 2005). The protein has also been identified in human gastric adenocarcinomas and prostate tumours (Gong et al., 2008; Urbanek et al., 2011). The presence of *M. hyorhinis* has been detected in paraffin embedded carcinoma sections of gastric and colon carcinomas as well as oesophagus, lung, breast and glioma carcinomas (Huang et al., 2001). The antibody used to identify the presence of *M. hyorhinis* targeted the 16 amino acid N-terminus of the p37 protein (Ning et al., 2003b). Persistent exposure to *M. hyorhinis* induces malignant transformation of human prostate cells (Namiki et al., 2009). Choi et al., (2014), inadvertently produced a monoclonal antibody against the p37 protein when searching for novel surface markers of circulating tumour cells. Using this antibody, Choi et al, (2014) are the first to discover the presence of mycoplasma infected circulating tumour cells in patients with hepatocellular carcinoma. Hence, p37 has been postulated to play a role in cancer progression. Indeed, sixteen of the eighteen genes we found most strongly up-regulated by p37 are associated with cancer progression (Table 3.2).

The mechanisms underlying increased invasivity through Matrigel of various cell lines following p37-treatment are unknown. Induction of *Mmp* genes may play a role. Similarly, the increased migration rates (wound healing) (Section 8.2.3) induced by p37 and reported by a number of laboratories are yet to be understood although Angptl4 enhances cell migration during wound healing (Goh et al., 2010) and increased Has2 levels facilitate the migration of melanoma cells (Kultti et al., 2012). The loss of heterotypic contact inhibition of locomotion in response to p37-treatment may be due to the activation of RhoA (Section 8.2.4).

9.3 THE EFFECTS ON p37-INDUCED GENE EXPRESSION OF BLOCKING IL6R OR STAT3

As described in Chapters 4 and 5, the presence of an IL6 receptor inhibitor (IL6Ri) or inhibition of STAT3 greatly enhanced the stimulatory effect of p37 on gene expression. Ara et al. (2009) found inhibition of IL6R/gp130, using a mAb, equivalently blocked STAT3 activation in human neuroblastoma (BMSC) cells. However, both IL6Ri and STAT3 inhibition treatments increased expression of genes that are regulated by STAT3, namely *C3*, *Dcn*, *Hp*, *Lcn2* and *Lum*, although the stimulation of *C3*, *Dcn*, and *Lum* was greater with the IL6Ri than with the STAT3 inhibitor. However, there were some anomalies. p37-induction of *Saa3* was very strong in the presence of the STAT3 inhibitor but did not change significantly when IL6Ri was present. *LIF* expression increased from 4- to 10-fold when IL6Ri was present but no p37-induction occurred in the presence of the STAT3 inhibitor. *Fkbp5* expression strongly increased (37-fold) when IL6Ri was combined with p37 but decreased when the STAT3 inhibitor was used. *Angptl4* expression is induced 20-fold by 25µg/ml p37 (24hr) and the inclusion of neither IL6Ri nor the STAT3 inhibitor had an effect. p37-induced *Il6* expression is strongly increased by both inhibitors. The variability in response of the *Il6*, *LIF*, *Angptl4* and *Saa3* genes to the inhibitors is interesting as all four genes are activated by the TLR4 signalling pathway (Figure 9.1). Suggestions as to how the inhibitors may be functioning are provided in the final sections of Chapters 4 and 5.

p37 may be up-regulating a number of pathways activating NF-κB. Toll-like receptor (TLR) pathways, in addition to TLR4, may be enhanced in the presence of a STAT3 inhibitor or IL6R inhibitor. This could be checked by using immunoblotting to examine IκB phosphorylation, an inhibitor of NF-κB. TLRs activate NF-κB regulated transcription of acute phase protein genes. The increased response to p37 in the presence of the STAT3 inhibitor is similar to that seen in *STAT3*-deficient bone marrow derived macrophages (Karim C. El Kasmi, University of Colorado, personal communication). The *STAT3*-deficient macrophages were found to have activated STAT1. Immunoblotting for phosphorylated STAT1, STAT3 and STAT6 in the presence of p37 and either inhibitor could determine if activation is occurring. Combined inhibition of STAT1 and STAT3 would also help identify the role of STAT1 in the increased p37-induced gene expression in NIH3T3 cells when

STAT3 is inhibited. The IL6R α antibody may also block endogenous IL6/STAT3 pathways which are subsequently compensated for by STAT1, resulting in enhanced gene expression following p37-treatment.

9.4 INTERACTION OF p37 WITH THE TOLL-LIKE 4 RECEPTOR

The C-terminus of p37 may be the region of the protein interacting with the TLR4 receptor on NIH3T3 fibroblasts as the truncated p37 no longer induced expression of seven selected genes (*Il6*, *LIF*, *Saa3*, *Dcn*, *Has2*, *C3* and *Lcn2*). Alternatively, removal of the 20 amino acids may change the overall conformation of p37 so that receptor binding can no longer occur.

The C-terminal 20 amino acids of p37 align significantly to a *Borrelia burgdorferi* surface located protein (LMP1) (Section 7.2.6). *B. burgdorferi* has been shown to induce expression of *TNF α* , *Ifn β* , *Il6*, and *Cxcl10* 6hr post incubation of bone marrow derived macrophages. Relative gene expression was reduced 30% (*TNF α*), 60% (*Ifn β*), 75% (*Il6*) and 80% (*Cxcl10*) in *TLR2* deficient bone marrow derived macrophages (Petnicki-Ocwieja et al., 2013). *B. burgdorferi* expressing a LMP1 protein lacking the C-terminal region which included the p37-related 20 amino acid sequence, reduced the ability of the bacterium to cause chronic inflammatory disease (Yang et al., 2009).

The role of thiamine pyrophosphate (TPP) in p37 is not known, however, Sippel et al. (2009) suggested that p37 binds TPP similar to the *E. coli* TbpA protein (Section 1.4). p37-like proteins may be activated by TPP which is then transported into the mycobacterium. When the four amino acids required for TPP binding were mutated, the mutated p37 no longer induced activation of the selected genes to the degree of native p37 (Chapter 7). Hence, TPP may maintain the structure/conformation of p37 required for receptor binding.

Mycoplasma pneumonia has been found to induce an inflammatory response through activation of TLR4 (Shimizu et al., 2014). Mycoplasmas lack a cell wall and do not produce LPS. The *Mycoplasma pneumonia* TLR4 ligand is unknown. Mycoplasmal lipoproteins studied so far interact with one or more of the TLR1, 2 and 6 receptors (Section 6.2.4). The lipid rather than the protein moiety of the lipoprotein is generally considered involved (Zuo et al., 2009). However, a 90 amino acid subfragment of the MG309 lipoprotein from *M. genitalium* elicits increased *Il6* and *Il8* secretion from human genital

epithelium cells but TLR2 and 6 are involved (McGowin et al., 2009). Comparison of the subfragment with p37 showed no significant similarities (Appendix XXXI).

9.5 FUTURE WORK

1. Use qPCR to determine if cytokines in addition to *Il6* and *LIF* are induced by p37 during the first 2-4hr of treatment. The microarray (24hr) analysis would not have detected them if their induction is rapid. Expression of the *TNF α* , *TNF β* , *Il8*, *Il10* and *Il12* family genes would be of interest as they are activated by LPS via TLR4.
2. Gene expression of NIH3T3 cells in the presence of the isotype control antibody LEAF™ Purified Rat IgG2b, κ Isotype Ctrl Antibody (Biolegend Cat# 400637) could be determined, to confirm specificity of the inhibiting Il6R antibody.
3. Inhibiting both STAT1 and STAT3 activity should indicate whether the increase in p37-induced gene expression when STAT3 is inhibited is due to STAT1 activity.
4. Inhibiting NF- κ B activation, using the PDTC inhibitor, would confirm its role in p37-induced gene expression.
5. Since blocking TLR4 inhibits up-regulation of p37-induced gene expression of NIH3T3 cells, ascertain the effects of blocking TLR4 on down-regulated p37-induced gene expression identified in Chapter 3.
6. Ascertain the effects of inhibiting the TLR4 receptor at 2, 4, 8 and 12hr exposure times of p37-treated NIH3T3 fibroblasts.
7. Determine the effect of blocking the TLR4 gene (e.g. using siRNA) on p37-induced gene expression to see if additional receptor pathways are involved. However, pleiotropic effects could make interpretation difficult.
8. Determine the change to the 3D-structure of p37 when the C-terminal 20 amino acids have been removed or the TPP is no longer present (targeted mutations).
9. Isolate p37-like proteins from selected Mycoplasma species and determine if their

effects on gene induction mimic those of p37 in NIH3T3 cells.

10. Use flow-cytometry to determine cellular size and volume of *p37*-transfected NIH3T3 cells and to analyse the expression of p37.

10. APPENDICES

A CD is provided with this thesis which contains the raw data of all qPCR experiments and the calculations for correlation and histogram graphs. The appendices which are located on the attached CD are indicated.

Appendix I

Mass Spec Analysis

Swiss Protein Database aligned the digested peptides (grey boxes) of purified p37 (Section 3.2.1) to the High Affinity transport system protein p37 (P37_MYCHR). The red boxes are multiple positive hits of amino acids.



Appendix II

Dataset obtained from the microarray analysis of 24hr, 15µg/ml p37-treated NIH3T3 (mouse) fibroblasts. The dataset consists of 288 genes significantly up regulated by ≥ 3 fold with a p-value of ≤ 0.001 . The eighteen genes selected for further analysis are presented in bold as well as the chemokines identified in the PCR array, discussed in Section 3.2.7.

Affymetrix Probe Set ID	Gene Symbol	Gene Title	p-value	Fold Change (Up)
1427747_a_at	Lcn2	lipocalin 2	1.9E-04	64
1448881_at	Hp	haptoglobin	1.0E-04	55
1450826_a_at	Saa3	serum amyloid A 3	8.9E-05	34
1417130_s_at	Angptl4	angiopoietin-like 4	2.4E-04	31
1423954_at	C3	complement component 3	8.6E-05	19
1450297_at	Il6	interleukin 6	5.5E-05	16
1423607_at	Lum	lumican	4.9E-05	13
1439925_at	Tm4sf1	transmembrane 4 superfamily member 1	1.1E-04	12
1449368_at	Dcn	decorin	3.1E-05	11
1449169_at	Has2	hyaluronan synthase 2	4.1E-04	9
1450854_at	Pa2g4	proliferation-associated 2G4	1.3E-04	9
1460238_at	Msln	mesothelin	3.6E-04	9
1420142_s_at	Pa2g4	proliferation-associated 2G4	4.3E-04	9
1438009_at	RP23-480B19.10	similar to histone 2a	7.0E-04	9
1418678_at	Has2	hyaluronan synthase 2	3.5E-05	8
1449017_at	Nutf2	nuclear transport factor 2	1.3E-04	8
1460302_at	Thbs1	thrombospondin 1 /// similar to thrombospondin 1	5.1E-04	8
1416721_s_at	Sfrs6	splicing factor, arginine/serine-rich 6	3.7E-04	8
1431375_s_at	Parva	parvin, alpha	1.7E-04	8
1423282_at	Pitpna	phosphatidylinositol transfer protein, alpha	1.0E-04	7
1455494_at	Col1a1	procollagen, type I, alpha 1	1.8E-04	7
1421811_at	Thbs1	thrombospondin 1	5.1E-04	7
1448735_at	Cp	ceruloplasmin	3.0E-04	7
1455505_at	Gatad2a	GATA zinc finger domain containing 2A	1.2E-06	7
1431213_a_at	LOC100041156	hypothetical protein LOC100041156 /// hypothetical protein LOC100041932	7.6E-04	7
1422535_at	Ccne2	cyclin E2	6.6E-04	7
1449550_at	Myo1c	myosin IC	1.2E-05	6
1438658_a_at	Edg3	endothelial differentiation, sphingolipid G-protein-coupled receptor, 3	9.3E-05	6
1439516_at	2610201A13Rik	RIKEN cDNA 2610201A13 gene	6.4E-04	6
1437611_x_at	Kif2c	kinesin family member 2C	1.9E-04	6
1416720_at	Sfrs6	splicing factor, arginine/serine-rich 6	1.5E-04	6
1430139_at	Hells	helicase, lymphoid specific	1.7E-04	6
1435338_at	Cdk6	cyclin-dependent kinase 6	5.1E-04	6
1416155_at	Hmgb3	high mobility group box 3	1.2E-04	6
1417586_at	Timeless	timeless homolog (Drosophila)	5.7E-05	6
1447898_s_at	Sfrs6	splicing factor, arginine/serine-rich 6	2.4E-04	6

1420380_at	Ccl2	chemokine (C-C motif) ligand 2	7.3E-06	6
1417625_s_at	Cxcr7	chemokine (C-X-C motif) receptor 7	3.1E-05	6
1448162_at	Vcam1	vascular cell adhesion molecule 1	1.2E-04	6
1423422_at	Asb4	ankyrin repeat and SOCS box-containing protein 4	1.8E-04	6
1434089_at	Synpo	synaptopodin	7.2E-04	6
1435047_at		Transcribed locus	2.0E-05	6
1435315_s_at	2900034E22Rik	RIKEN cDNA 2900034E22 gene	1.2E-04	6
1421207_at	Lif	leukemia inhibitory factor	4.1E-04	6
1448961_at	Plscr2	phospholipid scramblase 2	8.4E-05	6
1455529_at	Mex3a	mex3 homolog A (C. elegans)	2.0E-04	6
1452912_at	2600005O03Rik	RIKEN cDNA 2600005O03 gene	1.4E-04	6
1460212_at	Gnat1	guanine nucleotide binding protein, alpha transducing 1	6.3E-05	5
1455287_at	Cdk6	cyclin-dependent kinase 6	1.4E-04	5
1426529_a_at	Tagln2	transgelin 2	4.7E-05	5
1419749_at	Trdmt1	tRNA aspartic acid methyltransferase 1	2.1E-04	5
1435000_at	Gspt1	G1 to S phase transition 1	1.0E-04	5
1417495_x_at	Cp	ceruloplasmin	6.8E-04	5
1417155_at	Mycn	v-myc myelocytomatosis viral related oncogene, neuroblastoma derived (avian)	6.5E-04	5
1417494_a_at	Cp	ceruloplasmin	7.6E-04	5
1428069_at	Cdca7	cell division cycle associated 7	9.4E-04	5
1416125_at	Fkbp5	FK506 binding protein 5	5.1E-07	5
1419182_at	Svep1	sushi, von Willebrand factor type A, EGF and pentraxin domain containing 1	2.0E-04	5
1435972_at	Cast	calpastatin	6.9E-05	5
1449893_a_at	Lrig1	leucine-rich repeats and immunoglobulin-like domains 1	3.2E-04	5
1420980_at	Pak1	p21 (CDKN1A)-activated kinase 1	3.6E-05	5
1439407_x_at	Tagln2	transgelin 2	1.1E-04	5
1439191_at		0 day neonate eyeball cDNA, RIKEN full-length enriched library, clone:E130107G13 product:histocompatibility 2, T region locus 18, full insert sequence	4.9E-04	5
1447369_at	1190005F20Rik	RIKEN cDNA 1190005F20 gene	5.0E-05	5
1434552_at	Wdr77	WD repeat domain 77	5.1E-05	5
1433919_at	Asb4	ankyrin repeat and SOCS box-containing protein 4	1.4E-04	5
1448377_at	Slpi	secretory leukocyte peptidase inhibitor	4.3E-04	5
1437173_at	Edg3	endothelial differentiation, sphingolipid G-protein-coupled receptor, 3	2.0E-04	5
1419869_s_at	Hdlbp	high density lipoprotein (HDL) binding protein	6.7E-05	5
1437071_at	Eif1ay	eukaryotic translation initiation factor 1A, Y-linked	2.0E-04	5
1453181_x_at	Plscr1	phospholipid scramblase 1	7.2E-04	5
1424949_at	Huwe1	HECT, UBA and WWE domain containing 1	1.6E-04	5
1450070_s_at	Pak1	p21 (CDKN1A)-activated kinase 1	8.7E-05	5
1444531_at		Adult male urinary bladder cDNA, RIKEN full-length enriched library, clone:9530055M18 product:unclassifiable, full insert sequence	2.2E-04	5
1415810_at	Uhrf1	ubiquitin-like, containing PHD and RING finger domains, 1	4.9E-04	5
1428819_at	Mapre1	microtubule-associated protein, RP/EB family,	1.5E-05	5

		member 1		
1453708_a_at	Gsto2	glutathione S-transferase omega 2	2.8E-04	5
1439648_at	Anln	anillin, actin binding protein (scraps homolog, Drosophila)	9.8E-04	5
1448326_a_at	Crabp1	cellular retinoic acid binding protein I	5.9E-04	5
1434555_at	Anp32a	acidic (leucine-rich) nuclear phosphoprotein 32 family, member A	6.4E-05	5
1421228_at	Ccl7	chemokine (C-C motif) ligand 7	1.4E-04	5
1416129_at	Errfi1	ERBB receptor feedback inhibitor 1	4.8E-04	5
1427883_a_at	Col3a1	procollagen, type III, alpha 1	4.9E-04	5
1441855_x_at	Cxcl1	chemokine (C-X-C motif) ligand 1	1.5E-04	5
1416227_at	Arpc1b /// EG434782	actin related protein 2/3 complex, subunit 1B /// predicted gene, EG434782	1.6E-04	5
1450920_at	Ccnb2	cyclin B2	4.2E-04	5
1417587_at	Timeless	timeless homolog (Drosophila)	3.2E-04	5
1448734_at	Cp	ceruloplasmin	1.4E-04	5
1436349_at	2700094K13Rik	RIKEN cDNA 2700094K13 gene	8.9E-04	5
1429527_a_at	Plscr1	phospholipid scramblase 1	4.7E-04	4
1416258_at	Tk1	thymidine kinase 1	7.5E-05	4
1418255_s_at	Srf	serum response factor	1.9E-05	4
1416030_a_at	Mcm7	minichromosome maintenance deficient 7 (<i>S. cerevisiae</i>)	1.1E-04	4
1417019_a_at	Cdc6	cell division cycle 6 homolog (<i>S. cerevisiae</i>)	2.2E-04	4
1434311_at	Cnot6l	CCR4-NOT transcription complex, subunit 6-like	4.7E-05	4
1435977_at	Hdgfrp3	hepatoma-derived growth factor, related protein 3	2.7E-04	4
1438571_at	Bub1	Budding uninhibited by benzimidazoles 1 homolog (<i>S. cerevisiae</i>)	1.9E-04	4
1436036_at	Whsc1	Wolf-Hirschhorn syndrome candidate 1 (human)	2.0E-05	4
1455591_at			3.6E-05	4
1446791_at		Transcribed locus	3.3E-04	4
1451413_at	Cast	calpastatin	1.2E-04	4
1426897_at	Rcc2	regulator of chromosome condensation 2	4.9E-04	4
1455060_at	G3bp1	Ras-GTPase-activating protein SH3-domain binding protein 1	2.4E-05	4
1454946_at	Mybl2	myeloblastosis oncogene-like 2	5.2E-04	4
1440884_s_at	A530047J11Rik	RIKEN cDNA A530047J11 gene	6.7E-04	4
1449060_at	Kif2c	kinesin family member 2C	7.8E-06	4
1434210_s_at	Lrig1	leucine-rich repeats and immunoglobulin-like domains 1	3.0E-04	4
1455715_at	LOC100038746	hypothetical LOC100038746	1.7E-04	4
1416715_at	Gjb3	gap junction membrane channel protein beta 3	1.9E-04	4
1434850_at	Iqgap3	IQ motif containing GTPase activating protein 3	5.8E-04	4
1416593_at	Glrx	glutaredoxin	9.8E-05	4
1415996_at	Txnip	thioredoxin interacting protein	3.8E-04	4
1436186_at	E2f8	E2F transcription factor 8	8.6E-04	4
1428412_at	Tm9sf3	transmembrane 9 superfamily member 3	7.4E-04	4
1419816_s_at	Errfi1	ERBB receptor feedback inhibitor 1	4.8E-04	4
1428280_at	Fip11	FIP1 like 1 (<i>S. cerevisiae</i>)	1.9E-06	4
1415989_at	Vcam1	vascular cell adhesion molecule 1	2.7E-05	4
1416120_at	Rrm2	ribonucleotide reductase M2	1.1E-04	4
1452872_at	Ank3	ankyrin 3, epithelial	3.1E-04	4
1457687_at	Bcl2	B-cell leukemia/lymphoma 2	9.1E-04	4

1448584_at	Rsrc1	arginine/serine-rich coiled-coil 1	1.1E-05	4
1454995_at	Ddah1	dimethylarginine dimethylaminohydrolase 1	2.4E-05	4
1448226_at	Rrm2	ribonucleotide reductase M2	8.7E-04	4
1460208_at	Fbn1	fibrillin 1	7.5E-05	4
1452348_s_at	lfi203	interferon activated gene 203	3.9E-04	4
1418402_at	Adam19	a disintegrin and metallopeptidase domain 19 (meltrin beta)	7.7E-05	4
1416031_s_at	Mcm7	minichromosome maintenance deficient 7 (<i>S. cerevisiae</i>)	2.0E-04	4
1422692_at	Sub1	SUB1 homolog (<i>S. cerevisiae</i>)	4.6E-04	4
1418176_at	Vdr	vitamin D receptor	5.9E-04	4
1428142_at	Etv5	ets variant gene 5	4.2E-04	4
1438404_at	Rnf144	ring finger protein 144	6.5E-05	4
1436555_at	Slc7a2	solute carrier family 7 (cationic amino acid transporter, y+ system), member 2	2.4E-04	4
1419153_at	2810417H13Rik	RIKEN cDNA 2810417H13 gene	5.9E-05	4
1425528_at	Prrx1	paired related homeobox 1	5.5E-04	4
1417821_at	D17H6S56E-5	DNA segment, Chr 17, human D6S56E 5	3.0E-05	4
1434437_x_at	Rrm2	ribonucleotide reductase M2	3.9E-04	4
1416073_a_at	Nup85	nucleoporin 85	6.5E-05	4
1448669_at	Dkk3	dickkopf homolog 3 (<i>Xenopus laevis</i>)	5.0E-04	4
1435384_at	Ube2n	ubiquitin-conjugating enzyme E2N	9.0E-04	4
1417910_at	Ccna2	cyclin A2	1.5E-04	4
1440396_at			2.0E-04	4
1429095_at	Cenpp	centromere protein P	3.1E-04	4
1419639_at	Efnb2	ephrin B2	9.8E-05	4
1418175_at	Vdr	vitamin D receptor	8.4E-05	4
1434570_at	AK122525	cDNA sequence AK122525	4.4E-04	4
1452098_at	Chtf18	CTF18, chromosome transmission fidelity factor 18 homolog (<i>S. cerevisiae</i>)	8.4E-05	4
1429076_a_at	Gdpd2	glycerophosphodiester phosphodiesterase domain containing 2	8.5E-04	4
1449708_s_at	Chek1	checkpoint kinase 1 homolog (<i>S. pombe</i>)	1.5E-04	4
1448627_s_at	Pbk	PDZ binding kinase	2.9E-04	4
1417971_at	Nrm	nurim (nuclear envelope membrane protein)	4.9E-04	4
1419015_at	Wisp2	WNT1 inducible signalling pathway protein 2	5.5E-04	4
1450677_at	Chek1	checkpoint kinase 1 homolog (<i>S. pombe</i>)	5.4E-04	4
1455899_x_at	Socs3	suppressor of cytokine signalling 3	2.7E-04	4
1439901_at		Transcribed locus	5.4E-04	4
1455160_at	2610203C20Rik	RIKEN cDNA 2610203C20 gene	8.9E-05	4
1416454_s_at	Acta2	actin, alpha 2, smooth muscle, aorta	7.2E-04	4
1457644_s_at	Cxcl1	chemokine (C-X-C motif) ligand 1	9.6E-05	4
1455680_at	9630025H16Rik	RIKEN cDNA 9630025H16 gene	9.8E-04	4
1439899_at	Galnt13	UDP-N-acetyl-alpha-D-galactosamine:polypeptide N-acetylgalactosaminyltransferase 13	3.2E-04	4
1460415_a_at	Cd40	CD40 antigen	8.6E-04	4
1416953_at	Ctgf	connective tissue growth factor	4.3E-04	4
1416017_at	Copg	coatamer protein complex, subunit gamma	4.6E-04	4
1427348_at	Zc3h12a	zinc finger CCCH type containing 12A	7.8E-04	4
1431087_at	Spc24	SPC24, NDC80 kinetochore complex component, homolog (<i>S. cerevisiae</i>)	2.8E-05	4
1436917_s_at	Gpsm1	G-protein signalling modulator 1 (AGS3-like, C.	1.4E-04	4

		elegans)		
1436723_at	Cenpi	centromere protein I	4.3E-04	4
1433507_a_at	Hmgn2	high mobility group nucleosomal binding domain 2	8.2E-04	4
1416042_s_at	Nasp	nuclear autoantigenic sperm protein (histone-binding)	2.2E-04	4
1456221_at	ENSMUSG00000074134	Predicted gene, ENSMUSG00000074134	2.1E-04	4
1452881_at	Gins2	GIN5 complex subunit 2 (Psf2 homolog)	1.0E-04	4
1423877_at	Chaf1b	chromatin assembly factor 1, subunit B (p60)	3.7E-04	4
1419209_at	Cxcl1	chemokine (C-X-C motif) ligand 1	1.3E-04	4
1419603_at	lfi204	interferon activated gene 204	1.4E-04	4
1449314_at	Zfp2	zinc finger protein, multitype 2	3.4E-04	4
1416592_at	Glrx	glutaredoxin	2.8E-04	4
1452534_a_at	Hmgb2	high mobility group box 2	8.1E-04	4
1423775_s_at	Prc1	protein regulator of cytokinesis 1	5.0E-04	4
1426631_at	Pus7	pseudouridylate synthase 7 homolog (S. cerevisiae)	1.5E-04	4
1439740_s_at	Uck2	uridine-cytidine kinase 2	5.3E-04	3
1450496_a_at	2810433K01Rik	RIKEN cDNA 2810433K01 gene	2.2E-04	3
1453748_a_at	Kif23	kinesin family member 23	4.1E-05	3
1426864_a_at	Ncam1	neural cell adhesion molecule 1	4.3E-05	3
1455173_at	Gspt1	G1 to S phase transition 1	8.0E-05	3
1435170_at	Tsr2	TSR2, 20S rRNA accumulation, homolog (S. cerevisiae)	3.7E-04	3
1424991_s_at	Tyms /// Tymps	thymidylate synthase /// thymidylate synthase, pseudogene	2.7E-04	3
1424128_x_at	Aurkb	aurora kinase B	3.9E-05	3
1455352_at	AU023006	expressed sequence AU023006	2.5E-04	3
1424759_at	Arrdc4	arrestin domain containing 4	2.6E-04	3
1415945_at	Mcm5	minichromosome maintenance deficient 5, cell division cycle 46 (S. cerevisiae)	4.9E-04	3
1457614_at		Transcribed locus	7.5E-04	3
1435797_at	D5Wsu178e	DNA segment, Chr 5, Wayne State University 178, expressed	6.4E-04	3
1439394_x_at	Cdc20	cell division cycle 20 homolog (S. cerevisiae)	4.2E-04	3
1440169_x_at	lfnar2	interferon (alpha and beta) receptor 2	5.6E-05	3
1424046_at	Bub1	budding uninhibited by benzimidazoles 1 homolog (S. cerevisiae)	2.7E-04	3
1452387_a_at	Amotl2	angiomin like 2	4.2E-04	3
1451246_s_at	Aurkb	aurora kinase B	6.9E-06	3
1435306_a_at	Kif11	kinesin family member 11	2.2E-04	3
1436211_at	Thoc4	THO complex 4	3.3E-04	3
1428187_at	Cd47	CD47 antigen (Rh-related antigen, integrin-associated signal transducer)	4.4E-05	3
1439741_x_at	Uck2	uridine-cytidine kinase 2	6.9E-04	3
1435743_at	Klhl23	kelch-like 23 (Drosophila)	2.4E-04	3
1435594_at	Arl6ip2	ADP-ribosylation factor-like 6 interacting protein 2	9.9E-04	3
1433234_at	4930424E08Rik	RIKEN cDNA 4930424E08 gene	9.7E-04	3
1422628_at	4632417K18Rik	RIKEN cDNA 4632417K18 gene	9.0E-05	3
1436585_at	BB182297	expressed sequence BB182297	9.2E-05	3
1451206_s_at	Pscdbp	pleckstrin homology, Sec7 and coiled-coil domains, binding protein	4.1E-04	3

1436217_at	Zfp148	zinc finger protein 148	4.9E-04	3
1426818_at	Arrdc4	arrestin domain containing 4	1.3E-04	3
1456280_at	Clspn	claspin homolog (Xenopus laevis)	2.1E-04	3
1423714_at	Asf1b	ASF1 anti-silencing function 1 homolog B (S. cerevisiae)	1.2E-04	3
1432179_x_at	2810433K01Rik	RIKEN cDNA 2810433K01 gene	5.9E-04	3
1454788_at	Arl4c /// LOC632433	ADP-ribosylation factor-like 4C /// similar to ADP-ribosylation factor-like protein 7	3.1E-04	3
1426909_at	Uck2	uridine-cytidine kinase 2	4.0E-04	3
1460009_at		Transcribed locus	5.8E-04	3
1417938_at	Rad51ap1	RAD51 associated protein 1	3.0E-04	3
1423596_at	Nek6	NIMA (never in mitosis gene a)-related expressed kinase 6	2.1E-04	3
1428713_s_at	Gins2	GIN5 complex subunit 2 (Psf2 homolog)	6.1E-04	3
1426652_at	Mcm3	minichromosome maintenance deficient 3 (S. cerevisiae)	8.1E-05	3
1430530_s_at	Nmral1	NmrA-like family domain containing 1	1.1E-04	3
1439263_at	LOC14210	hypothetical LOC14210	7.7E-05	3
1419554_at	Cd47	CD47 antigen (Rh-related antigen, integrin-associated signal transducer)	2.5E-05	3
1451077_at	Rpl5	ribosomal protein L5	4.3E-04	3
1452314_at	Kif11	kinesin family member 11	1.6E-05	3
1431751_a_at	Mpped2	metallophosphoesterase domain containing 2	4.0E-05	3
1455737_at	C030002B11Rik	RIKEN cDNA C030002B11 gene	6.7E-04	3
1419838_s_at	Plk4	polo-like kinase 4 (Drosophila)	1.6E-04	3
1434232_a_at	2610030H06Rik	RIKEN cDNA 2610030H06 gene	9.3E-05	3
1424524_at	1200002N14Rik	RIKEN cDNA 1200002N14 gene	6.7E-04	3
1416664_at	Cdc20	cell division cycle 20 homolog (S. cerevisiae)	3.9E-04	3
1423805_at	Dab2	disabled homolog 2 (Drosophila)	5.6E-05	3
1448777_at	Mcm2	minichromosome maintenance deficient 2 mitotin (S. cerevisiae)	3.5E-04	3
1448291_at	Mmp9	matrix metalloproteinase 9	5.7E-04	3
1418012_at	Sh3glb1	SH3-domain GRB2-like B1 (endophilin)	1.9E-04	3
1416492_at	Ccne1	cyclin E1	1.6E-04	3
1448127_at	Rrm1	ribonucleotide reductase M1	1.1E-05	3
1436472_at	Slfn9	schlafen 9	4.0E-04	3
1418424_at	TNFAIP6	tumor necrosis factor alpha induced protein 6	2.5E-04	3
1419943_s_at	Ccnb1	cyclin B1	9.1E-04	3
1423690_s_at	Gpsm1	G-protein signalling modulator 1 (AGS3-like, C. elegans)	7.0E-04	3
1425295_at	Ear11	eosinophil-associated, ribonuclease A family, member 11	8.8E-04	3
1423774_a_at	Prc1	protein regulator of cytokinesis 1	4.8E-06	3
1454737_at	Dusp9	dual specificity phosphatase 9	1.4E-04	3
1438852_x_at	Mcm6	minichromosome maintenance deficient 6 (MIS5 homolog, S. pombe) (S. cerevisiae)	2.3E-04	3
1418133_at	Bcl3	B-cell leukemia/lymphoma 3	8.4E-04	3
1439269_x_at	Mcm7	minichromosome maintenance deficient 7 (S. cerevisiae)	3.7E-04	3
1435785_at	Ehd2	EH-domain containing 2	1.3E-04	3
1424501_at	Utp6	UTP6, small subunit (SSU) processome component, homolog (yeast)	2.6E-04	3
1452854_at	Sec63	SEC63-like (S. cerevisiae)	6.3E-05	3
1416961_at	Bub1b	budding uninhibited by benzimidazoles 1	2.5E-04	3

		homolog, beta (<i>S. cerevisiae</i>)		
1427183_at	Efemp1	epidermal growth factor-containing fibulin-like extracellular matrix protein 1	3.9E-04	3
1449513_at	Adam24	a disintegrin and metalloproteinase domain 24 (testase 1)	9.8E-04	3
1451782_a_at	Slc29a1	solute carrier family 29 (nucleoside transporters), member 1	6.9E-05	3
1424278_a_at	Birc5	baculoviral IAP repeat-containing 5	6.9E-04	3
1444459_at		Adult male urinary bladder cDNA, RIKEN full-length enriched library, clone:9530065A06 product:unclassifiable, full insert sequence	5.4E-04	3
1417856_at	Relb	avian reticuloendotheliosis viral (v-rel) oncogene related B	3.7E-04	3
1451989_a_at	Mapre2	microtubule-associated protein, RP/EB family, member 2	2.6E-06	3
1433807_at	6720463M24Rik	RIKEN cDNA 6720463M24 gene	3.1E-04	3
1439208_at	Chek1	checkpoint kinase 1 homolog (<i>S. pombe</i>)	6.2E-05	3
1435184_at	Npr3	natriuretic peptide receptor 3	8.5E-04	3
1417133_at	Pmp22	peripheral myelin protein	4.1E-04	3
1421052_a_at	Sms	spermine synthase	8.4E-04	3
1419938_s_at	Arhgef17	Rho guanine nucleotide exchange factor (GEF) 17	2.0E-04	3
1434475_at	Ppig	peptidyl-prolyl isomerase G (cyclophilin G)	3.5E-06	3
1427105_at	Cenpn	centromere protein N	2.1E-04	3
1424292_at	Depdc1a	DEP domain containing 1a	1.4E-04	3
1433813_at	Tmem48	transmembrane protein 48	6.0E-04	3
1460227_at	Timp1	tissue inhibitor of metalloproteinase 1	2.1E-04	3
1417534_at	Itgb5	integrin beta 5	4.2E-04	3
1448113_at	Stmn1	stathmin 1	2.4E-04	3
1442148_at	Psip1	PC4 and SFRS1 interacting protein 1	4.0E-04	3
1440478_at	LOC100047601	similar to DNA segment, Chr 10, ERATO Doi 438, expressed	4.1E-04	3
1420913_at	Slco2a1	solute carrier organic anion transporter family, member 2a1	1.0E-04	3
1449494_at	Rab3c	RAB3C, member RAS oncogene family	4.0E-04	3
1441559_at	LOC627626	similar to CG11212-PA	4.5E-04	3
1423666_s_at	Rpl5	ribosomal protein L5	1.7E-04	3
1446331_at	Ptgfr	prostaglandin F receptor	5.5E-04	3
1417533_a_at	Itgb5	integrin beta 5	3.9E-04	3
1448205_at	Ccnb1 /// Ccnb1-rs1	cyclin B1, related sequence 1 /// cyclin B1	8.4E-04	3
1417040_a_at	Bok	Bcl-2-related ovarian killer protein	2.4E-04	3
1435221_at		Adult male corpora quadrigemina cDNA, RIKEN full-length enriched library, clone:B230341P20 product:inferred: forkhead box P1, full insert sequence	3.6E-04	3
1423092_at	Incenp	inner centromere protein	1.8E-04	3
1439814_at		Transcribed locus	4.1E-04	3
1448899_s_at	Rad51ap1	RAD51 associated protein 1	4.7E-05	3
1455242_at	Foxp1	forkhead box P1	1.2E-04	3
1422814_at	Aspm	asp (abnormal spindle)-like, microcephaly associated (<i>Drosophila</i>)	9.6E-04	3
1449705_x_at	Mcm3	minichromosome maintenance deficient 3 (<i>S. cerevisiae</i>)	1.0E-05	3

1435162_at	Prkg2	protein kinase, cGMP-dependent, type II	3.5E-04	3
1425142_a_at	Hnrpd	heterogeneous nuclear ribonucleoprotein D	2.4E-04	3

Appendix III

Dataset obtained from the microarray analysis of 24hr ~15µg/ml p37-treated NIH3T3 (mouse) fibroblasts. The dataset consists of 249 genes significantly down regulated by ≤ 3 fold with a p-value of ≤ 0.001 . The genes discussed in Section 3.2.8 are bold.

Affymetrix Probe Set ID	Gene Symbol	Gene Title	p-value	Fold Change (Down)
1449382_at	Slc6a12	solute carrier family 6 (neurotransmitter transporter, betaine/GABA), member 12	1.5E-06	47
1438109_at	Clca5	chloride channel calcium activated 5	1.4E-04	32
1434195_at	Prss35	protease, serine, 35	2.6E-05	27
1455477_s_at	Pdzk1ip1	PDZK1 interacting protein 1	3.7E-05	21
1451322_at	Cmb1	carboxymethylenebutenolidase-like (Pseudomonas)	2.6E-04	20
1419378_a_at	Fxyd2	FXD domain-containing ion transport regulator 2	2.4E-06	19
1422478_a_at	Acss2	acyl-CoA synthetase short-chain family member 2	4.1E-07	18
1456601_x_at	Fxyd2	FXD domain-containing ion transport regulator 2	7.1E-07	17
1422479_at	Acss2	acyl-CoA synthetase short-chain family member 2	6.8E-07	16
1421153_at	Loxl4	lysyl oxidase-like 4	2.7E-05	16
1418925_at	Celsr1	cadherin EGF LAG seven-pass G-type receptor 1	3.4E-05	14
1417689_a_at	Pdzk1ip1	PDZK1 interacting protein 1	1.2E-04	13
1418595_at	S3-12	plasma membrane associated protein, S3-12	4.6E-05	13
1443921_at	Ranbp3l	RAN binding protein 3-like	5.3E-04	13
1419379_x_at	Fxyd2	FXD domain-containing ion transport regulator 2	1.4E-04	13
1439036_a_at	Atp1b1	ATPase, Na⁺/K⁺ transporting, beta 1 polypeptide	1.7E-04	12
1440700_a_at	Arhgef18	rho/rac guanine nucleotide exchange factor (GEF) 18	1.3E-04	12
1452388_at	Hspa1a	heat shock protein 1A	2.7E-05	12
1419872_at	Csf1r	colony stimulating factor 1 receptor	1.5E-06	12
1452418_at	Rik	RIKEN cDNA 1200016E24 gene	9.6E-04	12
1420558_at	Selp	selectin, platelet	4.8E-04	12
1416702_at	Serpini1	serine (or cysteine) peptidase inhibitor, clade I, member 1	2.1E-05	11
1456060_at	Maf	avian musculoaponeurotic fibrosarcoma (v-maf) AS42 oncogene homolog	4.5E-04	11
1418453_a_at	Atp1b1	ATPase, Na ⁺ /K ⁺ transporting, beta 1 polypeptide	2.8E-05	11
1448831_at	Angpt2	angiopoietin 2	7.4E-05	11
1425784_a_at	Olfm1	olfactomedin 1	3.8E-06	11
1417150_at	Slc6a4	solute carrier family 6 (neurotransmitter transporter, serotonin), member 4	5.4E-05	11
1427919_at	Srpx2	sushi-repeat-containing protein, X-linked 2	3.4E-05	11

1455796_x_at	Olfm1	olfactomedin 1	1.1E-06	10
1448619_at	Dhcr7	7-dehydrocholesterol reductase	1.1E-04	10
1425124_at	Rnf183	ring finger protein 183	7.2E-04	10
1450682_at	Fabp6	fatty acid binding protein 6, ileal (gastrotropin)	3.9E-05	10
1419873_s_at	Csf1r	colony stimulating factor 1 receptor	1.0E-04	10
1440173_x_at	Selp	selectin, platelet	1.7E-04	10
1460336_at	Ppargc1a	peroxisome proliferative activated receptor, gamma, coactivator 1 alpha	1.2E-05	10
1449906_at	Selp	selectin, platelet	3.9E-04	9
1458385_at	Hspa4l	heat shock protein 4 like	7.5E-04	9
1420354_at	Cnnm1	cyclin M1	8.2E-05	9
1416831_at	Neu1	neuraminidase 1	5.6E-05	9
1427359_at	Jhdm1d	jumonji C domain-containing histone demethylase 1 homolog D (<i>S. cerevisiae</i>)	4.2E-05	9
1436948_a_at	6430550H21Rik	RIKEN cDNA 6430550H21 gene	1.7E-04	8
1415935_at	Smoc2	SPARC related modular calcium binding 2	1.1E-05	8
1443841_x_at	Uap1l1	UDP-N-acetylglucosamine pyrophosphorylase 1-like 1	2.2E-04	8
1456768_a_at	Mmrn2	multimerin 2	5.6E-04	8
1426516_a_at	Lpin1	lipin 1	3.9E-05	8
1448136_at	Enpp2	ectonucleotide pyrophosphatase/phosphodiesterase 2	7.1E-05	8
1416455_a_at	Cryab	crystallin, alpha B	2.0E-04	8
1452946_a_at	Rftn2	raftlin family member 2	1.9E-04	8
1456395_at	Ppargc1a	peroxisome proliferative activated receptor, gamma, coactivator 1 alpha	7.4E-05	7
1436188_a_at	Ndrp4	N-myc downstream regulated gene 4	1.4E-04	7
1453265_at	4930579C15Rik	RIKEN cDNA 4930579C15 gene	1.3E-04	7
1429676_at		Adult male stomach cDNA, RIKEN full-length enriched library, clone:2210408O09 product:unclassifiable, full insert sequence	9.6E-04	7
1436742_a_at	Gm1967	gene model 1967, (NCBI)	1.7E-05	7
1449010_at	Hspa4l	heat shock protein 4 like	1.4E-05	7
1448663_s_at	Mvd	mevalonate (diphospho) decarboxylase	1.0E-04	7
1418288_at	Lpin1	lipin 1	8.8E-05	7
1455707_at	Ranbp3l	RAN binding protein 3-like	3.7E-04	7
1415894_at	Enpp2	ectonucleotide pyrophosphatase/phosphodiesterase 2	5.4E-05	6
1460684_at	Tm7sf2	transmembrane 7 superfamily member 2	7.7E-05	6
1448421_s_at	Aspn	asporin	4.2E-04	6
1437751_at	Ppargc1a	peroxisome proliferative activated receptor, gamma, coactivator 1 alpha	9.4E-05	6
1439006_x_at	6430550H21Rik	RIKEN cDNA 6430550H21 gene	4.7E-05	6
1428074_at	Tmem158	transmembrane protein 158	6.0E-06	6
1424463_at	2210010L05Rik	RIKEN cDNA 2210010L05 gene	1.1E-04	6
1419704_at	Cyp3a41a /// LOC100041375	cytochrome P450, family 3, subfamily a, polypeptide 41A /// similar to cytochrome P450	1.8E-05	6
1422155_at	Hist2h3c2	histone cluster 2, H3c2	5.7E-05	6
1422916_at	Fgf21	fibroblast growth factor 21	6.0E-05	6
1426663_s_at	Slc45a3	solute carrier family 45, member 3	3.5E-04	6
1434099_at	Ppargc1a	Peroxisome proliferative activated receptor, gamma, coactivator 1 alpha	7.5E-05	6
1419684_at	Ccl8 /// LOC100048554	chemokine (C-C motif) ligand 8 /// similar to monocyte chemoattractant protein-2 (MCP-2)	1.4E-04	6

1443653_at			8.5E-04	6
1418818_at	Aqp5 /// LOC100046616	aquaporin 5 /// similar to aquaporin 5	8.6E-04	6
1422170_at	Slc5a3	solute carrier family 5 (inositol transporters), member 3	9.9E-05	6
1435849_at	6330417G02Rik	RIKEN cDNA 6330417G02 gene	8.9E-04	6
1417263_at	Ptgs2	prostaglandin-endoperoxide synthase 2	1.1E-04	6
1460033_at	C030002C11Rik	RIKEN cDNA C030002C11 gene	7.9E-04	6
1452117_a_at	Fyb	FYN binding protein	1.2E-04	6
1426615_s_at	Ndrp4	N-myc downstream regulated gene 4	2.8E-04	6
1443503_at	lhpk3	inositol hexaphosphate kinase 3	8.1E-05	6
1434100_x_at	Ppargc1a	Peroxisome proliferative activated receptor, gamma, coactivator 1 alpha	1.1E-05	6
1458562_at			7.0E-05	6
1418025_at	Bhlhb2	basic helix-loop-helix domain containing, class B2	6.0E-05	6
1435761_at	Stfa1	stefin A1 /// cDNA sequence BC100530	9.4E-04	5
1417303_at	Mvd	mevalonate (diphospho) decarboxylase	1.2E-04	5
1429888_a_at	Hspb2	heat shock protein 2	2.1E-05	5
1418253_a_at	Hspa4l	heat shock protein 4 like	7.0E-05	5
1438160_x_at	Slco4a1	solute carrier organic anion transporter family, member 4a1	1.4E-04	5
1449848_at	Gna14	guanine nucleotide binding protein, alpha 14	8.4E-04	5
1416069_at	Pfkl	phosphofructokinase, platelet	4.2E-05	5
1456319_at			1.0E-04	5
1420013_s_at	Lss	lanosterol synthase	2.6E-04	5
1426562_a_at	Olfm1	olfactomedin 1	1.3E-04	5
1439093_at			2.1E-04	5
1439518_at	Mmrn2	multimerin 2	2.0E-04	5
1435680_a_at	Dpp7	dipeptidylpeptidase 7	5.0E-06	5
1451486_at	Slc46a3	solute carrier family 46, member 3	2.9E-04	5
1437332_at		Adult male corpora quadrigemina cDNA, RIKEN full-length enriched library, clone:B230334A10 product:unclassifiable, full insert sequence	3.9E-04	5
1435867_at	ENSMUSG0000 0073143	predicted gene, ENSMUSG00000073143	1.0E-04	5
1426664_x_at	Slc45a3	solute carrier family 45, member 3	2.8E-06	5
1434046_at	AA467197	expressed sequence AA467197	2.0E-04	5
1438704_at	Trim63	tripartite motif-containing 63	7.4E-04	5
1428896_at	Pdgfrl	platelet-derived growth factor receptor-like	2.3E-05	5
1438211_s_at	Dbp	D site albumin promoter binding protein	9.1E-06	5
1423606_at	Postn	periostin, osteoblast specific factor	1.1E-04	5
1436842_at	B230380D07Rik	RIKEN cDNA B230380D07 gene	8.9E-05	5
1425113_x_at		Transcribed locus	9.6E-05	5
1418188_a_at	Malat1	Metastasis associated lung adenocarcinoma transcript 1 (non-coding RNA)	1.2E-04	5
1449363_at	Atf3	activating transcription factor 3	9.5E-06	5
1428379_at	Slc17a6	solute carrier family 17 (sodium-dependent inorganic phosphate cotransporter), member 6	5.2E-05	5
1429106_at	4921509J17Rik	RIKEN cDNA 4921509J17 gene	1.5E-05	5
1436480_at	Dpp7	dipeptidylpeptidase 7	1.1E-04	5
1430964_at	2310034O05Rik	RIKEN cDNA 2310034O05 gene	2.2E-04	5
1451382_at	Chac1	ChaC, cation transport regulator-like 1 (E. coli)	9.4E-05	5
1437123_at	Mmrn2	multimerin 2	5.5E-05	5

1428834_at	Dusp4	dual specificity phosphatase 4	6.1E-04	5
1422529_s_at	Casq2	calsequestrin 2	8.8E-05	5
1451457_at	Sc5d	sterol-C5-desaturase (fungal ERG3, delta-5-desaturase) homolog (<i>S. cerevisiae</i>)	1.5E-04	5
1418219_at	Il15	interleukin 15	1.1E-04	5
1416046_a_at	Fuca2	fucosidase, alpha-L- 2, plasma	7.9E-05	5
1427126_at	Hspa1b	heat shock protein 1B	1.4E-04	5
1421594_a_at	Syt12	synaptotagmin-like 2	4.6E-05	5
1439072_at	Slc1a3	solute carrier family 1 (glial high affinity glutamate transporter), member 3	9.5E-05	5
1440227_at	Slc5a3	solute carrier family 5 (inositol transporters), member 3	3.4E-04	5
1450922_a_at	Tgfb2	transforming growth factor, beta 2	9.5E-04	5
1436479_a_at	Dpp7	dipeptidylpeptidase 7	2.0E-04	5
1452132_at	Tlcd1	TLC domain containing 1	1.5E-05	5
1449702_at	Zfand2a	zinc finger, AN1-type domain 2A	1.0E-04	5
1416625_at	Serping1	serine (or cysteine) peptidase inhibitor, clade G, member 1	6.2E-05	5
1429236_at	Galnt12	UDP-N-acetyl-alpha-D-galactosamine:polypeptide N-acetylgalactosaminyltransferase-like 2	5.2E-04	5
1430619_a_at	Mvk	mevalonate kinase	6.1E-05	5
1429060_at			8.4E-04	5
1424464_s_at	2210010L05Rik	RIKEN cDNA 2210010L05 gene	4.6E-04	5
1433944_at	Hectd2	HECT domain containing 2	1.0E-03	5
1455065_x_at	Gnpda1	glucosamine-6-phosphate deaminase 1	1.8E-04	4
1418359_at	Wbscr27	Williams Beuren syndrome chromosome region 27 (human)	1.8E-04	4
1452583_s_at	Galm	galactose mutarotase	1.3E-04	4
1424140_at	Gale	galactose-4-epimerase, UDP	8.0E-05	4
1434191_at	A530016O06Rik	RIKEN cDNA A530016O06 gene	2.6E-04	4
1450745_at	C1galt1	core 1 synthase, glycoprotein-N-acetylgalactosamine 3-beta-galactosyltransferase, 1	1.7E-05	4
1448596_at	Slc6a8	solute carrier family 6 (neurotransmitter transporter, creatine), member 8	5.3E-04	4
1426616_at	Tlcd1	TLC domain containing 1	2.9E-05	4
1440929_at			9.1E-04	4
1427893_a_at	Pmvk	phosphomevalonate kinase	8.5E-04	4
1419663_at	Ogn	osteoglycin	8.8E-05	4
1432976_at	2310038E17Rik	RIKEN cDNA 2310038E17 gene	2.9E-04	4
1423890_x_at	Atp1b1	ATPase, Na ⁺ /K ⁺ transporting, beta 1 polypeptide	7.6E-05	4
1448443_at	Serpin1	serine (or cysteine) peptidase inhibitor, clade I, member 1	1.8E-05	4
1415941_s_at	Zfand2a	zinc finger, AN1-type domain 2A	6.2E-04	4
1427534_at	4930535I16Rik	RIKEN cDNA 4930535I16 gene	4.0E-05	4
1436325_at	Rora	RAR-related orphan receptor alpha	6.0E-04	4
1421571_a_at	Ly6c2	lymphocyte antigen 6 complex, locus C1	4.2E-05	4
1441281_s_at	Ninj1	ninjurin 1	1.3E-05	4
1456611_at	D430015B01Rik	RIKEN cDNA D430015B01 gene	6.5E-04	4
1455269_a_at	Coro1a	coronin, actin binding protein 1A	1.5E-04	4
1441971_at		Transcribed locus	1.9E-04	4
1460122_at	Tmem41b	transmembrane protein 41B	2.6E-06	4

1450378_at	Tapbp	TAP binding protein	2.4E-04	4
1450134_at	Loxl4	lysyl oxidase-like 4	1.8E-04	4
1427287_s_at	Itpr2	inositol 1,4,5-triphosphate receptor 2	3.5E-05	4
1424834_s_at	Itpr2	inositol 1,4,5-triphosphate receptor 2	1.8E-04	4
1434369_a_at	Cryab	crystallin, alpha B	1.4E-04	4
1417664_a_at	Ndr3	N-myc downstream regulated gene 3	8.5E-05	4
1430307_a_at	Mod1	malic enzyme, supernatant	2.1E-05	4
1456590_x_at	Akr1b3	aldo-keto reductase family 1, member B3 (aldose reductase)	5.5E-05	4
1420062_at			2.9E-04	4
1452452_at		Intracisternal A-particle-related retroviral elements and envelope pseudogene	2.6E-04	4
1431046_at	Ppfia3	protein tyrosine phosphatase, receptor type, f polypeptide (PTPRF), interacting protein (liprin), alpha 3	2.8E-04	4
1449954_at	Hyal1 /// Nat6	hyaluronoglucosaminidase 1 /// N-acetyltransferase 6	2.5E-04	4
1452646_at	Trp53inp2	transformation related protein 53 inducible nuclear protein 2	1.3E-04	4
1416114_at	Sparcl1	SPARC-like 1 (mast9, hevin)	1.5E-04	4
1427127_x_at	Hspa1b	heat shock protein 1B	9.7E-05	4
1440282_at	Tulp4	tubby like protein 4	4.2E-04	4
1448417_at	Ninj1	ninjurin 1	1.1E-05	4
1440397_at	Cacna2d1	calcium channel, voltage-dependent, alpha2/delta subunit 1	8.7E-04	4
1416632_at	Mod1	malic enzyme, supernatant	5.3E-04	4
1424167_a_at	Pmm1	phosphomannomutase 1	8.2E-05	4
1445694_at		Transcribed locus	1.5E-04	4
1438426_at	Tmem58	transmembrane protein 58	3.1E-04	4
1431780_at	1700021K14Rik	RIKEN cDNA 1700021K14 gene	1.6E-05	4
1426936_at	BC005512 /// EG641366 /// LOC629242	cDNA sequence BC005512 /// hypothetical protein LOC629242 /// predicted gene, EG641366	6.5E-04	4
1424172_at	Hagh	hydroxyacyl glutathione hydrolase	6.4E-05	4
1417110_at	Man1a	mannosidase 1, alpha	6.5E-05	4
1436841_at	B230380D07Rik	RIKEN cDNA B230380D07 gene	1.2E-06	4
1448481_at	Neu1	neuraminidase 1	2.3E-04	4
1416274_at	Ctns	cystinosis, nephropathic	5.8E-05	4
1447774_x_at	5730469M10Rik	RIKEN cDNA 5730469M10 gene	2.1E-04	4
1437519_x_at	Hagh /// LOC100044022	hydroxyacyl glutathione hydrolase /// similar to Hydroxyacyl glutathione hydrolase	1.8E-04	4
1453011_at	Bdh2	3-hydroxybutyrate dehydrogenase, type 2	4.3E-04	4
1422433_s_at	Idh1	isocitrate dehydrogenase 1 (NADP+), soluble	3.9E-04	4
1436528_at	Kazald1	Kazal-type serine peptidase inhibitor domain 1	4.1E-04	4
1457102_at	A030001D16Rik	RIKEN cDNA A030001D16 gene	6.1E-05	4
1424443_at	Hdgfrp3 /// Tm6sf1	hepatoma-derived growth factor, related protein 3 /// transmembrane 6 superfamily member 1	6.3E-04	4
1429239_a_at	Stard4	StAR-related lipid transfer (START) domain containing 4	5.5E-04	4
1417109_at	Tinagl	tubulointerstitial nephritis antigen-like	6.4E-04	4
1458264_at	AW046200	Expressed sequence AW046200	1.8E-04	4
1448830_at	Dusp1	dual specificity phosphatase 1	8.4E-05	4
1424171_a_at	Hagh	hydroxyacyl glutathione hydrolase	1.9E-04	4

1417871_at	Hsd17b7	hydroxysteroid (17-beta) dehydrogenase 7	9.3E-05	4
1449869_at	Vpreb1	pre-B lymphocyte gene 1	7.8E-05	4
1417049_at	Rhd	Rh blood group, D antigen	4.9E-04	4
1450678_at	Itgb2	integrin beta 2	2.1E-04	4
1421061_at	Guca1a	guanylate cyclase activator 1a (retina)	4.1E-05	4
1452716_at	5730469M10Rik	RIKEN cDNA 5730469M10 gene	5.5E-04	4
1418601_at	Aldh1a7	aldehyde dehydrogenase family 1, subfamily A7	4.3E-05	4
1447252_s_at	Mep1a	mepirin 1 alpha	2.8E-04	4
1454797_at	Tmem55b	transmembrane protein 55b	2.0E-05	4
1420693_at	Myom1	myomesin 1	1.1E-04	4
1427285_s_at	Malat1	metastasis associated lung adenocarcinoma transcript 1 (non-coding RNA)	6.4E-04	4
1416926_at	Trp53inp1	transformation related protein 53 inducible nuclear protein 1	2.6E-04	4
1448183_a_at	Hif1a	hypoxia inducible factor 1, alpha subunit	4.2E-04	4
1423250_a_at	Tgfb2	transforming growth factor, beta 2	5.4E-04	4
1415940_at	Zfand2a	zinc finger, AN1-type domain 2A	2.6E-04	4
1445580_at			3.9E-04	4
1429777_at	Dnajb6	DnaJ (Hsp40) homolog, subfamily B, member 6	1.3E-04	4
1441288_at		Transcribed locus	6.1E-04	4
1435124_at	EG328644	predicted gene, EG328644	7.4E-04	4
1419132_at	TLR2	toll-like receptor 2	1.0E-04	4
1422924_at	TNFSf9	tumor necrosis factor (ligand) superfamily, member 9	2.7E-04	4
1449408_at	Jam2	junction adhesion molecule 2	7.6E-04	4
1426886_at	Cln5	ceroid-lipofuscinosis, neuronal 5	6.2E-05	4
1427546_at	Abca8b	ATP-binding cassette, sub-family A (ABC1), member 8b	1.0E-04	4
1430780_a_at	Pmm1	phosphomannomutase 1	1.3E-04	4
1447791_s_at	Gna14	guanine nucleotide binding protein, alpha 14	3.7E-04	4
1420784_at	Scn11a	sodium channel, voltage-gated, type XI, alpha	7.7E-04	4
1416246_a_at	Coro1a	coronin, actin binding protein 1A	2.5E-05	4
1438928_x_at	Ninj1	ninjurin 1	1.0E-04	4
1419124_at	2210010L05Rik	RIKEN cDNA 2210010L05 gene	1.4E-04	4
1436634_at	Robo3	roundabout homolog 3 (Drosophila)	6.5E-04	4
1417382_at	Entpd5	ectonucleoside triphosphate diphosphohydrolase 5	6.0E-05	4
1453008_at	2300002D11Rik	RIKEN cDNA 2300002D11 gene	2.7E-04	4
1418715_at	Pank1	pantothenate kinase 1	3.3E-04	4
1437642_at	Hrb1	HIV-1 Rev binding protein-like	9.9E-06	4
1426908_at	Galnt7	UDP-N-acetyl-alpha-D-galactosamine: polypeptide N-acetylgalactosaminyltransferase 7	4.4E-04	4
1454757_s_at	D12Ert647e	DNA segment, Chr 12, ERATO Doi 647, expressed	3.3E-05	4
1421812_at	Tapbp	TAP binding protein	2.0E-06	4
1452837_at	Lpin2	lipin 2	4.2E-04	4
1460346_at	Arsa	arylsulfatase A	2.5E-04	4
1438266_at	Adamts15	ADAMTS-like 5	5.6E-04	4
1441952_x_at	Lynx1	Ly6/neurotoxin 1	5.0E-04	4
1454161_s_at	0610007P14Rik	RIKEN cDNA 0610007P14 gene	5.4E-05	4
1416968_a_at	Hsd3b7	hydroxy-delta-5-steroid dehydrogenase, 3 beta- and steroid delta-isomerase 7	8.3E-04	3

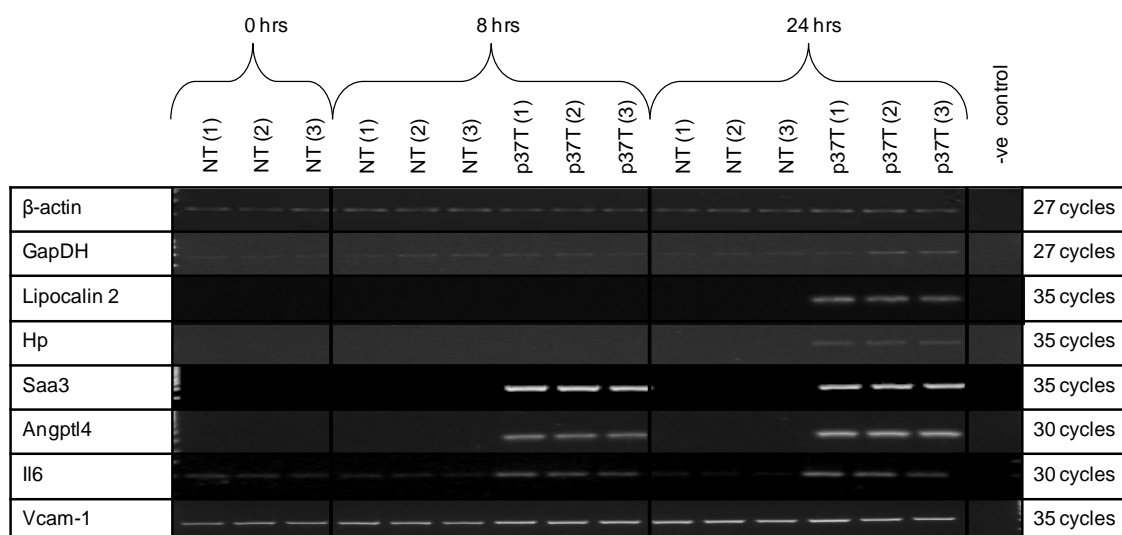
1452014_a_at	Igf1	insulin-like growth factor 1	5.8E-04	3
1419665_a_at	Nupr1	nuclear protein 1	4.3E-04	3
1453054_at	Scamp1	secretory carrier membrane protein 1	1.4E-04	3
1455717_s_at	Daam2	dishevelled associated activator of morphogenesis 2	1.6E-04	3
1418367_x_at	Hist1h2ad	histone cluster 2, H2aa1	6.7E-05	3
1415824_at	Scd2	stearoyl-Coenzyme A desaturase 2	3.9E-04	3
1420385_at	Gna14	guanine nucleotide binding protein, alpha 14	2.8E-04	3
1416262_at	Tmem19	transmembrane protein 19	2.9E-04	3
1454699_at	LOC100047324 /// Sesn1	sestrin 1 /// similar to Sesn1 protein	8.0E-05	3
1428025_s_at	Pitpnc1	phosphatidylinositol transfer protein, cytoplasmic 1	4.1E-04	3
1424940_s_at	BC022687	cDNA sequence BC022687	2.5E-04	3
1428190_at	Slc25a1	solute carrier family 25 (mitochondrial carrier, citrate transporter), member 1	1.2E-04	3
1452789_at	Snn	stannin	3.0E-05	3
1453080_at	Apol3	apolipoprotein L 3	4.1E-04	3
1434849_at	Tspyl2	TSPY-like 2	4.0E-04	3
1452318_a_at	Hspa1b	heat shock protein 1B	3.3E-04	3
1415865_s_at	Bpgm	2,3-bisphosphoglycerate mutase	5.3E-04	3
1454706_at	Uvrag	UV radiation resistance associated gene	1.5E-04	3
1424034_at	Rora	RAR-related orphan receptor alpha	4.9E-06	3
1418536_at	H2-Q6	histocompatibility 2, Q region locus 7	2.9E-07	3
1452290_at	Tmem106b	transmembrane protein 106B	1.2E-05	3
1459871_x_at	Mar-02	membrane-associated ring finger (C3HC4) 2	8.9E-05	3
1417283_at	Lynx1	Ly6/neurotoxin 1	3.3E-04	3
1436890_at	Uap111	UDP-N-acetylglucosamine pyrophosphorylase 1-like 1	2.0E-04	3
1435135_at	Aadacl1	arylacetamide deacetylase-like 1	4.4E-04	3
1431128_at	Tmem170	transmembrane protein 170	1.8E-04	3
1451533_at	BC022687	cDNA sequence BC022687	4.2E-04	3
1460022_at		Adult male epididymis cDNA, RIKEN full-length enriched library, clone:9230106K18 product:unclassifiable, full insert sequence	1.2E-04	3
1428352_at	Arrdc2	arrestin domain containing 2	3.4E-04	3
1421856_at	S100a3	S100 calcium binding protein A3	5.9E-04	3
1419100_at	Serpina3n	serine (or cysteine) peptidase inhibitor, clade A, member 3N	9.7E-04	3
1418435_at	Mkrn1	makorin, ring finger protein, 1	2.9E-04	3
1433711_s_at	LOC100047324 /// Sesn1	sestrin 1 /// similar to Sesn1 protein	4.3E-06	3
1437597_at		Transcribed locus	7.1E-05	3
1448163_at	Gnpda1	glucosamine-6-phosphate deaminase 1	4.8E-04	3
1435071_at	Zfyve1	zinc finger, FYVE domain containing 1	5.6E-04	3
1425281_a_at	Tsc22d3	TSC22 domain family 3	5.0E-05	3
1456721_at	Thsd7a	thrombospondin, type I, domain containing 7A	6.9E-04	3
1428895_at	Rftn2	raftlin family member 2	5.4E-04	3
1429841_at	Megf10	multiple EGF-like-domains 10	3.3E-04	3
1435902_at	Nudt18	nudix (nucleoside diphosphate linked moiety X)-type motif 18	6.8E-05	3
1448148_at	Grn	granulin	8.4E-04	3
1428586_at	Tmem41b	transmembrane protein 41B	6.3E-04	3
1442947_x_at		13 days embryo heart cDNA, RIKEN full-length	8.6E-04	3

		enriched library, clone:D330042P15 product:unclassifiable, full insert sequence		
1422064_a_at	Zbtb20	zinc finger and BTB domain containing 20	9.4E-04	3
1415864_at	Bpgm	2,3-bisphosphoglycerate mutase	5.8E-04	3
1450798_at	Tnxb	tenascin XB	8.1E-05	3
1423086_at	Npc1	Niemann Pick type C1	4.0E-05	3
1453102_at	Flrt3	fibronectin leucine rich transmembrane protein 3	3.3E-04	3
1422670_at	Rnd2	Rho family GTPase 2	2.6E-04	3
1433588_at	D6Wsu116e	DNA segment, Chr 6, Wayne State University 116, expressed	3.9E-05	3
1422038_a_at	TNFRsf22	tumor necrosis factor receptor superfamily, member 22	1.5E-05	3
1438931_s_at	LOC100047324 /// Sesn1	sestrin 1 /// similar to Sesn1 protein	4.5E-04	3
1437261_at	2900024O10Rik	RIKEN cDNA 2900024O10 gene	1.3E-04	3
1437704_at	2900024O10Rik	RIKEN cDNA 2900024O10 gene	1.6E-04	3
1423141_at	Lipa	lysosomal acid lipase A	2.1E-04	3
1426851_a_at	Nov	nephroblastoma overexpressed gene	5.6E-05	3
1419030_at	Ero1l	ERO1-like (<i>S. cerevisiae</i>)	1.3E-04	3
1431417_at	Jam2	junction adhesion molecule 2	4.6E-04	3
1424785_at	Angptl6	angiopoietin-like 6	1.4E-04	3
1441649_at		0 day neonate lung cDNA, RIKEN full-length enriched library, clone:E030001E08 product:unclassifiable, full insert sequence	8.0E-04	3
1445882_at	Cd300lb	CD300 antigen like family member B	6.7E-06	3
1432103_a_at	Sh3gl3	SH3-domain GRB2-like 3	4.0E-04	3
1431769_at	2210406O10Rik	RIKEN cDNA 2210406O10 gene	1.1E-04	3
1456744_x_at	Flcn	folliculin	5.5E-04	3
1450626_at	Manba	mannosidase, beta A, lysosomal	7.5E-04	3
1442140_at	Tnn	tenascin N	5.7E-04	3
1419666_x_at	Nupr1	nuclear protein 1	6.0E-04	3
1455011_at	Stard4	StAR-related lipid transfer (START) domain containing 4	2.3E-04	3
1424951_at	Baiap2l1	BAI1-associated protein 2-like 1	7.6E-05	3
1423593_a_at	Csf1r	colony stimulating factor 1 receptor	5.4E-04	3
1423662_at	Atp6ap2	ATPase, H+ transporting, lysosomal accessory protein 2	4.3E-04	3
1426315_a_at	6330416G13Rik	RIKEN cDNA 6330416G13 gene	2.6E-05	3
1438579_at	Utp14b	UTP14, U3 small nucleolar ribonucleoprotein, homolog B (yeast)	2.4E-04	3
1452956_a_at	D12Ertd647e	DNA segment, Chr 12, ERATO Doi 647, expressed	2.3E-04	3
1442893_at			4.7E-05	3
1452232_at	Galnt7	UDP-N-acetyl-alpha-D-galactosamine: polypeptide N-acetylgalactosaminyltransferase 7	6.8E-04	3
1418129_at	Dhcr24	24-dehydrocholesterol reductase	3.7E-04	3
1448696_at	Heph	hephaestin	3.4E-04	3
1417551_at	Cln3	ceroid lipofuscinosis, neuronal 3, juvenile (Batten, Spielmeyer-Vogt disease)	7.0E-04	3
1428195_at	4631427C17Rik	RIKEN cDNA 4631427C17 gene	1.9E-05	3
1425235_s_at	Col20a1	collagen, type XX, alpha 1	8.2E-04	3
1455820_x_at	Scarb1	scavenger receptor class B, member 1	9.2E-04	3

1428334_at	Ostm1	osteopetrosis associated transmembrane protein 1	1.4E-04	3
1435357_at	D4Wsu53e	DNA segment, Chr 4, Wayne State University 53, expressed	5.8E-04	3
1448200_at	Tcn2	transcobalamin 2	2.2E-04	3
1450708_at	Scg2	secretogranin II	1.2E-04	3
1423585_at	Igfbp7	insulin-like growth factor binding protein 7	5.4E-04	3
1426708_at	Antxr2	anthrax toxin receptor 2	8.4E-05	3
1441481_at	Mfap3l	microfibrillar-associated protein 3-like	1.6E-04	3
1435484_at	BF642829	expressed sequence BF642829	5.7E-05	3
1416830_at	0610031J06Rik	RIKEN cDNA 0610031J06 gene	7.7E-04	3
1433074_at	4931412I15Rik	RIKEN cDNA 4931412I15 gene	2.5E-04	3
1456056_a_at	D6Wsu116e	DNA segment, Chr 6, Wayne State University 116, expressed	4.5E-05	3
1433034_at	2310007H11Rik	RIKEN cDNA 2310007H11 gene	4.6E-05	3
1451799_at	Ccdc25	coiled-coil domain containing 25	7.7E-04	3
1450919_at	Mpp1	membrane protein, palmitoylated	2.1E-05	3
1419688_at	Gpc6	glypican 6	5.8E-04	3
1420833_at	Vamp2	vesicle-associated membrane protein 2	3.1E-04	3
1443882_at		Transcribed locus	2.8E-05	3
1437044_a_at	Gba	glucosidase, beta, acid	4.8E-04	3
1438167_x_at	Flcn	Folliculin	1.9E-04	3
1425140_at	Lactb2	lactamase, beta 2	1.9E-04	3
1456482_at	Pik3r3	phosphatidylinositol 3 kinase, regulatory subunit, polypeptide 3 (p55)	9.0E-05	3
1419006_s_at	Peli2	pellino 2	4.4E-04	3
1452271_at	Xpr1	xenotropic and polytropic retrovirus receptor 1	2.5E-04	3
1438415_s_at	Yipf2	Yip1 domain family, member 2	6.3E-04	3
1451152_a_at	Atp1b1	ATPase, Na ⁺ /K ⁺ transporting, beta 1 polypeptide	4.4E-05	3
1448319_at	Akr1b3	aldo-keto reductase family 1, member B3 (aldose reductase)	4.7E-05	3
1416265_at	Capn10	calpain 10	7.9E-05	3

Appendix IV

RT-PCR analysis of the genes whose expression was strongly up-regulated in the original microarray analysis. RNA was extracted from individual NIH3T3 (mouse fibroblast) cell cultures at 0, 8 and 24hrs. At 0hrs the cells had not been treated (NT) with purified p37 protein. At 8 and 24hrs mRNA was extracted from three biological replicates not treated [NT(1),(2)&(3)] and three biological replicates treated [p37T(1),(2)&(3)] with p37 protein. Samples (1) and (2) of the 24hr treated and non-treated were used in the original microarray analysis, while sample (3) was not. The PCRs (Section 2.11) were run out on a 2% agarose gel (Section 2.7) and observed under UV light. All bands were at the correct size and no gDNA was amplified. The bands were excised from the gel, purified (Section 2.7) and sent for sequencing (Section 2.8.2) to confirm the right genes were amplified.



Appendix V

Raw data of Microarray validation by qPCR presented in Figure 3.5.

Located on attached CD

Appendix VI

Reasons for fold change variations between qPCR and Microarray data

Variability observed in correlation graphs of qPCR and microarray data can be due to collection and processing of total RNA and data acquisition and analysis (Morey et al., 2006; Ach et al., 2008). The same total RNA was used for both the microarray and validating qPCRs therefore collection of total RNA in this correlation is not a factor lowering the Pearson correlation coefficient (Figure 3.6). The total RNA was checked for degradation before use in the microarray and checked again before use in qPCR. No degradation was observed. For the microarray, reverse transcription (RT) was performed using a kit purchased from Affymetrix while for qPCR the assay was performed using a kit purchased from Invitrogen. The Reverse Transcriptase may contribute to the low correlation. The microarray RNA was further amplified, labelled, purified, fragmented and hybridized to Affymetrix chips for the microarray, during which variations in expression may be introduced.

Different data acquisition techniques were also used. In the microarray a fluidics station is used to measure the fluorescence intensity of each gene spot from an image. The image intensities are scaled and used to calculate a fold change based on the difference between the controls and treated samples. Beckman et al. (2004) found that low correlation between microarray data and qPCR is influenced by low intensity spots in microarrays. Low intensity spots occur when treated samples give a lower fluorescence than the highest value of the controls. This can cause both false positive and negatives and, consequently, fold change errors within microarray data (Beckman et al., 2004; Morey et al., 2006). These issues can be resolved by increasing the number of biological and technical replicates. In the microarray analysis, biological triplicates were used, however not experimental triplicates. In qPCR an iCycler is used to measure the fluorescence of SYBR green that has been intercalated into double strand (ds) DNA during the amplification process. The cycle threshold (cycle number at which the fluorescence generated within a reaction crosses the threshold) values of two reference genes and the gene of interest are used to determine fold change. To ensure accurate acquisition of data from qPCR it is important that oligonucleotides are specific to the gene of interest and efficient in amplification.

All qPCR oligonucleotide efficiencies were established, as described in section 2.12 and listed in Section 0. The acceptable efficiency range was set between 90 - 110%, which is equivalent to an increase of 1.9 to 2.1-fold per amplification cycle. Amplification products were all assessed by a melting curve, gel electrophoresis (Section 2.7) and sequencing analysis (Section 2.8.2/2.8.3). Thallinger et al. (2012) found that high correlations were achievable if oligonucleotides from the microarray and qPCR matched. The further the PCR primers were located from the microarray probes the lower the correlation (Etienne et al., 2004). Matching oligonucleotides are not always possible as qPCR oligonucleotides have many selection rules to ensure efficient amplification. qPCR primers are usually designed to span an intron, indicating the presence of gDNA, and can detect a subset of splice variants. Microarray oligonucleotides bind all splice variants and reside entirely within an exon (Thallinger et al., 2012).

The analysis process of microarray and qPCR data can also decrease correlation. qPCR is normalised to two or more reference genes. In our correlation the qPCR data was normalised to B-actin and GAPDH. Microarray data is usually intensity scaled and then normalised to a set of 5 reference genes. B-actin and GAPDH were identified as good reference genes as their transcript levels did not change in response to p37 treated in the microarray and consistently have similar Ct values in samples with the same concentrations of cDNA.

Appendix VII

Calculations of correlation graphs and the histogram presented in Figure 3.6.

Located on attached CD

Appendix VIII

Raw data of gene expression of NIH3T3 (mouse) fibroblasts treated with different concentrations of purified p37 (0.5, 1, 5 and 25µg/ml) presented in Figure 3.7.

Located on attached CD

Appendix IX

Raw data of gene expression at time points after 5µg/ml p37 treatment of NIH3T3 cells presented in Table 3.3.

Located on attached CD

Appendix X

Calculations of RT²Profiler Array correlation graphs presented in Figure 3.8 and overview of Ct values presented in Figure 3.9.

Located on attached CD

Appendix XI

Gene expression of all the genes of the RT²Profiler Array. Those presented in Table 3.6, Figure 5.7 and Table 5.1.

NCBI Locus Number	Gene ID	Description	25µg/ml p37		S31-201		S31-201 + 25µg/ml p37	
			Fold change	p-value	Fold change	p-value	Fold change	p-value
NM_009778	C3	Complement component 3	10	0.178	1	0.847	36	0.005
NM_008176	Cxcl1	Chemokine (C-X-C motif) ligand 1	10	0.064	3	0.388	47	0.007
NM_013653	Ccl5	Chemokine (C-C motif) ligand 5	6	0.192	2	0.562	13	0.013
NM_009141	Cxcl5	Chemokine (C-X-C motif) ligand 5	5	0.084	2	0.472	33	0.016
NM_013654	Ccl7	Chemokine (C-C motif) ligand 7	4	0.175	3	0.252	33	0.007
NM_011333	Ccl2	Chemokine (C-C motif) ligand 2	4	0.192	3	0.089	35	0.000
NM_021274	Cxcl10	Chemokine (C-X-C motif) ligand 10	3	0.085	1	0.663	6	0.034
NM_007768	Crp	C-reactive protein, pentraxin-related	3	0.255	1	0.813	3	0.230
NM_011905	TLR2	Toll-like receptor 2	2	0.286	0	0.126	2	0.591
NM_031168	Il6	Interleukin 6	2	0.171	5	0.001	25	0.025
NM_010927	Nos2	Nitric oxide synthase 2, inducible	2	0.699	0	0.356	0	0.397
NM_207225	Hdac4	Histone deacetylase 4	2	0.758	2	0.201	2	0.241
NM_009883	Cebpb	CCAAT/enhancer binding protein (C/EBP), beta	2	0.961	2	0.859	4	0.100
NM_009744	Bcl6	B-cell leukemia/lymphoma 6	2	0.082	1	0.595	2	0.168
NM_010851	Myd88	Myeloid differentiation primary response gene 88	2	0.344	1	0.826	2	0.355
NM_008349	Il10rb	Interleukin 10 receptor, beta	2	0.451	4	0.002	9	0.000
NM_021443	Ccl8	Chemokine (C-C motif) ligand 8	1	0.729	0	0.261	4	0.425
NM_010735	Lta	Lymphotoxin A	1	0.426	1	0.552	2	0.195
NM_007719	Ccr7	Chemokine (C-C motif) receptor 7	1	0.877	0	0.399	2	0.714
NM_011331	Ccl12	Chemokine (C-C motif) ligand 12	1	0.790	0	0.273	1	0.728
NM_013520	Flt3l	FMS-like tyrosine kinase 3 ligand	1	0.589	1	0.592	2	0.204
SA_00104	RTC	Reverse Transcription Control	1	0.673	2	0.398	4	0.047
NM_009780	C4b	Complement component 4B (Childo blood group)	1	0.101	1	0.136	1	0.410
NM_007778	Csf1	Colony stimulating factor 1 (macrophage)	1	0.197	3	0.000	2	0.004
SA_00103	PPC	Positive PCR Control	1	0.631	1	0.978	2	0.236
NM_008518	Ltb	Lymphotoxin B	1	0.960	0	0.304	1	0.544

NM_019418	TNFSf14	Tumor necrosis factor (ligand) superfamily, member 14	1	0.891	0	0.313	2	0.983
SA_00104	RTC	Reverse Transcription Control	1	0.752	2	0.591	3	0.127
SA_00103	PPC	Positive PCR Control	1	0.642	2	0.370	3	0.053
NM_011611	Cd40	CD40 antigen	1	0.617	0	0.204	1	0.701
NM_008689	Nfkb1	Nuclear factor of kappa light polypeptide gene enhancer in B-cells 1, p105	1	0.709	1	0.865	3	0.045
SA_00103	PPC	Positive PCR Control	1	0.599	2	0.362	3	0.041
NM_008371	Il7	Interleukin 7	1	0.474	1	0.461	2	0.067
NM_031252	Il23a	Interleukin 23, alpha subunit p19	1	0.841	1	0.408	2	0.719
SA_00104	RTC	Reverse Transcription Control	1	0.652	2	0.302	4	0.035
NM_010548	Il10	Interleukin 10	1	0.564	1	0.638	2	0.444
NM_133211	TLR7	Toll-like receptor 7	1	0.735	0	0.211	2	0.385
NM_011330	Ccl11	Chemokine (C-C motif) ligand 11	1	0.761	1	0.749	5	0.077
NM_011888	Ccl19	Chemokine (C-C motif) ligand 19	1	0.706	0	0.122	1	0.977
NM_008337	lfng	Interferon gamma	1	0.614	0	0.354	2	0.618
NM_203320	Cxcl3	Chemokine (C-X-C motif) ligand 3	1	0.922	0	0.319	1	0.659
NM_011329	Ccl1	Chemokine (C-C motif) ligand 1	1	0.806	0	0.314	1	0.789
NM_016923	Ly96	Lymphocyte antigen 96	1	0.869	2	0.449	6	0.031
NM_021297	TLR4	Toll-like receptor 4	1	0.714	1	0.313	2	0.911
NM_010901	Nfatc3	Nuclear factor of activated T-cells, cytoplasmic, calcineurin-dependent 3	1	0.754	2	0.052	3	0.011
NM_009915	Ccr2	Chemokine (C-C motif) receptor 2	1	0.933	0	0.207	0	0.470
NM_010554	Il1a	Interleukin 1 alpha	1	0.998	0	0.283	12	0.056
NM_019577	Ccl24	Chemokine (C-C motif) ligand 24	1	0.947	0	0.273	1	0.563
NM_010177	Fasl	Fas ligand (TNF superfamily, member 6)	1	0.819	1	0.353	1	0.813
NM_009137	Ccl22	Chemokine (C-C motif) ligand 22	1	0.783	0	0.263	1	0.663
NM_023764	Tollip	Toll interacting protein	1	0.969	1	0.929	3	0.058
NM_016960	Ccl20	Chemokine (C-C motif) ligand 20	1	0.987	0	0.354	1	0.684
NM_008360	Il18	Interleukin 18	1	0.729	4	0.040	6	0.016
NM_008302	Hsp90ab1	Heat shock protein 90 alpha (cytosolic), class B member 1	1	0.891	2	0.199	3	0.009
NM_010368	Gusb	Glucuronidase, beta	1	0.944	1	0.922	2	0.188
NM_009911	Cxcr4	Chemokine (C-X-C motif) receptor 4	1	0.791	0	0.359	1	0.996

NM_138952	Ripk2	Receptor (TNFRSF)-interacting serine-threonine kinase 2	1	0.667	3	0.023	4	0.010
NM_008084	Gapdh	Glyceraldehyde-3-phosphate dehydrogenase	1	0.474	1	0.354	1	0.863
NM_144548	Il23r	Interleukin 23 receptor	1	0.820	0	0.357	1	0.866
SA_00106	MGDC	Mouse Genomic DNA Contamination	1	0.825	0	0.357	1	0.652
NM_008364	Il1rap	Interleukin 1 receptor accessory protein	1	0.860	1	0.612	2	0.226
NM_019494	Cxcl11	Chemokine (C-X-C motif) ligand 11	1	0.836	0	0.359	1	0.738
NM_031167	Il1rn	Interleukin 1 receptor antagonist	1	0.946	0	0.236	1	0.796
NM_126166	TLR3	Toll-like receptor 3	1	0.778	1	0.334	1	0.643
NM_013556	Hprt	Hypoxanthine guanine phosphoribosyl transferase	1	0.990	2	0.117	3	0.028
NM_008373	Il9	Interleukin 9	1	0.851	0	0.244	2	0.637
NM_013652	Ccl4	Chemokine (C-C motif) ligand 4	1	0.975	0	0.063	1	0.673
NM_008362	Il1r1	Interleukin 1 receptor, type I	1	0.914	5	0.002	10	0.002
NM_178258	Il22ra2	Interleukin 22 receptor, alpha 2	1	0.968	0	0.362	1	0.854
NM_009140	Cxcl2	Chemokine (C-X-C motif) ligand 2	1	0.976	0	0.364	1	0.998
NM_010559	Il6ra	Interleukin 6 receptor, alpha	1	0.879	2	0.116	1	0.271
NM_009916	Ccr4	Chemokine (C-C motif) receptor 4	1	0.934	0	0.221	1	0.852
NM_008404	Itgb2	Integrin beta 2	1	0.621	0	0.172	1	0.984
NM_009138	Ccl25	Chemokine (C-C motif) ligand 25	1	0.974	2	0.139	4	0.075
NM_010553	Il18rap	Interleukin 18 receptor accessory protein	1	0.998	0	0.010	0	0.014
NM_011337	Ccl3	Chemokine (C-C motif) ligand 3	1	0.973	0	0.184	2	0.400
NM_153077	Il1f10	Interleukin 1 family, member 10	1	0.967	0	0.355	1	0.547
NM_011332	Ccl17	Chemokine (C-C motif) ligand 17	1	0.901	3	0.174	3	0.121
NM_016971	Il22	Interleukin 22	1	0.970	0	0.364	1	0.771
NM_009912	Ccr1	Chemokine (C-C motif) receptor 1	1	0.830	0	0.109	1	0.438
NM_009909	Cxcr2	Chemokine (C-X-C motif) receptor 2	1	0.859	0	0.330	1	0.569
NM_013693	TNF	Tumor necrosis factor	1	0.939	0	0.356	1	0.528
NM_011616	Cd40lg	CD40 ligand	1	0.922	0	0.358	1	0.620
NM_054096	Tirap	Toll-interleukin 1 receptor (TIR) domain-containing adaptor protein	1	0.746	1	0.346	1	0.643
NM_007393	Actb	Actin, beta	1	0.455	1	0.396	1	0.771
NM_016928	TLR5	Toll-like receptor 5	1	0.839	0	0.362	1	0.949
NM_009914	Ccr3	Chemokine (C-C motif) receptor 3	1	0.794	0	0.368	1	0.500
NM_008361	Il1b	Interleukin 1 beta	1	0.728	0	0.361	1	0.644
NM_030682	TLR1	Toll-like receptor 1	1	0.746	2	0.113	3	0.025

NM_023125	Kng1	Kininogen 1	1	0.913	0	0.202	1	0.558
NM_011604	TLR6	Toll-like receptor 6	1	0.368	0	0.091	0	0.105
NM_008599	Cxcl9	Chemokine (C-X-C motif) ligand 9	1	0.457	0	0.037	1	0.691
NM_008173	Nr3c1	Nuclear receptor subfamily 3, group C, member 1	1	0.437	1	0.740	2	0.109
NM_009779	C3ar1	Complement component 3a receptor 1	1	0.881	0	0.270	1	0.413
NM_010234	Fos	FBJ osteosarcoma oncogene	1	0.440	1	0.764	2	0.430
NM_178241	Cxcr1	Chemokine (C-X-C motif) receptor 1	0.50	0.477	0	0.330	1	0.642

Appendix XII

Raw data of gene expression and correlation calculations for Section 4.2, Il6R inhibition, presented in Figure 4.2, Figure 4.3 and Figure 4.4.

Located on attached CD

Appendix XIII

Raw data of *STAT3* expression in p37 treated NIH3T3 cells at different concentrations, at different times and the affect of Il6R inhibition presented in Figure 5.1.

Located on attached CD

Appendix XIV

Raw data of gene expression for Section 5.2.2, effects of STAT3 inhibitor S31-201, presented in Figure 5.3 and Figure 5.4.

Located on attached CD

Appendix XV

Calculations of RT²Profiler Array correlation graphs presented in Figure 5.5 and the overview of Ct values presented in Figure 5.6.

Located on attached CD

Appendix XVI

Raw data of *Il6*, *Saa3* and *TNFaip6* gene expression in LPS treated NIH3T3 cells presented in Figure 6.2, *Saa3* gene expression of NIH3T3 cells treated with CP7 or VIPER presented in Figure 6.3 and dose-dependent effect of VIPER and CP7 on LPS-stimulated *Saa3* gene expression in NIH3T3 cells presented in Figure 6.4.

Located on attached CD

Appendix XVII

Raw data of 1μM VIPER or CP7 on gene expression in NIH3T3 cells, presented in Figure 6.5, and on p37-induced gene expression in NIH3T3 cells, presented in Figure 6.6.

Located on attached CD

Appendix XVIII

Raw data of 0.5 μ M VIPER or CP7 on gene expression in NIH3T3 cells, presented in Figure 6.7, and on p37-induced gene expression in NIH3T3 cells, presented in Figure 6.8.

Located on attached CD

Appendix XIX

The plasmids were sequenced and those containing the seven mutations were re-named pRA:mutp37

		20		40		60	
pRAp37	GATCTCGATC	CCGCGAAATT	AATACGACTC	ACTATAGGGA	GACCACAACG	GTTTCCCTCT	60
mutp37 (F1/R1)	-----	-----	-----	-----	-----	-----	
mutp37 (F2/R2)	-----	-----	-----	-----	-----	-----	
		80		100		120	
pRAp37	AGAAATAATT	TTGTTTAACT	TAAAGAAGGA	GATATACATA	TGCGGGGTTT	TCATCATCAT	120
mutp37 (F1/R1)	-----	-----CT	TAAAGAAGGA	GATATACATA	TGCGGGGTTT	TCATCATCAT	42
mutp37 (F2/R2)	-----	-----CT	TAAAGAAGGA	GATATACATA	TGCGGGGTTT	TCATCATCAT	42
		140		160		180	
pRAp37	CATCATCATG	GTATGGCTAG	CATGACTGGT	GGACAGCAAA	TGGGTCGGGA	TCTGTACGAC	180
mutp37 (F1/R1)	CATCATCATG	GTATGGCTAG	CATGACTGGT	GGACAGCAAA	TGGGTCGGGA	TCTGTACGAC	102
mutp37 (F2/R2)	CATCATCATG	GTATGGCTAG	CATGACTGGT	GGACAGCAAA	TGGGTCGGGA	TCTGTACGAC	102
		200		220		240	
pRAp37	GATGACGATA	AGGATCGATG	GGGATCCGCA	TGTTCTAATA	CAGGAGTAGT	CAAGCAAGAG	240
mutp37 (F1/R1)	GATGACGATA	AGGATCGATG	GGGATCCGCA	TGTTCTAATA	CAGGAGTAGT	CAAGCAAGAG	162
mutp37 (F2/R2)	GATGACGATA	AGGATCGATG	GGGATCCGCA	TGTTCTAATA	CAGGAGTAGT	CAAGCAAGAG	162
		260		280		300	
pRAp37	GATGTATCAG	TTAGTCAAGG	TCAATGGGAT	AAAAGTATAA	CATTTGGTGT	TTCAGAAGCT	300
mutp37 (F1/R1)	GATGTATCAG	TTAGTCAAGG	TCAATGGGAT	AAAAGTATAA	CATTTGGTGT	TTCAGAAGCT	222
mutp37 (F2/R2)	GATGTATCAG	TTAGTCAAGG	TCAATGGGAT	AAAAGTATAA	CATTTGGTGT	TTCAGAAGCT	222
		320		340		360	
pRAp37	TGGTTAAACA	AGAAAAAAGG	AGGTGAAAAA	GTTAACAAAG	AAGTTATTAA	TACATTTTTA	360
mutp37 (F1/R1)	TGGTTAAACA	AGAAAAAAGG	AGGTGAAAAA	GTTAACAAAG	AAGTTATTAA	TACATTTTTA	282
mutp37 (F2/R2)	TGGTTAAACA	AGAAAAAAGG	AGGTGAAAAA	GTTAACAAAG	AAGTTATTAA	TACATTTTTA	282
		380		400		420	
pRAp37	GAAAAATTTCA	AAAAAGAATT	TAATAAACTC	AAAAATGCAA	ATGATAAAAC	CAAAAACTTC	420
mutp37 (F1/R1)	GAAAAATTTCA	AAAAAGAATT	TAATAAACTC	AAAAATGCAA	ATGATAAAAC	CAAAAACTTC	342
mutp37 (F2/R2)	GAAAAATTTCA	AAAAAGAATT	TAATAAACTC	AAAAATGCAA	ATGATAAAAC	CAAAAACTTC	342
		440		460		480	
pRAp37	GATGACGTTG	ATTTTAAAGT	AACTCCAATT	CAAGACTTTA	CTGTGTTGTT	AAACAATTTA	480
mutp37 (F1/R1)	GATGACGTTG	ATTTTAAAGT	AACTCCAATT	CAAGACTTTA	CTGTGTTGTT	AAACAATTTA	402
mutp37 (F2/R2)	GATGACGTTG	ATTTTAAAGT	AACTCCAATT	CAAGACTTTA	CTGTGTTGTT	AAACAATTTA	402
		500		520		540	
pRAp37	TCTACTGACA	ATCCTGAATT	AGATTTTGGG	ATTAATGCTT	CAGGAAAATT	GGTAGAATTT	540
mutp37 (F1/R1)	TCTACTGACA	ATCCTGAATT	AGATTTTGGG	ATTAATGCTT	CAGGAAAATT	GGTAGAATTT	462
mutp37 (F2/R2)	TCTACTGACA	ATCCTGAATT	AGATTTTGGG	ATTAATGCTT	CAGGAAAATT	GGTAGAATTT	462
		560		580		600	
pRAp37	CTAAAAAATA	ATCCTGGTAT	AATAACTCCA	GCATTAGAAA	CAACAACATA	TTCTTTTGTA	600
mutp37 (F1/R1)	CTAAAAAATA	ATCCTGGTAT	AATAACTCCA	GCATTAGAAA	CAACAACATA	TTCTTTTGTA	522
mutp37 (F2/R2)	CTAAAAAATA	ATCCTGGTAT	AATAACTCCA	GCATTAGAAA	CAACAACATA	TTCTTTTGTA	522
		620		640		660	
pRAp37	TTTGACAAAG	AAAAAGATAA	ATTTTATGTT	GATGGTACAG	ATTCAGATCC	ACTTGTAATA	660
mutp37 (F1/R1)	TTTGACAAAG	AAAAAGATAA	ATTTTATGTT	GATGGTACAG	ATTCAGATCC	ACTTGTAATA	582
mutp37 (F2/R2)	TTTGACAAAG	AAAAAGATAA	ATTTTATGTT	GATGGTACAG	ATTCAGATCC	ACTTGTAATA	582
		680		700		720	
pRAp37	ATTGCTAAAG	AAATTAATAA	AATTTTTGTT	GAAACTCCAT	ATGCAAGTTG	GACTGATGAA	720
mutp37 (F1/R1)	ATTGCTAAAG	AAATTAATAA	AATTTTTGTT	GAAACTCCAT	ATGCAAGTTG	GACTGATGAA	642
mutp37 (F2/R2)	ATTGCTAAAG	AAATTAATAA	AATTTTTGTT	GAAACTCCAT	ATGCAAGTTG	GACTGATGAA	642
		740		760		780	
pRAp37	AATCATAAGT	GGAATGGTAA	TGTTTATCAA	AGTGTTCACG	ATCCAACGTG	TCAAGCTAAT	780
mutp37 (F1/R1)	AATCATAAGT	GGAATGGTAA	TGTTTATCAA	AGTGTTCACG	ATCCAACGTG	TCAAGCTAAT	702
mutp37 (F2/R2)	AATCATAAGT	GGAATGGTAA	TGTTTATCAA	AGTGTTCACG	ATCCAACGTG	TCAAGCTAAT	702
		800		820		840	
pRAp37	TTTTATAGAG	GAATGATTTG	GATAAAAGGT	AATGATGAAA	CTCTAGCTAA	AATTAATAAAA	840
mutp37 (F1/R1)	TTTTATAGAG	GAATGATTTG	GATAAAAGGT	AATGATGAAA	CTCTAGCTAA	AATTAATAAAA	762
mutp37 (F2/R2)	TTTTATAGAG	GAATGATTTG	GATAAAAGGT	AATGATGAAA	CTCTAGCTAA	AATTAATAAAA	762
		860		880		900	
pRAp37	GCTTGGAAATG	ATAAAGATTG	GAATACATTT	AGAAATTTTG	GAATTTTACA	CGGTAAAGAT	900
mutp37 (F1/R1)	GCTTGGAAATG	ATAAAGATTG	GAATACATTT	AGAAATTTTG	GAATTTTACA	CGGTAAAGAT	822
mutp37 (F2/R2)	GCTTGGAAATG	ATAAAGATTG	GAATACATTT	AGAAATTTTG	GAATTTTACA	CGGTAAAGAT	822
		920		940		960	
pRAp37	AATTCCTTTT	CTAAATTCAA	GTTAGAAGAA	ACTATATTAA	AAAACCACTT	TCAAAATAAA	960
mutp37 (F1/R1)	AATGCTGTTG	CTGAATTCAA	GTTAGAAGAA	ACTATATTAA	AAAACCACTT	TCAAAATAAA	882
mutp37 (F2/R2)	AATGTTGTTG	TTGTATTCAA	GTTAGAAGAA	ACTATATTAA	AAAACCACTT	TCAAAATAAA	882

			980		1,000		1,020	
pRAp37	TTTACAACAC	TAAATGAAGA		CAGAAGCGCA	CATCCAAACG	CATATAAACA	AAAATCTGCA	1020
mutp37 (F1/R1)	TTTACAACAC	TAAATGAAGA		CAGAAGCGCA	CATCCAAACG	CATATAAACA	AAAATCTGCA	942
mutp37 (F2/R2)	TTTACAACAC	TAAATGAAGA		CAGAAGCGCA	CATCCAAACG	CATATAAACA	AAAATCTGCA	942
			1,040		1,060		1,080	
pRAp37	GATACATTGG	GAACTTTAGA		TGATTTCCAT	ATTGCTTTTT	CAGAAGAAGG	TTCTTTTGTCT	1080
mutp37 (F1/R1)	GATACATTGG	GAACTTTAGA		TGATTTCCAT	ATTGCTTTTT	C-----	-----	983
mutp37 (F2/R2)	GATACATTGG	GAACTTTAGA		TGATTTCCAT	ATTGCTTTTT	C-----	-----	983
			1,100		1,120		1,140	
pRAp37	TGAACACATA	ACAAATCAGC		AACAAAACTT	TTTGAAACTA	AAGCAAATGA	AAAGATGGAA	1140
mutp37 (F1/R1)	-----	-----		-----	-----	-----	-----	983
mutp37 (F2/R2)	-----	-----		-----	-----	-----	-----	983
			1,160		1,180		1,200	
pRAp37	GCACTTATAG	TAACATAATCC		AATTCGGTAT	GATGTTGGAG	TGTTTAGAAA	AAGTGTTAAC	1200
mutp37 (F1/R1)	-----	-----		-----	-----	-----	-----	983
mutp37 (F2/R2)	-----	-----		-----	-----	-----	-----	983
			1,220		1,240		1,260	
pRAp37	CAATTAGAAC	AAAATTTAAT		TGTTCAAACA	TTCATTAATT	TAGCTAAAAA	TAAACAAGAT	1260
mutp37 (F1/R1)	-----	-----		-----	-----	-----	-----	983
mutp37 (F2/R2)	-----	-----		-----	-----	-----	-----	983
			1,280		1,300		1,320	
pRAp37	ACATATGGCC	CACTTTTAGG		GTATAATGGT	TATAAAAAAA	TTGACAATTT	CCAAAAAGAG	1320
mutp37 (F1/R1)	-----	-----		-----	-----	-----	-----	983
mutp37 (F2/R2)	-----	-----		-----	-----	-----	-----	983
			1,340					
pRAp37	ATTGTAGAAG	TTTATGAAAA		AGCCATTAAA	TAA			1353
mutp37 (F1/R1)	-----	-----		-----	---			983
mutp37 (F2/R2)	-----	-----		-----	---			983

Appendix XX

Raw data of mutant p37 (mutp37) affect on gene expression of NIH3T3 cells presented in Figure 7.9.

Located on attached CD

Appendix XXI

Sequence analysis of the four truncated p37 constructs (pRAp37-20, -60, -80 and -105) discussed in Section 7.2.4. The location of the forward primer is highlighted in blue and the location of the reverse primers are highlighted in purple.

		-200		-180		-160		-140	
p37									
pRAp37-20	GATCTCGATC	CCGCGAAATT	AATACGACTC	ACTATAGGGA	GACCAACAACG	GTTTCCTCT	AGAAATAATT	TTGTTTAACT	80
pRAp37-60	GATCTCGATC	CCGCGAAATT	AATACGACTC	ACTATAGGGA	GACCAACAACG	GTTTCCTCT	AGAAATAATT	TTGTTTAACT	80
pRAp37-80	GATCTCGATC	CCGCGAAATT	AATACGACTC	ACTATAGGGA	GACCAACAACG	GTTTCCTCT	AGAAATAATT	TTGTTTAACT	80
pRAp37-105	GATCTCGATC	CCGCGAAATT	AATACGACTC	ACTATAGGGA	GACCAACAACG	GTTTCCTCT	AGAAATAATT	TTGTTTAACT	80
		-120		-100		-80		-60	
p37									
pRAp37-20	TTAAGAAGGA	GATATACATA	TGCGGGGTTT	TCATCATCAT	CATCATCATG	GTATGGCTAG	CATGACTGGT	GGACAGCAA	160
pRAp37-60	TTAAGAAGGA	GATATACATA	TGCGGGGTTT	TCATCATCAT	CATCATCATG	GTATGGCTAG	CATGACTGGT	GGACAGCAA	160
pRAp37-80	TTAAGAAGGA	GATATACATA	TGCGGGGTTT	TCATCATCAT	CATCATCATG	GTATGGCTAG	CATGACTGGT	GGACAGCAA	160
pRAp37-105	TTAAGAAGGA	GATATACATA	TGCGGGGTTT	TCATCATCAT	CATCATCATG	GTATGGCTAG	CATGACTGGT	GGACAGCAA	160
		-40		-20		1		20	
p37							CA	TGTTCTAATA	
pRAp37-20	TGGGTCGGGA	TCTGTACGAC	GATGACGATA	AGGATCGATG	GGGATCCGCA	TGTTCTAATA	CAGGAGTAGT	CAAGCAAGAG	32
pRAp37-60	TGGGTCGGGA	TCTGTACGAC	GATGACGATA	AGGATCGATG	GGGATCCGCA	TGTTCTAATA	CAGGAGTAGT	CAAGCAAGAG	240
pRAp37-80	TGGGTCGGGA	TCTGTACGAC	GATGACGATA	AGGATCGATG	GGGATCCGCA	TGTTCTAATA	CAGGAGTAGT	CAAGCAAGAG	240
pRAp37-105	TGGGTCGGGA	TCTGTACGAC	GATGACGATA	AGGATCGATG	GGGATCCGCA	TGTTCTAATA	CAGGAGTAGT	CAAGCAAGAG	240
		40		60		80		100	
p37	GATGTATCAG	TTAGTCAAGG	TCAATGGGAT	AAAAGTATAA	CATTTGGTGT	TTCAGAAGCT	TGGTTAAACA	AGAAAAAGG	112
pRAp37-20	GATGTATCAG	TTAGTCAAGG	TCAATGGGAT	AAAAGTATAA	CATTTGGTGT	TTCAGAAGCT	TGGTTAAACA	AGAAAAAGG	320
pRAp37-60	GATGTATCAG	TTAGTCAAGG	TCAATGGGAT	AAAAGTATAA	CATTTGGTGT	TTCAGAAGCT	TGGTTAAACA	AGAAAAAGG	320
pRAp37-80	GATGTATCAG	TTAGTCAAGG	TCAATGGGAT	AAAAGTATAA	CATTTGGTGT	TTCAGAAGCT	TGGTTAAACA	AGAAAAAGG	320
pRAp37-105	GATGTATCAG	TTAGTCAAGG	TCAATGGGAT	AAAAGTATAA	CATTTGGTGT	TTCAGAAGCT	TGGTTAAACA	AGAAAAAGG	320
		120		140		160		180	
p37	AGGTGAAAAA	GTTAACAAAG	AAGTTATTTA	TACATTTTTA	GAAAAATTTCA	AAAAAGAATT	TAATAAACTC	AAAAATGCAA	192
pRAp37-20	AGGTGAAAAA	GTTAACAAAG	AAGTTATTTA	TACATTTTTA	GAAAAATTTCA	AAAAAGAATT	TAATAAACTC	AAAAATGCAA	400
pRAp37-60	AGGTGAAAAA	GTTAACAAAG	AAGTTATTTA	TACATTTTTA	GAAAAATTTCA	AAAAAGAATT	TAATAAACTC	AAAAATGCAA	400
pRAp37-80	AGGTGAAAAA	GTTAACAAAG	AAGTTATTTA	TACATTTTTA	GAAAAATTTCA	AAAAAGAATT	TAATAAACTC	AAAAATGCAA	400
pRAp37-105	AGGTGAAAAA	GTTAACAAAG	AAGTTATTTA	TACATTTTTA	GAAAAATTTCA	AAAAAGAATT	TAATAAACTC	AAAAATGCAA	400
		200		220		240		260	
p37	ATGATAAAAC	CAAAAACTTC	GATGACGTTG	ATTTTAAAGT	AACCTCCAAT	CAAGACTTTA	CTGTGTTGTT	AAACAATTTA	272
pRAp37-20	ATGATAAAAC	CAAAAACTTC	GATGACGTTG	ATTTTAAAGT	AACCTCCAAT	CAAGACTTTA	CTGTGTTGTT	AAACAATTTA	480
pRAp37-60	ATGATAAAAC	CAAAAACTTC	GATGACGTTG	ATTTTAAAGT	AACCTCCAAT	CAAGACTTTA	CTGTGTTGTT	AAACAATTTA	480
pRAp37-80	ATGATAAAAC	CAAAAACTTC	GATGACGTTG	ATTTTAAAGT	AACCTCCAAT	CAAGACTTTA	CTGTGTTGTT	AAACAATTTA	480
pRAp37-105	ATGATAAAAC	CAAAAACTTC	GATGACGTTG	ATTTTAAAGT	AACCTCCAAT	CAAGACTTTA	CTGTGTTGTT	AAACAATTTA	480
		280		300		320		340	
p37	TCTACTGACA	ATCCTGAATT	AGATTTTGGG	ATTAATGCTT	CAGGAAAAAT	GGTAGAATTT	CTAAAAAATA	ATCCTGGTAT	352
pRAp37-20	TCTACTGACA	ATCCTGAATT	AGATTTTGGG	ATTAATGCTT	CAGGAAAAAT	GGTAGAATTT	CTAAAAAATA	ATCCTGGTAT	560
pRAp37-60	TCTACTGACA	ATCCTGAATT	AGATTTTGGG	ATTAATGCTT	CAGGAAAAAT	GGTAGAATTT	CTAAAAAATA	ATCCTGGTAT	560
pRAp37-80	TCTACTGACA	ATCCTGAATT	AGATTTTGGG	ATTAATGCTT	CAGGAAAAAT	GGTAGAATTT	CTAAAAAATA	ATCCTGGTAT	560
pRAp37-105	TCTACTGACA	ATCCTGAATT	AGATTTTGGG	ATTAATGCTT	CAGGAAAAAT	GGTAGAATTT	CTAAAAAATA	ATCCTGGTAT	560
		360		380		400		420	
p37	AATAACTCCA	GCATTAGAAA	CAACAACCTAA	TTCTTTTGTA	TTTGACAAAG	AAAAAGATAA	ATTTTATGTT	GATGGTACAG	432
pRAp37-20	AATAACTCCA	GCATTAGAAA	CAACAACCTAA	TTCTTTTGTA	TTTGACAAAG	AAAAAGATAA	ATTTTATGTT	GATGGTACAG	640
pRAp37-60	AATAACTCCA	GCATTAGAAA	CAACAACCTAA	TTCTTTTGTA	TTTGACAAAG	AAAAAGATAA	ATTTTATGTT	GATGGTACAG	640
pRAp37-80	AATAACTCCA	GCATTAGAAA	CAACAACCTAA	TTCTTTTGTA	TTTGACAAAG	AAAAAGATAA	ATTTTATGTT	GATGGTACAG	640
pRAp37-105	AATAACTCCA	GCATTAGAAA	CAACAACCTAA	TTCTTTTGTA	TTTGACAAAG	AAAAAGATAA	ATTTTATGTT	GATGGTACAG	640
		440		460		480		500	
p37	ATTCAGATCC	ACTTGTAATA	ATTGCTAAAG	AAATTAATAA	AATTTTGTGT	GAAACTCCAT	ATGCAAGTTG	GACTGATGAA	512
pRAp37-20	ATTCAGATCC	ACTTGTAATA	ATTGCTAAAG	AAATTAATAA	AATTTTGTGT	GAAACTCCAT	ATGCAAGTTG	GACTGATGAA	720
pRAp37-60	ATTCAGATCC	ACTTGTAATA	ATTGCTAAAG	AAATTAATAA	AATTTTGTGT	GAAACTCCAT	ATGCAAGTTG	GACTGATGAA	720
pRAp37-80	ATTCAGATCC	ACTTGTAATA	ATTGCTAAAG	AAATTAATAA	AATTTTGTGT	GAAACTCCAT	ATGCAAGTTG	GACTGATGAA	720
pRAp37-105	ATTCAGATCC	ACTTGTAATA	ATTGCTAAAG	AAATTAATAA	AATTTTGTGT	GAAACTCCAT	ATGCAAGTTG	GACTGATGAA	720
		520		540		560		580	
p37	AATCATAAGT	GGAATGGTAA	TGTTTATCAA	AGTGTTTACG	ATCCAACGTG	TCAAGCTAAT	TTTTATAGAG	GAATGATTTG	592
pRAp37-20	AATCATAAGT	GGAATGGTAA	TGTTTATCAA	AGTGTTTACG	ATCCAACGTG	TCAAGCTAAT	TTTTATAGAG	GAATGATTTG	800
pRAp37-60	AATCATAAGT	GGAATGGTAA	TGTTTATCAA	AGTGTTTACG	ATCCAACGTG	TCAAGCTAAT	TTTTATAGAG	GAATGATTTG	800
pRAp37-80	AATCATAAGT	GGAATGGTAA	TGTTTATCAA	AGTGTTTACG	ATCCAACGTG	TCAAGCTAAT	TTTTATAGAG	GAATGATTTG	800
pRAp37-105	AATCATAAGT	GGAATGGTAA	TGTTTATCAA	AGTGTTTACG	ATCCAACGTG	TCAAGCTAAT	TTTTATAGAG	GAATGATTTG	800
		600		620		640		660	
p37	GATAAAAGGT	AATGATGAAA	CTCTAGCTAA	AATTAATAAA	GCTTGGAAATG	ATAAAGATTG	GAATACATTT	AGAAATTTTG	672
pRAp37-20	GATAAAAGGT	AATGATGAAA	CTCTAGCTAA	AATTAATAAA	GCTTGGAAATG	ATAAAGATTG	GAATACATTT	AGAAATTTTG	880
pRAp37-60	GATAAAAGGT	AATGATGAAA	CTCTAGCTAA	AATTAATAAA	GCTTGGAAATG	ATAAAGATTG	GAATACATTT	AGAAATTTTG	880
pRAp37-80	GATAAAAGGT	AATGATGAAA	CTCTAGCTAA	AATTAATAAA	GCTTGGAAATG	ATAAAGATTG	GAATACATTT	AGAAATTTTG	880
pRAp37-105	GATAAAAGGT	AATGATGAAA	CTCTAGCTAA	AATTAATAAA	GCTTGGAAATG	ATAAAGATTG	GAATACATTT	AGAAATTTTG	880
		680		700		720		740	
p37	GAATTTTACA	CGGTAAGAT	AATTCCTTTT	CTAAATTTCA	GTTAGAAGAA	ACTATATTTA	AAAACCCTT	TCAAAATAAA	752
pRAp37-20	GAATTTTACA	CGGTAAGAT	AATTCCTTTT	CTAAATTTCA	GTTAGAAGAA	ACTATATTTA	AAAACCCTT	TCAAAATAAA	960
pRAp37-60	GAATTTTACA	CGGTAAGAT	AATTCCTTTT	CTAAATTTCA	GTTAGAAGAA	ACTATATTTA	AAAACCCTT	TCAAAATAAA	960
pRAp37-80	GAATTTTACA	CGGTAAGAT	AATTCCTTTT	CTAAATTTCA	GTTAGAAGAA	ACTATATTTA	AAAACCCTT	TCAAAATAAA	960
pRAp37-105	GAATTTTACA	CGGTAAGAT	AATTCCTTTT	CTAAATTTCA	GTTAGAAGAA	ACTATATTTA	AAAACCCTT	TCAAAATAAA	960
		760		780		800		820	
p37	TTTACAACAC	TAAATGAAGA	CAGAAGCGCA	CATCCAAACG	CATATAAACA	AAAATCTGCA	GATACATTGG	GAACCTTTGA	832
pRAp37-20	TTTACAACAC	TAAATGAAGA	CAGAAGCGCA	CATCCAAACG	CATATAAACA	AAAATCTGCA	GATACATTGG	GAACCTTTGA	1040
pRAp37-60	TTTACAACAC	TAAATGAAGA	CAGAAGCGCA	CATCCAAACG	CATATAAACA	AAAATCTGCA	GATACATTGG	GAACCTTTGA	1040
pRAp37-80	TTTACAACAC	TAAATGAAGA	CAGAAGCGCA	CATCCAAACG	CATATAAACA	AAAATCTGCA	GATACATTGG	GAACCTTTGA	1040
pRAp37-105	TTTACAACAC	TAAATGAAGA	CAGAAGCGCA	CATCCAAACG	CATATAAACA	AAAATCTGCA	GATACATTGG	GAACCTTTGA	1040

		840		860		880		900	
p37	TGATTTCCAT	ATTGCTTTTT	CAGAAGAAGG	TTCTTTTGCT	TGGACACATA	ACAAATCAGC	AACAAAACCT	TTTGAAACTA	912
pRAp37-20	TGATTTCCAT	ATTGCTTTTT	CAGAAGAAGG	TTCTTTTGCT	TGGACACATA	ACAAATCAGC	AACAAAACCT	TTTGAAACTA	1120
pRAp37-60	TGATTTCCAT	ATTGCTTTTT	CAGAAGAAGG	TTCTTTTGCT	TGGACACATA	ACAAATCAGC	AACAAAACCT	TTTGAAACTA	1120
pRAp37-80	TGATTTCCAT	ATTGCTTTTT	CAGAAGAAGG	TTCTTTTGCT	TGGACACATA	ACAAATCAGC	AACAAAACCT	TTTGAAACTA	1110
pRAp37-105	-----	-----	-----	-----	-----	-----	-----	-----	1035
		840		860		880		900	
p37	TGATTTCCAT	ATTGCTTTTT	CAGAAGAAGG	TTCTTTTGCT	TGGACACATA	ACAAATCAGC	AACAAAACCT	TTTGAAACTA	912
pRAp37-20	TGATTTCCAT	ATTGCTTTTT	CAGAAGAAGG	TTCTTTTGCT	TGGACACATA	ACAAATCAGC	AACAAAACCT	TTTGAAACTA	1120
pRAp37-60	TGATTTCCAT	ATTGCTTTTT	CAGAAGAAGG	TTCTTTTGCT	TGGACACATA	ACAAATCAGC	AACAAAACCT	TTTGAAACTA	1120
pRAp37-80	TGATTTCCAT	ATTGCTTTTT	CAGAAGAAGG	TTCTTTTGCT	TGGACACATA	ACAAATCAGC	AACAAAACCT	TTTGAAACTA	1110
pRAp37-105	-----	-----	-----	-----	-----	-----	-----	-----	1035
		920		940		960		980	
p37	AAGCAAATGA	AAAGATGGAA	GCACTTATAG	TAACATAATCC	AATTCGGTAT	GATGTTGGAG	TGTTTAGAAA	AAGTGTTAAC	992
pRAp37-20	AAGCAAATGA	AAAGATGGAA	GCACTTATAG	TAACATAATCC	AATTCGGTAT	GATGTTGGAG	TGTTTAGAAA	AAGTGTTAAC	1200
pRAp37-60	AAGCAAATGA	AAAGATGGAA	GCACTTATAG	TAACATAATCC	AATTCGGTAT	-----	-----	-----	1170
pRAp37-80	-----	-----	-----	-----	-----	-----	-----	-----	1110
pRAp37-105	-----	-----	-----	-----	-----	-----	-----	-----	1035
		1,000		1,020		1,040		1,060	
p37	CAATTAGAAC	AAAATTTAAT	TGTTCAAACA	TTCATTAATT	TAGCTAAAAA	TAAACAAGAT	ACATATGGCC	CACTTTTAGG	1072
pRAp37-20	CAATTAGAAC	AAAATTTAAT	TGTTCAAACA	TTCATTAATT	TAGCTAAAAA	TAAACAAGAT	ACATATGGCC	CACTTTTAGG	1280
pRAp37-60	-----	-----	-----	-----	-----	-----	-----	-----	1170
pRAp37-80	-----	-----	-----	-----	-----	-----	-----	-----	1110
pRAp37-105	-----	-----	-----	-----	-----	-----	-----	-----	1035
		1,080		1,100		1,120		1,140	
p37	GTATAATGGT	TATAAAAAAA	TTGACAATTT	CCAAAAAGAG	ATTGTAGAAG	TTTATGAAAA	AGCCATTAAA	TAA-----	1145
pRAp37-20	GTATAATGGT	-----	-----	-----	-----	-----	-----	TAAACCATGGA	1300
pRAp37-60	-----	-----	-----	-----	-----	-----	-----	TAAACCATGGA	1180
pRAp37-80	-----	-----	-----	-----	-----	-----	-----	TAAACCATGGA	1120
pRAp37-105	-----	-----	-----	-----	-----	-----	-----	TAAACCATGGA	1045
		1,160		1,180		1,200		1,220	
p37	-----	-----	-----	-----	-----	-----	-----	-----	1145
pRAp37-20	ATTCGAAGCT	TGATCCGGCT	GCTAACAAAG	CCCAAAAGGA	AGCTGAGTTG	GCTGCTGCCA	CCGCTGAGCA	ATAACTAGCA	1380
pRAp37-60	ATTCGAAGCT	TGATCCGGCT	GCTAACAAAG	CCCAAAAGGA	AGCTGAGTTG	GCTGCTGCCA	CCGCTGAGCA	ATAACTAGCA	1260
pRAp37-80	ATTCGAAGCT	TGATCCGGCT	GCTAACAAAG	CCCAAAAGGA	AGCTGAGTTG	GCTGCTGCCA	CCGCTGAGCA	ATAACTAGCA	1200
pRAp37-105	ATTCGAAGCT	TGATCCGGCT	GCTAACAAAG	CCCAAAAGGA	AGCTGAGTTG	GCTGCTGCCA	CCGCTGAGCA	ATAACTAGCA	1125
		1,240		1,260					
p37	-----	-----	-----	-----	-----	-----	-----	-----	1145
pRAp37-20	TAACCCCTTG	GGGCCTCTAA	ACGGGTCTTG	AGG	AGG	AGG	AGG	AGG	1413
pRAp37-60	TAACCCCTTG	GGGCCTCTAA	ACGGGTCTTG	AGG	AGG	AGG	AGG	AGG	1293
pRAp37-80	TAACCCCTTG	GGGCCTCTAA	ACGGGTCTTG	AGG	AGG	AGG	AGG	AGG	1233
pRAp37-105	TAACCCCTTG	GGGCCTCTAA	ACGGGTCTTG	AGG	AGG	AGG	AGG	AGG	1158

Appendix XXII

Affect of gudHCL purified p37 and truncated p37 protein on gene expression discussed in Section 7.2.4.

NIH3T3 cells were treated with 25µg/ml gudHCL purified truncated p37-20 and p37-105, the shortest and longest truncations, respectively, for 24hrs. As a control 25µg/ml gudHCL purified wild type p37 protein was also incubated with NIH3T3 cells for 24hr. Quantitative (q) PCR was used to analyse mRNA expression (Section 2.12) of eight selected genes whose expression was previously found to be significantly increased with 25µg/ml p37 treatment (24hr). None of these purified proteins (including wt. p37) induced expression of the eight genes tested (Figure 10.1). Hence, denaturing the protein using gudHCL treatment is predicted to have affected protein structure and re-folding was presumably inadequate.

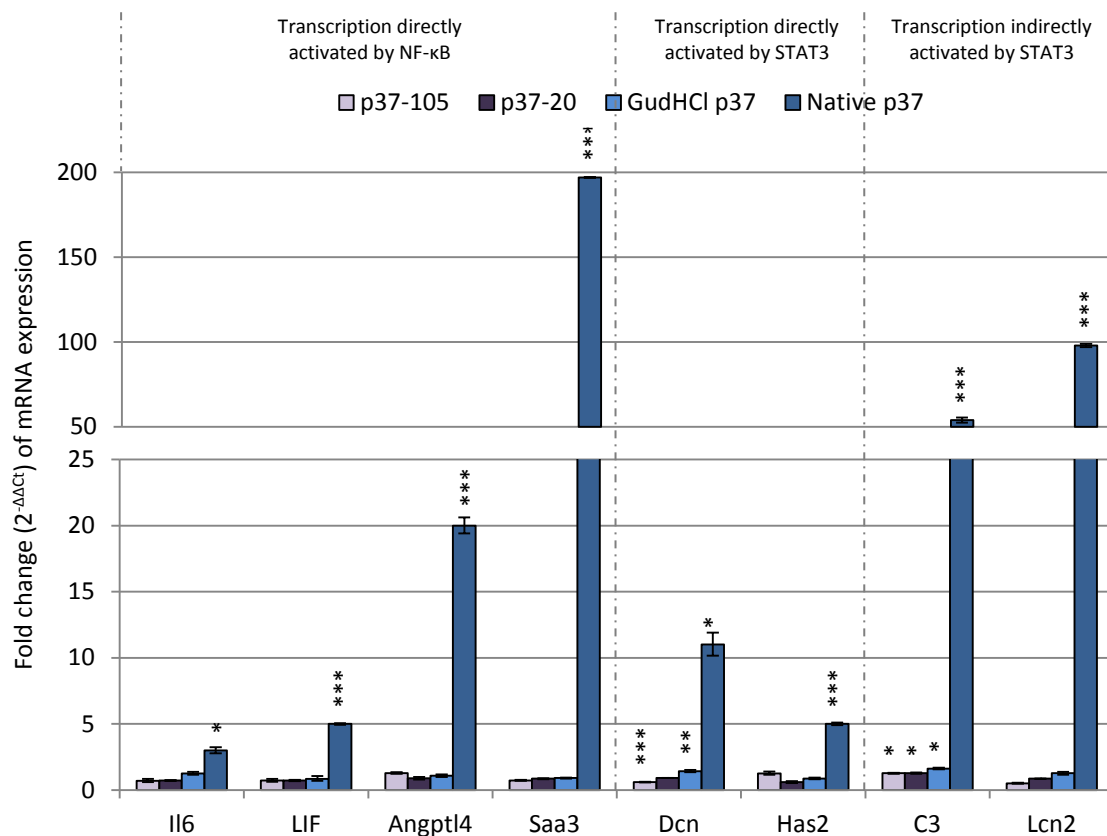


Figure 10.1: Affect of gudHCL purified native and truncated p37 protein on gene expression. NIH3T3 cells treated with either gudHCL purified p37-105, -20 and p37 for 24hr. Fold change ($2^{-\Delta\Delta C_t}$) is relative to untreated controls, normalised to reference genes *GAPDH* and *βactin* (Section 2.12). Significant differences between treated and untreated cells were calculated by ANOVA analysis (* $p < 0.05$, ** $p < 0.01$, *** $p < 0.001$) and error bars depict \pm SE in relation to fold change (Section 2.12.8). Fold change data of 24hr 25µg/ml p37 treated NIH3T3 cells from Chapter 3. Raw data presented in Appendix XXII, located on attached CD.

Appendix XXIII

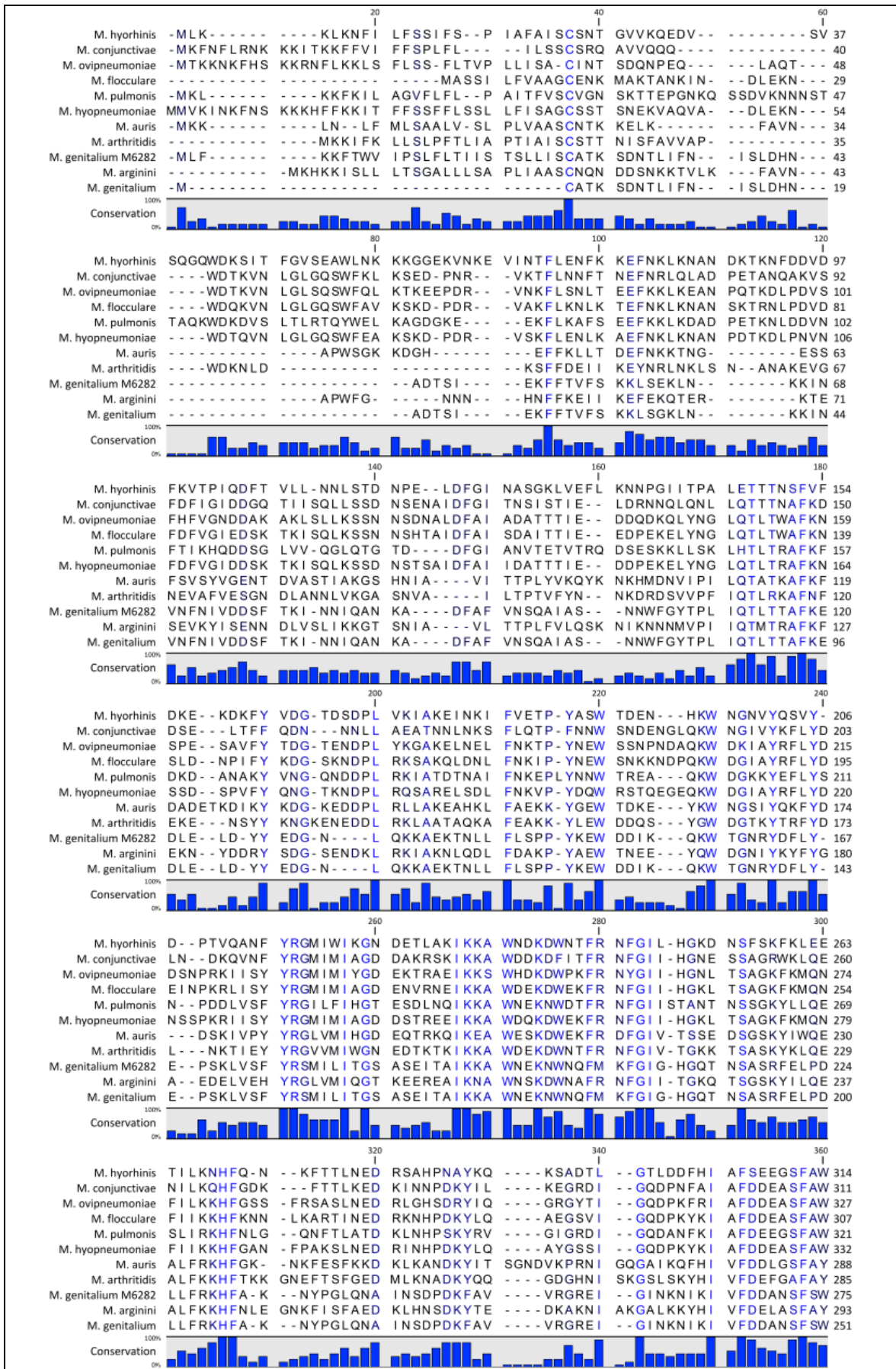
Raw data of affect of arginine soak purified truncated p37 on gene expression presented in Figure 7.13.

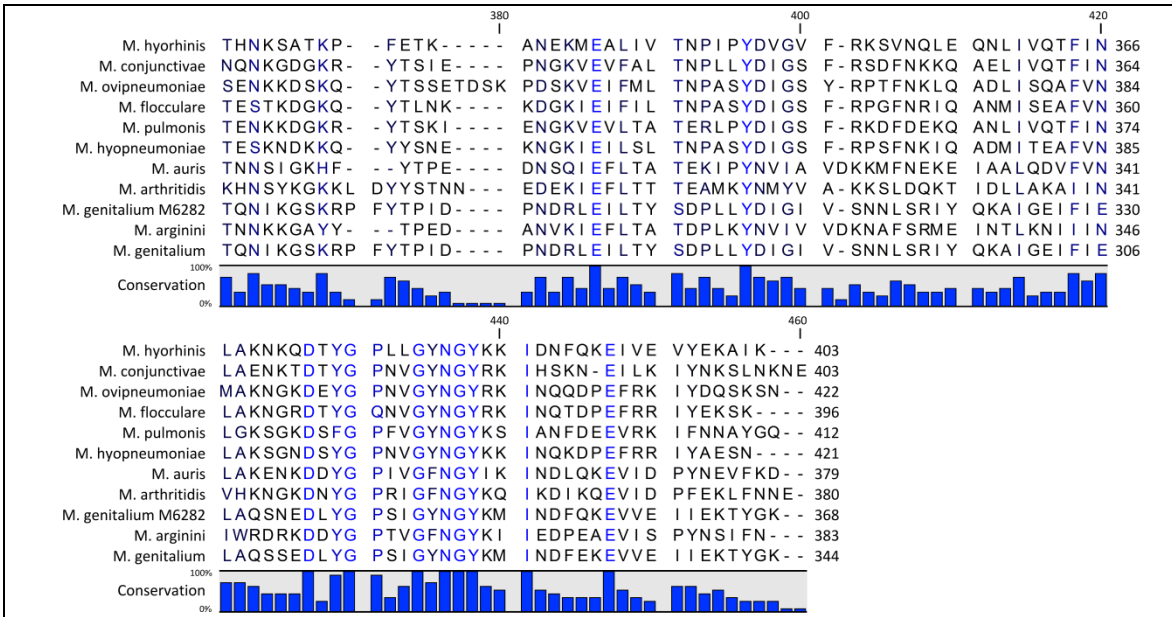
Located on attached CD

Appendix XXIV

Alignments of BLASTp hits against the full-length *Mycoplasma hyorhinis* p37 protein sequence and the raw data associated with the alignments presented in Table 7.6.

Mycoplasma species	Protein (Accession Number)	Score (Bits)	E-value	Identity	Positives	Gaps
<i>M. hyorhinis</i>	p37 (CAA32357.1)	N/A	N/A	N/A	N/A	N/A
<i>M. conjunctivae</i> HRC/581	putative P37-like ABC transporter substrate-bi (YP_002960563.1)	288	2E-92	178/404 (44%)	251/404 (62%)	30/404 (7%)
<i>M. ovipneumoniae</i>	DNA repair protein HhH-GPD (WP_010321138.1)	272	3E-86	158/413 (38%)	235/413 (56%)	24/413 (5%)
<i>M. flocculare</i>	P37-like ABC transporter substrate-binding lipoprotein (WP_002557691.1)	271	5E-86	157/400 (39%)	231/400 (57%)	21/400 (5%)
<i>M. pulmonis</i>	lipoprotein ABC transporter substrate -binding protein (WP_010925029.1)	268	1E-84	162/415 (39%)	240/415 (57%)	24/415 (5%)
<i>M. hyopneumoniae</i> 7448	P37-like ABC transporter substrate-binding lipoprotein (YP_287754.1)	266	6E-84	156/392 (40%)	230/392 (58%)	22/392 (5%)
<i>M. auris</i>	Alkylphosphonate ABC transporter, substrate-binding protein (PhnD) (WP_004423763.1)	210	5E-63	133/412 (32%)	213/412 (51%)	44/412 (10%)
<i>M. arthritidis</i> 158L3-1	P37-like ABC transporter substrate-binding lipoprotein (YP_001999750.1)	202	5E-60	139/410 (34%)	215/410 (52%)	52/410 (12%)
<i>M. genitalium</i> M6282	alkylphosphonate ABC transporter substrate-binding protein (YP_006600321.1)	200	4E-59	102/263 (39%)	157/263 (59%)	8/263 (3%)
<i>M. arginini</i>	Alkylphosphonate ABC transporter, substrate-binding component (WP_004416279.1)	199	8E-59	110/274 (40%)	165/274 (60%)	13/274 (4%)
<i>M. genitalium</i>	MG289 Chain A (3MYU)	198	8E-59	101/262 (39%)	157/262 (59%)	8/262 (3%)

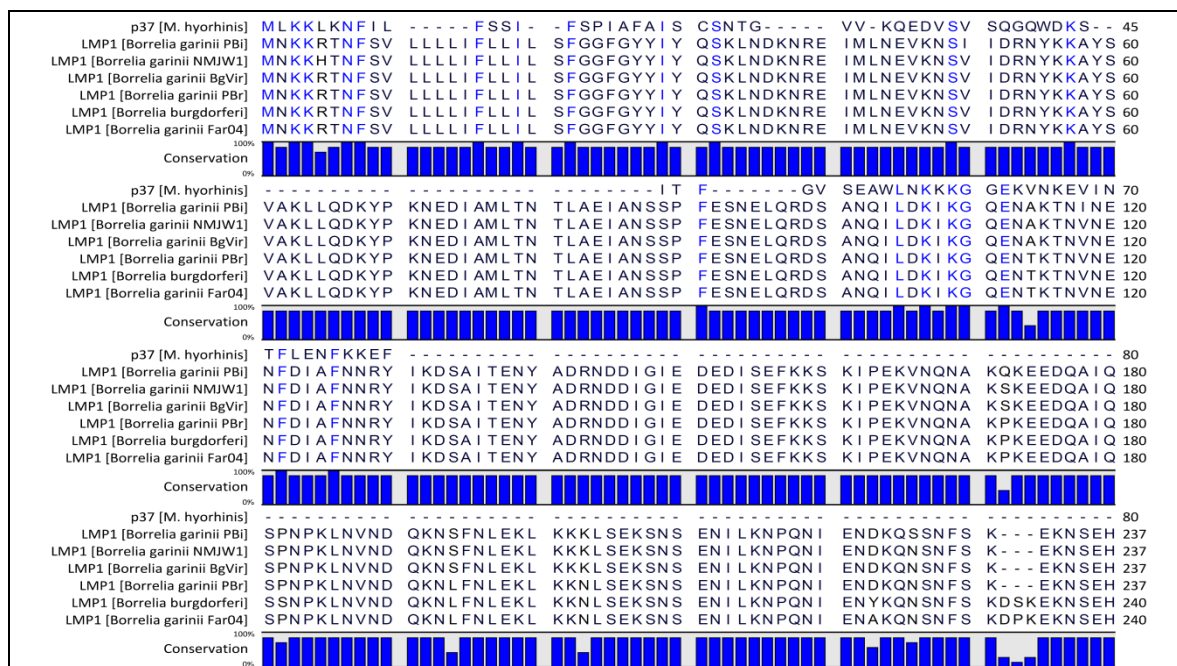




Appendix XXV

Alignments of BLASTp hits against the *Mycoplasma hyorhinis* p37 C-terminal 20aa and the raw data associated with the alignments presented in Table 8.7.

Mycoplasma species	Protein (Accession Number)	Score (bits)	E-value	Identity	Positives	Gaps
<i>Mycoplasma genitalium</i> M6282	alkylphosphonate ABC transporter substrate-binding protein (YP_006600321.1)	40.1	0.013	11/17 (65%)	15/17 (88%)	0/17 (0%)
<i>Mycoplasma genitalium</i> M2321	alkylphosphonate ABC transporter substrate-binding protein (YP_006599832.1)	38.4	0.044	11/21 (52%)	16/21 (76%)	4/21 (19%)
<i>Borrelia garinii</i> PBi	surface-located membrane protein 1 (YP_072659.1)	37.5	0.086	13/20 (65%)	16/20 (80%)	1/20 (5%)
<i>Borrelia garinii</i> NMJW1	surface-located membrane protein 1 (YP_006870908.1)	37.5	0.086	13/20 (65%)	16/20 (80%)	1/20 (5%)
<i>Borrelia garinii</i> BgVir	LMP1 (YP_006202902.1)	37.5	0.086	13/20 (65%)	16/20 (80%)	1/20 (5%)
<i>Borrelia garinii</i> PBr	tetratricopeptide repeat domain protein (ZP_03539481.1)	37.5	0.086	13/20 (65%)	16/20 (80%)	1/20 (5%)
<i>Borrelia burgdorferi</i>	LMP1 (AAK18802)	37.5	0.086	13/20 (65%)	16/20 (80%)	1/20 (5%)
<i>Borrelia garinii</i>	hypothetical protein (WP_004793842.1)	37.5	0.086	13/20 (65%)	16/20 (80%)	1/20 (5%)
<i>Mycoplasma genitalium</i> Mg289	Chain A (3MYU_A)	37.1	0.11	10/17 (59%)	15/17 (88%)	0/17 (0%)
<i>Mycoplasma genitalium</i> G37	phosphonate ABC transporter substrate-binding protein (NP_072955.1)	37.1	0.11	10/17 (59%)	15/17 (88%)	0/17 (0%)





Appendix XXVI

Sequence of the pSTp37 construct used for lipofection of NIH3T3 cells. TheTGA to TGG mutations are shaded blue.

pSecTag	GACGGATCGG	GAGATCTCCC	GATCCCCTAT	GGTCGACTCT	CAGTACAATC	TGCTCTGATG	60
p37	-----	-----	-----	-----	-----	-----	-----
pSTp37	GACGGATCGG	GAGATCTCCC	GATCCCCTAT	GGTCGACTCT	CAGTACAATC	TGCTCTGATG	60
pSecTag	CCGCATAGTT	AAGCCAGTAT	CTGCTCCCTG	CTTGTGTGTT	GGAGGTCGCT	GAGTAGTGCG	120
p37	-----	-----	-----	-----	-----	-----	-----
pSTp37	CCGCATAGTT	AAGCCAGTAT	CTGCTCCCTG	CTTGTGTGTT	GGAGGTCGCT	GAGTAGTGCG	120
pSecTag	CGAGCAAAAT	TTAAGCTACA	ACAAGGCAAG	GCTTGACCGA	CAATTGCATG	AAGAATCTGC	180
p37	-----	-----	-----	-----	-----	-----	-----
pSTp37	CGAGCAAAAT	TTAAGCTACA	ACAAGGCAAG	GCTTGACCGA	CAATTGCATG	AAGAATCTGC	180
pSecTag	TTAGGGTTAG	GCGTTTTGCG	CTGCTTCGCG	ATGTACGGGC	CAGATATACG	CGTTGACATT	240
p37	-----	-----	-----	-----	-----	-----	-----
pSTp37	TTAGGGTTAG	GCGTTTTGCG	CTGCTTCGCG	ATGTACGGGC	CAGATATACG	CGTTGACATT	240
pSecTag	GATTATTGAC	TAGTTATTA	TAGTAATCAA	TTACGGGGTC	ATTAGTTCAT	AGCCCATATA	300
p37	-----	-----	-----	-----	-----	-----	-----
pSTp37	GATTATTGAC	TAGTTATTA	TAGTAATCAA	TTACGGGGTC	ATTAGTTCAT	AGCCCATATA	300
pSecTag	TGGAGTTCCG	CGTTACATA	CCTACGGTAA	ATGGCCCGCC	TGGCTGACCG	CCCAACGACC	360
p37	-----	-----	-----	-----	-----	-----	-----
pSTp37	TGGAGTTCCG	CGTTACATA	CCTACGGTAA	ATGGCCCGCC	TGGCTGACCG	CCCAACGACC	360
pSecTag	CCCGCCCATT	GACGTCAATA	ATGACGTATG	TTCCCATAGT	AACGCCAATA	GGGACTTTCC	420
p37	-----	-----	-----	-----	-----	-----	-----
pSTp37	CCCGCCCATT	GACGTCAATA	ATGACGTATG	TTCCCATAGT	AACGCCAATA	GGGACTTTCC	420
pSecTag	ATTGACGTCA	ATGGGTGGAC	TATTTACGGT	AAACTGCCCA	CTTGGCAGTA	CATCAAGTGT	480
p37	-----	-----	-----	-----	-----	-----	-----
pSTp37	ATTGACGTCA	ATGGGTGGAC	TATTTACGGT	AAACTGCCCA	CTTGGCAGTA	CATCAAGTGT	480
pSecTag	ATCATATGCC	AAGTACGCC	CCTATTGACG	TCAATGACGG	TAAATGGCCC	GCCTGGCATT	540
p37	-----	-----	-----	-----	-----	-----	-----
pSTp37	ATCATATGCC	AAGTACGCC	CCTATTGACG	TCAATGACGG	TAAATGGCCC	GCCTGGCATT	540
pSecTag	ATGCCCAGTA	CATGACCTTA	TGGGACTTTC	CTACTTGGCA	GTACATCTAC	GTATTAGTCA	600
p37	-----	-----	-----	-----	-----	-----	-----
pSTp37	ATGCCCAGTA	CATGACCTTA	TGGGACTTTC	CTACTTGGCA	GTACATCTAC	GTATTAGTCA	600
pSecTag	TCGCTATTAC	CATGGTGATG	CGGTTTTGGC	AGTACATCAA	TGGGCGTGGA	TAGCGTTTTG	660
p37	-----	-----	-----	-----	-----	-----	-----
pSTp37	TCGCTATTAC	CATGGTGATG	CGGTTTTGGC	AGTACATCAA	TGGGCGTGGA	TAGCGTTTTG	660
pSecTag	ACTCACGGGG	ATTTCCAAGT	CTCCACCCCA	TTGACGTCAA	TGGGAGTTTG	TTTTGGCACC	720
p37	-----	-----	-----	-----	-----	-----	-----
pSTp37	ACTCACGGGG	ATTTCCAAGT	CTCCACCCCA	TTGACGTCAA	TGGGAGTTTG	TTTTGGCACC	720
pSecTag	AAAATCAACG	GGACTTTCCA	AAATGTCGTA	ACAACCTCCG	CCCATTGACG	CAAATGGGCG	780
p37	-----	-----	-----	-----	-----	-----	-----
pSTp37	AAAATCAACG	GGACTTTCCA	AAATGTCGTA	ACAACCTCCG	CCCATTGACG	CAAATGGGCG	780
pSecTag	GTAGGCGTGT	ACGGTGGGAG	GTCTATATAA	GCAGAGCTCT	CTGGCTAACT	AGAGAACCCA	840
p37	-----	-----	-----	-----	-----	-----	-----
pSTp37	GTAGGCGTGT	ACGGTGGGAG	GTCTATATAA	GCAGAGCTCT	CTGGCTAACT	AGAGAACCCA	840
pSecTag	CTGCTTACTG	GCTTATCGAA	ATTAATACGA	CTCACTATAG	GGAGACCCAA	GCTGGCTAGC	900
p37	-----	-----	-----	-----	-----	-----	-----
pSTp37	CTGCTTACTG	GCTTATCGAA	ATTAATACGA	CTCACTATAG	GGAGACCCAA	GCTGGCTAGC	900

pSecTag	CACCATGGAG	ACAGACACAC	TCCTGCTATG	GGTACTGCTG	CTCTGGGTTG	CAGGTTCCAC	960
p37	-----	-----	-----	-----	-----	-----	
pSTp37	CACCATGGAG	ACAGACACAC	TCCTGCTATG	GGTACTGCTG	CTCTGGGTTG	CAGGTTCCAC	960
pSecTag	TGGTGACGCG	GCCCAGCCGG	CCAGGCGCGC	GCGCCGTACG	AAGCTTGGTA	CCGAGCTCGG	1020
p37	-----	-----	-----	-----	-----	-----	
pSTp37	TGGTGACGCG	GCCCAGCCGG	CCAGGCGCGC	GCGCCGTACG	AAGCTTGGTA	CCGAGCTCGG	1020
pSecTag	ATCCAC	-----	-----	-----	-----	-----	1026
p37	-----CATGT	TCTAATACAG	GAGTAGTCAA	GCAAGAGGAT	GTATCAGTTA	GTCAAGGTCA	55
pSTp37	ATCCACATGT	TCTAATACAG	GAGTAGTCAA	GCAAGAGGAT	GTATCAGTTA	GTCAAGGTCA	1080
pSecTag	-----	-----	-----	-----	-----	-----	1026
p37	ATGAGATAAA	AGTATAACAT	TTGGTGT TTC	AGAAGCTTGG	TTAAACAAGA	AAAAAGGAGG	115
pSTp37	ATGGAGATAAA	AGTATAACAT	TTGGTGT TTC	AGAAGCTTGG	TTAAACAAGA	AAAAAGGAGG	1140
pSecTag	-----	-----	-----	-----	-----	-----	1026
p37	TGAAAAAGTT	AACAAAGAAG	TTATTAATAC	ATTTTTAGAA	AATTTCAAAA	AAGAATTTAA	175
pSTp37	TGAAAAAGTT	AACAAAGAAG	TTATTAATAC	ATTTTTAGAA	AATTTCAAAA	AAGAATTTAA	1200
pSecTag	-----	-----	-----	-----	-----	-----	1026
p37	TAAACTCAAA	AATGCAAATG	ATAAAACCAA	AAACTTCGAT	GACGTTGATT	TTAAAGTAAC	235
pSTp37	TAAACTCAAA	AATGCAAATG	ATAAAACCAA	AAACTTCGAT	GACGTTGATT	TTAAAGTAAC	1260
pSecTag	-----	-----	-----	-----	-----	-----	1026
p37	TCCAATTCAA	GACTTTACTG	TGTTGT TAAA	CAATTTATCT	ACTGACAATC	CTGAATTAGA	295
pSTp37	TCCAATTCAA	GACTTTACTG	TGTTGT TAAA	CAATTTATCT	ACTGACAATC	CTGAATTAGA	1320
pSecTag	-----	-----	-----	-----	-----	-----	1026
p37	TTTTGGAATT	AATGCTTCAG	GAAAATTGGT	AGAATTTCTA	AAAAATAATC	CTGGTATAAT	355
pSTp37	TTTTGGAATT	AATGCTTCAG	GAAAATTGGT	AGAATTTCTA	AAAAATAATC	CTGGTATAAT	1380
pSecTag	-----	-----	-----	-----	-----	-----	1026
p37	AACTCCAGCA	TTAGAAACAA	CAACTAATTC	TTTTGTATTT	GACAAAGAAA	AAGATAAATT	415
pSTp37	AACTCCAGCA	TTAGAAACAA	CAACTAATTC	TTTTGTATTT	GACAAAGAAA	AAGATAAATT	1440
pSecTag	-----	-----	-----	-----	-----	-----	1026
p37	TTATGTTGAT	GGTACAGATT	CAGATCCACT	TGTA AAAATT	GCTAAAGAAA	TTAATAAAAT	475
pSTp37	TTATGTTGAT	GGTACAGATT	CAGATCCACT	TGTA AAAATT	GCTAAAGAAA	TTAATAAAAT	1500
pSecTag	-----	-----	-----	-----	-----	-----	1026
p37	TTTTGTTGAA	ACTCCATATG	CAAGTTGAAC	TGATGAAAAT	CATAAGTGAA	ATGGTAATGT	535
pSTp37	TTTTGTTGAA	ACTCCATATG	CAAGTTGGAC	TGATGAAAAT	CATAAGTGGA	ATGGTAATGT	1560
pSecTag	-----	-----	-----	-----	-----	-----	1026
p37	TTATCAAAGT	GTTTACGATC	CAACTGTTCA	AGCTAATTTT	TATAGAGGAA	TGATTTGAAT	595
pSTp37	TTATCAAAGT	GTTTACGATC	CAACTGTTCA	AGCTAATTTT	TATAGAGGAA	TGATTTGGAT	1620
pSecTag	-----	-----	-----	-----	-----	-----	1026
p37	AAAAGGTAAT	GATGAAACTC	TAGCTAAAAT	TAAAAAAGCT	TGAAATGATA	AAGATTGAAA	655
pSTp37	AAAAGGTAAT	GATGAAACTC	TAGCTAAAAT	TAAAAAAGCT	TGGAATGATA	AAGATTGCAA	1680
pSecTag	-----	-----	-----	-----	-----	-----	1026
p37	TACATTTAGA	AATTTTGGAA	TTTTACACGG	TAAAGATAAT	TCTTTTTCTA	AATTC AAGTT	715
pSTp37	TACATTTAGA	AATTTTGGAA	TTTTACACGG	TAAAGATAAT	TCTTTTTCTA	AATTC AAGTT	1740
pSecTag	-----	-----	-----	-----	-----	-----	1026
p37	AGAAGAAACT	ATATTA AAAAA	ACCACTTTCA	AAATAAATTT	ACAACACTAA	ATGAAGACAG	775
pSTp37	AGAAGAAACT	ATATTA AAAAA	ACCACTTTCA	AAATAAATTT	ACAACACTAA	ATGAAGACAG	1800
pSecTag	-----	-----	-----	-----	-----	-----	1026
p37	AAGCGCACAT	CCAAACGCAT	ATAAACAAAA	ATCTGCAGAT	ACATTGGGAA	CTTTAGATGA	835
pSTp37	AAGCGCACAT	CCAAACGCAT	ATAAACAAAA	ATCTGCAGAT	ACATTGGGAA	CTTTAGATGA	1860

		1,880		1,900		1,920	
pSecTag	-----		-----		-----		1026
p37	TTTCCATATT	GCTTTTTTCAG	AAGAAGG TTC	TTTTGCTTGA	ACACATAACA	AATCAGCAAC	895
pSTp37	TTTCCATATT	GCTTTTTTCAG	AAGAAGG TTC	TTTTGCTTGC	ACACATAACA	AATCAGCAAC	1920
		1,940		1,960		1,980	
pSecTag	-----		-----		-----		1026
p37	AAAACCTTTT	GAAACTAAAG	CAAATGAAAA	GATGGAAGCA	CTTATAGTAA	CTAATCCAAT	955
pSTp37	AAAACCTTTT	GAAACTAAAG	CAAATGAAAA	GATGGAAGCA	CTTATAGTAA	CTAATCCAAT	1980
		2,000		2,020		2,040	
pSecTag	-----		-----		-----		1026
p37	TCCGTATGAT	GTTGGAGTGT	TTAGAAAAAG	TGTTAACCAA	TTAGAACAAA	ATTTAATTGT	1015
pSTp37	TCCGTATGAT	GTTGGAGTGT	TTAGAAAAAG	TGTTAACCAA	TTAGAACAAA	ATTTAATTGT	2040
		2,060		2,080		2,100	
pSecTag	-----		-----		-----		1026
p37	TCAAACATTC	ATTAATTTAG	CTAAAAATAA	ACAAGATACA	TATGGCCAC	TTTTAGGGTA	1075
pSTp37	TCAAACATTC	ATTAATTTAG	CTAAAAATAA	ACAAGATACA	TATGGCCAC	TTTTAGGGTA	2100
		2,120		2,140		2,160	
pSecTag	-----		-----		-----		1026
p37	TAATGGTTAT	AAAAAAATTG	ACAATTTCCA	AAAAGAGATT	GTAGAAGTTT	ATGAAAAAGC	1135
pSTp37	TAATGGTTAT	AAAAAAATTG	ACAATTTCCA	AAAAGAGATT	GTAGAAGTTT	ATGAAAAAGC	2160
		2,180		2,200		2,220	
pSecTag	-----CAG	ATATCCAGCA	CAGTGGCGGC	CGCTCGAGGA	GGGCCCGAAC	AAAAACTCAT	1079
p37	CATTAAATAA	-----	-----	-----	-----	-----	1145
pSTp37	CATTAAACAG	ATATCCAGCA	CAGTGGCGGC	CGCTCGAGGA	GGGCCCGAAC	AAAAACTCAT	2220
		2,240		2,260			
pSecTag	CTCAGAAGAG	GATCTGAATA	GCGCCGTCGA	CCATCATCAT	CATCATCATT	GA	1131
p37	-----	-----	-----	-----	-----	---	1145
pSTp37	CTCAGAAGAG	GATCTGAATA	GCGCCGTCGA	CCATCATCAT	CATCATCATT	GA	2272

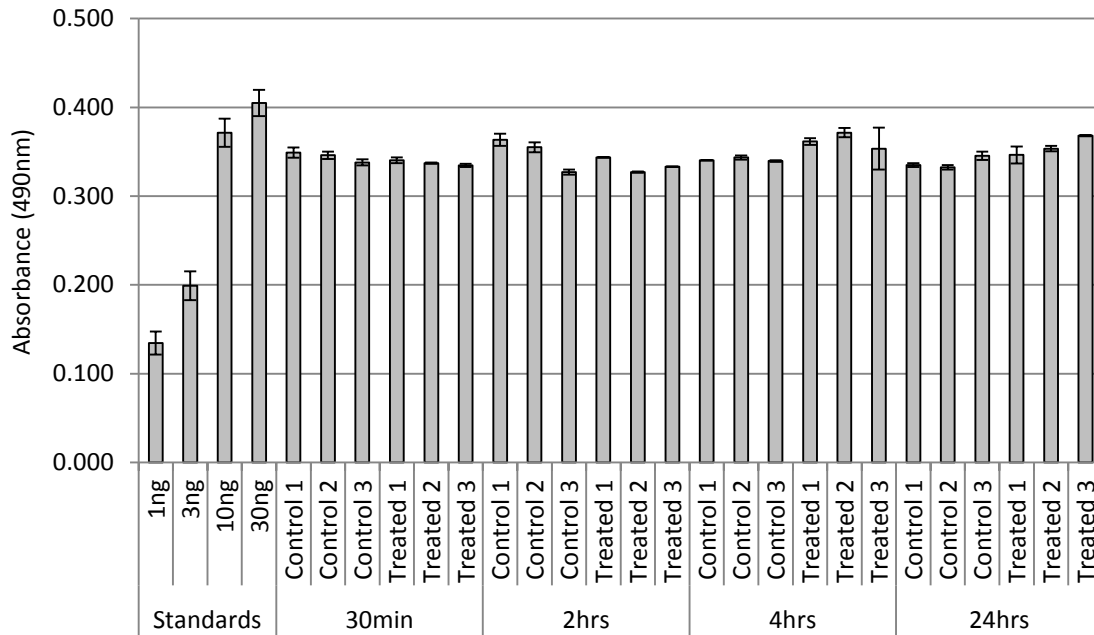
Appendix XXVII

Raw data of surface area (μm^2) covered by p37-treated and p37-transfected migrating cells presented in Figure 8.7 and the rate of cell migration presented in Table 8.1.

Located on attached CD

Appendix XXVIII

Raw data of the levels of total RhoA between the biological replicates and time points of the treated and control cells.



Appendix XXIX

Raw data of normalised active RhoA in p37-treated and non-treated (control) NIH3T3 cells presented in Figure 8.8.

Located on attached CD

Appendix XXX

Raw data of gene expression in p37-transfected NIH3T3 cells presented in Figure 8.9.

Located on attached CD

Appendix XXXI

BLASTp alignment of the *M. hyorhina* p37 protein (Query) and the *M. genitalium* MG309 (Sbjct) indicating no significant alignments.

Range 1: 268 to 304 GenPept Graphics ▼ Next Match ▲ Previous Match					
Score	Expect	Method	Identities	Positives	Gaps
20.0 bits(40)	0.36	Compositional matrix adjust.	13/38(34%)	18/38(47%)	1/38(2%)
Query 286	NAYKQKSADILGTLDDFHIAFSEEGSFAWTHNKSAIKP 323				
	N Y Q+ G + FHI S S+ T+NK+ P				
Sbjct 268	NKYNQQDNSIKGA-NGFHILASNLQSYVNTNNKTIDIP 304				
Range 2: 325 to 366 GenPept Graphics ▼ Next Match ▲ Previous Match ▲ First Match					
Score	Expect	Method	Identities	Positives	Gaps
18.9 bits(37)	0.89	Compositional matrix adjust.	9/42(21%)	20/42(47%)	0/42(0%)
Query 205	VYDPTVQANFYRGMWIKGNDETAKIKKAWNDKDWNTFRNF 246				
	+DP+ A F +G + ++ + + + +KD + NF				
Sbjct 325	TFDPSFSAAFIQGYLALQKKSKEAEQTEYTKLEKDKSIIENF 366				
Range 3: 914 to 925 GenPept Graphics ▼ Next Match ▲ Previous Match ▲ First Match					
Score	Expect	Method	Identities	Positives	Gaps
17.3 bits(33)	2.9	Compositional matrix adjust.	5/12(42%)	9/12(75%)	0/12(0%)
Query 310	GSFAWTHNKSAT 321				
	++ WT+NK+ T				
Sbjct 914	SAYNWNNKTPT 925				
Range 4: 838 to 857 GenPept Graphics ▼ Next Match ▲ Previous Match ▲ First Match					
Score	Expect	Method	Identities	Positives	Gaps
16.9 bits(32)	3.1	Compositional matrix adjust.	9/20(45%)	11/20(55%)	0/20(0%)
Query 134	LKNNPGIITPALETTNSFV 153				
	LKN + L ITNSF+				
Sbjct 838	LKNLQNLQAKLSRTNSFL 857				
Range 5: 756 to 766 GenPept Graphics ▼ Next Match ▲ Previous Match ▲ First Match					
Score	Expect	Method	Identities	Positives	Gaps
16.2 bits(30)	5.9	Compositional matrix adjust.	4/11(36%)	9/11(81%)	0/11(0%)
Query 234	AWNDKDWNTFR 244				
	+ N+++WN F+				
Sbjct 756	SLNNENWNIFK 766				
Range 6: 1093 to 1109 GenPept Graphics ▼ Next Match ▲ Previous Match ▲ First Match					
Score	Expect	Method	Identities	Positives	Gaps
15.8 bits(29)	7.9	Compositional matrix adjust.	9/17(53%)	11/17(64%)	2/17(11%)
Query 82	KLKNANDKT--KNFDDV 96				
	+LK A KT NF+DV				
Sbjct 1093	QLKQAQSKTNNNSNFNDV 1109				

BIBLIOGRAPHY

- Abdollahi-Roodsaz, S., Joosten, L.A., Roelofs, M.F., Radstake, T.R., Matera, G., Popa, C., van der Meer, J.W., Netea, M.G., and van den Berg, W.B. (2007). Inhibition of Toll-like receptor 4 breaks the inflammatory loop in autoimmune destructive arthritis. *Arthritis and Rheumatism* 56(9): 2957-2967.
- Abercrombie, M. (1979). Contact inhibition and malignancy. *Nature* 281: 259-262.
- Abercrombie, M., and Heaysman, J.E. (1953). Observations on the social behaviour of cells in tissue culture. I. Speed of movement of chick heart fibroblasts in relation to their mutual contacts. *Experimental Cell Research* 5(1): 111-131.
- Abercrombie, M., and Heaysman, J.E.M. (1976). Invasive behaviour between sarcoma and fibroblast populations in cell culture *Journal of the National Cancer Institute* 56(3): 561-569.
- Ach, R.A., Wang, H., and Curry, B. (2008). Measuring microRNAs: comparisons of microarray and quantitative PCR measurements, and of different total RNA prep methods. *BMC Biotechnology* 8(69): 1-16.
- Aldemir, M., Ener, K., Dehni, D., Agras, K., and Kayigil, O. (2010). Evaluation of the relationship between prostate cancer and serum inflammation markers. *International Journal of Nephrology & Urology* 2(1): 244-250.
- Allioli, N., Vincent, S., Vlaeminck-Guillem, V., Decaussin-Petrucci, M., Ragage, F., Ruffion, A., and Samarut, J. (2011). TM4SF1, a novel primary androgen receptor target gene over-expressed in human prostate cancer and involved in cell migration. *The Prostate* 71(11): 1239-1250.
- Anagnostopoulou, A., Vultur, A., Arulanandam, R., Cao, J., Turkson, J., Jove, R., Kim, J.S., Glenn, M., Hamilton, A.D., and Raptis, L. (2006). Differential effects of Stat3 inhibition in sparse vs confluent normal and breast cancer cells. *Cancer Letters* 242(1): 120-132.
- Anear, E., and Parish, R.W. (2012). The effects of modifying RhoA and Rac1 activities on heterotypic contact inhibition of locomotion. *FEBS Letters* 586(9): 1330-1335.
- Ara, T., Song, L., Shimada, H., Keshelava, N., Russell, H.V., Metelitsa, L.S., Groshen, S.G., Seeger, R.C., and DeClerck, Y.A. (2009). Interleukin-6 in the bone marrow microenvironment promotes the growth and survival of neuroblastoma cells. *Cancer Research* 69(1): 329-337.
- Arredouani, M.S., Kasran, A., Vanoirbeek, J.A., Berger, F.G., Baumann, H., and Ceuppens, J.L. (2005). Haptoglobin dampens endotoxin-induced inflammatory effects both in vitro and in vivo. *Immunology* 114(2): 263-271.
- Arulanandam, R., Vultur, A., Cao, J., Carefoot, E., Elliott, B.E., Truesdall, P.F., Larue, L.,

- Feracci, H., and Raptis, L. (2009). Cadherin-cadherin engagement promotes cell survival via Rac1/Cdc42 signal transducer and activator of transcription-3. *Molecular Cancer Research* 7(8): 1310-1327.
- Arwert, E.N., Hoste, E., and Watt, F.M. (2012). Epithelial stem cells, wound healing and cancer. *Nature Reviews: Cancer* 12(3): 170-180.
- Bacac, M., and Stamenkovic, I. (2008). Metastatic cancer cells. *Annual Review of Pathology: Mechanisms of Disease* 3: 221-247.
- Baker, H.M., Mason, A.B., He, Q.Y., MacGillivray, R.T., and Baker, E.N. (2001). Ligand variation in the transferrin family: the crystal structure of the H249Q mutant of the human transferrin N-lobe as a model for iron binding in insect transferrins. *Biochemistry* 40(39): 11670-11675.
- Barden, J.A., and Decker, J.L. (1971). *Mycoplasma hyorhinis* swine arthritis. I. Clinical and microbiologic features. *Arthritis and Rheumatism* 14(2): 193-201.
- Barnes, J., Lim, J.-M., Godard, A., Blanchard, F., Wells, L., and Steet, R. (2011). Extensive mannose phosphorylation on Leukemia Inhibitory Factor (LIF) controls its extracellular levels by multiple mechanisms. *The Journal of Biological Chemistry* 286(28): 24855-24855.
- Barre, B., Avril, S., and Coqueret, O. (2003). Opposite regulation of myc and p21waf1 transcription by STAT3 proteins. *The Journal of Biological Chemistry* 278(5): 2990-2996.
- Beckman, K.B., Lee, K.Y., Golden, T., and Melov, S. (2004). Gene expression profiling in mitochondrial disease: assessment of microarray accuracy by high-throughput Q-PCR. *Mitochondrion* 4(5): 453-470.
- Bekes, E.M., Schweighofer, B., Kupriyanova, T.A., Zajac, E., Ardi, V.C., Quigley, J.P., and Deryugina, E.I. (2011). Tumor-recruited neutrophils and neutrophil TIMP-free MMP-9 regulate coordinately the levels of tumor angiogenesis and efficiency of malignant cell intravasation. *The American Journal of Pathology* 179(3): 1455-1470.
- Betts, M.J., and Russel, R.B. (2003). Amino Acid Properties and Consequences of Substitutions. In *Bioinformatics for Geneticists*, M.R. Barnes, and I.C. Gray, eds. (Germany, John Wiley & Sons, Ltd.), pp. 291-316.
- Bi, X., Pohl, N.M., Qian, Z., Yang, G.R., Gou, Y., Guzman, G., Kajdacsy-Balla, A., Iozzo, R.V., and Yang, W. (2012). Decorin-mediated inhibition of colorectal cancer growth and migration is associated with E-cadheron *in vitro* and in mice. *Carcinogenesis* 33(2): 326-330.
- Bishop, A.L., and Hall, A. (2000). Rho GTPases and their effector proteins. *Biochemical Journal* 348(Pt2): 241-255.
- Blay, J.-Y., Negrier, S., Combaret, V., Attali, S., Goillot, E., Merrouche, Y., Mercatello, A.,

- Ravault, A., Touani, J.-M., Moskvotchenko, J.-F., Philip, T., and Favrot, M. (1992). Serum level of Interleukin 6 as a prognosis factor in metastatic renal cell carcinomas. *Cancer Research* 52(12): 3317-3322.
- Bond, C.S. (2003). TopDraw: a sketchpad for protein structure topology cartoons. *Bioinformatics* 19(2): 311-312.
- Boulanger, M.J., Chow, D., Brevnova, E.E., and Garcia, K.C. (2003). Hexameric Structure and Assembly of the Interleukin-6/IL-6 α -Receptor/gp130 Complex. *Science* 300(5628): 2101-2104.
- Bowman, T., Garcia, R., Turkson, J., and Jove, R. (2000). STATs in oncogenesis. *Oncogene* 19(21): 2474-2488.
- Carmona-Fontaine, C., Matthews, H.K., Kuriyama, S., Moreno, M., Dunn, G.A., Parsons, M., Stern, C.D., and Mayor, R. (2008). Contact inhibition of locomotion *in vivo* controls neural crest directional migration. *Nature* 456: 957-961.
- Catlett-Falcone, R., Landowski, T.H., Oshiro, M.M., Turkson, J., Levitzki, A., Savino, R., Ciliberto, G., Moscinski, L., Fernandez-Luna, J.L., Nunez, G., Dalton, W.S., and Jove, R. (1999). Constitutive activation of Stat3 signaling confers resistance to apoptosis in human U266 myeloma cells. *Immunity* 10(1): 105-115.
- Cavallaro, U., and Christofori, G. (2004). Cell adhesion and signalling by cadherins and Ig-CAMS in cancer. *Nature Reviews* 4: 118-132.
- Cazes, A., Galaup, A., Chomel, C., Bignon, M., Brechot, N., Jan, S.L., Weber, H., Corvol, P., Muller, L., Germain, S., and Monnot, C. (2006). Extracellular matrix-bound angiopoietin-like 4 inhibits endothelial cell adhesion, migration, and sprouting and alters actin cytoskeleton. *Circulation Research* 99(11): 1207-1215.
- Champagne, K.S., Sissler, M., Larrabee, Y., Doublet, S., and Francklyn, C.S. (2005). Activation of the hetero-octameric ATP phosphoribosyl transferase through subunit interface rearrangement by a tRNA synthetase paralog. *The Journal of Biological Chemistry* 280(40): 34096-34104.
- Chan, F.Y., and Torriani, A. (1996). PstB protein of the phosphate-specific transport system of *Escherichia coli* is an ATPase. *Journal of Bacteriology* 178(13): 3974-3977.
- Chen, H., Herndon, M.E., and Lawler, J. (2000). The cell biology of thrombospondin-1. *Matrix Biology* 19(7): 597-614.
- Chi, H., Barry, S.P., Roth, R.J., Wu, J.J., Jones, E.A., Bennett, A.M., and Flavell, R.A. (2006). Dynamic regulation of pro- and anti-inflammatory cytokines by MAPK phosphatase 1 (MKP-1) in innate immune responses. *Proceedings of the National Academy of Sciences of the United States of America* 103(7): 2274-2279.
- Choi, H.S., Lee, H.M., Kim, W.-T., Kim, M.K., Chang, H.J., Lee, H.R., Joh, J.-W., Kim, D.S., and Ryu, C.J. (2014). Detection of mycoplasma infection in circulating tumor cells in

- patients with hepatocellular carcinoma. *Biochemical and Biophysical Research Communications* 446(2): 620-625.
- Chu, H.W., Jeyaseelan, S., Rino, J.G., Voelker, D.R., Wexler, R.B., Campbell, K., Harbeck, R.J., and Martin, R.J. (2005). TLR2 signaling is critical for *Mycoplasma pneumoniae*-induced airway mucin expression. *Journal of Immunology* 174(9): 5713-5719.
- Cid, M.C., Grant, D.S., Hoffman, G.S., Auerbach, R., Fauci, A.S., and Kleinman, H.K. (1993). Angiogenic Activity of Haptoglobin. *The Journal of Clinical Investigation* 91: 977-985.
- Cifone, M.A., and Fidler, I.J. (1980). Correlation of patterns of anchorage-independent growth with *in vivo* behavior of cells from a murine fibrosarcoma. *Proceedings of the National Academy of Sciences of the United States of America* 77(2): 1039-1043.
- Cirl, C., Wieser, A., Yadav, M., Duerr, S., Schubert, S., Fischer, H., Stappert, D., Wantia, N., Rodriguez, N., Wagner, H., Svanborg, C., and Miethke, T. (2008). Subversion of Toll-like receptor signaling by a unique family of bacterial Toll/interleukin-1 receptor domain-containing proteins. *Nature Medicine* 14(4): 399-406.
- Colotta, F., Allavena, P., Sica, A., Garlanda, C., and Mantovani, A. (2009). Cancer-related inflammation, the seventh hallmark of cancer: links to genetic instability. *Carcinogenesis* 30(7): 1073-1081.
- Consortium, T.U. (2012). Reorganizing the protein space at the Universal Protein Resource (UniProt). *Nucleic Acids Research* 40: D71-75.
- Contassot, E., Beer, H.D., and French, L.E. (2012). Interleukin-1, inflammasomes, autoinflammation and the skin. *Swiss Medical Weekly: The European Journal of Medical Sciences* 142(w13590).
- Cornelissen, C., Lüscher-Firzlaff, J., Baron, J.M., and Lüscher, B. (2011). Signaling by IL-31 and functional consequences. *European Journal of Cell Biology* 91(6): 552-566.
- Costa-Pereira, A.P., Tininini, S., Strobl, B., Alonzi, T., Schlaak, J.F., Is'harc, H., Gesualdo, I., Newman, S.J., Kerr, I.M., and Poli, V. (2002). Mutational switch of an IL-6 response to an interferon-gamma-like response. *Proceedings of the National Academy of Sciences of the United States of America* 99(12): 8043-8047.
- Cowland, J.B., Sorensen, O.E., Sehested, M., and Borregaard, N. (2003). Neutrophil gelatinase-associated lipocalin is up-regulated in human epithelial cells by IL-1 beta, but not by TNF-alpha. *J Immunol* 171(12): 6630-6639.
- Cui, L.F., Guo, X.J., Wei, J., Liu, F.F., Fan, Y., Lang, R.G., Gu, F., Zhang, X.M., and Fu, L. (2008). Overexpression of TNF-alpha and TNFRII in invasive micropapillary carcinoma of the breast: clinicopathological correlations. *Histopathology* 53(4): 381-388.
- Dassa, E., and Hofnung, M. (1985). Sequence of gene malG in E. coli K12: homologies between integral membrane components from binding protein-dependent

transport systems. *The EMBO Journal* 4(9): 2287-2293.

Dayhoff, M.O., Schwartz, R.M., and Orcutt, B.C. (1978). Atlas of Protein Sequence and Structure, Vol 5 (National Biochemical Research Foundation, Washington DC).

DeMarco, M.L., and Woods, R.J. (2011). From agonist to antagonist: structure and dynamics of innate immune glycoprotein MD-2 upon recognition of variably acylated bacterial endotoxins. *Molecular Immunology* 49(1-2): 124-133.

Desai, L.P., Aryal, A.M., Ceacareanu, B., Hassid, A., and Waters, C.M. (2004). RhoA and Rac1 are both required for efficient wound closure of airway epithelial cells. *American Journal of Physiology Lung Cellular and Molecular Physiology* 287(6): L1134-1144.

Detopoulou, P., Panagiotakos, D.B., Antonopoulou, S., Pitsavos, C., and Stefanadis, C. (2008). Dietary choline and betaine intakes in relation to concentrations of inflammatory markers in healthy adults: the ATTICA study. *The American Journal of Clinical Nutrition* 87(2): 424-430.

Dil, N., and Banerjee, A.G. (2011). A role for aberrantly expressed nuclear localized decorin in migration and invasion of dysplastic and malignant oral epithelial cells. *Head and Neck Oncology* 3(44): 1-10.

Driessler, F., Venstrom, K., Sabat, R., Asadullah, K., and Schottelius, A.J. (2004). Molecular mechanisms of interleukin-10-mediated inhibition of NF-kappaB activity: a role for p50. *Clinical and Experimental Immunology* 135(1): 64-73.

Dudler, R., Schmidhauser, C., Parish, R.W., Wettenhall, R.E.H., and Schmidt, T. (1988). A mycoplasma high-affinity transport system and the *in vitro* invasiveness of mouse sarcoma cells. *The EMBO Journal* 7(12): 3963-3970.

Dunne, A., Ejdeback, M., Ludidi, P.L., O'Neill, L.A., and Gay, N.J. (2003). Structural complementarity of Toll/interleukin-1 receptor domains in Toll-like receptors and the adaptors Mal and MyD88. *The Journal of Biological Chemistry* 278(42): 41443-41451.

Elkind, E., Vaisid, T., Kornspan, J.D., Barnoy, S., Rottem, S., and Kosower, N.S. (2012). Calpastatin upregulation in *Mycoplasma hyorhinitis*-infected cells is promoted by the mycoplasma lipoproteins via the NF- κ B pathway. *Cellular Microbiology* 14(6): 840-851.

Etienne, W., Meyer, M.H., Peppers, J., and Meyer, R.A., Jr. (2004). Comparison of mRNA gene expression by RT-PCR and DNA microarray. *Biotechniques* 36(4): 618-620, 622, 624-616.

Fareed, G.C., Mendiaz, E., Sen, A., Juillare, G.J.F., Weisenburger, T.H., and Totanes, T.J. (1988). Novel antigenic markers of human tumor regression. *Journal of Biological Response Modifiers* 7(1): 11-23.

- Faruqi, T., Gomez, D., Bustelo, X., Bar-Sagi, D., and Reich, N. (2001). Rac1 mediates STAT3 activation by autocrine IL-6. *Proceedings of the National Academy of Sciences of the United States of America* 98(16): 9014-9019.
- Feng, X.-L., Wang, F., Zou, Y.-F., Li, W.-F., Tian, Y.-H., Pan, F.-M., and Huang, F. (2011). Association of FK506 binding protein 5 (FKBP5) gene rs4713916 polymorphism with mood disorders: a meta-analysis. *Acta Neuropsychiatrica* 23(1): 12-19.
- Ferdous, Z., Peterson, S.B., Tseng, H., Anderson, D.K., Iozzo, R.V., and Grande-Allen, K.J. (2009). A role for decorin in controlling proliferation, adhesion and migration of murine embryonic fibroblasts. *Journal of Biomedical Materials Research* 93(2): 419-428.
- Fernandez, C.A., Yan, L., Louis, G., Yang, J., Kutok, J.L., and Moses, M.A. (2005). The matrix metalloproteinase-9/neutrophil gelatinase-associated lipocalin complex plays a role in breast tumor growth and is present in the urine of breast cancer patients. *Clinical Cancer Research* 11(15): 5390-5395.
- Firlej, V., Mathieu, J.R.R., Gilbert, C., Lemonnier, L., Nakhle, J., Gallou-Kabani, C., Guarmit, B., Morin, A., Prevarskaya, N., Delongchamps, N.B., and Cabon, F. (2011). Thrombospondin-1 triggers cell migration and development of advanced prostate tumors. *Cancer Research* 71(24): 7649-7658.
- Flower, D.R. (1996). The lipocalin protein family: structure and function. *Biochemical Journal* 318(Pt1): 1-14.
- Gao, S.P., Mark, K.G., Leslie, K., Pao, W., Motoi, N., Gerald, W.L., Travis, W.D., Bornmann, W., Veach, D., Clarkson, B., and Bromberg, J.F. (2007). Mutations in the EGFR kinase domain mediate STAT3 activation via IL-6 production in human lung adenocarcinomas. *The Journal of Clinical Investigation* 117(12): 3846-3856.
- Geertsma, E.R., Nik Mahmood, N.A., Schuurman-Wolters, G.K., and Poolman, B. (2008). Membrane reconstitution of ABC transporters and assays of translocator function. *Nature Protocols* 3(2): 256-266.
- Germano, G., Mantovani, A., and Allavena, P. (2011). Targeting of the innate immunity/inflammation as complementary anti-tumor therapies. *Annals of Medicine* 43(8): 581-593.
- Geurts, J., van den Brand, B.T., Wolf, A., Abdollahi-Roodsaz, S., Arntz, O.J., Kracht, M., van den Berg, W.B., and van de Loo, F.A. (2011). Toll-like receptor 4 signalling is specifically TGF-beta-activated kinase 1 independent in synovial fibroblasts. *Rheumatology (Oxford)* 50(7): 1216-1225.
- Gilson, E., Alloing, G., Schmidt, T., Claverys, J., Dudler, R., and Hofnung, M. (1988). Evidence for high affinity binding-protein dependent transport systems in Gram-positive bacteria and in Mycoplasma. *The EMBO Journal* 7(12): 3971-3974.
- Glaros, T., Fu, Y., Xing, J., and Li, L. (2012). Molecular mechanism underlying persistent

induction of LCN2 by lipopolysaccharide in kidney fibroblasts. *PLoS One* 7(4): e34633.

- Goh, Y.Y., Pal, M., Chong, H.C., Zhu, P., Tan, M.J., Punugu, L., Tan, C.K., Huang, R.L., Sze, S.K., Tang, M.B., Ding, J.L., Kersten, S., and Tan, N.S. (2010). Angiopoietin-like 4 interacts with matrix proteins to modulate wound healing. *The Journal of Biological Chemistry* 285(43): 32999-33009.
- Gomes, N.J.C., Gauger, P.C., and Strait, E.L. (2012). Mycoplasma-associated arthritis: Critical points for diagnosis. *JSHAP* 20(2): 82-86.
- Gong, M., Meng, L., Jiang, B., Zhang, J., Yang, H., Wu, J., and Shou, C. (2008). p37 from *Mycoplasma hyorhinis* promotes cancer cell invasiveness and metastasis through activation of MMP-2 and followed by phosphorylation of EGFR. *Molecular Cancer Therapeutics* 7(3): 530-537.
- Gonzalez-Reyes, S., Marin, L., Gonzalez, L., Gonzalez, L.O., del Casar, J.M., Lamelas, M.L., Gonzalez-Quintana, J.M., and Vizoso, F.J. (2010). Study of TLR3, TLR4 and TLR9 in breast carcinomas and their association with metastasis. *BMC Cancer* 10(665): 1-9.
- Goodison, S., Nakamura, K., Iczkowski, K.A., Anai, S., and Boehlein, S.K. (2007). Exogenous mycoplasma p37 protein alters gene expression, growth and morphology of prostate cancer cells. *Cytogenetic and Genome Research* 118(2): 204-213.
- Green, J.A., Stockton, R.A., Johnson, C., and Jacobson, B.S. (2004). 5-lipoxygenase and cyclooxygenase regulate wound closure in NIH/3T3 fibroblast monolayers. *American Journal of Physiology Cell Physiology* 287(2): C373-383.
- Guilluy, C., Garcia-Mata, R., and Burridge, K. (2011). Rho protein crosstalk: another social network? *Trends in Cell Biology* 21(12): 718-726.
- Guo, F., Tang, J., Zhou, Z., Dou, Y., Van Lonkhuyzen, D., Gao, C., and Huan, J. (2012). GEF-H1-RhoA signaling pathway mediates LPS-induced NF- κ B transactivation and IL-8 synthesis in endothelial cells. *Molecular Immunology* 50(1-2): 98-107.
- Gutfeld, O., Prus, D., Ackerman, Z., Dishon, S., Linke, R.P., Levin, M., and Urieli-Shoval, S. (2006). Expression of serum amyloid A, in normal, dysplastic, and neoplastic human colonic mucosa: implication for a role in colonic tumorigenesis. *Journal of Histochemistry and Cytochemistry* 54(1): 63-73.
- Gyotoku, E., Morita, E., Kameyoshi, Y., Hiragun, T., Yamamoto, S., and Hide, M. (2001). The IL-6 family cytokines, interleukin-6, interleukin-11, oncostatin M, and leukemia inhibitory factor, enhance mast cell growth through fibroblast-dependent pathway in mice. *Archives of Dermatological Research* 293(10): 508-514.
- Hanna, R.A., Campbell, R.L., and Davies, P.L. (2008). Calcium-bound structure of calpain and its mechanism of inhibition by calpastatin. *Nature* 456: 409-413.
- Hashimoto, M., Shingu, M., Ezaki, I., Nobunaga, M., Minamihara, M., Kato, K., and

- Sumioki, H. (1994). Production of soluble ICAM-1 from human endothelial cells induced by IL-1 β and TNF- α . *Inflammation* 18(2): 163-173.
- Haynes, L.M., Moore, D.D., Kurt-Jones, E.A., Finberg, R.W., Anderson, L.J., and Tripp, R.A. (2001). Involvement of Toll-Like Receptor 4 in Innate Immunity to Respiratory Syncytial Virus. *Journal of Virology* 75(22): 10730-10737.
- He, F., Zhang, Q., Kuruba, R., Gao, X., Li, J., Li, Y., Gong, W., Jiang, Y., Xie, W., and Li, S. (2008). Upregulation of decorin by FXR in vascular smooth muscle cells. *Biochemical and Biophysical Research Communications* 372(4): 746-751.
- He, W., Qu, T., Yu, Q., Wang, Z., Wang, H., Zhang, J., and Smith, A.J. (2012). Lipopolysaccharide enhances decorin expression through the Toll-like receptor 4, myeloid differentiating factor 88, nuclear factor-kappa B, and mitogen-activated protein kinase pathways in odontoblast cells. *Journal of Endodontics* 38(4): 464-469.
- Heinrich, P.C., Behrmann, I., Haan, S., Hermanns, H.M., Müller-Newen, G., and Schaper, F. (2003). Principles of interleukin (IL)-6-type cytokine signalling and its regulation. *Biochemical Journal* 374(Pt1): 1-20.
- Helander, K.G. (1994). Kinetic Studies of Formaldehyde Binding in Tissue. *Biotechnic & Histochemistry* 69(3): 177-179.
- Henderson, B., Poole, S., and Wilson, M. (1996). Bacterial modulins: a novel class of virulence factors which cause host tissue pathology by inducing cytokine synthesis. *Microbiological Reviews* 60(2): 316-341.
- Hiles, I.D., Gallagher, M.P., Jamieson, D.J., and Higgins, C.F. (1987). Molecular characterization of the oligopeptide permease of *Salmonella typhimurium*. *Journal of Molecular Biology* 195(1): 125-142.
- Hopfe, M., Deenen, R., Degrandi, D., Köhrer, K., and Henrich, B. (2013). Host Cell Responses to Persistent Mycoplasmas - Different Stages in Infection of HeLa Cells with *Mycoplasma hominis*. *PLoS One* 8(1): e54219-54234.
- Howlett, M., Menheniott, T.R., Judd, L.M., and Giraud, A.S. (2009). Cytokine signalling via gp130 in gastric cancer. *Biochimica et Biophysica Acta* 1793(11): 1623-1633.
- Huang, J.H., and Liao, W.S. (1999). Synergistic induction of mouse serum amyloid A3 promoter by the inflammatory mediators IL-1 and IL-6. *Journal of Interferon and Cytokine Research* 19(12): 1403-1411.
- Huang, S., Li, J.Y., Wu, J., Meng, L., and Shou, C.C. (2001). Mycoplasma infections and different human carcinomas. *World Journal of Gastroenterology* 7(2): 266-269.
- Huang, Z., Hoffmann, F.W., Norton, R.L., Hashimoto, A.C., and Hoffmann, P.R. (2011). Selenoprotein K is a novel target of m-calpain, and cleavage is regulated by Toll-like receptor-induced calpastatin in macrophages. *J Biol Chem* 286(40): 34830-34838.
- Iacobuzio-Donahue, C.A., Ashfaq, R., Maitra, A., Adsay, N.V., Shen-Ong, G.L., Berg, K.,

- Hollingsworth, M.A., Cameron, J.L., Yeo, C.J., Kern, S.E., Goggins, M., and Hruban, R.H. (2003). Highly expressed genes in pancreatic ductal adenocarcinomas: a comprehensive characterization and comparison of the transcription profiles obtained from three major technologies. *Cancer Research* 63(24): 8614-8622.
- Iannetti, A., Pacifico, F., Acquaviva, R., Lavorgna, A., Crescenzi, E., Vascotto, C., Tell, G., Salzano, A.M., Scaloni, A., Vuttariello, E., Chiappetta, G., Formisano, S., and Leonardi, A. (2008). The neutrophil gelatinase-associated lipocalin (NGAL), a NF- κ B-regulated gene, is a survival factor for thyroid neoplastic cells. *Proceedings of the National Academy of Sciences of the United States of America* 105(37): 14058-14063.
- Ilantzis, C., Thomson, D., Michaelidou, A., Benchimol, S., and Stanners, C.P. (1993). Identification of a human cancer related organ-specific neoantigen. *Microbiology and Immunology* 37(2): 119-128.
- Jayagopala Reddy, N.R., Wilkie, B.N., Borgs, P., and Mallard, B.A. (2000). Cytokines in *Mycoplasma hyorhinis*-induced arthritis in pigs bred selectively for high and low immune responses. *Infection and Immunity* 68(3): 1150-1155.
- Jiang, D., Liang, J., Fan, J., Yu, S., Chen, S., Luo, Y., Prestwich, G.D., Mascarenhas, M.M., Garg, H.G., Quinn, D.A., Homer, R.J., Goldstein, D.R., Bucala, R., Lee, P.J., Medzhitov, R., and Noble, P.W. (2005a). Regulation of lung injury and repair by Toll-like receptors and hyaluronan. *Nature Medicine* 11(11): 1173-1179.
- Jiang, Z., Georgel, P., Du, X., Shamel, L., Sovath, S., Mudd, S., Huber, M., Kalis, C., Keck, S., Galanos, C., Freudenberg, M., and Beutler, B. (2005b). CD14 is required for MyD88-independent LPS signaling. *Nature Immunology* 6(6): 565-570.
- Jones, S.A., and Rose-John, S. (2002). The role of soluble receptors in cytokine biology: the agonistic properties of the sIL-6/IL-6 complex. *Biochimica et Biophysica Acta* 1592(3): 251-263.
- Jurgenson, C.T., Begley, T.P., and Ealick, S.E. (2009). The Structural and Biochemical Foundations of Thiamin Biosynthesis. *Annual Review of Biochemistry* 78: 569-603.
- Kang, S.-M., Sung, H.-J., Ahn, J.-M., Park, J.-Y., Lee, S.-Y., Park, C.-S., and Cho, J.-Y. (2011). The Haptoglobin B chain as a supportive biomarker for human lung cancers. *Molecular Biosystems* 7: 1167-1175.
- Kano, A., Wolfgang, M.J., Gao, Q., Jacoby, J., Chai, G.X., Hansen, W., Iwamoto, Y., Pober, J.S., Flavell, R.A., and Fu, X.Y. (2003). Endothelial cells require STAT3 for protection against endotoxin-induced inflammation. *The Journal of Experimental Medicine* 198(10): 1517-1525.
- Kanoh, Y., Ohtani, H., Egawa, S., Baba, S., and Akahoshi, T. (2011). Levels of acute inflammatory biomarkers in advanced prostate cancer patients with α_2 -macroglobulin deficiency. *International Journal of Oncology* 39: 1553-1558.

- Kao, W.W.-Y., Funderburgh, J.L., Xia, Y., Liu, C.-Y., and Conrad, G.W. (2006). Focus on Molecules: Lumican. *Experimental Eye Research* 82(1): 3-4.
- Kawahito, Y., Ichinose, S., Sano, H., Tsubouchi, Y., Kohno, M., Yoshikawa, T., Tokunaga, D., Hojo, T., Harasawa, R., Nakano, T., and Matsuda, K. (2008). *Mycoplasma fermentans* glycolipid-antigen as a pathogen of rheumatoid arthritis. *Biochemical and Biophysical Research Communications* 369(2): 561-566.
- Kawai, T., and Akira, S. (2007). Signaling to NF-kappaB by Toll-like receptors. *Trends in Molecular Medicine* 13(11): 460-469.
- Ketcham, C.M., Anai, S., Reutzel, R., Sheng, S., Schuster, S.M., Brenes, R.B., Agbandje-McKenna, M., McKenna, R., Rosser, C.J., and Boehlein, S.K. (2005). p37 induces tumor invasiveness. *Molecular Cancer Therapeutics* 4(7): 1031-1038.
- Kevil, C.G., Orr, A.W., Langston, W., Mickett, K., Murphy-Ullrich, J., Patel, R.P., Kucik, D.F., and Bullard, D.C. (2004). Intracellular adhesion molecule-1 (ICAM-1) regulates endothelial cell motility through nitric oxide-dependent pathway. *The Journal of Biological Chemistry* 279(18): 19230-19238.
- Kim, B., Lee, K., Han, K., Kim, D., Ha, Y., Kim, C.H., Oh, Y., Kang, I., Lee, J., and Chae, C. (2010). Development of *in situ* hybridization for the detection of *Mycoplasma hyorhinis* in formalin-fixed paraffin-embedded tissues from naturally infected pigs with polyserositis. *The Journal of Veterinary Medical Science* 72(9): 1225-1227.
- Kim, S., Takahashi, H., Lin, W., Descargues, P., Grivennikov, S., Kim, Y., Luo, J., and Karin, M. (2009). Carcinoma-produced factors activate myeloid cells through TLR2 to stimulate metastasis. *Nature* 457(7225): 102-106.
- Kisseleva, T., Bhattacharya, S., Braunstein, J., and Schindler, C.W. (2002). Signaling through the JAK/STAT pathway, recent advances and future challenges. *Gene* 285(1): 1-24.
- Kitt, K.N., and Nelson, W.J. (2011). Rapid suppression of activated Rac1 by cadherins and nectins during de novo cell-cell adhesion. *PLoS One* 6(3): e17841-17850.
- Klein, G., Vellenga, E., Fraaije, M.W., Kamphaus, W.A., and de Bont, E.S.J.M. (2004). The possible role of matrix metalloproteinase (MMP)-2 and MMP-9 in cancer, e.g. acute leukemia. *Critical Reviews in Oncology/Hematology* 50(2): 87-100.
- Kolch, W. (2000). Meaningful relationship: the regulation of the Ras/Raf/MEK/ERK pathway by protein interactions. *Biochemical Journal* 351(Pt2): 289-305.
- Koliwad, S.K., Gray, N.E., and Wang, J.C. (2012). Angiopoietin-like 4 (Angptl4): A glucocorticoid-dependent gatekeeper of fatty acid flux during fasting. *Adipocyte* 1(3): 182-187.
- Kopfstein, L., and Christofori, G. (2006). Metastasis: cell-autonomous mechanisms versus contributions by the tumor microenvironment. *Cellular and Molecular Life Sciences*

63(4): 449-468.

- Kornspan, J.D., Tarshis, M., and Rottem, S. (2010). Invasion of melanoma cells by *Mycoplasma hyorhinis*: Enhancement by protease treatment. *Infection and Immunity* 78(2): 611-617.
- Kostyal, D.A., Butler, G.H., and Beezhold, D.H. (1995). *Mycoplasma hyorhinis* molecules that induce tumor necrosis factor alpha secretion by human monocytes. *Infection and Immunity* 63(10): 3858 - 3863.
- Kubben, F.J., Sier, C.F., Hawinkels, L.J., Tschesche, H., van Duijn, W., Zuidwijk, K., van der Reijden, J.J., Hanemaaijer, R., Griffioen, G., Lamers, C.B., and Verspaget, H.W. (2007). Clinical evidence for a protective role of lipocalin-2 against MMP-9 autodegradation and the impact for gastric cancer. *European Journal of Cancer* 43(12): 1869-1876.
- Kultti, A., Li, X., Jiang, P., Thompson, C.B., Frost, G.I., and Shepard, H.M. (2012). Therapeutic targeting of hyaluronan in the tumor stroma. *Cancers* 4(3): 873-903.
- Kurt-Jones, E.A., Sandor, F., Ortiz, Y., Bowen, G.N., Counter, S.L., Wang, T.C., and Finberg, R.W. (2004). Use of murine embryonic fibroblasts to define Toll-like receptor activation and specificity. *Journal of Endotoxin Research* 10(6): 419-424.
- Lambert, L.C., Trummell, H.Q., Singh, A., Cassell, G.H., and Bridges, R.J. (1998). *Mycoplasma pulmonis* inhibits electrogenic ion transport across murine tracheal epithelial cell monolayers. *Infection and Immunity* 66(1): 272-279.
- Lawler, J. (2000). The functions of thrombospondin-1 and -2. *Current Opinion in Cell Biology* 12: 634-640.
- Lee, I.K., VanSaun, M.N., Shim, J.H., Matrisian, L.M., and Gordan, D.L. (2012). Increased metastases are associated with inflammation and matrix metalloproteinase-9 activity at incision sites in a murine model of peritoneal dissemination of colorectal cancer. *Journal of Surgical Research* 180(2): 252-259.
- Lee, J.W., Kim, Y.H., Park, K.D., Jee, K.S., Shin, J.W., and Hahn, S.B. (2004). Importance of integrin β 1-mediated cell adhesion on biodegradable polymers under serum depletion in mesenchymal stem cells and chondrocytes *Biomaterials* 25(10): 1901 - 1909.
- Lee, T.H., Wisniewski, H., and Vilcek, J. (1992). A novel secretory tumor necrosis factor-inducible protein (TSG-6) is a member of the family of hyaluronate binding proteins, closely related to the adhesion receptor CD44. *The Journal of Cell Biology* 116(2): 545-557.
- Leow-Dyke, S., Allen, C., Denes, A., Nilsson, O., Maysami, S., Bowie, A.G., Rothwell, N.J., and Pinteaux, E. (2012). Neuronal toll-like receptor 4 signaling induces brain endothelial activation and neutrophil transmigration in vitro. *Journal of Neuroinflammation* 9(230): 1-11.

- Leung, L., Radulovich, N., Zhu, C.-Q., Organ, S., Bandarchi, B., Pintilie, M., To, C., Panchal, D., and Tsao, M.S. (2012). Lipocalin 2 Promotes Invasion, Tumorigenicity and Gemcitabine Resistance in Pancreatic Ductal Adenocarcinoma. *PLoS One* 7(10): e46677-46687.
- Ley, K., and Huo, Y. (2001). VCAM-1 is critical in atherosclerosis. *The Journal of Clinical Investigation* 107(10): 1255-1262.
- Li, H., Xu, H., and Liu, S. (2011). Toll-like receptors 4 induces expression of matrix metalloproteinase-9 in human aortic smooth muscle cells. *Mol Biol Rep* 38(2): 1419-1423.
- Li, L., Asteriou, T., Bernert, B., Heldin, C.H., and Heldin, P. (2007). Growth factor regulation of hyaluronan synthesis and degradation in human dermal fibroblasts: importance of hyaluronan for the mitogenic response of PDGF-BB. *The Biochemical Journal* 404(2): 327-336.
- Liang, C.C., Park, A.Y., and Guan, J.L. (2007). In vitro scratch assay: a convenient and inexpensive method for analysis of cell migration in vitro. *Nature Protocols* 2(2): 329-333.
- Lim, R., Ahmed, N., Borregaard, N., Riley, C., Wafai, R., Thompson, E.W., Quinn, M.A., and Rice, G.E. (2007). Neutrophil gelatinase-associated lipocalin (NGAL) an early-screening biomarker for ovarian cancer: NGAL is associated with epidermal growth factor-induced epithelio-mesenchymal transition. *International Journal of Cancer* 120(11): 2426 - 2434.
- Linker, R.A., Luhder, F., Kallen, K.-J., Lee, D.-H., Engelhardt, B., Rose-John, S., and Gold, R. (2008). IL-6 transsignalling modulates the early effector phase of EAE and targets the blood-brain barrier. *Journal of Neuroimmunology* 205(1): 64-72.
- Litvak, V., Ramsey, S.A., Rust, A.G., Zak, D.E., Kennedy, K.A., Lampano, A.E., Nykter, M., Shmulevich, I., and Aderem, A. (2009). Function of C/EBPdelta in a regulatory circuit that discriminates between transient and persistent TLR4-induced signals. *Nature Immunology* 10(4): 437-443.
- Liu, W., Ren, T., Jiang, B., Gong, M., and Shou, C. (2007). Mycoplasma membrane protein p37 promotes malignant changes in mammalian cells. *Canadian Journal of Microbiology* 53(2): 270-276.
- Liu, W., Zhang, J., Jiang, B., Ren, T., Gong, M., Meng, L., and Shou, C. (2006). Lipoprotein p37 from *Mycoplasma hyorhinis* inhibiting mammalian cell adhesion. *Journal of Biomedical Science* 13(3): 323-331.
- Liu, Z., de Matos, D.G., Fan, H.Y., Shimada, M., Palmer, S., and Richards, J.S. (2009). Interleukin-6: an autocrine regulator of the mouse cumulus cell-oocyte complex expansion process. *Endocrinology* 150(7): 3360-3368.
- Lu, B., Moser, A., Shigenaga, J.K., Grunfeld, C., and Feingold, K.R. (2010). The acute phase

response stimulates the expression of angiopoietin like protein 4. *Biochem Biophys Res Commun* 391(4): 1737-1741.

Lu, X., Mu, E., Wei, Y., Riethdorf, S., Yang, Q., Yuan, M., Yan, J., Hua, Y., Tiede, B.J., Lu, X., Haffty, B.G., Pantel, K., Massague', J., and Kang, Y. (2011). VCAM-1 promotes osteolytic expansion of indolent bone micrometastasis of breast cancer by engaging $\alpha 4\beta 1$ -positive osteoclast progenitors. *Cancer Cell* 20(6): 701-714.

Lu, Y.C., Yeh, W.C., and Ohashi, P.S. (2008). LPS/TLR4 signal transduction pathway. *Cytokine* 42(2): 145-151.

Lysakova-Devine, T., Keogh, B., Harrington, B., Nagpal, K., Halle, A., Golenbock, D.T., Monie, T., and Bowie, A.G. (2010). Viral inhibitory peptide of TLR4, a peptide derived from vaccinia protein A46, specifically inhibits TLR4 by directly targeting MyD88 adaptor-like and TRIF-related adaptor molecule. *Journal of Immunology* 185(7): 4261-4271.

Ma, T., Jham, B.C., Hu, J., Friedman, E.R., Basile, J.R., Molinolo, A., Sodhi, A., and Montaner, S. (2010). Viral G protein-coupled receptor up-regulates Angiopoietin-like 4 promoting angiogenesis and vascular permeability in Kaposi's sarcoma. *Proceedings of the National Academy of Sciences of the United States of America* 107(32): 14363-14368.

Machacek, M., Hodgson, L., Welch, C., Elliott, H., Pertz, O., Nalbant, P., Abell, A., Johnson, G.L., Hahn, K.M., and Danuser, G. (2009). Coordination of Rho GTPase activities during cell protrusion. *Nature* 461(7260): 99-103.

Maniloff, J., McElhaney, R.N., Finch, L.R., and Baseman, J.B. (1992). *Mycoplasmas: molecular biology and pathogenesis* (American Society for Microbiology, Washington, DC.).

Mannelqvist, M., Stefansson, I.M., Wik, E., Kusonmano, K., Raeder, M.B., Oyan, A.M., Kalland, K.-H., Moses, M.A., Salvesen, H.B., and Akslen, L.A. (2012). Lipocalin 2 expression is associated with aggressive features of endometrial cancer. *BMC Cancer* 12(169): 1471-2470.

Mantovani, A. (2009). Cancer: Inflaming metastasis. *Nature* 457(7225): 36-37.

Mantovani, A., Allavena, P., Sica, A., and Balkwill, F. (2008). Cancer-related inflammation. *Nature* 454: 436-444.

Marques, L., Auriac, A., Willemetz, A., Banha, J., Silva, B., Canonne-Hergaux, F., and Costa, L. (2012). Immune cells and hepatocytes express glycosylphosphatidylinositol-anchored ceruloplasmin at their cell surface. *Blood Cells, Molecules, and Diseases* 48(2): 110-120.

Marui, N., Offermann, M.K., Swerlick, R., Kunsch, C., Rosen, C.A., Ahmad, M., Alexander, R.W., and Medford, R.M. (1993). Vascular cell adhesion molecule-1 (VCAM-1) gene transcription and expression are regulated through an antioxidant-sensitive

mechanism in human vascular endothelial cells. *Journal of Clinical Investigation* 92(4): 1866-1874.

Maunsell, F.P., Woolums, A.R., Francoz, D., Rosenbusch, R.F., Step, D.L., Wilson, D.J., and Janzen, E.D. (2011). *Mycoplasma bovis* Infections in Cattle. *Journal of Veterinary Internal Medicine* 25(4): 772-783.

Mayor, R., and Carmona-Fontaine, C. (2010). Keeping in touch with contact inhibition of locomotion. *Trends in Cell biology* 20(6): 319-328.

McFarland, B.C., Gray, G.K., Nozell, S.E., Hong, S.W., and Benveniste, E.N. (2013). Activation of the NF- κ B Pathway by the STAT3 Inhibitor JSI-124 in Human Glioblastoma Cells. *Molecular Cancer Research* 11(5): 494-505.

McGowin, C.L., Ma, L., Martin, D.H., and Pyles, R.B. (2009). *Mycoplasma genitalium*-encoded MG309 activates NF- κ B via Toll-like receptors 2 and 6 to elicit proinflammatory cytokine secretion from human genital epithelial cells. *Infection and Immunity* 77(3): 1175-1181.

Medzhitov, R., and Janeway, J.C. (2000). The Toll receptor family and microbial recognition. *Trends in Microbiology* 8(10): 452-456.

Minami, Y., Ikeda, W., Kajita, M., Fujito, T., Monden, M., and Takai, Y. (2007). Involvement of up-regulated Necl-5/Tage4/PVR/CD155 in the loss of contact in transformed NIH3T3 cells. *Biochemical and Biophysical Research Communications* 352(4): 856-860.

Monach, P.A., Verschoor, A., Jacobs, J.P., Carroll, M.C., Wagers, A.J., Benoist, C., and Mathis, D. (2007). Circulating C3 is necessary and sufficient for autoantibody-mediated arthritis. *Arthritis and Rheumatism* 56(9): 2968-2974.

Morey, J.S., Ryan, J.C., and Van Dolah, F.M. (2006). Microarray validation: factors influencing correlation between oligonucleotide microarrays and real-time PCR. *Biological Procedures Online* 8: 175-193.

Mori, S., Chang, J.T., Andrechek, E.R., Matsumura, N., Baba, T., Yao, G., Kim, J.W., Gatza, M., Murphy, S., and Nevins, J.R. (2009). Anchorage-independent cell growth signature identifies tumors with metastatic potential. *Oncogene* 28(31): 2796-2805.

Mu, H.H., Pennock, N.D., Humphreys, J., Kirschning, C.J., and Cole, B.C. (2005). Engagement of Toll-like receptors by mycoplasmal superantigen: downregulation of TLR2 by MAM/TLR4 interaction. *Cellular Microbiology* 7(6): 789-797.

Mu, H.H., Sawitzke, A.D., and Cole, B.C. (2001). Presence of Lps(d) mutation influences cytokine regulation in vivo by the *Mycoplasma arthritidis* mitogen superantigen and lethal toxicity in mice infected with *M. arthritidis*. *Infection and Immunity* 69(6): 3837-3844.

Muller-Newen, G., Kuster, A., Hemmann, U., Keul, R., Horsten, U., Martens, A., Graeve, L.,

- Wijdenes, J., and Heinrich, P.C. (1998). Soluble interleukin-6 receptor potentiates the antagonistic activity of soluble gp130 on interleukin-6 responses. *The Journal of Immunology* 161(11): 6347-6355.
- Myles, A., and Aggarwal, A. (2011). Expression of Toll-like receptors 2 and 4 is increased in peripheral blood and synovial fluid monocytes of patients with enthesitis-related arthritis subtype of juvenile idiopathic arthritis. *Rheumatology (Oxford)* 50(3): 481-488.
- Nagase, H., and Woessner, J.F. (1999). Matrix Metalloproteinases. *The Journal of Biological Chemistry* 274(31): 21491-21494.
- Nagyeri, G., Radacs, M., Ghassemi-Nejad, S., Trynieszewska, B., Olasz, K., Hutas, G., Gyorfy, Z., Hascall, V.C., Glant, T.T., and Mikecz, K. (2011). TSG-6 Protein, a negative Regulator of Inflammatory Arthritis, Forms a Ternary Complex with Murine Mast Cell Trypsases and Heparin. *The Journal of Biological Chemistry* 286(26): 23559-23569.
- Naito, Z. (2005). Role of the small leucine-rich proteoglycan (SLRP) family in pathological lesions and cancer cell growth. *Journal of Nippon Medical School* 72(3): 137-145.
- Nakamura, N., Shimaoka, Y., Tougan, T., Onda, H., Okuzaki, D., Zhao, H., Fujimori, A., Yabuta, N., Nagamori, I., Tanigawa, A., Sato, J., Oda, T., Hayashida, K., Suzuki, R., Yukioka, M., Nojima, H., and Ochi, T. (2006). Isolation and expression profiling of genes upregulated in bone marrow-derived mononuclear cells of rheumatoid arthritis patients. *DNA Research* 13: 169-183.
- Namiki, K., Goodison, S., Porvasnik, S., Allan, R.W., Iczkowski, K.A., Urbanek, C., Reyes, L., Sakamoto, N., and Rosser, C.J. (2009). Persistent exposure to mycoplasma induces malignant transformation of human prostate cells. *PLoS One* 4(9): 1-9.
- Netea, M.G., Van der Graaf, C., Van der Meer, J.W., and Kullberg, B.J. (2004). Recognition of fungal pathogens by Toll-like receptors. *European Journal of Clinical Microbiology and Infectious Diseases* 23(9): 672-676.
- Niessen, C.M., and Yap, A.S. (2006). Another job for the talented p120-catenin. *Cell* 127(5): 875-877.
- Nikaido, K., Liu, P.Q., and Ames, G.F. (1997). Purification and characterization of HisP, the ATP-binding subunit of a traffic ATPase (ABC transporter), the histidine permease of *Salmonella typhimurium*. Solubility, dimerization, and ATPase activity. *The Journal of Biological Chemistry* 272(44): 27745-27752.
- Ning, J., Huang, S., Wu, J., Meng, L., and Shou, C. (2003a). Protein p37 of *Mycoplasma hyorhinis* induces secretion of TNF- α from human peripheral blood mononuclear cells. *Chinese Science Bulletin* 48(7): 658-662.
- Ning, J., Sun, G., Huang, S., Ma, H., An, P., Meng, L., Song, S., Wu, J., and Shou, C. (2003b). Identification of antigens by monoclonal antibody PD4 and its expression in

Escherichia coli. *World Journal of Gastroenterology* 9(10): 2164-2168.

- Nir-Paz, R., Prevost, M., Nicolas, P., Blanchard, A., and Wroblewski, H. (2002). Susceptibilities of *Mycoplasma fermentans* and *Mycoplasma hyorhinis* to membrane-active peptides and enrofloxain in human tissue cell culture. *Antimicrobial Agents and Chemotherapy* 46(5): 1218-1225.
- Nishimoto, N. (2006). Interleukin-6 in rheumatoid arthritis. *Current Opinion in Rheumatology* 18(3): 277-281.
- Nishimoto, N. (2010). Interleukin-6 as a therapeutic target in candidate inflammatory diseases. *Clinical Pharmacology and Therapeutics* 87(4): 483-487.
- Nishimoto, N., and Kishimoto, T. (2008). Humanized antihuman IL-6 receptor antibody, tocilizumab. *Therapeutic Antibodies: Handbook of Experimental Pharmacology* 181: 151-160.
- Nishimoto, N., Terao, K., Mima, T., Nakahara, H., Takagi, N., and Takeuchi, T. (2008). Mechanisms and pathologic significances in increase in serum interleukin-6 (IL-6) and soluble IL-6 receptor after administration of an anti-IL-6 receptor antibody, tocilizumab, in patients with rheumatoid arthritis and Castleman disease. *Blood* 112(10): 3959-3964.
- Norris, S.J. (2006). The dynamic proteome of Lyme disease *Borrelia*. *Genome Biology* 7(3): 209-214.
- Obara, H., and Harasawa, R. (2008). L-ascorbic acid enhances apoptosis in human gastric carcinoma cell Line AZ-521 cells infected with *Mycoplasma hyorhinis*. *The Journal of Veterinary Medical Science* 71(1): 11 - 15.
- Oldham, M.L., and Chen, J. (2011). Crystal structure of the maltose transporter in a pretranslocation intermediate state. *Science* 332(6034): 1202-1205.
- Omelchenko, T., Fetisova, E., Ivanova, O., Bonder, E.M., Feder, H., Vasiliev, J.M., and Gelfand, I.M. (2001). Contact interactions between epitheliocytes and fibroblasts: Formation of heterotypic cadherin-containing adhesion sites accompanied by local cytoskeletal reorganization. *Proceedings of the National Academy of Sciences* 98(15): 8632-8637.
- Oshiumi, H., Sasai, M., Shida, K., Fujita, T., Matsumoto, M., and Seya, T. (2003). TIR-containing adapter molecule (TICAM)-2, a bridging adapter recruiting to toll-like receptor 4 TICAM-1 that induces interferon-beta. *The Journal of Biological Chemistry* 278(50): 49751-49762.
- Paddock, S.W., and Dunn, G.A. (1986). Analysing collisions between fibroblasts and fibrosarcoma cells: Fibrosarcoma cells show an active invasionary response. *Journal of Cell Science* 81: 163-187.
- Padua, D., Zhang, X.H., Wang, Q., Nadal, C., Gerald, W.L., Gomis, R.R., and Massague, J.

- (2008). TGF β primes breast tumors for lung metastasis seeding through angiopoietin-like 4. *Cell* 133(1): 66-77.
- Perona, R., Montaner, S., Saniger, L., Sanchez-Perez, I., Bravo, R., and Lacal, J.C. (1997). Activation of the nuclear factor-kappaB by Rho, CDC42, and Rac-1 proteins. *Genes and Development* 11(4): 463-475.
- Peters, M., Solem, F., Goldschmidt, J., Schirmacher, P., and Rose-John, S. (2001). Interleukin-6 and the soluble interleukin-6 receptor induce stem cell factor and Flt-3L expression in vivo and in vitro. *Experimental Hematology* 29(2): 146-155.
- Petnicki-Ocwieja, T., Chung, E., Acosta, D.I., Ramos, L.T., Shin, O.S., Ghosh, S., Kobzik, L., Li, X., and Hu, L.T. (2013). TRIF Mediates Toll-Like Receptor 2-Dependent Inflammatory Responses to *Borrelia burgdorferi*. *Infection and Immunity* 81(2): 402-410.
- Pletnev, S., Magracheva, E., Wlodawer, A., and Zdanov, A. (2005). A model of the ternary complex of interleukin-10 with its soluble receptors. *BMC Structural Biology* 5(10): 1-15.
- Pollard, J.W. (2004). Tumour-educated macrophages promote tumour progression and metastasis. *Nature Reviews* 4(1): 71-78.
- Poltorak, A., He, X., Smirnova, I., Liu, M.Y., Van Huffel, C., Du, X., Birdwell, D., Alejos, E., Silva, M., Galanos, C., Freudenberg, M., Ricciardi-Castagnoli, P., Layton, B., and Beutler, B. (1998). Defective LPS signaling in C3H/HeJ and C57BL/10ScCr mice: mutations in Tlr4 gene. *Science* 282(5396): 2085-2088.
- Quaglino, A., Schere-Levy, C., Romorini, L., Meiss, R.P., and Kordon, E.C. (2007). Mouse mammary tumors display Stat3 activation dependent on leukemia inhibitory factor signaling. *Breast Cancer Research* 9(R69): 1-12.
- Raftopoulou, M., and Hall, A. (2004). Cell migration: Rho GTPases lead the way. *Developmental Biology: Review* 265(1): 23-32.
- Rakesh, M., Cate, M., Vijay, R., Shrikant, A., and Shanjana, A. (2012). A TLR4-interacting peptide inhibits lipopolysaccharide-stimulated inflammatory responses, migration and invasion of colon cancer SW480 cells. *Oncoimmunology* 1(9): 1495-1506.
- Ramirez, A.S., Rosas, A., Hernandez-Berianin, J.A., Orengo, J.C., Saavedra, P., de la Fe, C., Fernandez, A., and Poveda, J.B. (2005). Relationship between rheumatoid arthritis and *Mycoplasma pneumoniae*: a case-control study. *Rheumatology* 44(7): 912-914.
- Ramos-DeSimone, N., Hahn-Dantona, E., Siple, J., Nagase, H., French, D.L., and Quigley, J.P. (1999). Activation of Matrix Metalloproteinase-9 (MMP-9) via a Converging Plasmin/Stromelysin-1 Cascade Enhances Tumor Cell Invasion. *Journal of Biological Chemistry* 274(19): 13066-13076.
- Raptis, L., Arulanandam, R., Geletu, M., and Turkson, J. (2011). The R(h)oads to Stat3:

- Stat3 activation by the Rho GTPases. *Experimental Cell Research* 317(13): 1787-1795.
- Raptis, L., Arulanandam, R., Vultur, A., Geletu, M., Chevalier, S., and Feracci, H. (2009). Beyond structure, to survival: activation of Stat3 by cadherin engagement. *Biochemistry and Cell Biology* 87(6): 835-843.
- Ray, J.M., and Stetler-Stevenson, W.G. (1994). The role of matrix metalloproteases and their inhibitors in tumour invasion, metastasis and angiogenesis. *European Respiratory Journal* 7(11): 2062-2072.
- Razin, S., Yogev, D., and Naot, Y. (1998). Molecular biology and pathogenicity of Mycoplasmas. *Microbiology and Molecular Biology Reviews* 62(4): 1094-1156.
- Re, F., and Strominger, J.L. (2002). Monomeric Recombinant MD-2 Binds Toll-like Receptor 4 Tightly and Confers Lipopolysaccharide Responsiveness. *Journal of Biological Chemistry* 277(26): 23427-23432.
- Rebouissou, S., Amessou, M., Couchy, G., Poussin, K., Imbeaud, S., Pilati, C., Izard, T., Balabaud, C., Bioulac-Sage, P., and Zucman-Rossi, J. (2009). Frequent in-frame somatic deletions activate gp130 in inflammatory hepatocellular tumours. *Nature* 457(7226): 200-204.
- Reigstad, C.S., Lunden, G.O., Felin, J., and Backhed, F. (2009). Regulation of serum amyloid A3 (SAA3) in mouse colonic epithelium and adipose tissue by the intestinal microbiota. *PLoS One* 4(6): 5842-5851.
- Reilly, P.T., Teo, W.L., Low, M.J., Amoyo-Brion, A.A., Dominguez-Brauer, C., Elia, A.J., Berger, T., Greicius, G., Pettersson, S., and Mak, T.W. (2012). Lipocalin 2 performs contrasting, location-dependent roles in APCmin tumor initiation and progression. *Oncogene* 32(10): 1233-1239.
- Ren, Y., Li, R., Zheng, Y., and Busch, H. (1998). Cloning and characterization of GEF-H1, a microtubule-associated guanine nucleotide exchange factor for Rac and Rho GTPases. *The Journal of Biological Chemistry* 273(52): 34954-34960.
- Riley, J.K., Takeda, K., Akira, S., and Schreiber, R.D. (1999). Interleukin-10 Receptor Signaling through the JAK-STAT Pathway: Requirement for two distinct receptor derived signals for anti-inflammatory action. *Journal of Biological Chemistry* 274(23): 16513-16521.
- Rossol, M., Heine, H., Meusch, U., Quandt, D., Klein, C., Sweet, M.J., and Hauschildt, S. (2011). LPS-induced cytokine production in human monocytes and macrophages. *Critical Reviews in Immunology* 3(5): 379-446.
- Rutkowski, M., Sughrue, M.E., Kane, A.J., Mills, S.A., and Parsa, A.T. (2010). Cancer and the Complement Cascade. *Molecular Cancer Research* 8(11): 1453-1465.
- Sacht, G., Marten, A., Deiters, U., Submuth, R., Jung, G., Wingender, E., and Muhlradt, P.F.

- (1998). Activation of nuclear factor- κ B in macrophages by mycoplasma lipopeptides. *European Journal of Immunology* 28(12): 4207-4212.
- Sadrzadeh, S.M.H., and Bozorgmehr, J. (2004). Haptoglobin Phenotypes in Health and Disorders. *American Society for Clinical Pathology* 121: S97-104.
- Sahu, A., and Lambris, J.D. (2001). Structure and biology of complement protein C3, a connecting link between innate and acquired immunity. *Immunology Reviews* 180: 35-48.
- Sansone, P., Storci, G., Tavolari, S., Guarnieri, T., Giovannini, C., Taffurelli, M., Ceccarelli, C., Santini, D., Paterini, P., Marcu, K.B., Chieco, P., and Bonafe, M. (2007). IL-6 triggers malignant features in mammospheres from human ductal breast carcinoma and normal mammary gland. *The Journal of Clinical Investigation* 117(12): 3988-4002.
- Scheller, J., Chalaris, A., Schmidt-Arras, D., and Rose-John, S. (2011). The pro- and anti-inflammatory properties of the cytokine interleukin-6. *Biochimica et Biophysica Acta* 1813(5): 878-888.
- Schindler, R., Mancilla, J., Endres, S., Ghorbani, R., Clark, S.C., and Dinarello, C.A. (1990). Correlations and interactions in the production of interleukin-6 (IL-6), IL-1, and tumor necrosis factor (TNF) in human blood mononuclear cells: IL-6 suppresses IL-1 and TNF. *Blood* 75(1): 40-47.
- Schmidhauser, C., Dudler, R., Schmidt, T., and Parish, R.W. (1990). A mycoplasma protein influences tumor cell invasiveness and contact inhibition *in vitro*. *Journal of Cell Science* 95(Pt3): 499-506.
- Schrodinger, LLC (2010). The PyMOL Molecular Graphics System, Version 1.3r1.
- Seya, T., Tanaka, N., Shinji, S., Yokoi, K., Koizumi, M., Teranishi, N., Yamashita, K., Tajiri, T., Ishiwata, T., and Naito, Z. (2006). Lumican expression in advanced colorectal cancer with nodal metastasis correlates with poor prognosis. *Oncology Reports* 16(6): 1225-1230.
- Shain, K.H., Yarde, D.N., Meads, M.B., Huang, M., Jove, R., Hazlehurst, L.A., and Dalton, W.S. (2009). Beta1 integrin adhesion enhances IL-6-mediated STAT3 signaling in myeloma cells: implications for microenvironment influence on tumor survival and proliferation. *Cancer Research* 69(3): 1009-1015.
- Sherry, M.M., Reeves, A., Wu, J.K., and Cochran, B.H. (2009). STAT3 is required for proliferation and maintenance of multipotency in glioblastoma stem cells. *Stem Cells* 27(10): 2383-2392.
- Shibolet, O., Giallourakis, C., Rosenberg, I., Mueller, T., Xavier, R.J., and Podolsky, D.K. (2007). AKAP13, a RhoA GTPase-specific guanine exchange factor, is a novel regulator of TLR2 signaling. *The Journal of Biological Chemistry* 282(48): 35308-35317.

- Shimazu, R., Akashi, S., Ogata, H., Nagai, Y., Fukudome, K., Miyake, K., and Kimoto, M. (1999). MD-2, a molecule that confers lipopolysaccharide responsiveness on Toll-like receptor 4. *The Journal of Experimental Medicine* 189(11): 1777-1782.
- Shimizu, S., Tahara, M., Ogata, S., Hashimoto, K., Morishige, K., Tasaka, K., and Murata, Y. (2007a). Involvement of nuclear factor- κ B activation through RhoA/Rho-kinase pathway in LPS-induced IL-8 production in human cervical stromal cells. *Molecular Human Reproduction* 13(3): 181-187.
- Shimizu, T., Kida, Y., and Kuwano, K. (2004). Lipid-associated membrane proteins of *Mycoplasma fermentans* and *M. penetrans* activate human immunodeficiency virus long-terminal repeats through Toll-like receptors. *Immunology* 113(1): 121-129.
- Shimizu, T., Kida, Y., and Kuwano, K. (2005). A dipalmitoylated lipoprotein from *Mycoplasma pneumoniae* activates NF-kappa B through TLR1, TLR2, and TLR6. *Journal of Immunology* 175(7): 4641-4646.
- Shimizu, T., Kida, Y., and Kuwano, K. (2007b). Triacylated lipoproteins derived from *Mycoplasma pneumoniae* activate nuclear factor- κ B through toll-like receptors 1 and 2. *Immunology* 121(4): 473-483.
- Shimizu, T., Kimura, Y., Kida, Y., Kuwano, K., Tachibana, M., Hashino, M., and Watarai, M. (2014). Cytadherence of *Mycoplasma pneumoniae* Induces Inflammatory Responses through Autophagy and Toll-like Receptor 4. *Infection and Immunity* 5: 1-5.
- Siddiquee, K., Zhang, S., Guida, W.C., Blaskovich, M.A., Greedy, B., Lawrence, H.R., Yip, M.L., Jove, R., McLaughlin, M.M., Lawrence, N.J., Sebt, S.M., and Turkson, J. (2007). Selective chemical probe inhibitor of Stat3, identified through structure-based virtual screening, induces antitumor activity. *Proceedings of the National Academy of Sciences of the United States of America* 104(18): 7391-7396.
- Sidhu, A., Miller, P.J., and Hollenbach, A.D. (2011). FOXO1 stimulates ceruloplasmin promoter activity in human hepatoma cells treated with IL-6. *Biochemical and Biophysical Research Communications* 404(4): 963-967.
- Sippel, K.H., Robbins, A.H., Reutzel, R., Boehlein, S.K., Namiki, K., Goodison, S., Agbandji-McKenna, M., Rosser, C.J., and McKenna, R. (2009). Structural insights into the extracytoplasmic thiamine-binding lipoprotein p37 of *Mycoplasma hyorhinae*. *Journal of Bacteriology* 191(8): 2585-2592.
- Sippel, K.H., Robbins, A.H., Reutzel, R., Domsic, J., Boehlein, S.K., Govindasamy, L., Agbandji-McKenna, M., Rosser, C.J., and McKenna, R. (2008). Structure determination of the cancer-associated *Mycoplasma hyorhinae* protein Mh-p37. *Biological Crystallography* 64(Pt11): 1172-1178.
- Sirand-Pugnet, P., Citti, C., Barre, A., and Blanchard, A. (2007). Evolution of mollicutes: down a bumpy road with twists and turns. *Research in Microbiology* 158(10): 754-766.

- Sledge Jr., G.W., and Miller, K.D. (2003). Exploiting the hallmarks of cancer: the future conquest of breast cancer. *European Journal of Cancer* 39(12): 1668-1675.
- Solinas, G., Marchesi, F., Garlanda, C., Mantovani, A., and Allavena, P. (2010). Inflammation-mediated promotion of invasion and metastasis. *Cancer Metastasis Reviews* 29(2): 243-248.
- Soriano, E.V., Rajashankar, K.R., Hanes, J.W., Bale, S., Begley, T.P., and Ealick, S.E. (2008). Structural similarities between thiamin-binding protein and Thiaminase-I suggest a common ancestor. *Biochemistry* 47(5): 1346-1357.
- Spano, D., and Zollo, M. (2012). Tumor microenvironment: a main actor in the metastasis process. *Clinical and Experimental Metastasis* 29(4): 381-395.
- Spirig, R., Tsui, J., and Shaw, S. (2012). The Emerging Role of TLR and Innate Immunity in Cardiovascular Disease. *Cardiol Res Pract* 2012(181394): 1-11.
- Stack, J., and Bowie, A.G. (2012). Poxviral protein A46 antagonizes Toll-like receptor 4 signaling by targeting BB loop motifs in Toll-IL-1 receptor adaptor proteins to disrupt receptor:adaptor interactions. *The Journal of Biological Chemistry* 287(27): 22672-22682.
- Stack, J., Haga, I.R., Schroder, M., Bartlett, N.W., Maloney, G., Reading, P.C., Fitzgerald, K.A., Smith, G.L., and Bowie, A.G. (2005). Vaccinia virus protein A46R targets multiple Toll-like-interleukin-1 receptor adaptors and contributes to virulence. *The Journal of Experimental Medicine* 201(6): 1007-1018.
- Steensberg, A., Fischer, C.P., Keller, C., Møller, K., and Pedersen, B.K. (2003). IL-6 enhances plasma IL-1ra, IL-10, and cortisol in humans. *American Journal of Physiology - Endocrinology And Metabolism* 285(2): E433-E437.
- Steinemann, C., Fenner, M., Binz, H., and Parish, R.W. (1984a). Invasive behaviour of mouse sarcoma cells is inhibited by blocking a 37,000-dalton plasma membrane glycoprotein with Fab fragments. *Proceedings of the National Academy of Sciences of the United States of America* 81(12): 3747-3750.
- Steinemann, C., Fenner, M., Parish, R., and Binz, H. (1984b). Studies of the invasiveness of the chemically induced mouse sarcoma FS9. I. Monoclonal antibodies to a 37,000 dalton membrane glycoprotein inhibit invasion of fibroblasts *in vitro*. *International Journal of Cancer* 34(3): 407-414.
- Storr, S.J., Mohammeda, R.A.A., Woolston, C.M., Green, A.R., Parr, T., Spiteri, I., Caldas, C., Ball, G.R., Ellis, I.O., and Martin, S.G. (2011). Calpastatin is associated with lymphovascular invasion in breast cancer. *The Breast* 20(5): 413-418.
- Szlosarek, P., Charles, K.A., and Balkwill, F.R. (2006). Tumour necrosis factor- α as a tumour promoter. *European Journal of Cancer* 42(6): 745-750.
- Taga, T., and Kishimoto, T. (1997). gp130 and the interleukin-6 family of cytokines. *Annual*

Review of Immunology 1997(15): 797-819.

- Takeda, K., and Akira, S. (2005). Toll-like receptors in innate immunity. *International Immunology* 17(1): 1-14.
- Takeda, K., Clausen, B.E., Kaisho, T., Tsujimura, T., Terada, N., Forster, I., and Akira, S. (1999). Enhanced Th1 activity and development of chronic enterocolitis in mice devoid of Stat3 in macrophages and neutrophils. *Immunity* 10(1): 39-49.
- Takeuchi, O., Kaufmann, A., Grote, K., Kawai, T., Hoshino, K., Morr, M., Mühlradt, P.F., and Akira, S. (2000). Cutting Edge: Preferentially the R-Stereoisomer of the Mycoplasma Lipopeptide Macrophage-Activating Lipopeptide-2 Activates Immune Cells Through a Toll-Like Receptor 2- and MyD88-Dependent Signaling Pathway. *The Journal of Immunology* 164(2): 554-557.
- Tam, R., and Saier, M.H.J. (1993). Structural, functional, and evolutionary relationships among extracellular solute-binding receptors of bacteria. *Microbiology and Molecular Biology Reviews* 57(2): 320-346.
- Tamm, I., Kikuchi, T., Cardinale, I., and Krueger, J.G. (1994). Cell-adhesion-disrupting action of interleukin-6 in human ductal breast carcinoma cells. *The Proceedings of the National Academy of Sciences USA* 91: 3329 - 3333.
- Terry, S.J., Zihni, C., Elbediwy, A., Vitiello, E., Leefa Chong San, I.V., Balda, M.S., and Matter, K. (2011). Spatially restricted activation of RhoA signalling at epithelial junctions by p114RhoGEF drives junction formation and morphogenesis. *Nature Cell Biology* 13(2): 159-166.
- Thallinger, G.G., Obermayr, E., Charoentong, P., Tong, D., Trajanoski, Z., and Zeillinger, R. (2012). A Sequence Based Validation of Gene Expression Microarray Data. *American Journal of Bioinformatics* 1(1): 1-9.
- Tilg, H., Trehu, E., Atkins, M., Dinarello, C., and Mier, J. (1994). Interleukin-6 (IL-6) as an anti-inflammatory cytokine: induction of circulating IL-1 receptor antagonist and soluble tumor necrosis factor receptor p55. *Blood* 83(1): 113-118.
- Tsai, S., Wear, D.J., Shih, J.W., and Lo, S.C. (1995). Mycoplasmas and oncogenesis: Persistent infection and multistage malignant transformation. *Proceedings of the National Academy of Sciences of the United States of America* 92(22): 10197-10201.
- Tsumoto, K., Abe, R., Ejima, D., and Arakawa, T. (2010). Non-denaturing solubilization of inclusion bodies. *Current Pharmaceutical Biotechnology* 11(3): 309-312.
- Turner, J.J., Foxwell, K.M., Kanji, R., Brenner, C., Wood, S., Foxwell, B.M., and Feldmann, M. (2010). Investigation of nuclear factor- κ B inhibitors and interleukin-10 as regulators of inflammatory signalling in human adipocytes. *Clinical and Experimental Immunology* 162(3): 487-493.
- Uphoff, C.C., and Drexler, H.G. (2002). Comparative PCR analysis for detection of

mycoplasma infections in continuous cell lines. *In Vitro Cellular & Developmental Biology: Animal* 38(2): 79-85.

Urbanek, C., Goodison, S., Chang, M., Porvasnik, S., Sakamoto, N., Li, C., Boehlein, S.K., and Rosser, C.J. (2011). Detection of antibodies directed at *M. hyorhinitis* p37 in the serum of men with newly diagnosed prostate cancer. *BMC Cancer* 11(233): 1-6.

Ushio, S., Iwaki, K., Taniai, M., Ohta, T., Fukuda, S., Sugimura, K., and Kurimoto, M. (1995). Metastasis-promoting activity of a novel molecule, Ag 243-5, derived from Mycoplasma, and the complete nucleotide sequence. *Microbiology and Immunology* 39(6): 393-400.

Visse, R., and Nagase, H. (2003). Matrix metalloproteinases and tissue inhibitors of metalloproteinases: structure, function and biochemistry. *Circulation Research* 92(8): 827-839.

Wan, F., and Lenardo, M.J. (2010). The nuclear signaling of NF- κ B: current knowledge, new insights, and future perspectives. *Cell Research* 20(1): 24-33.

Wang, J., Hori, K., Ding, J., Huang, Y., Kwan, P., Ladak, A., and Tredget, E.E. (2011a). Toll-like receptors expressed by dermal fibroblasts contribute to hypertrophic scarring. *J Cell Physiol* 226(5): 1265-1273.

Wang, Q., Rozelle, A.L., Lepus, C.M., Scanzello, C.R., Song, J.J., Larsen, D.M., Crish, J.F., Bebek, G., Ritter, S.Y., Lindstrom, T.M., Hwang, I., Wong, H.H., Punzi, L., Encarnacion, A., Shamloo, M., Goodman, S.B., Wyss-Coray, T., Goldring, S.R., Banda, N.K., Thurman, J.M., Gobezie, R., Crow, M.K., Holers, V.M., Lee, D.M., and Robinson, W.H. (2011b). Identification of a central role for complement in osteoarthritis. *Nature Medicine* 17(12): 1674-1680.

Wang, Y., Li, L., Guo, X., Jin, X., Sun, W., Zhang, X., and Xu, R.C. (2012). Interleukin-6 signaling regulates anchorage-independent growth, proliferation, adhesion and invasion in human ovarian cancer cells. *Cytokine* 59(2): 228-236.

Wang, Y., Lu, X., Zhu, L., Shen, Y., Chengedza, S., Feng, H., Wang, L., Jung, J.U., Gutkind, J.S., and Fe, P. (2013). IKK epsilon kinase is crucial for viral G protein-coupled receptor tumorigenesis. *Proceedings of the National Academy of Sciences of the United States of America* 14: 1-6.

Weber-Nordt, R.M., Riley, J.K., Greenlund, A.C., Moore, K.W., Darnell, J.E., and Schreiber, R.D. (1996). Stat3 recruitment by two distinct ligand-induced, tyrosine-phosphorylated docking sites in the interleukin-10 receptor intracellular domain. *The Journal of Biological Chemistry* 271(44): 27954-27961.

Welm, A.L. (2008). TGF β primes breast tumor cells for metastasis. *Cell* 133(1): 27-28.

Wender, P.A., Mitchell, D.J., Pattabiraman, K., Pelkey, E.T., Steinman, L., and Rothbard, J.B. (2000). The design, synthesis, and evaluation of molecules that enable or enhance cellular uptake: peptoid molecular transporters. *Proceedings of the*

National Academy of Sciences of the United States of America 97(24): 13003-13008.

- Wennerberg, K., Rossman, K.L., and Der, C.J. (2005). The Ras superfamily at a glance. *Journal of Cell Science* 118(Pt5): 843-846.
- Wildenburg, G.A., Dohn, M.R., Carnahan, R.H., Davis, M.A., Lobdell, N.A., Settlemen, J., and Reynolds, A.B. (2006). p120-Catenin and p190RhoGap regulate cell-cell adhesion by coordinating antagonism between Rac and Rho. *Cell* 127: 1027 - 1039.
- Williams, K., Fulford, L.A., and Albig, A.R. (2011). Lumican reduces tumor growth via induction of Fas-mediated endothelial cell apoptosis. *Cancer Microenvironment* 4(1): 115-126.
- Williams, L.M., Sarma, U., Willets, K., Smallie, T., Brennan, F., and Foxwell, B.M.J. (2007). Expression of Constitutively Active STAT3 Can Replicate the Cytokine-suppressive Activity of Interleukin-10 in Human Primary Macrophages. *Journal of Biological Chemistry* 282(10): 6965-6975.
- Wirth, M., Berthold, E., Grashoff, M., Pftitzner, H., Schubert, U., and Hauser, H. (1994). Detection of mycoplasma contaminations by the polymerase chain reaction. *Cytotechnology* 16: 67-77.
- Wright, S.D., Ramos, R.A., Tobias, P.S., Ulevitch, R.J., and Mathison, J.C. (1990). CD14, a receptor for complexes of lipopolysaccharide (LPS) and LPS binding protein. *Science* 249(4975): 1431-1433.
- Wu, F., Vij, N., Roberts, L., Lopez-Briones, S., Joyce, S., and Chakravarti, S. (2007). A novel role of the lumican core protein in bacterial lipopolysaccharide-induced innate immune response. *The Journal of Biological Chemistry* 282(36): 26409-26417.
- Wu, Y., Qiu, H., Zeng, Y., You, X., Deng, Z., Yu, M., and Zhu, C. (2008). *Mycoplasma genitalium* lipoproteins induce human monocytic cell expression of proinflammatory cytokines and apoptosis by activating nuclear factor kappaB. *Mediators of Inflammation* 2008: 195427.
- Xiong, H., Zhang, Z.G., Tian, X.Q., Sun, D.F., Liang, Q.C., Zhang, Y.J., Lu, R., Chen, Y.X., and Fang, J.Y. (2008). Inhibition of JAK1, 2/STAT3 signaling induces apoptosis, cell cycle arrest, and reduces tumor cell invasion in colorectal cancer cells. *Neoplasia* 10(3): 287-297.
- Yang, H., Qu, L., Ma, Chen, L., Liu, W., Liu, C., Meng, L., Wu, J., and Shou, C. (2010a). *Mycoplasma hyorhinis* infection in gastric carcinoma and its effects on the malignant phenotypes of gastric cancer cells. *BMC Gastroenterology* 10(132): 1-8.
- Yang, H., Zhang, J., and Shou, C. (2010b). Detection of *Mycoplasma hyorhinis* infection in Ovarian Cancer with *in situ* hybridization and immunohistochemistry. *Clinical Oncology of Cancer Research* 7: 294-298.
- Yang, J., McNeish, B., Butterfield, C., and Moses, M.A. (2012). Lipocalin 2 is a novel

regulator of angiogenesis in human breast cancer. *FASEB Journal* 27(1): 1-6.

- Yang, X., Coleman, A.S., Anguita, J., and Pal, U. (2009). A chromosomally encoded virulence factor protects the Lyme disease pathogen against host-adaptive immunity. *PLoS Pathogens* 5(3): e1000326-1000312.
- Yang, X., Lenhart, T.R., Kariu, T., Anguita, J., Akins, D.R., and Pal, U. (2010c). Characterization of unique regions of *Borrelia burgdorferi* surface-located membrane protein 1. *Infection and Immunity* 78(11): 4477-4487.
- Yavlovich, A., Higazi, A.A., and Rottem, S. (2001). Plasminogen binding and activation by *Mycoplasma fermentans*. *Infection and Immunity* 69(4): 1977-1982.
- Yavlovich, A., Katzenell, A., Tarshia, M., Higazi, A.R., and Rottem, S. (2004). *Mycoplasma fermentans* binds to and invades HeLa cells: Involvement of plasminogen and urokinase. *Infection and Immunity* 72(9): 5004-5011.
- Yokota, S., Okabayashi, T., Rehli, M., Fujii, N., and Amano, K. (2010). *Helicobacter pylori* lipopolysaccharides upregulate toll-like receptor 4 expression and proliferation of gastric epithelial cells via the MEK1/2-ERK1/2 mitogen-activated protein kinase pathway. *Infection and Immunity* 78(1): 468-476.
- Yoshio-Hoshino, N., Adachi, Y., Aoki, C., Pereboev, A., Curiel, D.T., and Nishimoto, N. (2007). Establishment of a new interleukin-6 (IL-6) receptor inhibitor applicable to the gene therapy for IL-6-dependent tumor. *Cancer Research* 67(3): 871-875.
- Zanoni, I., Ostuni, R., Marek, L.R., Barresi, S., Barbalat, R., Barton, G.M., Granucci, F., and Kagan, J.C. (2011). CD14 controls the LPS-induced endocytosis of Toll-like receptor 4. *Cell* 147(4): 868-880.
- Zhang, H., Wong, C.C.L., Wei, H., Gilkes, D.M., Korangath, P., Chaturvedi, P., Schito, L., Chen, J., Krishnamachary, B., Winnard Jr, P.T., Ramen, V., Zhen, L., Mitzner, W.A., Sukumar, S., and Semenza, G.L. (2012). HIF-1-dependent expression of angiopoietin-like 4 and L1CAM mediates vascular metastasis of hypoxic breast cancer cells to the lungs. *Oncogene* 31(14): 1757-1770.
- Zhang, H., Xu, L., Xiao, D., Xie, J., Zeng, H., Wang, Z., Zhang, X., Niu, Y., Shen, Z., Shen, J., Wu, X., and Li, E. (2007). Upregulation of neutrophil gelatinase-associated lipocalin in oesophageal squamous cell carcinoma: significant correlation with cell differentiation and tumour invasion. *Journal of Clinical Pathology* 60(5): 555-561.
- Zheng, L., Baumann, U., and Reymond, J.-L. (2004). An efficient one-step site-directed and site-saturation mutagenesis protocol. *Nucleic Acids Research* 32(14): e111-115.
- Zheng, Y. (2001). Dbl family guanine nucleotide exchange factors. *Trends in Biochemical Sciences* 26(12): 724-732.
- Zhou, Y., Holmseth, S., Hua, R., Lehre, A.C., Olofsson, A.M., Poblete-Naredo, I., Kempson, S.A., and Danbolt, N.C. (2012). The betaine-GABA transporter (BGT1, slc6a12) is

predominantly expressed in the liver and at lower levels in the kidneys and at the brain surface. *American Journal of Physiology Renal Physiology* 302(3): 316-328.

Zhu, P., Tan, M.J., Huang, R.-L., Tan, C.K., Chong, H.C., Pal, M., Lam, C.R.I., Boukamp, P., Pan, J.Y., Tan, S.H., Kersten, S., Li, H.Y., Ding, J.L., and Tan, N.S. (2011). Angiopoietin-like 4 protein elevates the prosurvival intracellular $O_2^-:H_2O_2$ ration and confers anikis resistance to tumors. *Cancer Cell* 19(3): 401-415.

Zukauskas, A., Merley, A., Li, D., Ang, L.-H., Sciuto, T.E., Salman, S., Dvorak, A.M., Dvorak, H.F., and Jaminet, S.-C.S. (2011). TM4SF1: a tetraspanin-like protein necessary for nanopodia formation and endothelial cell migration. *Angiogenesis* 14(3): 345-354.

Zuo, L.L., Wu, Y.M., and You, X.X. (2009). Mycoplasma lipoproteins and Toll-like receptors. *Journal of Zhejiang University Science B* 10(1): 67-76.